

**CRYSTAL ENGINEERING STUDIES OF METAL 1,1'-
DITHIOLATES: COORDINATION POLYMERS AND BEYOND**

TAN YEE SENG

**FACULTY OF SCIENCE
UNIVERSITY OF MALAYA
KUALA LUMPUR**

2016

CRYSTAL ENGINEERING STUDIES OF METAL 1,1'-
DITHIOLATES: COORDINATION POLYMERS AND
BEYOND

TAN YEE SENG

THESIS SUBMITTED IN FULFILMENT OF THE
REQUIREMENTS FOR THE DEGREE OF DOCTOR OF
PHILOSOPHY

FACULTY OF SCIENCE
UNIVERSITY OF MALAYA
KUALA LUMPUR

2016

UNIVERSITY OF MALAYA
ORIGINAL LITERARY WORK DECLARATION

Name of Candidate: TAN YEE SENG

Registration/Matric No: SHC 130011

Name of Degree: SHC - DOCTOR OF PHILOSOPHY (EXCEPT MATHEMATICS
& SCIENCE PHILOSOPHY)

Title of Project Paper/Research Report/Dissertation/Thesis ("this Work"):

Crystal Engineering Studies of Metal 1,1'-Dithiolates: Coordination Polymers and
Beyond

Field of Study: Inorganic Chemistry

I do solemnly and sincerely declare that:

- (1) I am the sole author/writer of this Work;
- (2) This Work is original;
- (3) Any use of any work in which copyright exists was done by way of fair dealing and for permitted purposes and any excerpt or extract from, or reference to or reproduction of any copyright work has been disclosed expressly and sufficiently and the title of the Work and its authorship have been acknowledged in this Work;
- (4) I do not have any actual knowledge nor do I ought reasonably to know that the making of this work constitutes an infringement of any copyright work;
- (5) I hereby assign all and every rights in the copyright to this Work to the University of Malaya ("UM"), who henceforth shall be owner of the copyright in this Work and that any reproduction or use in any form or by any means whatsoever is prohibited without the written consent of UM having been first had and obtained;
- (6) I am fully aware that if in the course of making this Work I have infringed any copyright whether intentionally or otherwise, I may be subject to legal action or any other action as may be determined by UM.

Candidate's Signature

Date:

Subscribed and solemnly declared before,

Witness's Signature

Date:

Name:

Designation:

ABSTRACT

Crystal engineering was implemented by conducting three distinctive projects, covering a total of 22 compounds. These compounds were fully characterised *via* various spectroscopic techniques and materials analysis, including FT-IR, UV-Vis, PL, SCXRD, PXRD, NMR, TGA, DSC and CHN elemental analysis. Crystallographic study of all compounds forms the core focus of current research for delineation of crystal engineering. The first project assessed seven crystal structures of same metal centre and ligand, with two forming one-dimensional coordination polymers. The factors leading to formation of solvomorph and supramolecular isomers were investigated. Solvomorph were obtained from different crystallisation parameters and solvent systems, while unanticipated non-reversible single crystal to single crystal transformations were found to afford two pairs of supramolecular isomers (**1** to **2** and **6** to **7**), stimulated by stabilisation energy in crystal systems and atmospheric moisture. The above ‘non-reversible transformations’ were, however interconverted by developing a solvent-induced reversible transformation system. Hexamethylenetetramine, a multidentate linker, was employed in the second project, which revealed its adoption of multiple coordination modes through the complexation with different cadmium xanthates. Unexpectedly, the coordination mode of hexamethylenetetramine was not affected despite varying the mole ratio of linker and precursor, *i.e.* 1:1, 1:2, and 2:1, identical adducts were obtained in respective synthesis. Hexamethylenetetramine functioned as μ_2 and μ_3 to form one-dimensional coordination polymers in compound **8** and **9**, and μ_1 in the dimeric motif of compound **10**. The coordination modes of hexamethylenetetramine depend upon the orientation of cadmium xanthate in the molecule, as demonstrated by compounds **8** and **9**. The highly packing crystal system of compound **8** oriented the methyl group of xanthate which prevented the coordination of third nitrogen atom of hexamethylenetetramine; while the steric effect

induced by the ethyl group resulted in a position which allowed the third coordination of hexamethylenetetramine in compound **9**. The third project aims to introduce the C–H $\cdots\pi$ (PdS₂C) interactions in palladium xanthate. Palladium xanthate **11** – **22**, a total of 12 compounds were prepared and the C–H $\cdots\pi$ (PdS₂C) interactions were successfully implemented in 11 out of 12 compounds, with some structures displayed up to a maximum of six interactions per molecule. Compound **13** was subjected to density functional theory calculations; the C–H $\cdots\pi$ (PdS₂C) was verified as second important interactions to support the respective crystal system, followed after Pd \cdots S interactions. In addition to the above, the crystal system was also stabilised by hydrophobic interactions of side-by-side aliphatic chains.

ABSTRAK

Tiga projek penyelidikan telah dijalankan untuk mengkaji aspek berbeza dalam bidang kejuruteraan hablur. Sejumlah 22 sebatian telah disediakan dimana kesemua sebatian telah dicirikan dengan pelbagai teknik spektroskopi dan analisis bahan termasuk FT-IR, UV-Vis, PL, SCXRD, PXRD, NMR, TGA dan lain-lain. Pencirian sebatian adalah termasuk pembelauan hablur tunggal, dimana ianya adalah kajian terpenting untuk mendalami bidang kejuruteraan hablur. Projek pertama mengkaji tujuh struktur hablur yang telah diperolehi dari logam dan ligan yang sama, dimana dua daripadanya adalah koordinasi polimer satu-dimensi yang berbeza. Kajian terperinci telah dijalankan untuk mengenalpasti faktor yang menyebabkan sebatian tersebut boleh wujud dalam pelbagai fenomena; *solvomorph* dan isomer supramolekul. Fenomena *solvomorph* didapati terjadi disebabkan parameter penghabluran serta sistem pelarut yang berbeza dan menunjukkan transformasi sehala, dimana ianya menghasilkan dua pasangan isomer supramolekul (**1** dan **6** kepada **2** dan **7**), jangkaan daripada pengiraan tenaga kestabilan molekul dan kelembapan atmosfera. Transformasi sehala tersebut walaubagaimanapun boleh dijadikan dua hala dengan membina sistem transformasi pelarut-pendorong dua hala. Untuk projek kedua, kajian melibatkan molekul hexamethylenetetramina, sebagai penyambung multi-kelat. Pelbagai mod koordinasi telah dipamerkan dalam struktur hablur apabila penyambung tersebut digabungkan dengan sebatian koordinatan kadmium(II) xanthate yang berbeza. Walaubagaimanapun, mod koordinasi hexamethylenetetramina tidak terpengaruh dengan mempelbagaikan nisbah penyambung dan bahan pemula; 1:1, 1:2 dan 2:1 dimana hasil yang sama telah dihasilkan. Hexamethylenetetramina berfungsi sebagai μ_2 dan μ_3 dalam koordinasi polimer satu-dimensi dalam sebatian **8** dan **9**, dan μ_1 dalam motif dimer dalam sebatian **10**. Mod pengkoordinatan hexamethylenetetramina bergantung kepada orientasi kadmium(II) xanthate dalam molekul, seperti yang dibuktikan dalam sebatian **8** dan **9**. Kepadatan sistem hablur sebatian **8** mengorientasikan

kumpulan metil pada xanthate telah menghalang koordinatan atom nitrogen yang ketiga pada hexamethylenetetramina sementara kesan sterik hasil dari kumpulan etil mewujudkan satu orientasi yang membolehkan kadmium(II) xanthate membuat ikatan koordinasi yang ketiga kepada hexamethylenetetramina dalam sebatian **9**. Projek ketiga bertujuan untuk menunjukkan interaksi $C-H\cdots\pi(PdS_2C)$ dalam sebatian palladium(II) xanthate. Sejumlah 12 sebatian koordinatan palladium(II) xanthate, iaitu **11** – **22** telah disediakan dan interaksi $C-H\cdots\pi(PdS_2C)$ telah berjaya diimplimentasikan dalam 11 sebatian dimana setiap struktur hablur mempamerkan sebanyak enam interaksi tersebut dalam setiap molekul. Sebatian **13** telah dipilih untuk kajian lanjut untuk pengiraan teori kepadatan fungsi dan didapati bahawa interaksi $C-H\cdots\pi(PdS_2C)$ adalah kedua terpenting untuk menyokong sistem hablur setelah interaksi $Pd\cdots S$. Selain daripada itu, sistem hablur juga distabilkan oleh interaksi hidrofobik; sebelah menyebelah rantai alifatik.

ACKNOWLEDGEMENTS

First and foremost, I would like to thank my supervisor, Professor Dr Edward R. T. Tiekink, and co-supervisor Dr Siti Nadiah Binti Abdul Halim for their contributions of time, idea and funding to support my research program. I have also acquired various analysing and wonderful crystal solving skills from their area of expertise. Besides, I am grateful for the freedom provided throughout my postgraduate program in organising relevant projects. They have been providing care more than supervisors, mentors and friends.

I would like to show my appreciation to the ex-post-doctorate in the group, Dr Seng Hoi Ling for expanding my knowledge in bioinorganic chemistry. Her generous sharing and contribution on one of my research projects has widened my understanding in the bioassay study. My gratitude is also directed to the other group members under Professor Tiekink and Dr Nadiah who have been offering bountiful knowledge sharing and kind help during my Ph.D. program.

Over and above, I would like to thank all of the collaborators, including Professor Dr Kieran C. Molloy and Dr Anna L. Sudlow (University of Bath, United Kingdom); Professor Dr Kiyoshi Fujisawa, and Ms. Yui Morishima (Ibaraki University, Japan); Professor Dr William Henderson and Ms. Wendy J. Jackson, (University of Waikato, New Zealand); Professor Dr Ionel Haiduc and Dr Marius V. Câmpian, (Babes-Bolyai University, Romania); Dr Alberto Otero-de-la-Roza (National Institute for Nanotechnology, National Research Council of Canada, Canada). Last but not least, I would like to thank local collaborators and their students, Dr Cheah Yoke-Kqueen, Dr Abdah Md Akim, Mr. Ooi Kah Kooi and Mr. Ang Kok Pian from University Putra Malaysia. Their collaborations are vital as to provide substantial complementing analysis for the projects conducted.

TABLE OF CONTENTS

ABSTRACT	iii
ABSTRAK	v
ACKNOWLEDGEMENTS	vii
TABLE OF CONTENTS	viii
LIST OF FIGURES	xi
LIST OF TABLES	xiv
LIST OF SYMBOLS AND ABBREVIATIONS	xv
LIST OF COMPOUND	xvi
LIST OF APPENDICES	xvii
CHAPTER 1: INTRODUCTION & LITERATURE REVIEW	1
1.1. 1,1'- Dithiolate Coordination Compounds.....	1
1.1.1. 1,1'- Dithiolate Ligands	1
1.1.1.1. Dithiocarbamate.....	2
1.1.1.2. Xanthate	3
1.1.2. Coordination Chemistry of 1, 1'- Dithiolate Ligand.....	4
1.2. Coordination Polymer Chemistry.....	4
1.2.1. 1,1'-Dithiolate Coordination Polymer	5
1.2.2. Coordination Mode of Multidendate Linker for Coordination Polymer.....	8
1.3. Crystal Engineering	9
1.3.1. Retrospective Crystal Engineering	9
1.3.2. Crystal Engineering for Secondary Interaction.....	10
1.4. Miscellaneous Studies	11
1.4.1. Crystallisation	11
1.4.1.1. Polymorphism.....	11
1.4.1.2. Single Crystal to Single Crystal Transformation.....	12
1.5. Aims of study	13
CHAPTER 2: REVERSIBLE, SOLVENT MEDIATED SUPRAMOLECULAR ISOMERISM IN A CADMIUM BIS (N-HYDROXYETHYL, N-ISOPROPYLDITHIOCARBAMATE) COMPOUND, Cd[S₂CN(iPr)CH₂CH₂OH]₂, AND UNEXPECTED CRYSTALLISATION OUTCOMES	14

2.1.	Introduction and Literature Review	14
2.2.	Methodology	17
2.2.1.	Synthesis	18
2.2.2.	X-ray crystallography	20
2.3.	Results and Discussion.....	22
2.3.1.	Synthesis and solution characterization	22
2.3.2.	Single crystal X-ray crystallography.....	23
2.3.3.	Powder X-ray diffraction (PXRD).....	28
2.3.4.	Thermal degradation	29
2.3.5.	Relationship between SI formed from $\text{Cd}[\text{S}_2\text{CN}(\text{iPr})\text{CH}_2\text{CH}_2\text{OH}]_2$	30
2.3.6.	Conversion between SIs.....	31
2.3.7.	Complementary crystallization experiments.....	33
2.4.	Conclusion.....	41
CHAPTER 3: SERENDIPITOUS COMPOSITIONAL AND STRUCTURAL DIVERSITY IN UROTROPINE ADDUCTS OF BINARY CADMIUM XANTHATES		42
3.1.	Introduction and Literature Review	42
3.2.	Methodology	46
3.2.1.	Synthesis of xanthate ligands.....	47
3.2.2.	Synthesis of binary cadmium xanthates.....	47
3.2.3.	Synthesis of $\text{Cd}(\text{S}_2\text{COR})_2(\text{hmta})_n$ adducts, R = Me (8), Et (9) and iPr (10).	48
3.2.4.	X-ray data collection and structure determination.....	49
3.3.	Results and Discussion.....	52
3.3.1.	Syntheses and spectroscopy	52
3.3.2.	Crystal and molecular structures.....	53
3.3.3.	Rationale for the adoption of different structural motifs in 8–10	59
3.3.4.	UV-visible and photoluminescence studies	60
3.3.5.	Thermogravimetric analysis.....	63
3.4.	Conclusion.....	64
CHAPTER 4: A COMBINED CRYSTALLOGRAPHIC AND COMPUTATIONAL STUDY OF THE PERSISTENCE OF C–H···π(CHELATE RING) INTERACTIONS IN THE CRYSTAL STRUCTURES OF PALLADIUM BIS (O-ALKYLDITHIOCARBONATE)S, $\text{Pd}(\text{S}_2\text{COR})_2$		65
4.1.	Introduction and Literature Review	65

4.2. Methodology	67
4.2.1. Synthesis	67
4.2.2. X-ray crystallography	68
4.3. Results and Discussion.....	68
4.3.1. Molecular Structures	70
4.3.2. Supramolecular Structures	71
4.3.3. Computational Study	86
4.3.4. Conclusion.....	89
CHAPTER 5: CONCLUSION.....	90
REFERENCES	92
LIST OF SELECTED PUBLICATION AND CONFERENCE ATTENDED.....	118

LIST OF FIGURES

Figure 1.1: Generic structures of mono-thiolate.	1
Figure 1.2: Generic chemical structures and resonance structure of 1,1'-dithiolate ligands.	2
Figure 1.3: Chemical structures of N-isopropyl-N-hydroxyethyl dithiocarbamate.	3
Figure 1.4: Chemical structures of xanthate ligands employed in the present study.	6
Figure 1.5: Coordination modes of dithiocarbamate (X= NRR') and xanthate (X= OR).	7
Figure 1.6: Molecular structure of the simplest urotropine, hexamethylenetetramine. ...	8
Figure 1.7: Scheme of crystal engineering and reverse crystal engineering.	10
Figure 2.1: Formation of crystals of needles of 1 and blocks of 2 in ethanol solution. ..	23
Figure 2.2: Asymmetric, molecular structures and molecular packing of 1	26
Figure 2.3: Asymmetric, molecular structures and molecular packing of 2	27
Figure 2.4: A view of the unit cell contents of 2 shown in projection down the a-axis highlighting the stacking of layers.	28
Figure 2.5: Asymmetric, molecular structures and molecular packing of 6 and 7	29
Figure 2.6: Schematic images of the three SI derived from Cd[S ₂ CN(iPr)CH ₂ CH ₂ OH] ₂	31
Figure 2.7: Solvent mediated interconversion between 1 , 2 , 6 , and 7	32
Figure 2.8: Asymmetric, molecular structures and molecular packing of 3	36
Figure 2.9: Proposed cyclisation derived from N-hydroxyethyl, N-isopropyl dithiocarbamate ligand.	37
Figure 2.10: Overlay diagram of the 3-(propan-2-yl)-1,3-oxazolidine-2-thione molecules and view of the unit cell contents of 3	37

Figure 2.11: Asymmetric, molecular structures and molecular packing of 4	38
Figure 2.12: Asymmetric, molecular structures and molecular packing of 5	39
Figure 2.13: View of unit cell content of 5	40
Figure 3.1: Generic chemical structures, resonance structure and chemical structure of xanthate, dithiocarbamate, dithiophosphate and hmta.	42
Figure 3.2: The three different structural motifs adopted by binary cadmium xanthates.	44
Figure 3.3: Asymmetric, and molecular structures of 8	53
Figure 3.4: View of unit cell of 8	54
Figure 3.5: Asymmetric, and molecular structures of 9	55
Figure 3.6: Molecular packing in 9	56
Figure 3.7: Molecular Structure of 10	57
Figure 3.8: Molecular packing in 10	57
Figure 3.9: End-on and side-on views of the CPs in (a) 8 and (b) 9	60
Figure 3.10: Solid-state emission spectra for 8–10	62
Figure 3.11: TGA (red trace) and DTA (blue trace) for (a) 8 , (b) 9 and (c) 10	63
Figure 4.1: Chemical structures of the palladium(II) bis(xanthate)s (11–22) investigated herein.....	67
Figure 4.2: Calculated UV/visible spectrum for bis(O-n-propylxanthato)palladium(II), [Pd(S ₂ COPr) ₂] (13).	70
Figure 4.3: Molecular structure of 18	71
Figure 4.4: Supramolecular aggregation in 11 , 13 , 12 , and 14	73

Figure 4.5: Views of the unit cell contents for bis(O-methylxanthato)palladium(II), [Pd(S ₂ COMe) ₂] (11).....	74
Figure 4.6: Views of the unit cell contents for bis(O-n-propylxanthato)palladium(II), [Pd(S ₂ COPr) ₂] (13).	75
Figure 4.7: View of the unit cell contents for bis(O-ethylxanthato)palladium(II), [Pd(S ₂ COEt) ₂] (12).	77
Figure 4.8: View of the unit cell contents for bis(O-isopropylxanthato)palladium(II), [Pd(S ₂ CO-i-Pr) ₂] (14).....	78
Figure 4.9: Supramolecular aggregation in 19 , 15 , 18 , 16 , and 22	80
Figure 4.10: View of the unit cell contents for bis(O-neopentylxanthato)palladium(II), [Pd(S ₂ CO-neo-Pent) ₂] (19).	81
Figure 4.11: View of the unit cell contents for bis(O-n-butylxanthato)palladium(II), [Pd(S ₂ CO-n-Bu) ₂] (15).....	81
Figure 4.12: Views of the crystal packing in bis(O-n-pentylxanthato)palladium(II), [Pd(S ₂ CO-n-Pent) ₂] (17).	82
Figure 4.13: Views of the crystal packing in bis(O-n-hexylxanthato)palladium(II), [Pd(S ₂ CO-n-Hex) ₂] (20).....	83
Figure 4.14: Views of the crystal packing in bis(O-isohexylxanthato)palladium(II), [Pd(S ₂ CO-i-Hex) ₂] (21).	84
Figure 4.15: View of the crystal packing in bis(O-isopentylxanthato)palladium(II), [Pd(S ₂ CO-i-Pent) ₂] (18).	84
Figure 4.16: View of the crystal packing in bis(O-isobutylxanthato)palladium(II), [Pd(S ₂ CO-i-Bu) ₂] (16).	85
Figure 4.17: View of the crystal packing in bis(O-neohexylxanthato)palladium(II), [Pd(S ₂ CO-neo-Hex) ₂] (22).....	85
Figure 4.18: NCI plots in the molecular packing of 13	87

LIST OF TABLES

Table 2.1: Crystal data and refinement details for 1–5	25
Table 3.1: Crystal data, data collection and refinement parameters for compounds 8–10	51
Table 3.2: UV-visible (λ_{max} , nm; ϵ , Lcm ⁻¹ mol ⁻¹) and photoluminescence data (λ , nm; λ_{ex} = 295 and 360 nm) for Cd(S ₂ COR) ₂ , R = Me, Et and iPr, and 8–10	61

University of Malaya

LIST OF SYMBOLS AND ABBREVIATIONS

CCDC	Cambridge Crystallographic Database Centre
CE	Crystal Engineering
CP	Coordination Polymer
CSD	Cambridge Structural Database
FT-IR	Fourier Transform Infrared
Hmta	Hexamethylenetetramine
MOFs	Metal-Organic Frameworks
NCI	Non-Covalent Interaction
NMR	Nuclear Magnetic Resonance
PXRD	Powder X-Ray Diffraction
RCE	Retrospective Crystal Engineering
SCSC	Single Crystal to Single Crystal Transformation
SCXRD	Single-Crystal X-Ray Diffraction
SI	Supramolecular Isomer
TGA	Thermogravimetric Analysis
UV-Vis	Ultraviolet- Visible

LIST OF COMPOUNDS

- 1 $[\{ \text{Cd}[\text{S}_2\text{CN}(\text{iPr})\text{CH}_2\text{CH}_2\text{OH}]_2 \} . \text{EtOH}]_\infty$
- 2 $\{ \text{Cd}[\text{S}_2\text{CN}(\text{iPr})\text{CH}_2\text{CH}_2\text{OH}]_2 \}_2 . 2\text{EtOH}$
- 3 $\{ \text{Cd}[\text{S}_2\text{CN}(\text{iPr})\text{CH}_2\text{CH}_2\text{OH}]_2 \}_2 : 2[3\text{-(propan-2-yl)-1,3-oxazolidin-2-thione}]$
- 4 $[\text{iPrNH}_2(\text{CH}_2\text{CH}_2\text{OH})]_4[\text{SO}_4]_2 \{ \text{Cd}[\text{S}_2\text{CN}(\text{iPr})\text{CH}_2\text{CH}_2\text{OH}]_2 \}_2$
- 5 $[\text{iPrNH}_2(\text{CH}_2\text{CH}_2\text{OH})] \{ \text{Cd}[\text{S}_2\text{CN}(\text{iPr})\text{CH}_2\text{CH}_2\text{OH}]_3 \}$
- 6 $[\{ \text{Cd}[\text{S}_2\text{CN}(\text{iPr})\text{CH}_2\text{CH}_2\text{OH}]_2 \}_3 . \text{MeCN}]_\infty$
- 7 $\{ \text{Cd}[\text{S}_2\text{CN}(\text{iPr})\text{CH}_2\text{CH}_2\text{OH}]_2 \}_2 . 2\text{H}_2\text{O} . 2\text{MeCN}$
- 8 $[\text{Cd}(\text{S}_2\text{COMe})_2 . \text{hmta}]_\infty$
- 9 $\{ [\text{Cd}(\text{S}_2\text{COEt})_2]_2 . \text{hmta} \}_\infty$
- 10 $[\text{Cd}(\text{S}_2\text{COi-Pr})_2] . \text{hmta} \}_\infty$
- 11 $[\text{Pd}(\text{S}_2\text{COMe})_2]$
- 12 $[\text{Pd}(\text{S}_2\text{COEt})_2]$
- 13 $[\text{Pd}(\text{S}_2\text{CO-n-Pr})_2]$
- 14 $[\text{Pd}(\text{S}_2\text{CO-i-Pr})_2]$
- 15 $[\text{Pd}(\text{S}_2\text{CO-n-Bu})_2]$
- 16 $[\text{Pd}(\text{S}_2\text{CO-i-Bu})_2]$
- 17 $[\text{Pd}(\text{S}_2\text{CO-n-Pent})_2]$
- 18 $[\text{Pd}(\text{S}_2\text{CO-i-Pent})_2]$
- 19 $[\text{Pd}(\text{S}_2\text{CO-neo-Pent})_2]$
- 20 $[\text{Pd}(\text{S}_2\text{CO-n-Hx})_2]$
- 21 $[\text{Pd}(\text{S}_2\text{CO-i-Hx})_2]$
- 22 $[\text{Pd}(\text{S}_2\text{CO-neo-Hx})_2]$

LIST OF APPENDICES

APPENDIX A	129
APPENDIX B	130
APPENDIX C	131
APPENDIX D	132
APPENDIX E	133
APPENDIX F	134
APPENDIX G	135
APPENDIX H	136
APPENDIX I	138
APPENDIX J	139
APPENDIX K	140
APPENDIX L	141
APPENDIX M	153
APPENDIX N	156
APPENDIX O	157

CHAPTER 1: INTRODUCTION & LITERATURE REVIEW

1.1. 1,1'- Dithiolate Coordination Compounds

A coordination compound can also be named as a metal complex, and comprises two components namely, the metal centre and ligand(s) (Garnovskii *et al.*, 2009). The compound is formed *via* chemical bonding between the metal and ligand, which can be termed as coordination bond or dative bond (Fiorillo *et al.*, 2004). A 1,1'- Dithiolate coordination compound is obtained from the coordination of 1,1'- dithiolate ligand to the metal centre using the ligating sulphur atoms available.

1.1.1. 1,1'- Dithiolate Ligands

The use of thiolate ligand is prevalent in coordination chemistry. Thiolate ligand can be further categorised into mono- and di-thiolate ligand based on the number of the sulphur atom(s) available for coordination. Mono thiolate ligand provides only one sulphur atom in the molecule for interaction with metal centre, with the most common examples being mercapto (HS-R) and thioamide (ROC(=S)NHR') as illustrated in Figure 1.1.

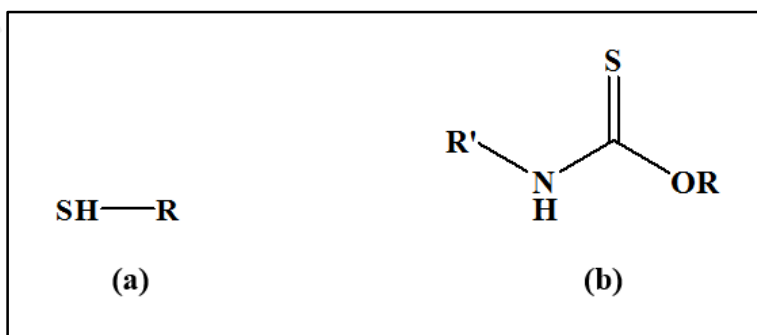


Figure 1.1: Generic structures of mono-thiolate.

(a) Mercapto and (b) thioamide ligand with R, R' = alkyl and/or aryl.

1,1'-Dithiolate ligand offers fascinating chemistry with the presence of two sulphur atoms that could act as the ligating atoms in the molecule. There are four main

types of 1,1'- dithiolate ligand reported in the literature, including dithiocarbamate (S_2CNR_2), xanthate (S_2COR), dithiophosphate [$\text{S}_2\text{P(OR)}_2$], and dithiophosphinate (S_2PR_2) (Figure 1.2). Dithiocarbamate and xanthate form the main focus of this dissertation, and the crystal engineering and respective application studies of their coordination compounds are reported herein.

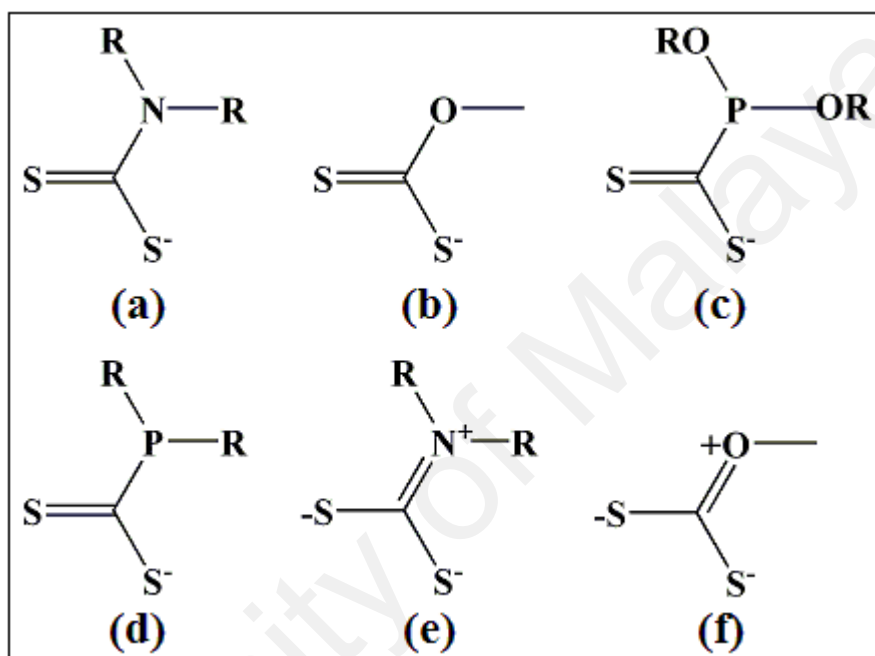


Figure 1.2: Generic chemical structures and resonance structure of 1,1'-dithiolate ligands.

(a) Dithiocarbamate, (b) xanthate, (c) dithiophosphate, (d) dithiophosphinate. (e) resonance dithiocarbamate anion, and (f) resonance xanthate anion. R, R' = alkyl and/or aryl.

1.1.1.1. Dithiocarbamate

Dithiocarbamate, with general formula of $\text{S}_2\text{CNRR}'$ in which R and R' can be identical or different, is obtained by the insertion of carbon disulphide, CS_2 , to non-tertiary amine where the formation of a covalent bond between the carbon from CS_2 and the nitrogen atom from amine is observed. The ligand commonly exists as milky white, pale yellow, yellowish, or light orange solid with an unpleasant smell. Synthesis of

dithiocarbamate has been well documented (Aly *et al.*, 2012; Nabipour *et al.*, 2010). Owing to its common application as flocculent, pesticide and *etc.*, some of the dithiocarbamates are commercially available such as sodium dimethyldithiocarbamate hydrate (CAS: 207233-95-2), and sodium diethyldithiocarbamate trihydrate (CAS: 20624-25-3), to name a few. Only the *N*-isopropyl-*N*-hydroxyethyl dithiocarbamate as depicted in Figure 1.3 being focused and applied in obtaining coordination compounds.

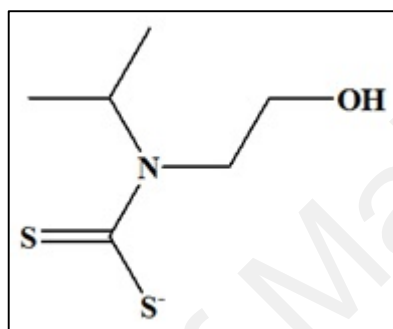


Figure 1.3: Chemical structure of *N*-isopropyl-*N*-hydroxyethyl dithiocarbamate.

1.1.1.2. Xanthate

Xanthate, with general formula of S_2COR , commonly appears as pale yellow solid with disagreeable smell. As presented in Figure 1.4, xanthate has only one R group attached to the oxygen atom and hence, the manipulation of this molecule in the realm of crystal engineering is comparably easier than the other 1,1'-dithiolate ligands having two R groups, *e.g.* dithiocarbamate, dithiophosphate and dithiophosphinate. In most cases, when R group comprises of hydrocarbon chain, it is predicted to have a zig-zag conformation and to be co-planar with the -CS_2 moiety. The synthetic procedure of xanthate occurs as a single step reaction where the CS_2 is inserted to a de-protonated alcohol (Zohir *et al.*, 2009). Similar to the dithiocarbamate, some xanthates can be sourced commercially, including potassium *O*-isopropyl xanthate (CAS: 140-92-1), potassium *O*-n-hexyl xanthate (CAS: 2720-76-5), and *etc.* There are a total of 12

xanthates employed in present study, with R group ranging from one to six carbon(s) number and the chain is ended with primary, secondary or tertiary hydrocarbon. Chapter 4 elucidates the influence exerted on the respective coordination compounds interactions by varying the R group of xanthate ligands.

1.1.2. Coordination Chemistry of 1, 1'-Dithiolate Ligand

1, 1'-Dithiolate ligand presents remarkable coordination chemistry (Mensforth *et al.*, 2013) owing to the various coordination modes exhibited by the molecules. Dithiocarbamate and xanthate display a wide range of denticity from as low as monodentate up to tetradentate upon their complexation to metal cation.

Searches on Cambridge Structural Database (CSD) reveal that dithiolate ligands generally favour coordination mode of form I as depicted in Figure 1.5 for each of the monodentate (Arman *et al.*, 2012; Drake *et al.*, 1992; Javed *et al.*, 2013; Mohamed-Ibrahim *et al.*, 2000; Tiekink, 2001; Yang Farina *et al.*, 2000), bidentate (Chan *et al.*, 2004; Cox, 1999; Decken *et al.*, 2004; Ewings *et al.*, 1976), tridentate (Duhme *et al.*, 1990; Malik *et al.*, 1996; Tiekink, 1988; van Poppel, Groy, & Tyler Caudle, 2004), and tetradentate (Duhme *et al.*, 1990; Malik *et al.*, 1996; Tiekink, 1988; van Poppel, Groy, & Tyler Caudle, 2004).

1.2. Coordination Polymer Chemistry

Coordination polymer (CP) defines one of the prominent fields under coordination chemistry; it is generally regarded as self-assembly of monomer through the coordination active sites in a growing macromolecule (Biradha *et al.*, 2009; Leong *et al.*, 2011). Differing from molecular coordination compounds, which intermolecular forces are mainly secondary interactions, CP is a polymeric array of coordination compound with coordination bonded ligand bridges metal centres and each of the metal centre is

coordinated with more than one ligand. CP can be extended to one-, two- or three-dimension by repeating the building block (Batten *et al.*, 2012).

1.2.1. 1,1'-Dithiolate Coordination Polymer

Repetition of 1,1'-dithiolate coordination compound through the formation of repeating bridging coordination bond between monomers is termed as 1,1'-dithiolate CP. 1,1'-Dithiolate compounds provide promising ability to form CP of one- (Okubo, Kuwamoto, *et al.*, 2011; Tiekink, 1987, 1988; Young Jr *et al.*, 2002), two- (Cox *et al.*, 1999; Ikeda *et al.*, 1966; Okubo *et al.*, 2013; Rietveld *et al.*, 1965) and three- (Okubo, Tanaka, *et al.*, 2011) dimensional through self-assembly.

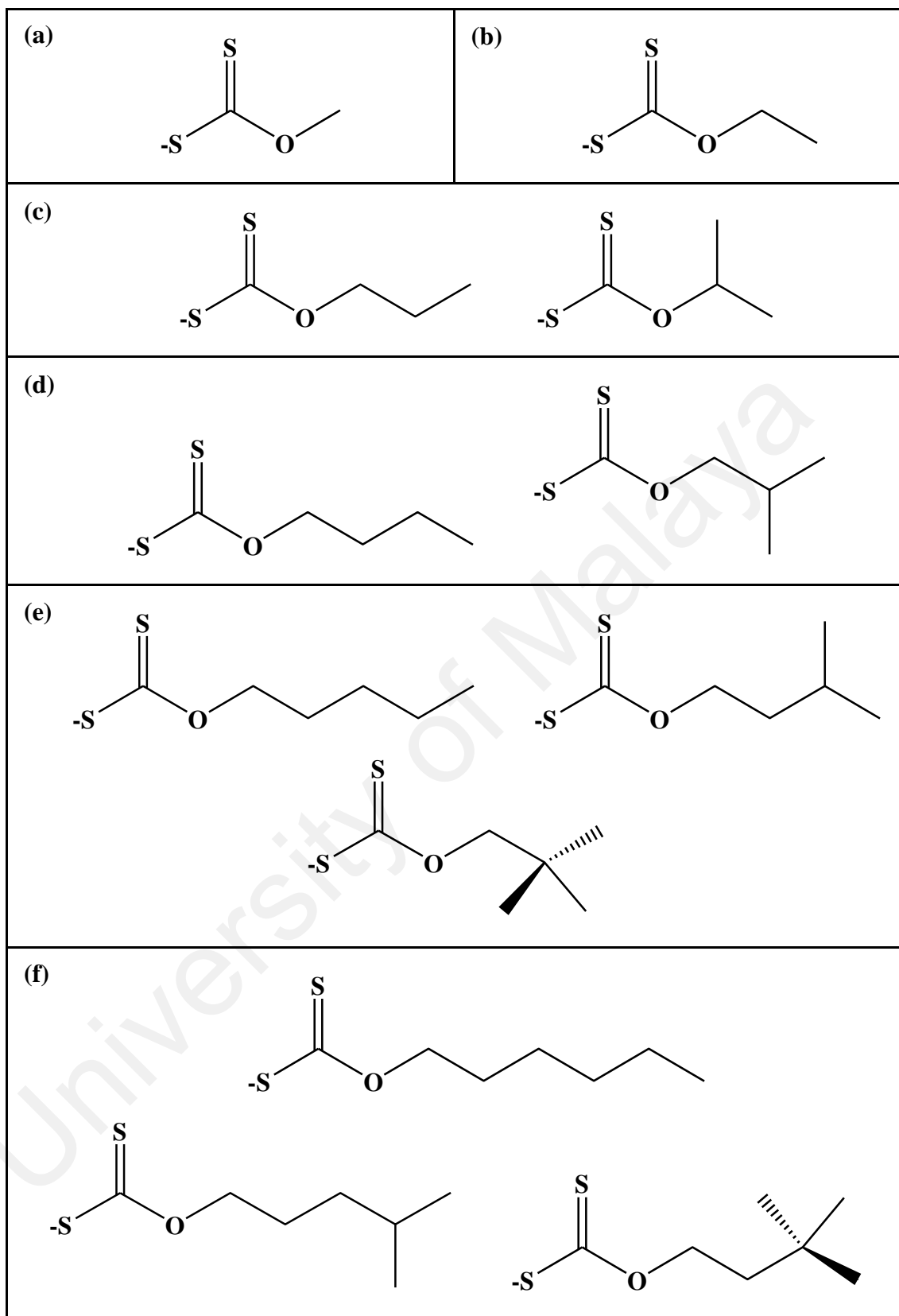


Figure 1.4: Chemical structures of xanthate ligands employed in the present study.

R group with (a) one carbon, (b) two carbons, (c) three carbons, (d) four carbons, (e) five carbons, and (f) six carbons.

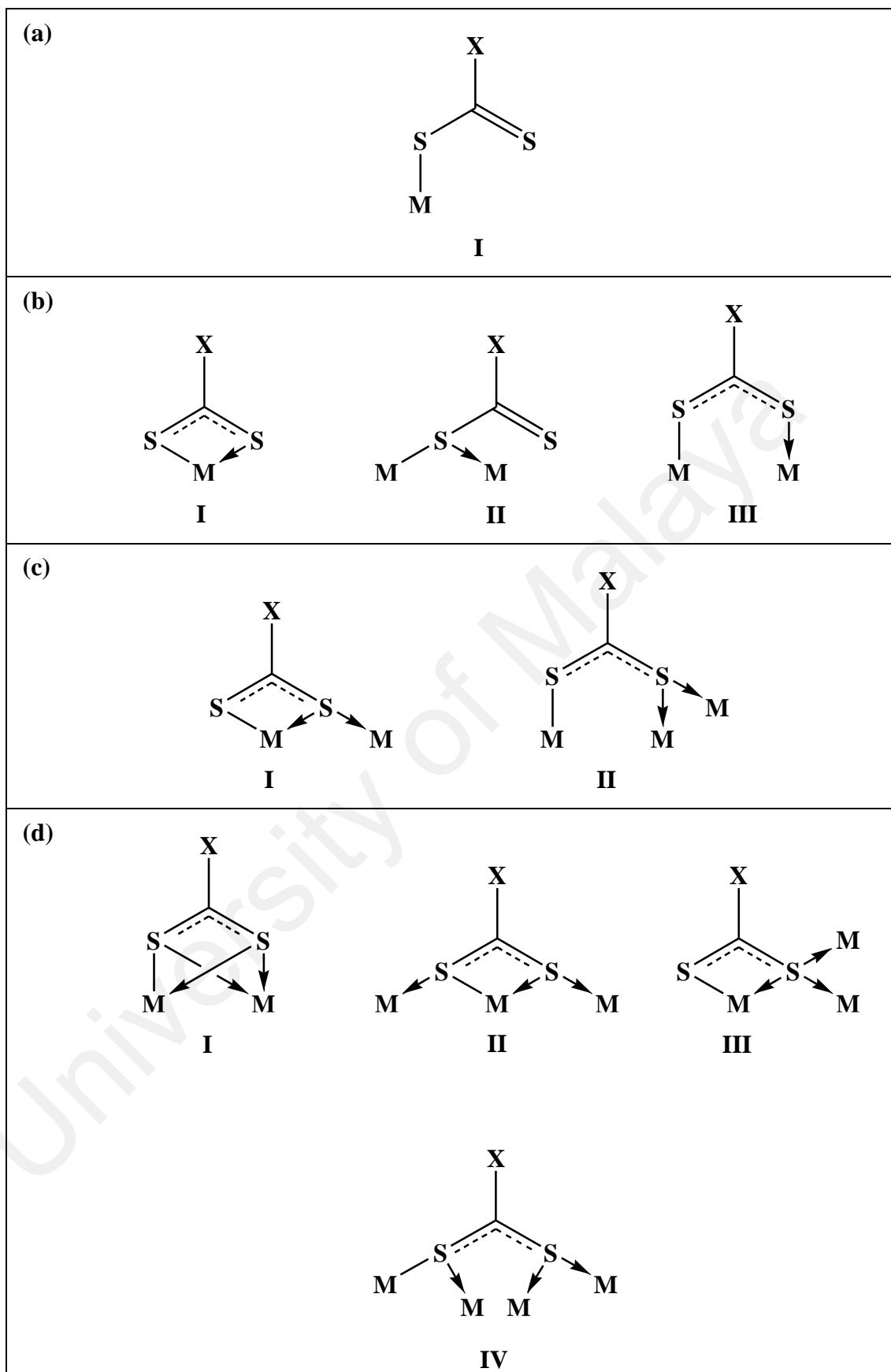


Figure 1.5: Coordination modes of dithiocarbamate ($X = \text{NRR}'$) and xanthate ($X = \text{OR}$).

(a) Monodentate, (b) bidentate, (c) tridentate and (d) tetradentate.

1.2.2. Coordination Mode of Multidentate Linker for Coordination Polymer

Self-assembly of coordination compound monomers through coordination bonding leads to the formation of CP, this is however not the only route to achieve the above. Alternatively, incorporation of linkers also affords coordination polymer formation. Generally, linker is a type of multidentate ligand with the ability to bridge coordination compounds and further leads to polymeric motif. Amongst these, bipyridine-type molecules being the most prominent example of linker (Avila *et al.*, 2006; Chai *et al.*, 2003; Kang *et al.*, 2010). Despite a linker may present more than one potential ligating atom, it is however not necessary for all of the ligating atoms to be involved in coordination (Broker *et al.*, 2011; Konarev *et al.*, 2008). The reasons contributing to the above may include the saturation of metal centre coordination number and steric effect attributed to electron rich moiety such as metalloaromatic ring.

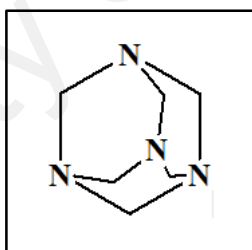


Figure 1.6: Molecular structure of the simplest urotropine, hexamethylenetetramine.

Hexamethylenetetramine, abbreviated as hmta, is employed in the present study for its application in coordination polymer formation. This molecule comprises four potential ligating nitrogen atoms and thus it is highly predicted to assume tetradentate coordination mode. Unpredictably, this remarkable molecule returns only one hit in CSD database where it defines a monodentate coordination mode towards cadmium dithiophosphate (Konarev *et al.*, 2008). Detailed discussion on the various coordination modes exhibited by hmta in cadmium 1,1'-dithiolates is presented in Chapter 3.

1.3. Crystal Engineering

Crystal engineering (CE) refers to the knowledge applied in design, synthesis and crystal growth to obtain new solid state structures with the desired properties. It is essential to study the interactions leading to crystal packing, as the understanding of the above is vital in the design of novel compounds (Desiraju, 1989). Initially, CE is aimed for structural design of synthetic compounds. In recent years, application of CE is however shifted to properties design *e.g.* manipulation of compounds physical and chemical properties (Desiraju, 2001; Moulton *et al.*, 2001).

The utilisation of CE in cocrystallisation offers significant implication from pharmaceutical aspect. Bioavailability and therapeutic effect of a compound can be enhanced by fine-tuning its solubility by employing appropriate cocrystal former (Smith, Kavuru, *et al.*, 2013; Smith, Kim, *et al.*, 2013). Practicing CE in material science such as CP or metal-organic frameworks (MOFs) also gives rise to material with intended properties such as gas storage, gas separation, catalysis and *etc.* (Nugent *et al.*, 2013).

1.3.1. Retrospective Crystal Engineering

Despite researchers generally apply CE to design expected interactions, bonding formation between atoms and molecules are sometimes unpredictable. Under certain circumstances, crystals form by serendipity, retrospective crystal engineering (RCE) comes in later for the investigation of interactions involved. Figure 1.7 shows a simplified scheme correlating the relationship of chemical interactions and crystal formation. Contrary to CE, RCE identifies and study the interactions that present in a crystal system. With the thorough understanding of underlying interactions, this aids in designing respective interactions in similar compound. RCE is practiced when a synthetic strategy ‘reticular synthesis’ is developed upon diligent study of similar compounds (Yaghi *et al.*, 2003). Similarly, RCE is applied in present study to delineate factors and interactions leading to crystal formation as discussed in Chapter 2 and 3.

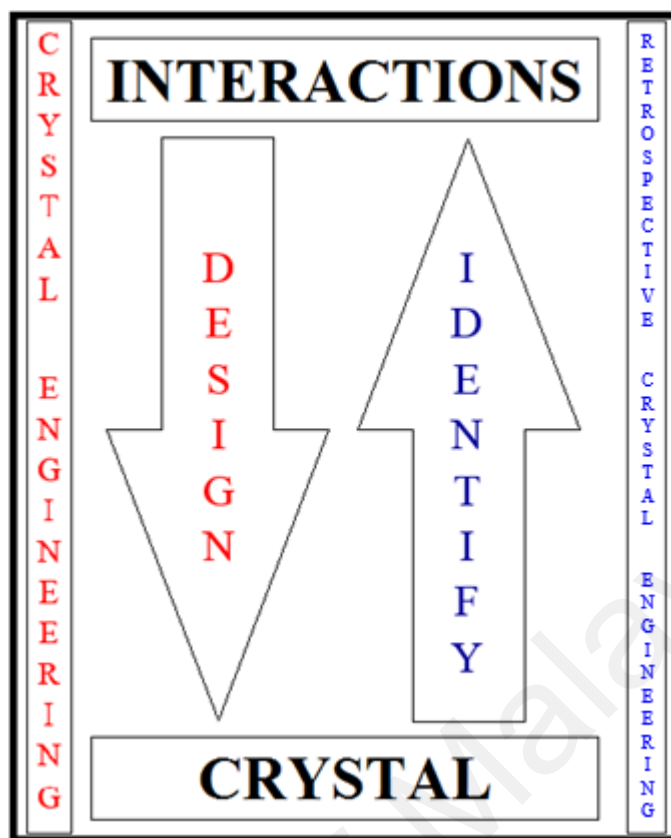


Figure 1.7: Scheme of crystal engineering and reverse crystal engineering.

1.3.2. Crystal Engineering for Secondary Interaction

Study of C–H to metalloaromatic ring, particularly C–H $\cdots\pi$ (MS₂C) was initiated by Tiekink and co-worker (Tiekink *et al.*, 2011); this provides a guideline for categorisation of related interaction. Chapter 4 detailed a thorough study evaluating the propensity of C–H to interact with metalloaromatic ring in a series of palladium xanthate. The selection of palladium(II) as the metal centre and xanthate as the ligand is based upon the CE concept to design a molecule with desired interactions. Palladium is generally tetra-coordinate in a square planar geometry and this is termed as molecular square (Stang *et al.*, 1997). Xanthate on the other hand consists of only one R group, this reduces molecular bulkiness and possible induce steric effects. With the planarity on palladium coordination compound and structural simplicity of xanthate ligand, this permits appreciable space for ease of approach of C–H to attain C–H $\cdots\pi$ (MS₂C) interactions.

1.4. Miscellaneous Studies

In addition to the discussion above, other factors are taken into consideration in investigation of compounds synthesised. This includes synthesis methodology, polymorphism, and single crystal to single crystal transformation which will be discussed in the following sections.

1.4.1. Crystallisation

Crystal structures are indispensable for in depth understanding of CE. It is however requiring effort to obtain good quality of crystals and hence, various crystallisation techniques are developed including conventional slow evaporation (Mishra *et al.*, 2014; Upreti *et al.*, 2011), solvent-solvent diffusion (Hwang *et al.*, 2013), vapour-solvent diffusion (Kimble *et al.*, 1995), solvent mixture system (Gangavaram *et al.*, 2012; Srinivasan *et al.*, 2009), solvo/hydrothermal (Luo *et al.*, 2013), temperature gradient (Akhbari *et al.*, 2013), and gel diffusion (Prasanna *et al.*, 2011), to name a few.

The most widely employed crystallisation technique is no doubt slow evaporation. Samples are dissolve in solvent and left for evaporation until supersaturation is achieved that further allows crystal nucleation. When different solvent system is employed, diverse crystal packing systems may be attained, this phenomenon is known as polymorphism.

1.4.1.1. Polymorphism

Remarkably, different crystal systems could be achieved by a compound through the fine-tuning of parameters for crystal growing. For instance, manipulating the solvent system for slow evaporation and/or controlling the working temperature for solvo/hydrothermal crystallisation. Despite out of the same compound, different solvent systems may give rise to a numbers of morphisms: polymorphism, solvomorphism (pseudo-polymorph) and supramolecular isomerism.

Polymorphism generally refers to multiple crystal systems for a molecule (López-Mejías *et al.*, 2012). When the same molecule gives rise to different crystal systems with solvate or guest molecule co-existing, solvomorphism is denoted (Nangia *et al.*, 1999). Supramolecular isomer (SI) on the other hand applies when different connectivity or interaction arise from various coordination modes and/or geometries for a coordination compound, with empirical formula for the coordination framework remains (Moulton *et al.*, 2001). In this case, guest molecules or solvates are not being concerned. Genuine SI specifically applies for isomers which are identical in molecular formula (Dobrzańska, 2015; Zhang *et al.*, 2009).

1.4.1.2. Single Crystal to Single Crystal Transformation

Single crystal to single crystal transformation (SCSC) is a phenomena where the atoms or molecules inside the crystal undergo rearrangement, but retain the crystallinity. The phenomena may being induced with the presence of external stimulations such as temperature (Zhang *et al.*, 2005), light irradiation (Park *et al.*, 2014), desolvation/solvation (Kaneko *et al.*, 2007) *etc.* The stabilisation energy involved in the molecular packing could act as a factor that mediated the transformation (Zhang *et al.*, 2014). This is especially applicable in the cases where transformation occurs despite the environment condition for a given crystal remain the same conditions and without additional stimulation. Other than providing opportunities for fundamental study of crystallography, crystal transformation also places impact on applied science such as gas storage (Tanaka *et al.*, 2008).

1.5. Aims of study

1,1'-Dithiolate coordination compounds were prepared to study crystal engineering which is the core focus of this postgraduate program. Three research projects were developed to evaluate CE from various perspective angles. One of them includes adopting polymorphs and method to attain variable crystal systems in cadmium dithiocarbamates. Secondly, to explore characteristic coordination modes of hmta towards cadmium xanthate. Denticity of hmta will be evaluated by its complexation with three cadmium xanthate precursors. Next, to incorporate and/or design C-H \cdots π (MS₂C) in respective 1,1'-dithiolate coordination compounds through a thoughtful selection of metal centre and ligand. The compounds prepared will be characterised and evaluated using various spectroscopic techniques and material analysis, such as FT-IR, UV-Vis, PI, NMR, SCXRD, PXRD, TGA, DSC, and CHN elemental analysis.

CHAPTER 2: REVERSIBLE, SOLVENT MEDIATED SUPRAMOLECULAR ISOMERISM IN A CADMIUM BIS(*N*-HYDROXYETHYL, *N*-ISOPROPYLDITHIOCARBAMATE) COMPOUND, $\text{Cd}[\text{S}_2\text{CN}(\text{iPr})\text{CH}_2\text{CH}_2\text{OH}]_2$, AND UNEXPECTED CRYSTALLISATION OUTCOMES

2.1. Introduction and Literature Review

Contemporary applications, *e.g.*, medicinal (Hogarth, 2012) and as single source precursors for nanoparticle generation of chalcogenides (Afzaal *et al.*, 2010), complement well established uses, *e.g.*, as lubricants, in the vulcanization of rubber, as flotation agents, *etc.* (Coucouvani, 2007; van Zyl *et al.*, 2013; Winter, 1980) of metal 1,1'-dithiolates containing ligands such as dithiocarbamate (S_2CNR_2), xanthate (S_2COR), and dithiophosphate [$\text{S}_2\text{P}(\text{OR})_2$]. Therefore it is not surprising that a vast amount of structural data for this class of compound exists as summarized in bibliographic reviews (Cookson *et al.*, 2007; Haiduc *et al.*, 1996; Heard, 2005; Hogarth, 2005; Tiekink *et al.*, 2005). An enormous range of structures have been characterized, ranging from zero- to three-dimensional architectures, and their adoption often rationalized in terms of the role of steric bulk of the remote substituents in mitigating secondary $\text{M}\cdots\text{S}$ interactions (Alcock, 1972), offering a new paradigm in the design of supramolecular assembly (Lai *et al.*, 2002; Lai *et al.*, 2003; Tiekink, 2003, 2006). In the context of the present study the structural diversity of these systems is very well illustrated in the binary cadmium xanthates, $\text{Cd}(\text{S}_2\text{COR})_2$, where zero- (mononuclear) (Abrahams *et al.*, 1988), one- (Young Jr *et al.*, 2002) and two-dimensional (Iimura, 1973; Iimura *et al.*, 1972; Jiang *et al.*, 2002; Rietveld *et al.*, 1965; Tiekink, 2000; Tomlin *et al.*, 1999) aggregation patterns are observed depending on the bridging propensity of the xanthate ligands. For the cadmium dithiophosphates both zero- (binuclear) (Casas *et al.*, 1995; Ivanov *et al.*, 2007; Lawton *et al.*, 1969) and one-dimensional (Ito *et al.*, 1996; Al. V. Ivanov *et al.*, 2005; Yin *et al.*, 2003) aggregation is found. By contrast to this diversity the structural chemistry of cadmium dithiocarbamates is remarkably less varied. In the almost 50 years since the

original report of the crystal structure of binuclear $[\text{Cd}(\text{S}_2\text{CNEt}_2)_2]_2$ (Domenicano *et al.*, 1968), a large number of related dialkyl species have been described as having the same binuclear structural motif, *i.e.*, with two each of κ^2 -chelating and $\mu_2\kappa^2$ -tridentate dithiocarbamate ligands leading to penta coordinate geometries, regardless of whether the R groups were the same (Casas *et al.*, 1989; Cox *et al.*, 1999; Dee *et al.*, 2002; Domenicano *et al.*, 1968; Glinskaya *et al.*, 1999; A. V. Ivanov *et al.*, 2005; Ivanov *et al.*, 2008; F.-F. Jian *et al.*, 1999; F. Jian *et al.*, 1999; Konarev *et al.*, 2006; Saravanan *et al.*, 2004; Yin *et al.*, 2004; Zhong *et al.*, 2004), dissimilar (Cox *et al.*, 1999; Kant *et al.*, 2012), incorporated within a cyclic system (Ivanov *et al.*, 2006; Manohar *et al.*, 2005; Thirumaran *et al.*, 2012), or whether the compound was cocrystallized with another species (Cox *et al.*, 1999; Konarev *et al.*, 2006; Manohar *et al.*, 2005), or that the R group carried additional potential oxygen donor atoms (Kant *et al.*, 2012; Zhong *et al.*, 2004). This situation changed in 2013 with the report of a CP, $[\{\text{Cd}[\text{S}_2\text{CN}(\text{iPr})\text{CH}_2\text{CH}_2\text{OH}]_2\}_3 \cdot \text{MeCN}]_\infty$ (**PUBLICATION 1**). Further diversity was described in 2014 with the report of a centrosymmetric trinuclear species having an octahedrally coordinated cadmium centre flanked by two square pyramidal centres (Kumar *et al.*, 2014). For completeness it is noted that $\{\text{Cd}[\text{S}_2\text{CN}(\text{H})\text{R}]_2\}_\infty$ R = *n*-C₅H₁₁ and *n*-C₁₂H₂₅, are linear CPs with octahedrally coordinated cadmium atoms (van Poppel, Groy, & Caudle, 2004).

The linear polymeric $[\{\text{Cd}[\text{S}_2\text{CN}(\text{iPr})\text{CH}_2\text{CH}_2\text{OH}]_2\}_3 \cdot \text{MeCN}]_\infty$ structure was of particular interest as when it was allowed to stand in the mother liquor over a period of several days it transformed to $\{\text{Cd}[\text{S}_2\text{CN}(\text{iPr})\text{CH}_2\text{CH}_2\text{OH}]_2\}_2 \cdot 2\text{H}_2\text{O} \cdot 2\text{MeCN}$ which has the normally adopted binuclear motif. The conversion from the polymer to dimeric form was reported to be mediated by adventitious water (**PUBLICATION 1**). These two species are examples of SI being supramolecular variants of the basic building block $\text{Cd}[\text{S}_2\text{CN}(\text{iPr})\text{CH}_2\text{CH}_2\text{OH}]_2$. SI originally referred to the phenomenon whereby distinct

supramolecular arrangements are constructed from the same building blocks (Moulton *et al.*, 2001). While this definition allowed for the presence of additional species such as solvent, a more recent definition refers to “genuine SI” where the molecular formula of each isomer is identical (Zhang *et al.*, 2009); for a recent discussion on SI terminology see (Dobrzańska, 2015). The terms polymorphism/pseudo polymorphism for the above species are excluded as the nature of the Cd–S bonding is quite distinct in the two structures. Several factors are known to influence the formation of SI with the most significant being solvent (Frahm *et al.*, 2014; Han *et al.*, 2015; Li *et al.*, 2011; Li *et al.*, 2015; Manna *et al.*, 2015; Peedikakkal *et al.*, 2011) and temperature (du Plessis *et al.*, 2012; Liu *et al.*, 2012; Nagarkar *et al.*, 2012; Sun *et al.*, 2005; Wang *et al.*, 2011) but other factors such as guest molecules (Meng *et al.*, 2013), concentration of reagents (Hou *et al.*, 2015; Xia *et al.*, 2015), conformation of molecules (Chen *et al.*, 2013), molar ratio of reactants (Lee *et al.*, 2013), and pH of reaction (An *et al.*, 2015; Lago *et al.*, 2013) are also known to lead to SI.

The transformation of $[\{\text{Cd}[\text{S}_2\text{CN}(\text{iPr})\text{CH}_2\text{CH}_2\text{OH}]_2\}_3 \cdot \text{MeCN}]_\infty$ to $\{\text{Cd}[\text{S}_2\text{CN}(\text{iPr})\text{CH}_2\text{CH}_2\text{OH}]_2\}_2 \cdot 2\text{H}_2\text{O} \cdot 2\text{MeCN}$ mentioned above is an example of solvent induced SI (**PUBLICATION 1**). Given the great interest in SI, including recent studies of SI in dithiocarbamates (Poplaukhin *et al.*, 2012; Poplaukhin *et al.*, 2010; Rojas-Leon *et al.*, 2012), it was thought of interest to explore the influence of other solvent systems upon SI in $\text{Cd}[\text{S}_2\text{CN}(\text{iPr})\text{CH}_2\text{CH}_2\text{OH}]_2$. With ethanol as the solvent two new SI, polymeric $[\{\text{Cd}[\text{S}_2\text{CN}(\text{iPr})\text{CH}_2\text{CH}_2\text{OH}]_2\} \cdot \text{EtOH}]_\infty$ (**1**) and binuclear $\{\text{Cd}[\text{S}_2\text{CN}(\text{iPr})\text{CH}_2\text{CH}_2\text{OH}]_2\}_2 \cdot 2\text{EtOH}$ (**2**), were characterized; their interconversion has also been investigated along with their relationships with the original $[\{\text{Cd}[\text{S}_2\text{CN}(\text{iPr})\text{CH}_2\text{CH}_2\text{OH}]_2\}_3 \cdot \text{MeCN}]_\infty$ and $\{\text{Cd}[\text{S}_2\text{CN}(\text{iPr})\text{CH}_2\text{CH}_2\text{OH}]_2\}_2 \cdot 2\text{H}_2\text{O} \cdot 2\text{MeCN}$ SI. From other solvent systems/crystallization conditions a cocrystal (**3**) and a cocrystal salt (**4**), each containing

binuclear $\{\text{Cd}[\text{S}_2\text{CN}(\text{iPr})\text{CH}_2\text{CH}_2\text{OH}]_2\}_2$, and a salt **(5)**, with $\{\text{Cd}[\text{S}_2\text{CN}(\text{iPr})\text{CH}_2\text{CH}_2\text{OH}]_3\}^-$, were also studied crystallographically. The results of this investigation are reported herein.

2.2. Methodology

All chemicals and reagents were used as received without purification: *N*-isopropyl ethanol amine (70% purity; Aldrich), carbon disulfide (99.9% purity; Merck), sodium hydroxide ($\geq 99.0\%$ purity; Merck), CdCl_2 (99.0% purity; Across Organic), $\text{Cd}(\text{acetate})_2 \cdot 2\text{H}_2\text{O}$ (Fluka), d^6 -DMSO (MagniSolv™, Merck), and Emsure® ethanol, acetone, chloroform, hydrochloric acid (37%), and acetonitrile (Merck). Acetonitrile and ethanol used in the solvent mediated transformation experiments were dried over molecular sieve 3 Å (Merck). For the gel experiments, sodium silicate hexahydrate (99.0% purity; R&M Chemicals) was employed.

Melting points were determined on a Krüss KSP1N melting point meter. Elemental analyses were performed on a Perkin Elmer PE 2400 CHN Elemental Analyser. ^1H and $^{13}\text{C}\{^1\text{H}\}$ NMR spectra were recorded in d^6 -DMSO solution on a Bruker Avance 400 MHz NMR spectrometer with chemical shifts relative to tetramethylsilane as internal reference; abbreviations for NMR assignments: *s*, singlet; *d*, doublet; *t*, triplet; *sept*, septet; *m*, multiplet; *dq*, doublet of quartets. The optical absorption spectra were measured in the range 190–1100 nm on an Agilent Cary 60 UV-Vis spectrophotometer. IR spectra were measured on a Perkin Elmer Spectrum 400 FT Mid-IR/Far-IR spectrophotometer from 4000 to 400 cm^{-1} . Thermogravimetric analyses were performed on a Perkin-Elmer TGA 4000 Thermogravimetric Analyser (TGA) in the range of 30 – 900 °C at a rate of 10 °C/min. Powder X-ray diffraction (PXRD) data were recorded with a PANalytical Empyrean XRD system with Cu K α 1 radiation ($\lambda = 1.54056$ Å) in the 2 θ range of 5 to 40° with a step size of 0.026°. Comparison between experimental and calculated (from CIFs) PXRD patterns was performed with X'Pert HighScore Plus

("X'Pert HighScore Plus," 2009). Spectroscopic data are given below. See Results and Discussion for discussion of PXRD and thermal decomposition results.

2.2.1. Synthesis

All reactions were carried out under ambient conditions. The sodium salt of $\text{S}_2\text{CN}(\text{iPr})\text{CH}_2\text{CH}_2\text{OH}$ was prepared by reacting NaOH, *N*-isopropyl ethanol amine and CS_2 as detailed earlier (**PUBLICATION 1**). To prepare the $\text{Cd}[\text{S}_2\text{CN}(\text{iPr})\text{CH}_2\text{CH}_2\text{OH}]_2$ precursor, $\text{Na}[\text{S}_2\text{CN}(\text{iPr})\text{CH}_2\text{CH}_2\text{OH}]$ (5.000 g, 0.0248 mol) and CdCl_2 (2.273 g, 0.0124 mol) were each dissolved in water (50 ml). The CdCl_2 solution was added slowly into the solution containing the dithiocarbamate anion with stirring. A milky white precipitate formed immediately. This was extracted into chloroform (100 ml), a process repeated several times. The chloroform extract was filtered and dried on a hotplate at 80 °C overnight (yield (based on Cd): 4.460 g, 77%). The compound exhibited the same spectroscopic features as reported earlier (**PUBLICATION 1**). This material was used for the generation of each of **1–4**.

Compounds **1** and **2** were obtained by crystallization of the $\text{Cd}[\text{S}_2\text{CN}(\text{iPr})\text{CH}_2\text{CH}_2\text{OH}]_2$ precursor in Emsure[®] ethanol with **1** being the first crystals formed. With time **1** transformed to **2** as detailed below in the Results and Discussion.

To obtain a sufficient quantity of **1** for physiochemical characterization $\text{Cd}[\text{S}_2\text{CN}(\text{iPr})\text{CH}_2\text{CH}_2\text{OH}]_2$ (0.5 g) was dissolved in Emsure[®] ethanol (50 ml). Needles of **1**, with composition $[\{\text{Cd}[\text{S}_2\text{CN}(\text{iPr})\text{CH}_2\text{CH}_2\text{OH}]_2\} \cdot \text{EtOH}]_\infty$ (see later), were harvested after 3 h (yield (based on Cd): 0.3894 g, 78%); M.pt: 152.5-156.1 °C. Elemental analysis: C, 32.43; H, 5.83; N, 5.11. $\text{C}_{14}\text{H}_{30}\text{CdN}_2\text{O}_3\text{S}_4$ requires: C, 32.65; H, 5.87; N, 5.44. IR (cm^{-1}): 1446 m $\nu(\text{C}-\text{N})$, 1162 m, 964 m $\nu(\text{C}-\text{S})$. The full IR spectrum is given in Appendix Aa. ^1H NMR $\{d_6\text{-DMSO}\}$: δ 5.21 (*sept*, CH, 2H, 6.67 Hz), 4.81 (*t*, $\text{CH}_2\text{CH}_2\text{OH}$, 2H, 5.52 Hz), 4.35 (*t*, $\text{CH}_3\text{CH}_2\text{OH}$, 1H, 5.08 Hz), 3.60-3.80 (*m*, $\text{NCH}_2\text{CH}_2\text{O}$, 8H), 3.44 (*dq*, $\text{CH}_3\text{CH}_2\text{OH}$, 2H, $J_q = 6.98$ Hz, $J_d = 5.10$ Hz), 1.17 (*d*, CHCH_3 , 12H, 6.72

Hz), 1.06 (*t*, $\text{CH}_3\text{CH}_2\text{OH}$, 3H, 7.00 Hz) ppm. ^{13}C $\{^1\text{H}\}$ $\{d^6\text{-DMSO}\}$: δ 205.12 (CS_2), 58.09 (OCH_2), 56.46 (NCH_2), 55.92 ($\text{CH}_3\text{CH}_2\text{OH}$), 50.33 (CH), 19.76 (CH_3), 18.45 ($\text{CH}_3\text{CH}_2\text{OH}$) ppm. UV-Vis (EtOH:MeCN 1/1 *v/v*; 10 μM): $\lambda_{\text{max}} = 261 \text{ nm}$ ($\epsilon = 28450 \text{ cm}^{-1} \text{ M}^{-1}$); 283 (17830); 338 (199); the spectrum is given in Appendix B.

Under the same crystallization conditions, blocks of **2** (yield (based on Cd): 0.3392 g, 68%) were harvested after three days with composition $\{\text{Cd}[\text{S}_2\text{CN}(\text{iPr})\text{CH}_2\text{CH}_2\text{OH}]_2\} \cdot 2\text{EtOH}$; M.pt: 149.0-149.5 °C. Elemental analysis: C, 32.30; H, 5.74; N, 5.45. $\text{C}_{28}\text{H}_{60}\text{Cd}_2\text{N}_4\text{O}_6\text{S}_8$ requires: C, 32.65; H, 5.87; N, 5.44. IR (cm^{-1}): 1451 *m* $\nu(\text{C}-\text{N})$, 1160 *m*, 969 *m* $\nu(\text{C}-\text{S})$. The full IR spectrum is given in Appendix Ab. ^1H NMR $\{d_6\text{-DMSO}\}$: δ 5.21 (*sept*, CH, 2H, 6.66Hz), 4.81 (*t*, $\text{CH}_2\text{CH}_2\text{OH}$, 2H, 5.52 Hz), 4.35 (*t*, $\text{CH}_3\text{CH}_2\text{OH}$, 1H, 5.08 Hz), 3.60-3.80 (*m*, $\text{NCH}_2\text{CH}_2\text{O}$, 8H), 3.44 (*dq*, $\text{CH}_3\text{CH}_2\text{OH}$, 2H, $J_q = 6.69 \text{ Hz}$, $J_d = 5.08 \text{ Hz}$), 1.17 (*d*, CHCH_3 , 12H, 6.72 Hz), 1.06 (*t*, $\text{CH}_3\text{CH}_2\text{OH}$, 3H, 7.00 Hz) ppm. ^{13}C $\{^1\text{H}\}$ $\{d^6\text{-DMSO}\}$: δ 205.11 (CS_2), 58.09 (OCH_2), 56.46 (NCH_2), 55.92 ($\text{CH}_3\text{CH}_2\text{OH}$), 50.32 (CH), 19.76 (CH_3), 18.45 ($\text{CH}_3\text{CH}_2\text{OH}$) ppm. UV-Vis (EtOH:MeCN 1/1 *v/v*; 10 μM): $\lambda_{\text{max}} = 261 \text{ nm}$ ($\epsilon = 30200 \text{ cm}^{-1} \text{ M}^{-1}$); 283 (18860); 340 (213); the spectrum is given in Appendix B.

Crystals of **3**, characterized crystallographically as a 1:2 cocrystal comprising $\{\text{Cd}[\text{S}_2\text{CN}(\text{iPr})\text{CH}_2\text{CH}_2\text{OH}]_2\} \cdot 2[3\text{-(propan-2-yl)-1,3-oxazolidine-2-thione}]$, were obtained by slow evaporation of a portion of one the chloroform solutions (100 ml) used for the extraction of the $\text{Cd}[\text{S}_2\text{CN}(\text{iPr})\text{CH}_2\text{CH}_2\text{OH}]_2$ precursor.

Crystals of **4** were obtained by dissolving $\text{Cd}[\text{S}_2\text{CN}(\text{iPr})\text{CH}_2\text{CH}_2\text{OH}]_2$ (0.5 g) in acetone (100 ml). The solution was stirred at 50 °C for 1 h. After filtration the solution was kept under ambient conditions which yielded a small number of crystals after 2 days. These were formulated on the basis of X-ray crystallography as the salt cocrystal $[\text{iPrNH}_2(\text{CH}_2\text{CH}_2\text{OH})]_2[\text{SO}_4]\{\text{Cd}[\text{S}_2\text{CN}(\text{iPr})\text{CH}_2\text{CH}_2\text{OH}]_2\} \cdot 2$.

Crystals of **5** were isolated from a crystallization experiment in a sodium silicate gel. Cd(acetate)₂·2H₂O (0.5683 g, 2.13 mmol) was dissolved in a sodium silicate gel solution (35 ml of 1.03 g ml⁻¹). The pH of the solution was adjusted to 6.0-7.0 by 5M hydrochloric acid. The gel solution was transferred to an 80 ml test tube and allowed to stand overnight. Na[S₂CN(iPr)CH₂CH₂OH] (0.8584 g, 4.26 mmol) dissolved in water (35 ml) was carefully layered on top of the gel. A small number of crystals formed after 1 month. These were formulated as the salt [iPrNH₂(CH₂CH₂OH)][Cd[S₂CN(iPr)CH₂CH₂OH]₃] by X-ray crystallography.

As only a matter of a few crystals were obtained for each of **3–5** there was insufficient sample for additional physiochemical characterization.

The detail of crystallisation of **6** and **7** refer to Publication 1.

2.2.2. X-ray crystallography

Single crystal X-ray diffraction data for colourless **1** (0.06 x 0.08 x 0.12 mm; cut from a needle), **2** (0.15 x 0.20 x 0.25 mm) and **3** (0.13 x 0.20 x 0.20 mm) were measured on a Bruker SMART APEX CCD diffractometer. Data for colourless **4** (0.05 x 0.10 x 0.20 mm) and yellow **5** (0.20 x 0.25 x 0.30 mm) were measured on an Agilent Technologies SuperNova Dual diffractometer fitted with an Atlas (Mo) detector. Data collections were measured at 100 K and employed Mo K α radiation ($\lambda = 0.71073$ Å) to θ_{max} of 27.5°. A multi-scan absorption correction was applied in each case ("CrysAlisPro," 2014; Sheldrick, 1996). The structures were solved by direct methods (SHELXS97) (Sheldrick, 2008) and refined (anisotropic displacement parameters (ADP), C-bound H atoms in the riding model approximation and a weighting scheme of the form $w = 1/[\sigma^2(F_o^2) + aP^2 + bP]$ where $P = (F_o^2 + 2F_c^2)/3$) with SHELXL2014 on F^2 (Sheldrick, 2015). The O-bound H atoms were located from difference maps and generally included in the refinement with O–H = 0.84±0.01 Å. When present N-bound H atoms were refined with N–H = 0.91±0.01 Å. Crystal data and refinement details are collected in Table 2.1.

Several of the refinements were non-trivial. In **1** the methylene group of the ethanol molecule was statistically disordered. The ADP for both components of the disorder were constrained to be equal and along with the terminal methyl group to be approximately isotropic. Further, some soft distance restraints were employed for this molecule *i.e.*, C–O, C–C, and O···C(methyl) were refined with 1.47 ± 0.01 , 1.50 ± 0.01 Å, and 2.45 ± 0.01 Å, respectively. All acidic protons were found to be disordered over two positions in locations consistent with hydrogen bonding to O atoms. In the final refinement O–H bond lengths were fixed in their as located positions *i.e.*, 0.83–0.85 Å. Three reflections *i.e.*, (0 0 2), (–1 0 10), and (–3 0 30), were omitted from the final cycles of refinement owing to poor agreement. Finally, the maximum and minimum residual electron density peaks, Table 2.1, were located 0.75 and 0.72 e Å^{–3} from the Cd1 and Cd2 atoms, respectively. In **2**, both the ethanol- and O1-hydroxyethyl-OH groups were statistically disordered; ADP for the chemically equivalent disordered components were constrained to be equal. For the ethanol molecule both O atoms were connected to the same H atom. For the O1-hydroxyl group only one position was found for the hydroxyl-H atom (assigned full weight) based on anticipated O–H···O hydrogen bonding. Four reflections were omitted from the final refinement of **3** *i.e.*, (–6 –5 1), (12 –1 1), (–6 –5 14), and (–2 6 1). For **4**, the O2-hydroxyethyl residue, with the exception of the hydroxyl-H atom, was disordered over two positions in a ratio 0.851(2):0.149(2). The ADP of matching pairs of atoms were constrained to be equal and nearly isotropic. Further, chemically equivalent bond lengths were constrained to be nearly equal. The residual electron density peaks, Table 2.1, were located 1.46 and 0.67 e Å^{–3} from the S4 and S5 atoms, respectively. Two reflections were omitted from the final refinement of **5** *i.e.*, (0 2 0) and (–1 0 1) owing to poor agreement. The displacement ellipsoid diagrams were drawn with ORTEP-3 for Windows (Farrugia, 2012) at the 50% probability level and other crystallographic diagrams were drawn with DIAMOND (Brandenburg, 2006).

2.3. Results and Discussion

2.3.1. Synthesis and solution characterization

As reported earlier (**PUBLICATION 1**), the metathetical reaction between CdCl_2 and 2 molar equivalents of $\text{Na}[\text{S}_2\text{CN}(\text{iPr})\text{CH}_2\text{CH}_2\text{OH}]$ yielded the anticipated cadmium bis(dithiocarbamate) compound (based on ^1H and ^{13}C NMR), $\text{Cd}[\text{S}_2\text{CN}(\text{iPr})\text{CH}_2\text{CH}_2\text{OH}]_2$; this was isolated as an analytically pure powder. Recrystallization from Emsure[®] ethanol solution resulted in X-ray quality acicular crystals of **1** within 3 h, Figure 2.1a. After only an additional hour of crystallization blocks of **2** started to appear with the needles of **1** being subsumed, Figure 2.1b, with the transformation nearly complete after 6 h, Figure 2.1c. After 3 days there was no evidence for acicular crystals, Figure 2.1d. Such transformation and change in morphology indicates disassembly of the original crystals and reassembly into the new form (Dubraja *et al.*, 2015).

The IR spectra recorded on freshly isolated crystals presented a very similar pattern of absorptions with minor differences in wavenumbers, see Appendix A. ^1H NMR spectroscopy conducted on analytically pure crystals of **1** and **2** were indistinguishable in terms of chemical shifts, integration and multiplicity indicating they have the same chemical composition confirmed by X-ray crystallography (see below). Remarkably both hydroxyethyl- and ethanol-OH protons appeared as well defined triplets. Similarly the ^{13}C NMR were indistinguishable as were the UV-Vis spectra, see Appendix B.

The crystal and molecular structures of **1** and **2** were determined showing the compositions of the needles and blocks to be polymeric $[\{\text{Cd}[\text{S}_2\text{CN}(\text{iPr})\text{CH}_2\text{CH}_2\text{OH}]_2\} \cdot \text{EtOH}]_\infty$ (**1**) and binuclear $\{\text{Cd}[\text{S}_2\text{CN}(\text{iPr})\text{CH}_2\text{CH}_2\text{OH}]_2\}_2 \cdot 2\text{EtOH}$ (**2**), respectively *i.e.*, to be (genuine) SIs in the sense that the empirical formula of each of **1** and **2** is identical. The similarity of the

solution characterization (^1H and $^{13}\text{C}\{^1\text{H}\}$ NMR and UV-Vis) for both species proves the observed SI to be a solid state phenomenon.

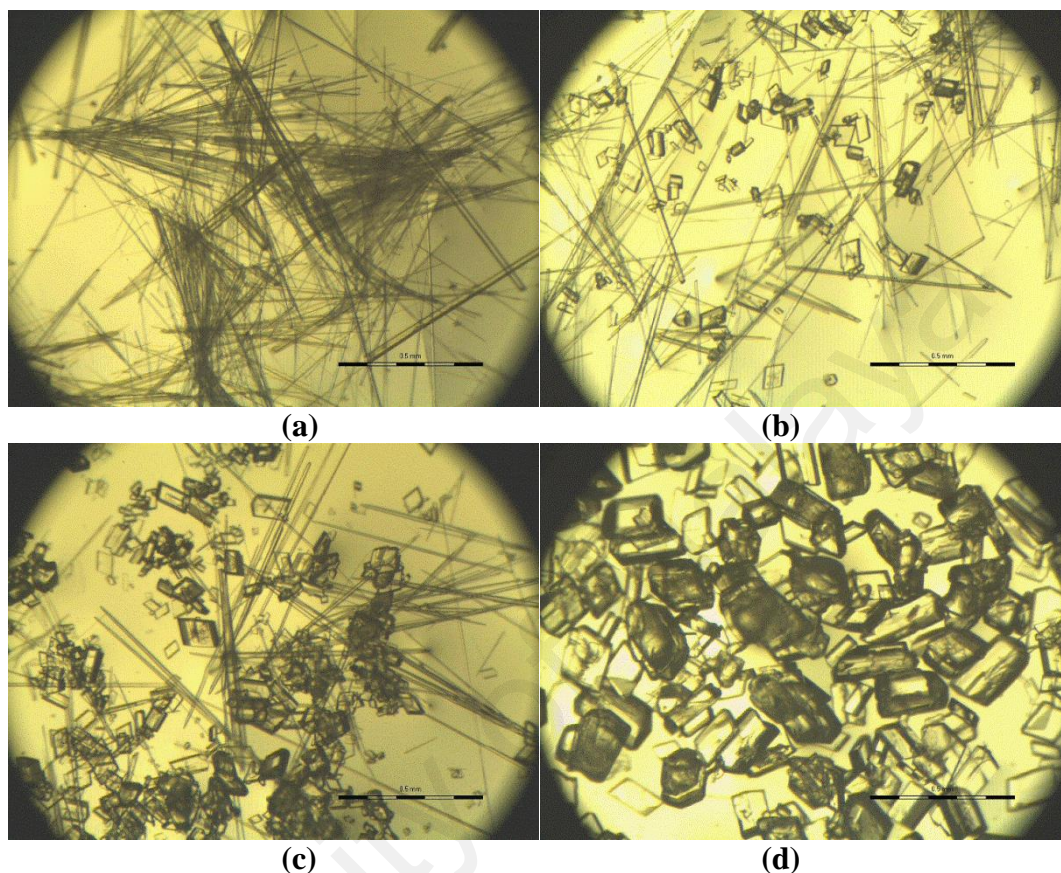


Figure 2.1: Formation of crystals of needles of **1** and blocks of **2** in ethanol solution. After: (a) 3 h, (b) 4 h, (c) 5 h, and (d) 3 days.

2.3.2. Single crystal X-ray crystallography

The crystallographic asymmetric unit of $[\{\text{Cd}[\text{S}_2\text{CN}(\text{iPr})\text{CH}_2\text{CH}_2\text{OH}]_2\} \cdot \text{EtOH}]_\infty$ (**1**), comprises two independent Cd atoms, each located on a 2-fold axis, two dithiocarbamate ligands and an ethanol molecule, Figure 2.2a. Both dithiocarbamate ligands coordinate in a $\mu_2\kappa^2$ -tridentate mode simultaneously chelating one Cd atom and bridging another. This results in octahedrally coordinated Cd atoms and the formation of a one-dimensional CP comprising alternating Cd1 and Cd2 atoms aligned along the *b*-axis, Figure 2.2b. The Cd–S bond lengths, Appendix C.1, span a relatively narrow range with the range for the Cd1 atom, *i.e.*, 2.6331(8) to 2.7412(9) Å, being wider than for Cd2,

i.e., 2.6556(9) to 2.7122(9) Å. Distortions from the ideal octahedral geometry can be related to the restricted bite angles of the dithiocarbamate ligands, *i.e.*, 67-68°. The *trans*-S–Cd–S angles lie in a narrow range *i.e.*, 167-168°.

In the crystal packing of **1** supramolecular chains are formed by O–H···O hydrogen bonding involving the hydroxylethyl- and ethanol-hydroxyl groups with one orientation of these interactions illustrated in Figure 2.2c; the geometric characteristics of the intermolecular interactions operating in the crystal structures of **1** and **2** are listed in Table 2.3. The one-dimensional CPs are connected by hydrogen bonding along both the *a*- and *c*-axes so that a three-dimensional architecture arises, Figure 2.2d.

As illustrated in Figure 2.3a, the asymmetric unit of **2** comprises half a molecule of {Cd[S₂CN(iPr)CH₂CH₂OH]₂}₂ and an ethanol molecule. The full molecule of {Cd[S₂CN(iPr)CH₂CH₂OH]₂}₂ is generated by the application of a centre of inversion, Figure 2.3b, *i.e.*, being the common structural motif for molecules of the general formula {Cd[S₂CNRR']₂}₂ (Casas *et al.*, 1989; Cox *et al.*, 1999; Dee *et al.*, 2002; Domenicano *et al.*, 1968; Glinskaya *et al.*, 1999; Ivanov *et al.*, 2006; A. V. Ivanov *et al.*, 2005; Ivanov *et al.*, 2008; F.-F. Jian *et al.*, 1999; F. Jian *et al.*, 1999; Kant *et al.*, 2012; Konarev *et al.*, 2006; Manohar *et al.*, 2005; Saravanan *et al.*, 2004; Thirumaran *et al.*, 2012; Yin *et al.*, 2004; Zhong *et al.*, 2004). In this structure the S1- and S3 dithiocarbamate ligands are κ^2 -chelating and $\mu_2\kappa^2$ -tridentate, respectively resulting in five coordinate geometries based on square pyramidal geometries as seen in the τ value of 0.08 which compares to τ values of 0.00 and 1.00 for ideal square pyramidal and trigonal bipyramidal geometries, respectively (Addison *et al.*, 1984). In this description the bridging S4 atom occupies the axial position.

Table 2.1: Crystal data and refinement details for **1–5**.

Parameter	1	2	3	4	5
Formula	C ₁₂ H ₂₄ CdN ₂ O ₂ S ₄ CH ₃ CH ₂ OH	C ₂₄ H ₄₈ Cd ₂ N ₄ O ₄ S ₈ 2CH ₃ CH ₂ OH	C ₂₄ H ₄₈ Cd ₂ N ₄ O ₄ S ₈ 2(C ₆ H ₁₁ NOS)	C ₂₄ H ₄₈ Cd ₂ N ₄ O ₄ S ₈ 4(C ₅ H ₁₄ NO), 2(SO ₄)	C ₁₈ H ₃₆ CdN ₃ O ₃ S ₆ C ₅ H ₁₄ NO
Formula weight	515.04	1030.10	1228.50	1546.75	751.43
Crystal system	monoclinic	triclinic	triclinic	monoclinic	monoclinic
Space group	<i>P</i> 2/ <i>c</i>	<i>P</i> 1	<i>P</i> 1	<i>C</i> 2/ <i>c</i>	<i>P</i> 2 ₁ / <i>n</i>
<i>a</i> , Å	10.2768(2)	9.2310(18)	10.419(2)	29.3471(6)	10.6261(2)
<i>b</i> , Å	7.6850(2)	9.2847(19)	11.120(2)	11.2512(2)	17.7820(4)
<i>c</i> , Å	27.9859(6)	13.671(3)	13.119(3)	21.9269(4)	17.8128(4)
α , °	90	83.15(3)	106.64(3)	90	90
β , °	90.839(1)	82.22(3)	102.07(3)	101.959(2)	91.274(2)
γ , °	90	71.73(3)	107.68(3)	90	90
<i>V</i> , Å ³	2210.01(9)	1098.7(4)	1312.5(5)	7082.9(2)	3364.96(12)
<i>Z</i>	4	1	1	1	4 4
Density, g/cm ³ (calculated)	1.548	1.557	1.554	1.450	1.483
μ /mm ⁻¹	1.380	1.388	1.253	0.956	1.055
Reflections collected	20074	13965	16418	28643	22504
Independent reflections	5069	4962	5907	8005	7715
Reflections with $I \geq 2\sigma(I)$	4033	4526	5085	7010	6382
<i>R</i> (observed data)	0.037	0.023	0.025	0.025	0.027
<i>a</i> , <i>b</i> in weighting scheme	0.018, 6.753	0.026, 0.169	0.034, 0	0.029, 7.020	0.017, 0.735
<i>R</i> _w (all data)	0.076	0.054	0.064	0.062	0.057
Largest diff. peak and hole e Å ⁻³	1.46 and -1.40	0.40 and -0.50	0.69 and -0.48	1.41 and -0.40	0.42 and -0.42
CCDC deposition number	1405102	1405103	1405104	1405105	1405106

* Please refer Publication 1 for Crystal data and refinement details of **6** and **7**

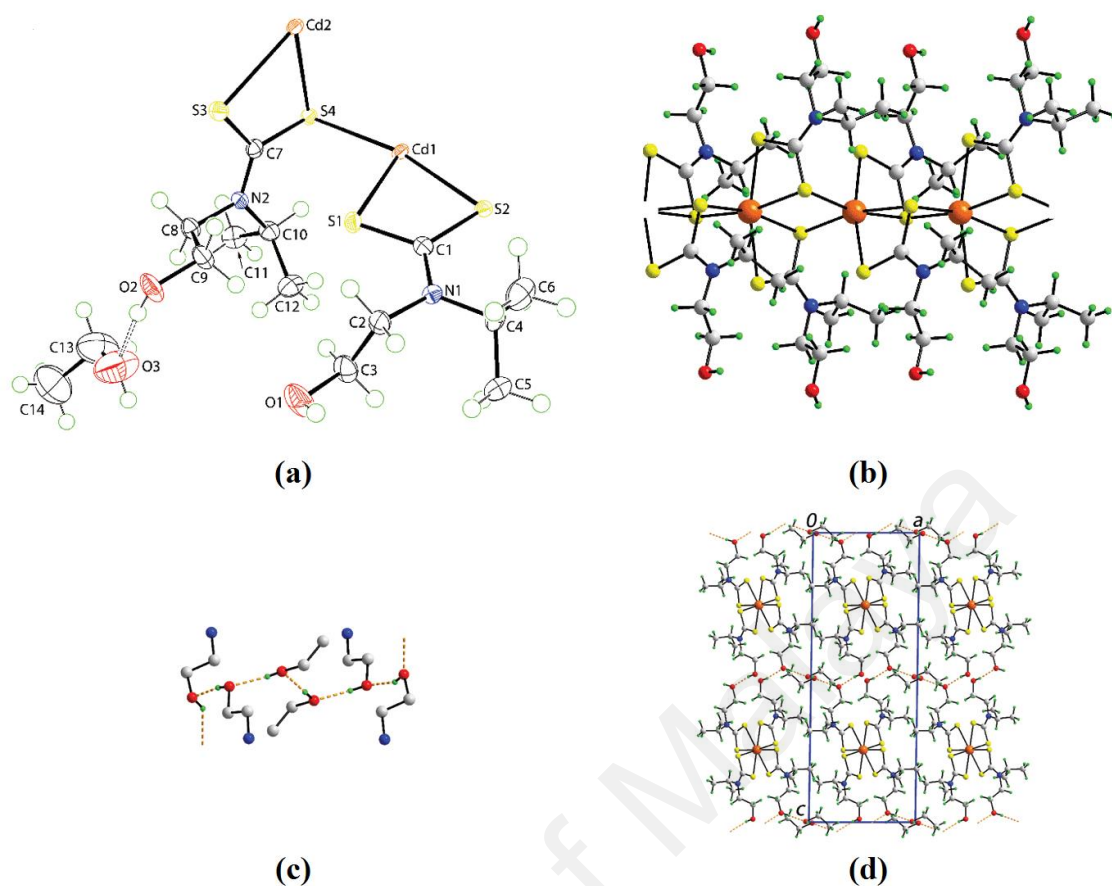


Figure 2.2: Asymmetric, molecular structures and molecular packing of **1**.

(a) Asymmetric unit for **1** showing atom labelling scheme; only one orientation of the disordered components is shown. (b) One-dimensional CP with ethanol molecules omitted. (c) A supramolecular chain mediated by O–H...O hydrogen bonding (orange dashed lines) with most atoms omitted. (d) A view of the unit cell contents in projection down the b-axis. In all images only one orientation of the acidic-H atoms is shown.

The most prominent feature of the crystal packing is the formation of centrosymmetric 12-membered $\{\cdots\text{HO}\}_6$ synthons with both hydroxyethyl- and ethanol-hydroxyl groups participating in donor and acceptor O–H...O hydrogen bonds, Appendix C.2 and Figure 2.3c. The hydrogen bonding leads to the formation of layers parallel to (0 2 1), Figure 2.3d; layers stack without specific interactions between them (Figure 2.4)

Structure of related SIs, **6** and **7** are shown in Figure 2.5. Please refer to Publication 1 for detail of crystallography description and information.

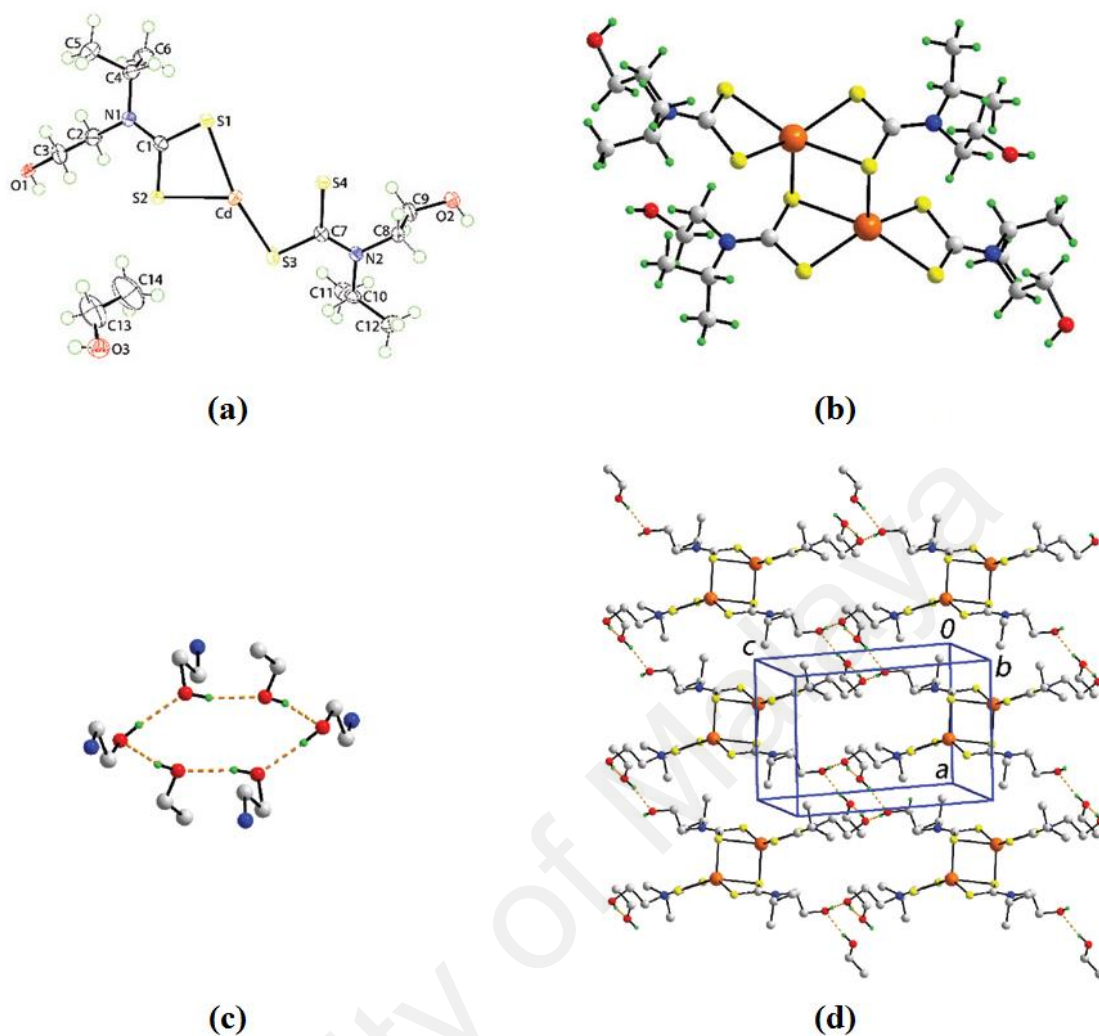


Figure 2.3: Asymmetric, molecular structures and molecular packing of **2**.

(a) Asymmetric unit for **2** showing atom labelling scheme. (b) A view of the centrosymmetric binuclear molecule with ethanol molecules omitted. (c) A supramolecular 12-membered ring mediated by O–H...O hydrogen bonding (orange dashed lines) with most atoms omitted. (d) A view of the supramolecular layer parallel to (0 2 1). In all images only one orientation of the disordered components is shown.

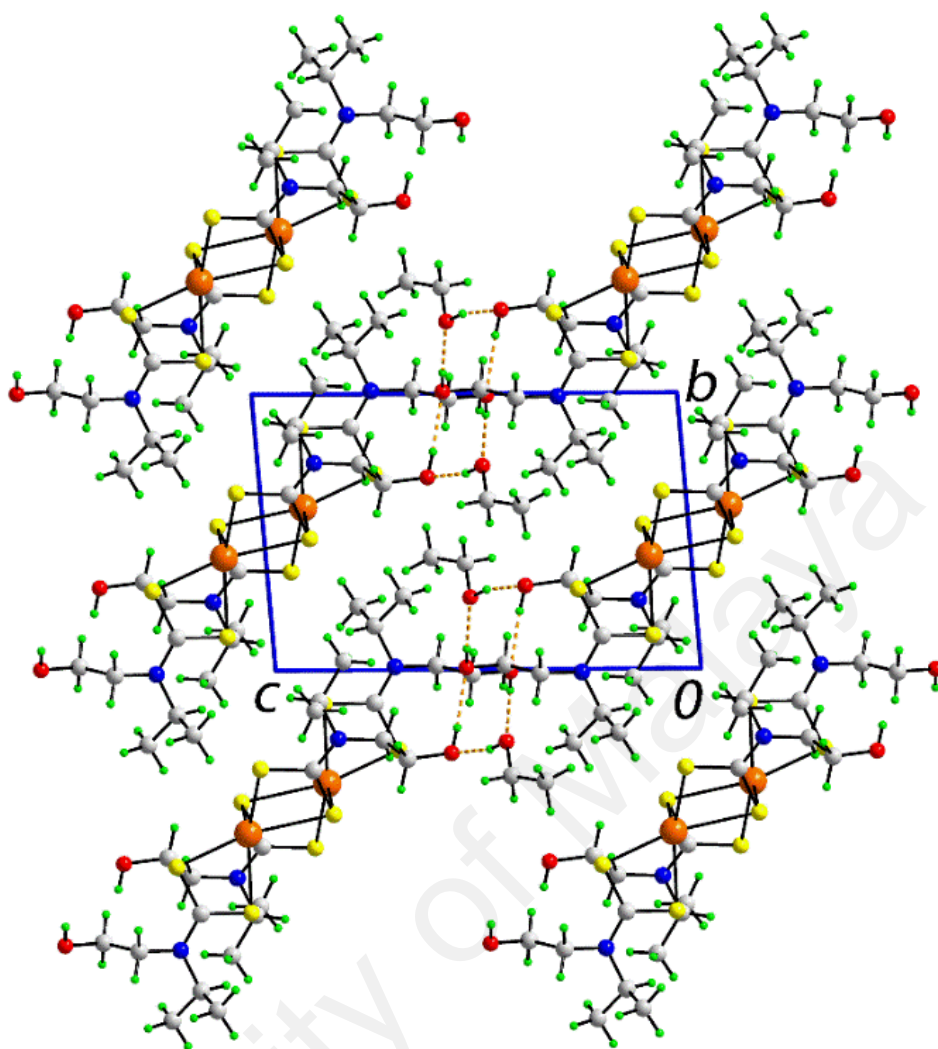


Figure 2.4: A view of the unit cell contents of **2** shown in projection down the a-axis highlighting the stacking of layers.

2.3.3. Powder X-ray diffraction (PXRD)

PXRD experiments were performed on freshly isolated **1** and **2** and compared with the simulated patterns calculated from the single crystal (SCXRD) experiments measured at 100 K. As both pairs of patterns matched, the SCXRD results are representative of the bulk materials (see Appendix Da and b). The stability of **1** and **2** with respect to loss of ethanol was also investigated using PXRD. Time dependent PXRD were measured on freshly harvested crystals and subsequently at 2, 6, 12, and 24 h; the experimental traces are given in Appendix Ea and b. For both **1** and **2** changes were apparent before 2 h indicating loss of the original crystal structure. The patterns obtained

for **1** and **2** after 24 h were distinct from each other and different from the original material used for recrystallization, *i.e.*, $\text{Cd}[\text{S}_2\text{CN}(\text{iPr})\text{CH}_2\text{CH}_2\text{OH}]_2$; see Appendix E (c).

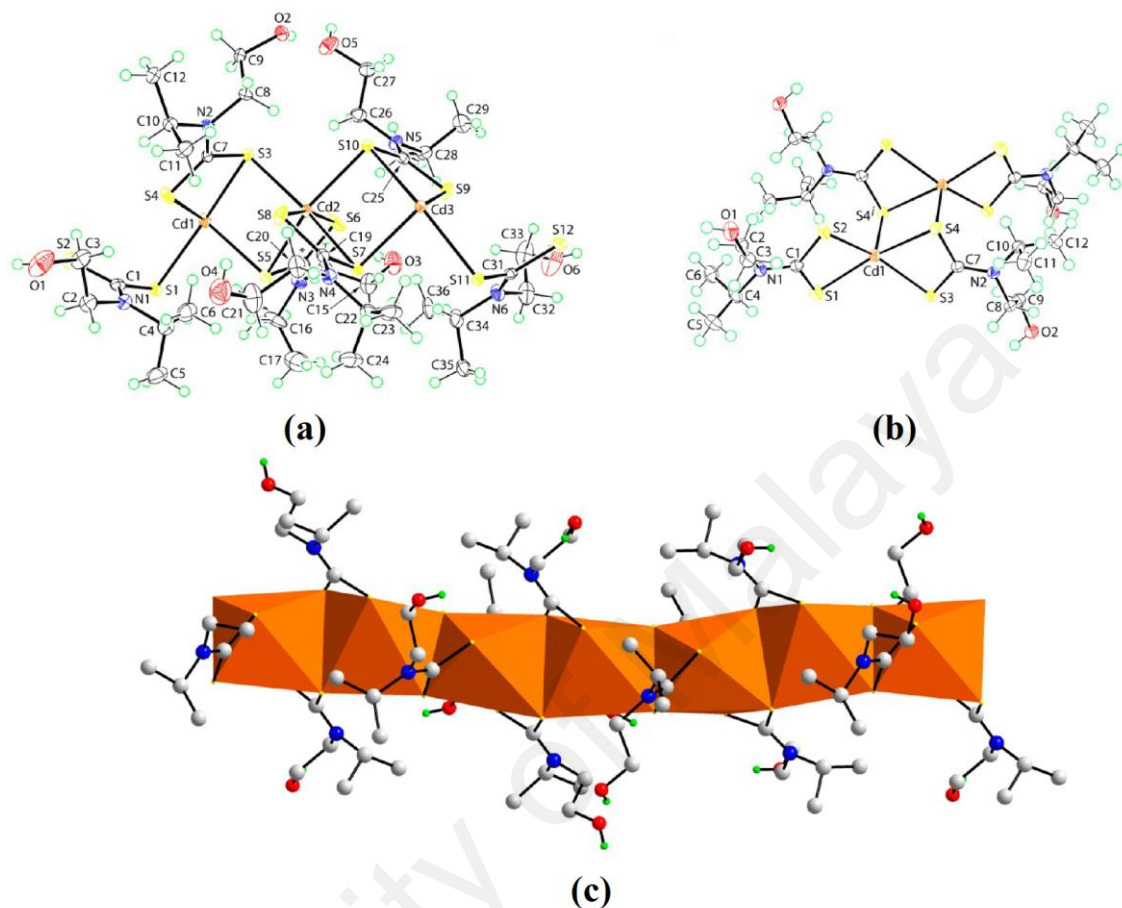


Figure 2.5: Asymmetric, molecular structures and molecular packing of **6** and **7**.

(a) Asymmetric unit (less acetonitrile molecule) in **6** showing atom labelling scheme. The atom indicated with an * is C13, and atoms C14, C18 and C30 are obscured. (b) Centrosymmetric dimeric aggregate in **7** showing atom labelling scheme. (c) Extended polymeric chain in **6** highlighting the edge shared polyhedra; all but O–H hydrogen atoms have been omitted. Solvent molecules have been omitted from all images.

2.3.4. Thermal degradation

The TGA traces for **1** and **2** are shown in Appendix Fa and b. Each decomposes in two well-defined steps to yield CdS. For **1** the desolvation of lattice ethanol occurred in the first step between 57 and 120 °C with a weight loss of 7.1% cf. calcd. 8.9%. The second step between 120 and 338 °C left a residue of 27.2 % cf. calcd. 28.0% corresponding to CdS; cadmium dithiocarbamates (Afzaal *et al.*, 2010) and the nitrogen

adducts (Mlowe *et al.*, 2014) are known to be excellent synthetic precursors for the deposition of CdS nanoparticles. The corresponding temperature ranges for **2** are 65 to 149 °C (obs., calcd. weight loss: 8.0, 8.9%) and 149 to 356 °C (29.6, 28.0%). The stability of **1** and **2** was also monitored by time dependent TGA where scans were performed on a fresh sample and then at 2, 6, 12, and 24 h; see Appendix F. By 6 h, practically all of the lattice ethanol had evaporated, a process that resulted in a change in crystal structure as indicated by the time dependent PXRD study (see above).

2.3.5. Relationship between SI formed from $\text{Cd}[\text{S}_2\text{CN}(\text{iPr})\text{CH}_2\text{CH}_2\text{OH}]_2$.

With the characterization of **1** and **2**, there are now three distinct SI derived from the basic building block, $\text{Cd}[\text{S}_2\text{CN}(\text{iPr})\text{CH}_2\text{CH}_2\text{OH}]_2$, with the third being the previously reported $[\{\text{Cd}[\text{S}_2\text{CN}(\text{iPr})\text{CH}_2\text{CH}_2\text{OH}]_2\}_3 \cdot \text{MeCN}]_\infty$ (**6**) (**PUBLICATION 1**) see Publication 1; the SI in $\{\text{Cd}[\text{S}_2\text{CN}(\text{iPr})\text{CH}_2\text{CH}_2\text{OH}]_2\}_2 \cdot 2\text{H}_2\text{O} \cdot 2\text{MeCN}$ (**7**) (**PUBLICATION 1**) matches that of **2**. Figure 2.6 shows simplified representations of the three SI, *i.e.*, the dimer in **2** (and **7**), and the linear CPs in each of **1** and **6**. The relationships between the SI are quite straight forward. In **2**, only one dithiocarbamate ligand forms Cd–S bridges so that a dimeric aggregate is formed. By contrast, in each of **1** and **6**, both dithiocarbamates form Cd–S bridges leading to linear CPs. The primary difference between **1** and **6** rests with the relative orientation of the dithiocarbamate ligands. In **1**, with crystallographically imposed 2-fold symmetry, the dithiocarbamate ligands are oriented in the same direction whereas in **6**, with neighbouring cadmium atoms related by centres of inversion, alternate dithiocarbamate ligands are oriented in opposite directions.

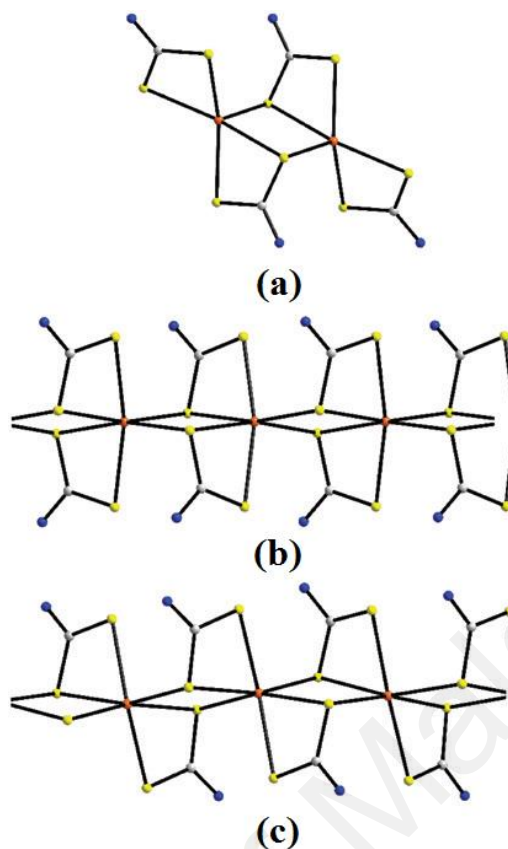


Figure 2.6: Schematic images of the three SI derived from $\text{Cd}[\text{S}_2\text{CN}(\text{iPr})\text{CH}_2\text{CH}_2\text{OH}]_2$. (a) Dimeric **2**, (b) linear CPs **1**, and (c) **6**. Alkyl substituents have been removed for clarity.

2.3.6. Conversion between SIs

Conversion between CPs, including SI, in the solid state has been reviewed (Vittal, 2007). Examples exist whereby reversible single crystal single crystal transformations mediated by solvent guests (Liu *et al.*, 2012; Park *et al.*, 2013), recrystallization (Jeon *et al.*, 2014), and microwave irradiation/rehydration (Li *et al.*, 2013; Zou *et al.*, 2014). Given the similarity in the SI derived from $\text{Cd}[\text{S}_2\text{CN}(\text{iPr})\text{CH}_2\text{CH}_2\text{OH}]_2$, it was thought of interest to investigate whether solvent mediated interconversion between them was possible.

The in situ conversion of $[\{\text{Cd}[\text{S}_2\text{CN}(\text{iPr})\text{CH}_2\text{CH}_2\text{OH}]_2\} \cdot \text{EtOH}]_\infty$ (**1**) to $\{\text{Cd}[\text{S}_2\text{CN}(\text{iPr})\text{CH}_2\text{CH}_2\text{OH}]_2\}_2 \cdot 2\text{EtOH}$ (**2**) indicates that the kinetic SI, **1**, transforms to the thermodynamic form, **2**, with time. In the previous study of

$[\{\text{Cd}[\text{S}_2\text{CN}(\text{iPr})\text{CH}_2\text{CH}_2\text{OH}]_2\}_3 \cdot \text{MeCN}]_\infty$ (6) and

$\{\text{Cd}[\text{S}_2\text{CN}(\text{iPr})\text{CH}_2\text{CH}_2\text{OH}]_2\}_2 \cdot 2\text{H}_2\text{O} \cdot 2\text{MeCN}$ (7) it was concluded that adventitious water mediated the in situ transformation of **6** to **7** (PUBLICATION 1). In order to investigate if it was possible to interconvert the SI, additional experiments were conducted. In these experiments freshly isolated samples (0.1 g) of **1**, **2**, **6** and **7** were taken up in dry (3 Å molecular sieves) and laboratory grade Emsure® MeCN or EtOH, covered with parafilm (with a few holes), and allowed to crystallize over seven days. The resultant crystals were analysed by PXRD (see Appendix G). Figure 2.7 summarizes the observed conversions between the SI achieved under these conditions.

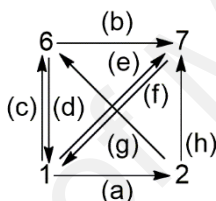


Figure 2.7: Solvent mediated interconversion between **1**, **2**, **6**, and **7**.

Conditions: (a) Hours in dry or lab. grade EtOH, ambient conditions. (b) Dry MeCN, and adventitious water. (c) Dry MeCN, and stored in a desiccator. (d) Dry EtOH, desiccator. (e) Dry or lab. grade MeCN, ambient. (f) Lab. EtOH, ambient. (g) Dry MeCN, desiccator. (h) Dry or lab. grade MeCN, ambient.

A reversible transformations between polymeric **1** and **6** was accomplished by recrystallization from dry acetonitrile and ethanol, respectively. When water was present, adventitious or otherwise, **1** could be converted to dimeric **7** but this was reversible in an excess of dry ethanol presumably as the water released from **7** was associated with the bulk solvent; evidence for a small amount of original **7** was seen in the PXRD for the transformation of **7** to **1** (see Appendix Ge). Dimeric **2** was mainly (there was also a trace of an unknown species, see Appendix Gf) transformed to polymeric **6** in an excess of dry acetonitrile but **6** could not be converted back to **2** by simple recrystallization. Similarly **2** was transformed irreversibly to dimeric **7**. A noteworthy observation is that **1**, which is thermodynamically unstable with “genuine SI” **2**, can be maintained in the presence of

MeCN. In summary, the above observations are consistent with the overall preferential formation of dimeric **2** and **7**, a result consistent with the literature precedents which overwhelmingly adopt the dimeric motif (Casas *et al.*, 1989; Cox *et al.*, 1999; Dee *et al.*, 2002; Domenicano *et al.*, 1968; Glinskaya *et al.*, 1999; Ivanov *et al.*, 2006; A. V. Ivanov *et al.*, 2005; Ivanov *et al.*, 2008; F.-F. Jian *et al.*, 1999; F. Jian *et al.*, 1999; Kant *et al.*, 2012; Konarev *et al.*, 2006; Manohar *et al.*, 2005; Saravanan *et al.*, 2004; Thirumaran *et al.*, 2012; Yin *et al.*, 2004; Zhong *et al.*, 2004).

2.3.7. Complementary crystallization experiments

Given the interesting SI of and interrelationships between **1**, **2**, **6** and **7**, it was thought of interest to explore other crystallizing solvents and techniques to investigate whether other SIs could be revealed. In all, three additional compounds, namely **3–5**, two of which contain binuclear{Cd[S₂CN(iPr)CH₂CH₂OH]₂}₂ (**3** and **4**) and one with the {Cd[S₂CN(iPr)CH₂CH₂OH]₃}⁻ anion (**5**), were discovered and these are described in turn below.

Compound **3** was isolated from the slow evaporation of a chloroform extract and is formulated as a 1:2 cocrystal, {Cd[S₂CN(iPr)CH₂CH₂OH]₂}₂:2[3-(propan-2-yl)-1,3-oxazolidine-2-thione], with the asymmetric unit comprising half a molecule of the former and a full molecule of the latter, Figure 2.8a. The binuclear molecule, Figure 2.8b, is centrosymmetric and to a first approximation exhibits the same features as seen in **2** with the most notable difference being the weakening of the transannular interaction formed by the bridging S2 atom to 3.0448(9) Å, Appendix H.1, cf. the equivalent bond in **2**, Appendix C.1. This has the result that the eight-membered {CdSCS}₂ ring lacks the internal Cd₂S₂ square. The reason for this structural difference is not immediately clear but the bridging bond formed by S2 has shortened to 2.5545(11) Å. The oxazolidine molecule is known to be a decomposition/cyclization product derived from the S₂CN(iPr)CH₂CH₂OH anion (proposed mechanism as Figure 2.9)(Tan *et al.*, 2014), a

phenomenon reported for related species (Mothes *et al.*, 2015; Nomura *et al.*, 1985), and its molecular structure (Tan *et al.*, 2014) matches closely that observed in **3** as seen the overlay diagram in Figure 2.10a.

In the crystal packing, hydroxyl-O–H \cdots O(hydroxyl) hydrogen bonds link the binuclear molecules into supramolecular chains aligned along the *a*-axis. Connected to either side of the chain via hydroxyl-O–H \cdots S(oxazolidine) hydrogen bonds are the 3-(propan-2-yl)-1,3-oxazolidine-2-thione molecules, Appendix H.2 and Figure 2.8c. The chains are connected into a supramolecular layer parallel to (0 1 1) *via* a strong methyl-C–H \cdots O(hydroxyl) and several C–H \cdots S(dithiocarbamate) interactions; see Figure 2.10b.

When a sample of Cd[S₂CN(iPr)CH₂CH₂OH]₂ was taken in acetone and left to evaporate a small number of crystals formed and these were formulated from X-ray crystallography as the salt cocrystal [iPrNH₂(CH₂CH₂OH)]₄[SO₄]₂{Cd[S₂CN(iPr)CH₂CH₂OH]₂}₂ (**4**). The asymmetric unit, Figure 2.11a, comprises half a centrosymmetric {Cd[S₂CN(iPr)CH₂CH₂OH]₂}₂ molecule, two ammonium [iPrNH₂(CH₂CH₂OH)]⁺ cations and a sulfate dianion. Presumably the ions are derived from the decomposition and subsequent protonation and oxidation of dithiocarbamate residues, respectively. The neutral species is binuclear and features the same pattern of Cd–S bond lengths as for **2**, Appendix H.1. There are no literature precedents (Groom *et al.*, 2014) for the structure of the cation (see discussion below). The key feature of the crystal packing is the formation of supramolecular chains along the *b*-axis sustained by charge-assisted N–H \cdots O(sulfate) and hydroxyl-O–H \cdots O(sulfate) hydrogen bonds, Figure 2.11b and Appendix H.2. The neutral molecules are connected to the chain *via* hydroxyl-O–H \cdots O(ammonium-hydroxyl and sulfate) hydrogen bonds. In this scheme each of the sulfate-O5, O7 and O8 atoms is bifurcated. The result of the aggregation between the chains and neutral molecules is a three-dimensional architecture, Figure 2.11c.

In another attempt to expand the structural landscape of $\text{Cd}[\text{S}_2\text{CN}(\text{iPr})\text{CH}_2\text{CH}_2\text{OH}]_2$ a crystallization reaction between $\text{Cd}(\text{acetate})_2 \cdot 2\text{H}_2\text{O}$ and two molar equivalents of $\text{Na}[\text{S}_2\text{CN}(\text{iPr})\text{CH}_2\text{CH}_2\text{OH}]$ was attempted in a sodium silicate gel. X-ray crystallography showed the small number of crystals that formed had composition $[\text{iPrNH}_2(\text{CH}_2\text{CH}_2\text{OH})]\{\text{Cd}[\text{S}_2\text{CN}(\text{iPr})\text{CH}_2\text{CH}_2\text{OH}]_3\}$ (**5**). The asymmetric unit comprises a $[\text{iPrNH}_2(\text{CH}_2\text{CH}_2\text{OH})]^+$ cation and a $\{\text{Cd}[\text{S}_2\text{CN}(\text{iPr})\text{CH}_2\text{CH}_2\text{OH}]_3\}^-$ anion, Figure 2.12a. The Cd atom in the anion is coordinated by three dithiocarbamate ligands and forms a relatively narrow range of Cd–S bond lengths, Appendix H.1, indicating a decidedly more symmetric mode of coordination than observed in **1–4**. The coordination geometry is distorted from the ideal octahedral geometry owing to the restricted bite distance of the ligands. The twist angle between the two trigonal faces is estimated to be 38° , compared with 60° in an ideal octahedron, indicating a twist towards a trigonal prismatic geometry. $\{\text{Cd}[\text{S}_2\text{CN}(\text{iPr})\text{CH}_2\text{CH}_2\text{OH}]_3\}^-$ anions have precedents in the literature being formed when reacting $\{\text{Cd}[\text{S}_2\text{CNEt}_2]_2\}_2$ with aliphatic Lewis bases (Glinskaya *et al.*, 1992; McCleverty *et al.*, 1982; Zemskova *et al.*, 1999). By contrast, there are no structurally characterized structures of the cations found in **4** and **5**. As seen from Appendix I, which presents overlay diagrams for the cations, there is great conformational flexibility in these species with the hydroxyl adopting three very distinct conformations when viewed down the $\text{CH}_2\text{--CH}_2$ bond.

In the crystal packing of **5** centrosymmetrically related cations associate *via* charge-assisted $\text{N--H}\cdots\text{O}(\text{hydroxyl})$ bonds, forming two interactions to the O4 atom. The dimeric aggregates are linked to anions *via* charge-assisted $\text{N--H}\cdots\text{O}(\text{hydroxyl})$ and hydroxyl- $\text{O--H}\cdots\text{O}(\text{hydroxyl})$ hydrogen bonds, Figure 2.12b and Appendix H.2. The anions are linked into supramolecular layers in the *ac*-plane by a network of $\text{O--H}\cdots\text{S}$ hydrogen bonds and incorporating strong $\text{C--H}\cdots\text{S}$ interactions, Figure 2.12c and Appendix H.2. Anionic layers stack along the *b*-axis and are linked into a three-

dimensional structure by the interactions with the interdigitated cationic aggregates, Figure 2.13.

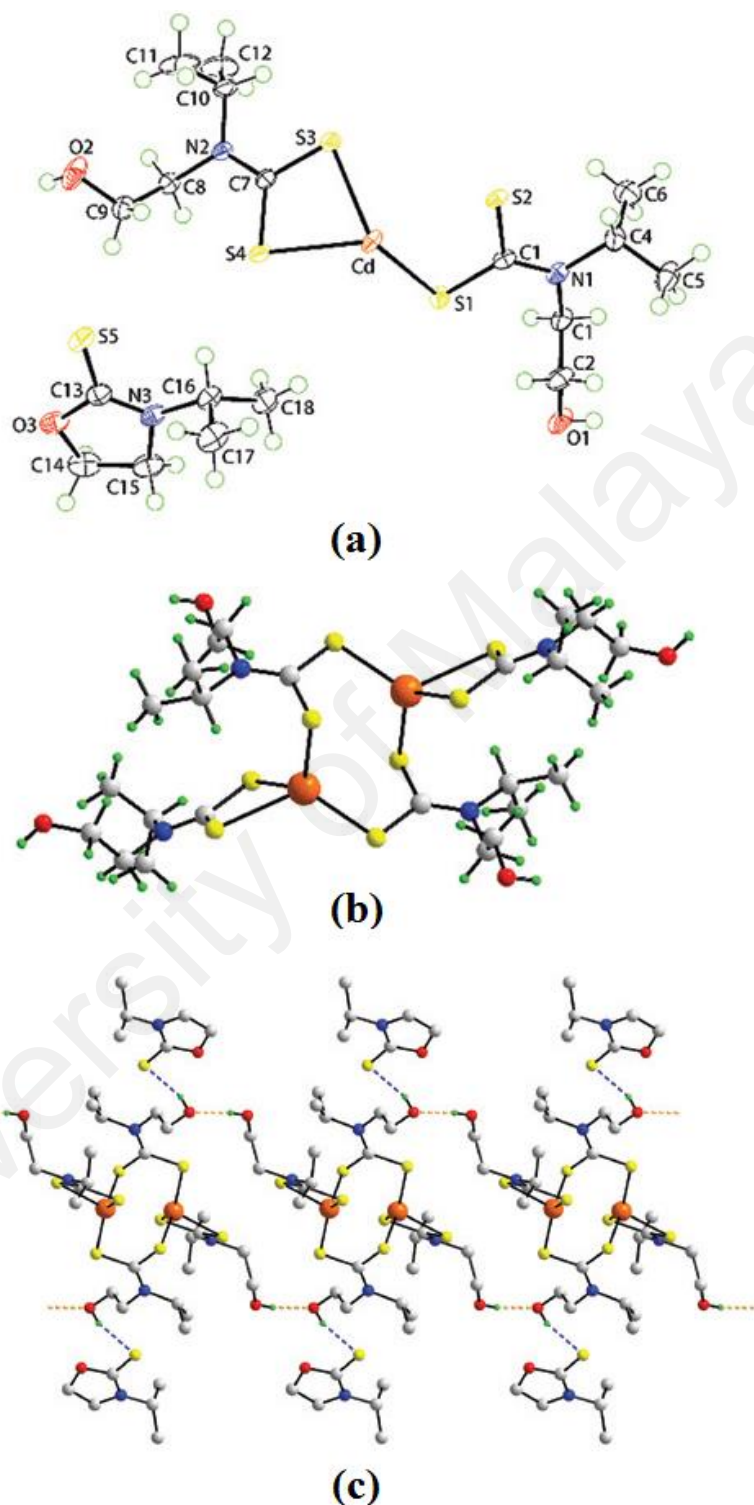


Figure 2.8: Asymmetric, molecular structures and molecular packing of **3**.

- (a) Asymmetric unit for cocrystal **3** showing atom labelling scheme. (b) A view of the centrosymmetric binuclear molecule with oxazolidine molecules omitted. (c) A supramolecular chain mediated by O-H...O hydrogen bonding (orange dashed lines) being connected to molecules *via* O-H...S hydrogen bonds (blue dashed lines) with non-participating H atoms omitted.

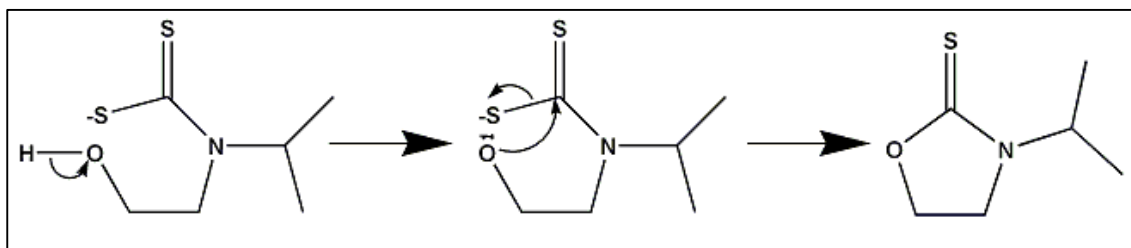
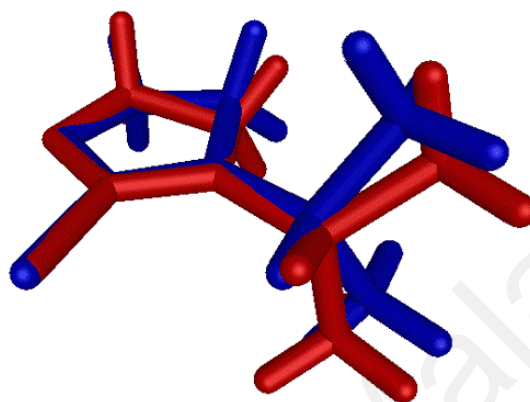
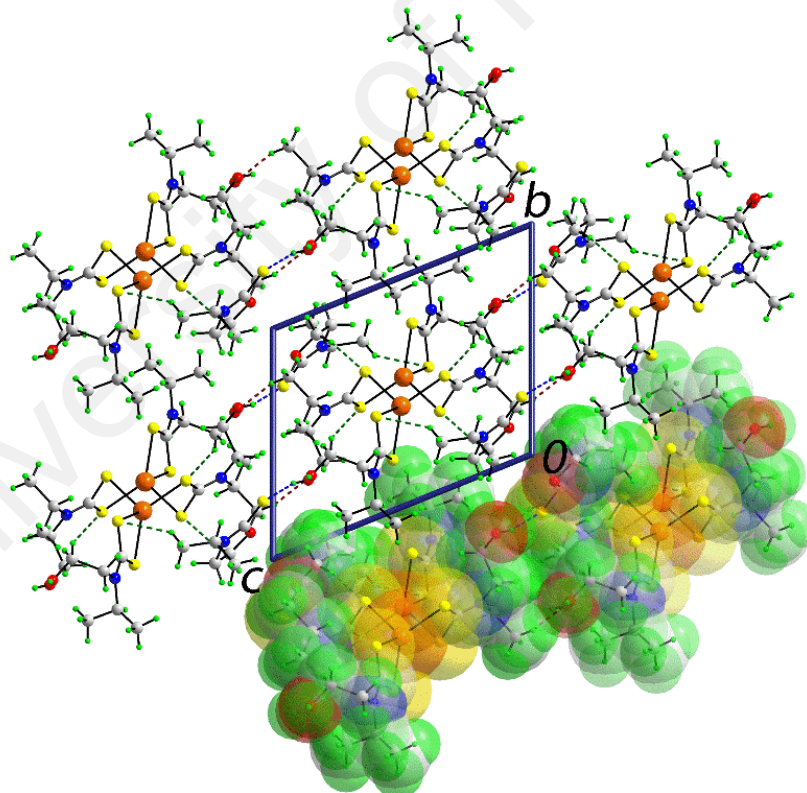


Figure 2.9: Proposed cyclisation derived from *N*-hydroxyethyl, *N*-isopropyl dithiocarbamate ligand.



(a)



(b)

Figure 2.10: Overlay diagram of the 3-(propan-2-yl)-1,3-oxazolidine-2-thione molecules and view of the unit cell contents of **3**.

(a) Overlay diagram of the 3-(propan-2-yl)-1,3-oxazolidine-2-thione molecules in **3** (red image) and in the free form (blue image). (b) A view of the unit cell contents of **3** shown in projection down the *a*-axis highlighting the stacking of layers; one layer is shown in space filling mode.

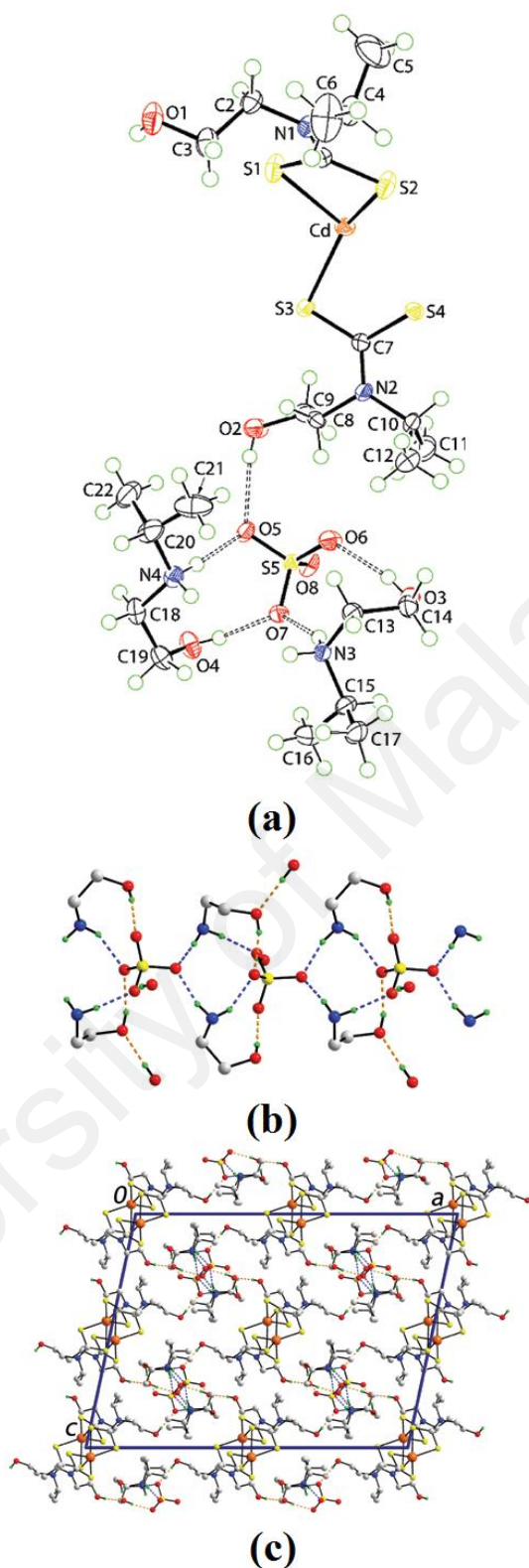


Figure 2.11: Asymmetric, molecular structures and molecular packing of **4**.

- (a) Asymmetric unit for salt cocrystal **4** showing atom labelling scheme. (b) A view of the supramolecular chain along the b-axis sustained by charge-assisted N–H \cdots O(sulfate) (blue dashed lines) and O–H \cdots O(sulfate) hydrogen bonds, and the hydroxyl–O–H \cdots O(hydroxyl) hydrogen bonds (orange) linking the chains to the neutral molecules. (c) A view of the unit cell contents in projection down the b-axis showing the links between the chains of ions and the neutral molecules with non-participating H atoms omitted.

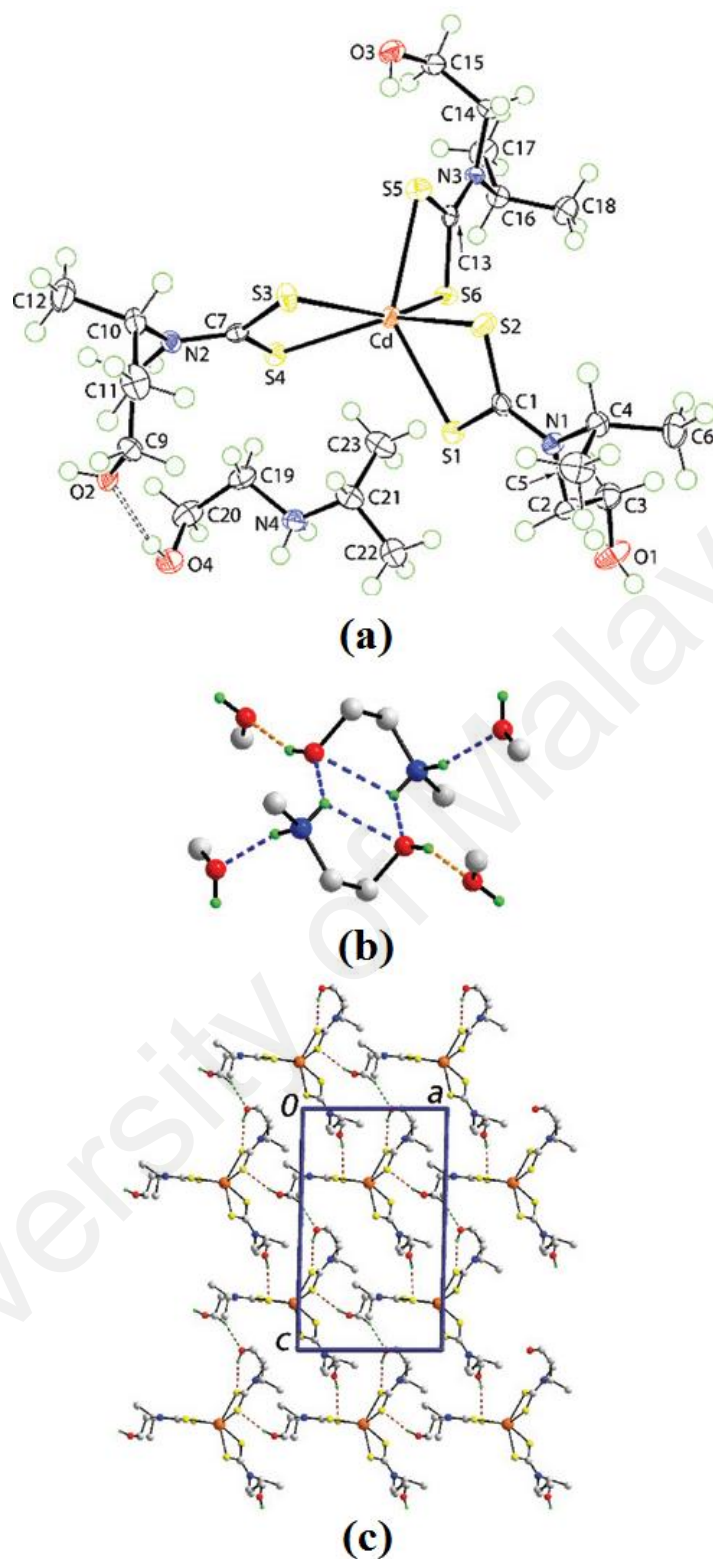


Figure 2.12: Asymmetric, molecular structures and molecular packing of **5**.

(a) Asymmetric unit for salt **5** showing atom labelling scheme. (b) A view of the bifurcated N–H···O(hydroxyl) hydrogen bonds (blue dashed lines) between atoms and the interaction of these *via* N–H···O(hydroxyl anion) (blue) and hydroxyl–O–H···O(anion hydroxyl) (orange) hydrogen bonds. (c) A view of the supramolecular layer in the *ac*-plane comprising anions connected by O–H···S and incorporating strong C–H···S hydrogen bonding (brown and green dashed lines, respectively) with non-participating H atoms omitted.

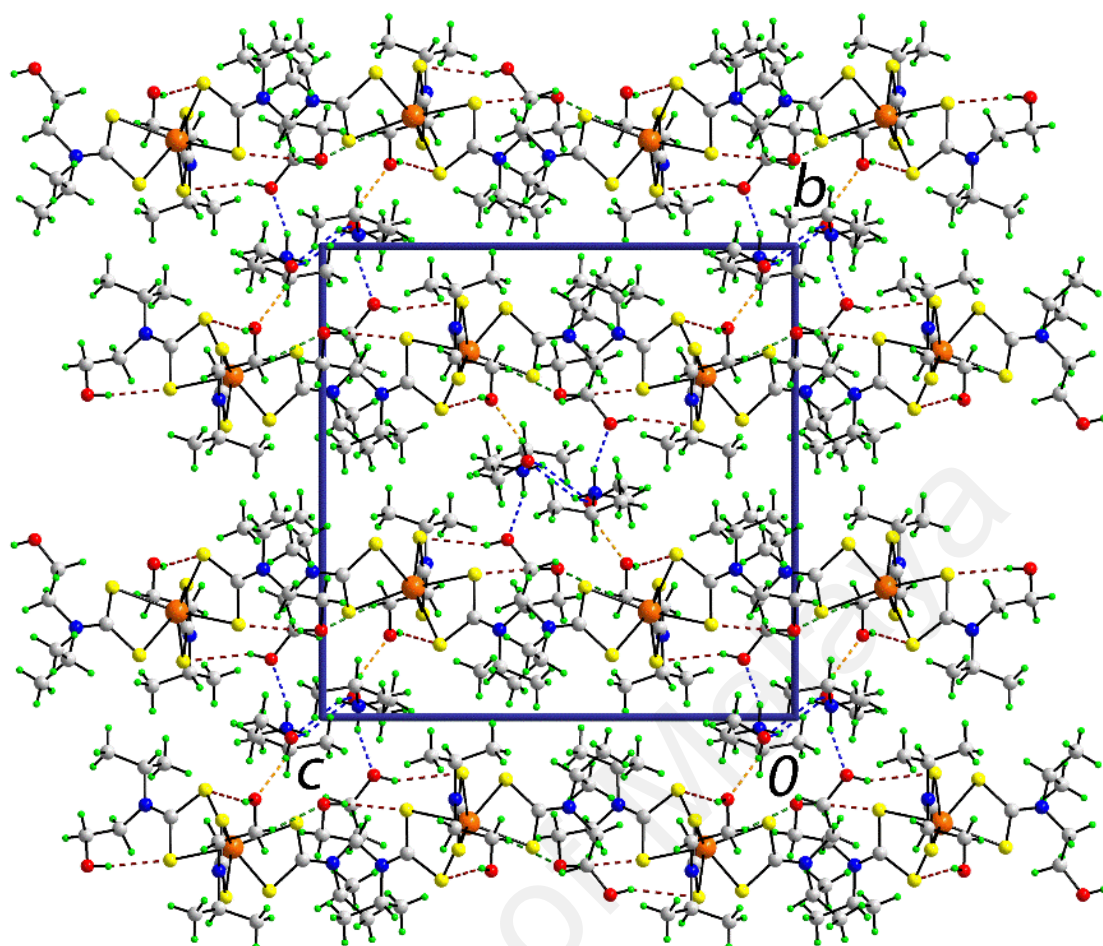


Figure 2.13: View of unit cell content of **5**.

A view of the unit cell contents of **5** shown in projection down the a-axis highlighting the stacking of anionic layers along the b-axis being interdigitated by cationic dimeric aggregates.

2.4. Conclusion

Needles of CP $[\{\text{Cd}[\text{S}_2\text{CN}(\text{iPr})\text{CH}_2\text{CH}_2\text{OH}]_2\} \cdot \text{EtOH}]_\infty$ (**1**) were isolated within three hours of recrystallization of $\text{Cd}[\text{S}_2\text{CN}(\text{iPr})\text{CH}_2\text{CH}_2\text{OH}]_2$ from ethanol. If the solution is left standing for longer periods the needles transform into blocks which is a genuine SI (Zhang *et al.*, 2009), having the same empirical formula including solvent, being binuclear $\{\text{Cd}[\text{S}_2\text{CN}(\text{iPr})\text{CH}_2\text{CH}_2\text{OH}]_2\}_2 \cdot 2\text{EtOH}$ (**2**). These results complements the previous characterization “non-genuine” SI, *i.e.*, $[\{\text{Cd}[\text{S}_2\text{CN}(\text{iPr})\text{CH}_2\text{CH}_2\text{OH}]_2\}_3 \cdot \text{MeCN}]_\infty$ (**6**) and $\{\text{Cd}[\text{S}_2\text{CN}(\text{iPr})\text{CH}_2\text{CH}_2\text{OH}]_2\}_2 \cdot 2\text{H}_2\text{O} \cdot 2\text{MeCN}$ (**7**) with the former transforming into the binuclear compound in the presence of water (**PUBLICATION 1**). The initial appearance of the one-dimensional CPs is correlated with reduced solubility of these species, and the ultimate appearance of the zero-dimensional binuclear species is correlated with it being the thermodynamically more stable, proven in the case of **1** and **2**, and implied in the case of **6** and **7**, solvent mediated transformations between **1**, **2**, **6** and **7**, and the appearance of the binuclear species in 1:2 cocrystal $\{\text{Cd}[\text{S}_2\text{CN}(\text{iPr})\text{CH}_2\text{CH}_2\text{OH}]_2\}_2 : 2[3\text{-(propan-2-yl)-1,3-oxazolidine-2-thione}]$ (**3**) and salt cocrystal $[\text{iPrNH}_2(\text{CH}_2\text{CH}_2\text{OH})]_2[\text{SO}_4]\{\text{Cd}[\text{S}_2\text{CN}(\text{iPr})\text{CH}_2\text{CH}_2\text{OH}]_2\}_2$ (**4**). In summary, despite the unvaried structural chemistry for the binary cadmium dialkyldithiocarbamates since the report of the first structure in 1968 (Domenicano *et al.*, 1968), recent studies (Kumar *et al.*, 2014; Tan *et al.*, 2013) indicate that varied crystallization conditions and careful observation can reveal fascinating crystal chemistry for this class of compound.

CHAPTER 3: SERENDIPITOUS COMPOSITIONAL AND STRUCTURAL DIVERSITY IN UROTROPINE ADDUCTS OF BINARY CADMIUM XANTHATES

3.1. Introduction and Literature Review

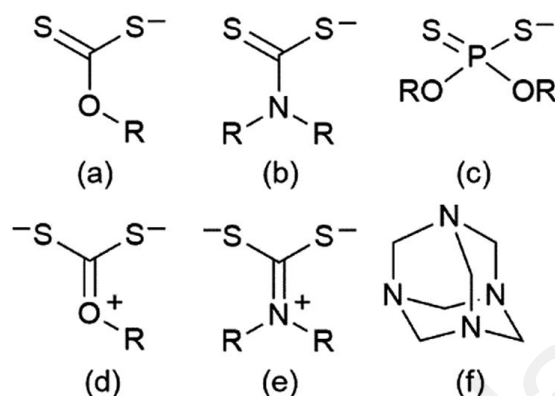


Figure 3.1: Generic chemical structures, resonance structure and chemical structure of xanthate, dithiocarbamate, dithiophosphate and hmta.

Generic structure of (a) xanthate, (b) dithiocarbamate and (c) dithiophosphate anions. Resonance structures for the (d) xanthate and (e) dithiocarbamate anions. (f) Chemical structure of urotropine (hmta).

Dithiocarbonates (xanthates), dithiocarbamates and dithiophosphates are important members of the 1,1'-dithiolate class of compounds, Figure 3.1 (Haiduc, 2003, 2007; Haiduc *et al.*, 1996; Heard, 2005; Hogarth, 2005; Tiekink *et al.*, 2005). Being easy to prepare and having a great propensity for complexing heavy elements ranging from the transition metals, lanthanides, and relevant to the present study, main group elements, it is not surprising that there is an enormous wealth of structural data for metal 1,1'-dithiolates (Haiduc, 2003, 2007; Haiduc *et al.*, 1996; Heard, 2005; Hogarth, 2005; Tiekink *et al.*, 2005). Amongst these, the structural chemistry exhibited by the binary cadmium xanthates, $\text{Cd}(\text{S}_2\text{COR})_2$ is remarkable for its diversity and complexity (Tiekink *et al.*, 2005). Thus, three distinct structural motifs are observed for these compounds, Figure 3.2, ranging from zero-dimensional in the case of the mononuclear compound found for $\text{R} = \text{CH}_2\text{CH}_2\text{OMe}$ (Abrahams *et al.*, 1988), one-dimensional in the form of a supramolecular chain when $\text{R} = \text{Me}$ (Young Jr *et al.*, 2002), and two-dimensional, as extended sheets, when $\text{R} = \text{Et}$, iPr and n-Bu (Iimura, 1973; Iimura *et al.*, 1972; Jiang *et*

al., 2002; Rietveld *et al.*, 1965; Tiekink, 2000; Tomlin *et al.*, 1999). Contrasting this behaviour are the structures of the binary cadmium dithiocarbamates, $\text{Cd}(\text{S}_2\text{CNR}_2)_2$, which normally features a binuclear, zero-dimensional structure as a result of two chelating ligands and two ligands which simultaneously chelate one cadmium centre while bridging another, *i.e.* $\mu_2\kappa^2$ -tridentate (Casas *et al.*, 1989; Cox *et al.*, 1999; Dee *et al.*, 2002; Domenicano *et al.*, 1968; Glinskaya *et al.*, 1999; Ivanov *et al.*, 2006; A. V. Ivanov *et al.*, 2005; Ivanov *et al.*, 2008; F.-F. Jian *et al.*, 1999; F. Jian *et al.*, 1999; Kant *et al.*, 2012; Konarev *et al.*, 2006; Manohar *et al.*, 2005; Saravanan *et al.*, 2004; Thirumaran *et al.*, 2012; Yin *et al.*, 2004; Zhong *et al.*, 2004). This dramatic difference in structural outcomes is rationalised in terms of the significant contribution of the canonical structure shown in Figure 3.1e, up to 40%, which makes dithiocarbamate ligands effective chelating agents certainly compared with the xanthate ligand where the equivalent canonical structure, Figure 3.1d, contributes no more than 20% to the overall electronic structure of the anion (Haiduc, 2003, 2007; Haiduc *et al.*, 1996; Heard, 2005; Hogarth, 2005; Tiekink *et al.*, 2005). However, the “staid” coordination chemistry for $\text{Cd}(\text{S}_2\text{CNR}_2)_2$ has been challenged recently by the characterisation of a one-dimensional CP, $[\{\text{Cd}[\text{S}_2\text{CN}(\text{iPr})\text{CH}_2\text{CH}_2\text{OH}]_2\}_3 \cdot \text{MeCN}]_\infty$ (**PUBLICATION 1**), for which all dithiocarbamate ligands are $\mu_2\kappa^2$ -tridentate, and its SI (Moulton *et al.*, 2001; Zhang *et al.*, 2009), $\{\text{Cd}[\text{S}_2\text{CN}(\text{iPr})\text{CH}_2\text{CH}_2\text{OH}]_2\}_2 \cdot 2\text{H}_2\text{O} \cdot 2\text{MeCN}$; this is properly classified as a “non-genuine” pair of SIs as the composition of the crystals differ (Zhang *et al.*, 2009). Further, a zero-dimensional trinuclear aggregate has been isolated recently, $\{\text{Cd}[\text{S}_2\text{CN}(\text{methylbenzyl})(\text{methylfurfuryl})]_2\}_3$, where the ratio of $\mu_2\kappa^2$ -tridentate to chelating ligands is 2:1 leading to a central octahedrally coordinated cadmium flanked by two square pyramidal cadmium atoms (Kumar *et al.*, 2014). The structural chemistry of the binary cadmium dithiophosphates resembles that of $\text{Cd}(\text{S}_2\text{CNR}_2)_2$ in that both zero- (binuclear) (Casas *et al.*, 1995; Ivanov *et al.*, 2007; Lawton *et al.*, 1969) and one-

dimensional (Ito *et al.*, 1996; Al. V. Ivanov *et al.*, 2005; Yin *et al.*, 2003) aggregation patterns are observed.

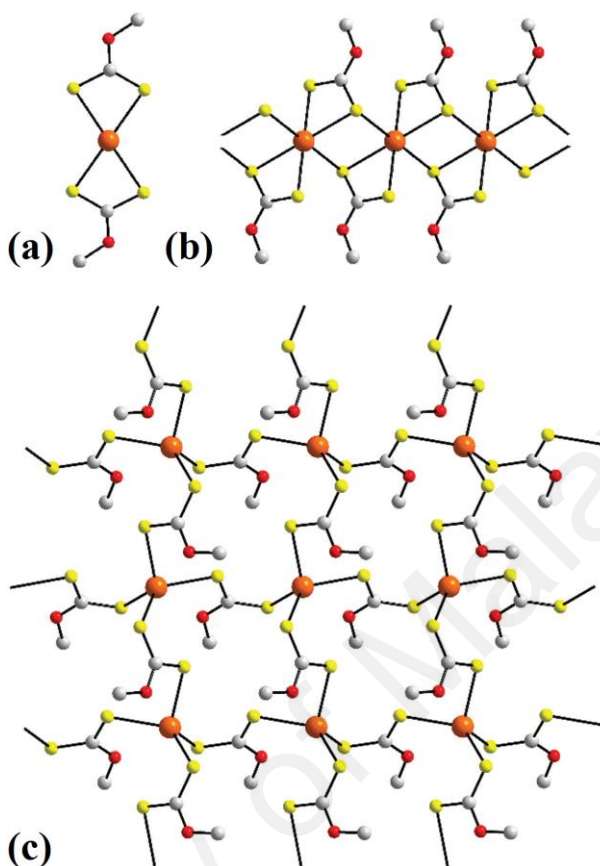


Figure 3.2: The three different structural motifs adopted by binary cadmium xanthates.

(a) Zero-dimensional, mononuclear found for $R = \text{CH}_2\text{CH}_2\text{OMe}$, (b) one-dimensional supramolecular chain found for $R = \text{Me}$, and (c) two-dimensional supramolecular layer found for $R = \text{Et}$, $i\text{-Pr}$ and $n\text{-Bu}$. All hydrogen atoms and all by the alkyl-carbon atoms bound to oxygen have been omitted.

While the mainstay of the construction of CPs of metal carboxylates has been to incorporate neutral and multidentate pyridine-donor ligands of which 4,4'-bipyridine (4,4'-bipy) is a prominent exemplar, the analogous chemistry of 1,1'-dithiolates is far less developed. In fact, there is only one example of structurally characterised cadmium xanthate with bridging bipyridine-type ligands, namely $[\text{Cd}(\text{S}_2\text{COiPr})_2(4,4'\text{-bipy})]_n$, which is a linear polymer (Abrahams *et al.*, 1990), even though structures with bidentate bipyridine donors are well known (Câmpian *et al.*, 2013; Larionov *et al.*, 2005). A linear CP is also noted in the structure of $\{\text{Cd}[\text{S}_2\text{CN}(\text{CH}_2\text{Ph})_2]_2(4,4'\text{-bipy})\}_n$.^{10a} This structure is complemented by highly flattened zig-zag polymers in each of $\{\text{Cd}(\text{S}_2\text{CNEt}_2)_2[1,2\text{-}$

bis(4-pyridyl)ethane]]_n (Avila *et al.*, 2006) and {Cd(S₂CNEt₂)₂[1,2-bis(4-pyridyl)ethylene]]_n (Chai *et al.*, 2003). By contrast to the aforementioned, the chemistry of cadmium dithiophosphates with bridging bipyridine-type ligands is far more developed (Lai & Tiekink, 2004; Lai *et al.*, 2006, 2006; Li *et al.*, 2004, 2005; Li *et al.*, 2006), with 17 different structures found in the Cambridge Structural Database (Groom *et al.*, 2014). A systematic study focussed on the influence of the steric profile of the remote organic substituents upon CP formation and, when formed, topology (Lai & Tiekink, 2004; Lai *et al.*, 2006, 2006). The controlling influence of steric bulk in influencing supramolecular aggregation patterns, in particular in militating secondary interactions (Alcock, 1972; Haiduc, 2007), in main group 1,1'-dithiolate chemistry is now well established (Lai *et al.*, 2002; Lai, Liu, *et al.*, 2004; Lai *et al.*, 2003; Tiekink, 2003, 2006). It is noted that in none of the cadmium structures with bridging bipyridine-type ligands were the 1,1'-dithiolate ligands bridging so that only one-dimensional architectures were formed. In an attempt to increase the dimensionality of the ensuing CP, attention was directed to the potentially polydentate ligand urotropine (hexamethylenetetramine, hereafter hmta), Figure 3.1f.

The utility of hmta in the construction of CPs has been reviewed recently which summarised a variety of “inverse coordination modes”, *i.e.* where hmta is regarded as the coordination centre (Kirillov, 2011). Bridging, *i.e.* μ_2 -, μ_3 - and even μ_4 -hmta, predominates with terminal coordination of hmta observed in less than 5% of the discussed CPs (Kirillov, 2011). Herein, an exploration of adduct formation between each of Cd(S₂COR)₂, R = Me, Et and iPr, and hmta is described in which the ratio of Cd(S₂COR)₂ to hmta was varied from 1:1, 2:1 and 1:2. Remarkably, from the nine possible products only three compounds could be prepared, namely Cd(S₂COMe)₂(hmta) (**8**), Cd(S₂COEt)₂(hmta)_{0.5} (**9**) and Cd(S₂COiPr)₂(hmta) (**10**), *i.e.* each with a different composition. Even more remarkably, the crystallographically determined structures of **8–10** are quite different owing to the different coordination modes of hmta, *i.e.*

monodentate, μ_2 -bidentate and μ_3 -tridentate so that different architectures are generated. The results of this investigation are reported herein.

3.2. Methodology

All chemicals and solvents were used as purchased without purification and reactions were carried out under ambient conditions. Elemental analyses were performed on a Perkin Elmer PE 2400 CHN Elemental Analyser. ^1H and $^{13}\text{C}\{^1\text{H}\}$ NMR spectra were recorded in d_6 -DMSO solutions on a Bruker Avance 400 MHz NMR spectrometer with chemical shifts relative to tetramethylsilane; abbreviations for NMR assignments: *s*, singlet; *d*, doublet; *t*, triplet; *q*, quartet; *sept*, septet. IR spectra were measured on a Perkin Elmer Spectrum 400 FT Mid-IR/Far-IR spectrophotometer from 4000 to 400 cm^{-1} ; abbreviations: vs, very strong; s, strong; m, medium; w, weak. The optical absorption spectra were measured on 10 and 100 μM ethanol:acetonitrile (1:1) solutions in the range 190–1100 nm on a single-beam Agilent Cary 60 UV-Vis spectrophotometer. Photoluminescence (PL) measurements were carried out at room temperature on 1 mM in acetonitrile:ethanol (1:1) solutions using an Agilent Varian Cary Eclipse Fluorescence Spectrophotometer with a Xenon flash lamp as the excitation source. Solid-state PL measurements were carried out using the same instrument. Solid samples were loaded on a SH1 plain sample holder of an Optistat DN2 (Oxford Instrument Nanoscience) attachment; liquid nitrogen was loaded into the cryostat system for low temperature (77 K) measurements. Thermogravimetric analyses were performed on a Perkin Elmer TGA 4000 Thermogravimetric Analyser in the range of 35–900 $^{\circ}\text{C}$ at the rate of 10 $^{\circ}\text{C}/\text{min}$. Powder X-ray diffraction (PXRD) data were recorded with a PANalytical Empyrean XRD system with Cu $K\alpha_1$ radiation ($\lambda = 1.54056 \text{ \AA}$) in the 2θ range 5 to 50 $^{\circ}$. The comparison between experimental and calculated (from CIF's) PXRD patterns were performed with X'Pert HighScore Plus ("X'Pert HighScore Plus," 2009).

3.2.1. Synthesis of xanthate ligands

The potassium salts of the three xanthate ligands, $K[S_2COR]$ for $R = \text{Me, Et and iPr}$, were prepared by dissolving KOH (*ca* 0.05 mol) in an excess of the respective alcohol followed by the slow addition of an equivalent amount of CS_2 . The precipitate which immediately formed was filtered off, dried *in vacuo* at room temperature and used as prepared.

3.2.2. Synthesis of binary cadmium xanthates

The same method was employed for the preparation of each of $Cd(S_2COR)_2$ for $R = \text{Me, Et and iPr}$. An aqueous solution (25 ml) of $CdCl_2$ (99.0% purity; Acros Organic; 2.75 g) was added to 2 molar equivalents of the respective xanthate taken up in ethanol ($R = \text{Me}$: 25 ml) or water ($R = \text{Et, iPr}$: 25 ml). The resulting mixture was stirred for 1 h and the precipitate that formed was suction filtered and air-dried. The products were characterised spectroscopically and used for subsequent reaction with hmta (Acros Organic).

$Cd(S_2COMe)_2$: Yield 4.26 g (87 %) as pale-yellow needles. 1H NMR (d_6 -DMSO, 25° C): δ 3.95 (s, 3H, OCH_3) ppm. $^{13}C\{^1H\}$ NMR (d_6 -DMSO, 25° C): δ 230.1 (C_q), 62.7 (OCH_3) ppm. IR (cm^{-1}): 1218 (vs) $\nu(C-O)$, 1029 (vs) $\nu(C-S)$.

$Cd(S_2COEt)_2$: Yield 4.74 g (89 %) as a milky-white powder. 1H NMR (d_6 -DMSO, 25 °C): δ 4.34 (q, 2H, OCH_2 , $J = 7.07$ Hz), 1.30 (t, 3H, CH_3 , $J = 7.08$ Hz) ppm. $^{13}C\{^1H\}$ NMR (d_6 -DMSO, 25 °C): δ 229.2 (C_q), 72.3 (OCH_2), 14.0 (CH_3) ppm. IR (cm^{-1}): 1195 (vs) $\nu(C-O)$, 1029 (vs) $\nu(C-S)$.

Cd(S₂COiPr)₂: Yield: 4.48 g (78 %) as a yellow powder. ¹H NMR (d₆-DMSO, 25 °C): δ 5.12 (*sept*, 1H, OCH, J = 6.17 Hz), 1.30 (*t*, 6H, CH₃, J = 6.20 Hz) ppm. ¹³C{¹H} NMR (d₆-DMSO, 25 °C): δ 228.2 (C_q), 80.4 (OCH), 21.3 (CH₃) ppm. IR (cm⁻¹): 1202 (vs) ν(C–O), 1021 (vs) ν(C–S).

hmta: ¹H NMR (d₆-DMSO, 25 °C): δ 4.52 (*s*, 12H, CH₂) ppm. ¹³C{¹H} NMR (d₆-DMSO, 25 °C): δ 73.8 (CH₂) ppm. IR (cm⁻¹): 1456 (m) ν_{as}(C–H), 1369 (s) ν_s(C–H), 1234 (vs) ν(C–N).

3.2.3. Synthesis of Cd(S₂COR)₂(hmta)_n adducts, R = Me (8), Et (9) and iPr (10).

The methods employed for the preparation of the hmta adducts were similar and hence, only details for the experiments involving the R = Me precursor will be given. In separate experiments, to a suspension of Cd(S₂COMe)₂ (0.65 g) in ethanol (25 ml) was added 0.5, 1.0 and 2.0 molar equivalents of hmta in ethanol (25 ml). The resulting mixtures were stirred for 1 h at 50 °C on a hot-plate. After cooling to room temperature, the solution was filtered and the filtrate left for slow evaporation, yielding crystals typically after 3 days. The crystals obtained from each reaction were screened by PXRD. From the nine experiments, three new compounds were isolated.

Cd(S₂COMe)₂(hmta) (8). Yield: 0.51 g (55 %) as colourless crystals. Anal. Calc. for C₁₀H₁₈CdN₄O₂S₄: C, 25.72; H, 3.89; N, 12.00. Found: C, 25.44; H, 3.87; N, 11.69. ¹H NMR (d₆-DMSO, 25 °C): δ 4.60 (*s*, 12H, CH₂), 3.95 (*s*, 6H, OCH₃) ppm. ¹³C{¹H} NMR (d₆-DMSO, 25 °C): δ 230.0 (C_q), 73.4 (CH₂), 62.6 (OCH₃) ppm. IR (cm⁻¹): 1460 (m) ν_{as}(C–H), 1375 (w) ν_s(C–H), 1238 (s) ν(C–N), 1200 (vs) ν(C–O), 1016 (vs) ν(C–S).

Cd(S₂COEt)₂(hmta)_{0.5} (**9**). Yield: 1.26 g (74 %) as pale-yellow crystals. Anal. Calc. for C₁₈H₃₂Cd₂N₄O₄S₈: C, 25.44; H, 3.80; N, 6.59. Found: C, 25.12; H, 3.70; N, 6.54. ¹H NMR (d₆-DMSO, 25 °C): δ 4.58 (*s*, 12H, CH₂), 4.34 (*q*, 8H, OCH₂, J = 7.05 Hz), 1.30 (*t*, 12H, CH₃, J = 7.06 Hz) ppm. ¹³C{¹H} NMR (d₆-DMSO, 25 °C): δ 229.2 (C_q), 73.7 (CH₂), 72.3 (OCH₂), 14.0 (CH₃) ppm. IR (cm⁻¹): 1461 (*m*) ν_{as}(C–H), 1365 (*w*) ν_s(C–H), 1232 (*m*) ν(C–N), 1197 (*vs*) ν(C–O), 1014 (*vs*) ν(C–S).

Cd(S₂COiPr)₂(hmta) (**10**). Yield: 0.81 g (77 %) as pale-yellow crystals. Anal. Calc. for C₂₈H₅₂Cd₂N₈O₄S₈: C, 32.15; H, 5.01; N, 10.71. Found: C, 31.97; H, 5.07; N, 10.49. ¹H NMR (d₆-DMSO, 25 °C): δ 5.13 (*sept*, 2H, OCH, J = 6.17 Hz), 4.58 (*s*, 12H, CH₂), 1.30 (*t*, 12H, CH₃, J = 6.20 Hz) ppm. ¹³C{¹H} NMR (d₆-DMSO, 25 °C): δ 228.3 (C_q), 80.6 (OCH), 73.7 (CH₂), 21.3 (CH₃) ppm. IR (cm⁻¹): 1459 (*m*) ν_{as}(C–H), 1370 (*w*) ν_s(C–H), 1246 (*s*) ν(C–N), 1206 (*vs*) ν(C–O), 1013 (*vs*) ν(C–S).

3.2.4. X-ray data collection and structure determination

A Rigaku AFC12κ/SATURN724 diffractometer fitted with Mo Kα radiation (λ = 0.71073 Å) was employed to measure intensity data for **8** at 98 K. Data processing and absorption corrections were accomplished with CrystalClear ("CrystalClear. User Manual. Rigaku/MSI Inc.," 2005) and ABSCOR (Higashi, 1995), respectively. Intensity data for **9** and **10** were measured at 100 K on an Agilent Technologies SuperNova Dual CCD with an Atlas detector also fitted with Mo Kα radiation. Data processing and absorption correction were accomplished with CrysAlis PRO ("CrysAlisPro," 2014). With the use of SHELXS-97 (Sheldrick, 2008) and SHELXL-2014/7 (Sheldrick, 2015) programs integrated into WinGX (Farrugia, 2012), the structures were solved by direct methods and refined on *F*² by full-matrix least-squares with anisotropic displacement parameters for all non-hydrogen atoms. The C-bound H atoms were placed on stereochemical grounds and refined in the riding model approximation with *U*_{iso} = 1.2-

$1.5U_{eq}(\text{carrier atom})$. A weighting scheme of the form $w = 1/[\sigma^2(F_o^2) + (aP)^2 + bP]$ where $P = (F_o^2 + 2F_c^2)/3$ was introduced in each case. For **10**, owing to poor agreement, perhaps due to the effect of the beam-stop, two low angle reflections, *i.e.* (1 0 0) and (0 1 0), were omitted from the final refinement. Generally, relatively high motion was observed for the terminal methyl groups and in particular for C4. However, multiple sites could not be resolved in this low temperature (100 K) study. This was despite the observation that the maximum residual electron density peaks were located in this region of the structures, *i.e.* the maximum and minimum residual electron density peaks of 1.20 and 1.00 Å⁻³, respectively, were located 0.48 and 0.44 Å from the H4a and C4 atoms, respectively. Unit cell data, X-ray data collection parameters, and details of the structure refinement are given in Table 3.1. The programs ORTEP-3 for Windows (Farrugia, 2012), PLATON (Spek, 2009), and DIAMOND (Brandenburg, 2006) were also used in the analysis.

Table 3.1: Crystal data, data collection and refinement parameters for compounds **8–10**.

	8	9	10
Formula	C ₁₀ H ₁₈ CdN ₄ O ₂ S ₄ C ₁₄ H ₂₆ CdN ₄ O ₂ S ₄	C ₁₈ H ₃₂ Cd ₂ N ₄ O ₄ S ₈	
Formula weight	466.92	849.75	523.03
Crystal size (mm)	0.10 x 0.10 x 0.30	0.08 x 0.11 x 0.14	0.20 x 0.20 x 0.20
Crystal system	monoclinic	triclinic	triclinic
Space group	<i>C2/c</i>	<i>P1</i>	<i>P1</i>
<i>a</i> /Å	17.321(4)	9.8286(3)	9.6453(4)
<i>b</i> /Å	10.3733(18)	11.7331(3)	9.7342(5)
<i>c</i> /Å	11.744(2)	13.3667(3)	11.9457(4)
α /°	90	90.639(2)	85.258(3)
β /°	129.836(2)	90.981(2)	78.488(3)
γ /°	90	105.455(2)	69.138(4)
<i>V</i> (Å ³)	1620.3(6)	1485.29(7)	1026.88(8)
<i>Z</i>	4	2	2
<i>D_x</i> /g cm ⁻³	1.914	1.900	1.692
μ /mm ⁻¹	1.871	2.027	1.486
θ range/°	2.5–27.5	2.2–27.5	2.6–27.6
Reflections measured	5452	25768	17439
Independent reflections; <i>R</i> _{int}	1855; 0.020	6812; 0.028	4745; 0.047
Reflections with <i>I</i> > 2 σ (<i>I</i>)	1812	6170	4221
Number of parameters	99	332	230
<i>R</i> (<i>F</i>) [<i>I</i> > 2 σ (<i>I</i>) reflns]	0.019	0.019	0.029
<i>a</i> , <i>b</i> in wght scheme	0.021, 2.409	0.014, 0.599	0.026, 0.251
<i>wR</i> (<i>F</i> ²) (all data)	0.046	0.042	0.063
GoF(<i>F</i> ²)	1.07	1.04	1.04
$\Delta\rho_{\max, \min}$ (e Å ⁻³)	0.54, -0.62	0.51, -0.43	1.20, -1.00

3.3. Results and Discussion

3.3.1. Syntheses and spectroscopy

The reactions between $\text{Cd}(\text{S}_2\text{COR})_2$, $\text{R} = \text{Me, Et and iPr}$, and hmta yielded three new compounds regardless of the ratio between the reagents, *i.e.* 1:1, 2:1 and 1:2. The structures of $\text{Cd}(\text{S}_2\text{COMe})_2(\text{hmta})$ (**8**), $\text{Cd}(\text{S}_2\text{COEt})_2(\text{hmta})_{0.5}$ (**9**) and $\text{Cd}(\text{S}_2\text{COiPr})_2(\text{hmta})$ (**10**) were established by single crystal X-ray crystallography as discussed below. Powder X-ray patterns (PXRD) were measured on the powdered samples of the crystals isolated from all reactions. These were compared with the simulated patterns calculated based on the single crystal data (using the respective CIF's) obtained for **8–10** ("X'Pert HighScore Plus," 2009). The agreement between the experimental and calculated patterns for **8–10** indicates the single crystal results are representative of the isolated materials, see Appendix J.

The multiplicity and integration observed in the ^1H NMR spectra were consistent with the expected formulae. The resonances due to the CH_2 protons of hmta were observed as singlets at δ 4.60 (**8**) and 4.58 (**9** and **10**) compared with δ 4.52 ppm for hmta measured under the same conditions, perhaps indicating a small downfield shift upon coordination. Very small upfield shifts were noted in the $^{13}\text{C}\{^1\text{H}\}$ NMR spectra with δ (NCH_2) being 73.4 (**8**) and 73.7 (**9** and **10**) compared with δ 73.8 ppm for hmta. By contrast, in terms of the xanthate ligands, the ^1H and $^{13}\text{C}\{^1\text{H}\}$ NMR of **8–10** were practically indistinguishable from those recorded for $\text{Cd}(\text{S}_2\text{COR})_2$, $\text{R} = \text{Me, Et and iPr}$. Further discussion relating to the question whether hmta remains coordinated in solution is found below. At least, the appearance of a single resonance for the hmta molecules in the ^1H and $^{13}\text{C}\{^1\text{H}\}$ spectra of **8–10** indicates fluxional behaviour. The IR spectra (see Appendix K) showed characteristic absorptions, *i.e.* $\nu_{\text{as}}(\text{C-H})$, $\nu_{\text{s}}(\text{C-H})$ and $\nu(\text{C-N})$, due to hmta. In the same way, characteristic xanthate absorptions, *i.e.* $\nu(\text{C-O})$ and $\nu(\text{C-S})$, were observed, with systematic blue-shifts noted for the latter.

3.3.2. Crystal and molecular structures

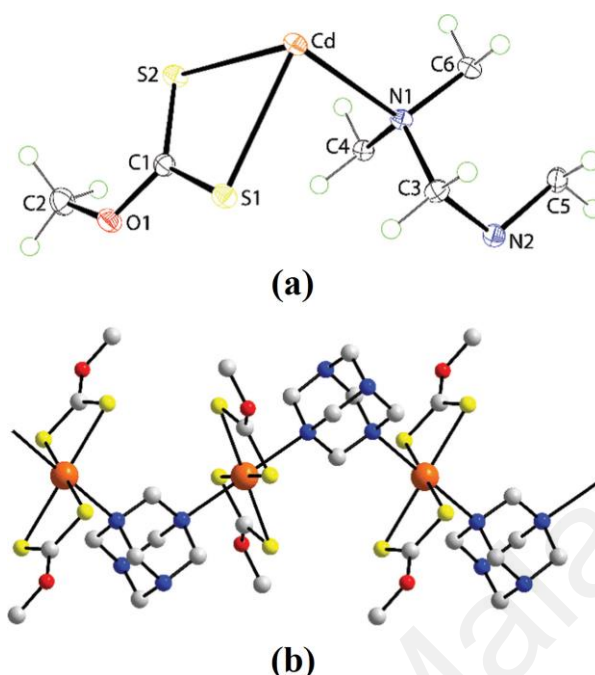


Figure 3.3: Asymmetric, and molecular structures of **8**.

(a) The asymmetric unit in the crystal structure of **8** showing atom-labelling and displacements ellipsoids at the 50% probability level; the Cd atom is located on a crystallographic centre of inversion and N4 is located about a 2-fold axis. (b) The one-dimensional CP in **8**. Selected geometric parameters: Cd–S1 2.6435(7), Cd–S2 2.6844(6) and Cd–N1 2.5476(15) Å.

The crystal structures of $[\text{Cd}(\text{S}_2\text{COMe})_2(\text{hmta})]_n$ (**8**), $[\text{Cd}(\text{S}_2\text{COEt})_2(\text{hmta})_{0.5}]_n$ (**9**) and $\text{Cd}(\text{S}_2\text{COiPr})_2(\text{hmta})$ (**10**) were established by X-ray crystallography; selected geometric parameters are given in the respective figure captions. The crystallographic asymmetric unit in the crystal structure of **8** comprises half of $\text{Cd}(\text{S}_2\text{COMe})_2$, with the Cd atom located on a crystallographic centre of inversion, and half of a molecule of hmta, as this is located about a 2-fold axis, Figure 3.3a, so that there is a 1:1 ratio between $\text{Cd}(\text{S}_2\text{COMe})_2$ and hmta. The methylxanthate ligand chelates the cadmium and forms almost symmetric Cd–S bond lengths. From symmetry, the cadmium atom is six-coordinate within a N_2S_4 donor set with the nitrogen atoms being mutually *trans*. Distortions from the ideal octahedral geometry are related to the acute bite angle of the xanthate ligand, S1–Cd–S2 is $68.572(13)^\circ$. The N4 ligand is μ_2 -bidentate, spanning two cadmium atoms so that a one-dimensional CP is formed. This is orientated along the

[101] direction and has a zigzag topology, Figure 3.3b. In the crystal packing, chains pack with no specific intermolecular interactions between them according to the criteria embodied in PLATON (Spek, 2009); the unit cell contents for **8** are shown in Figure 3.4.

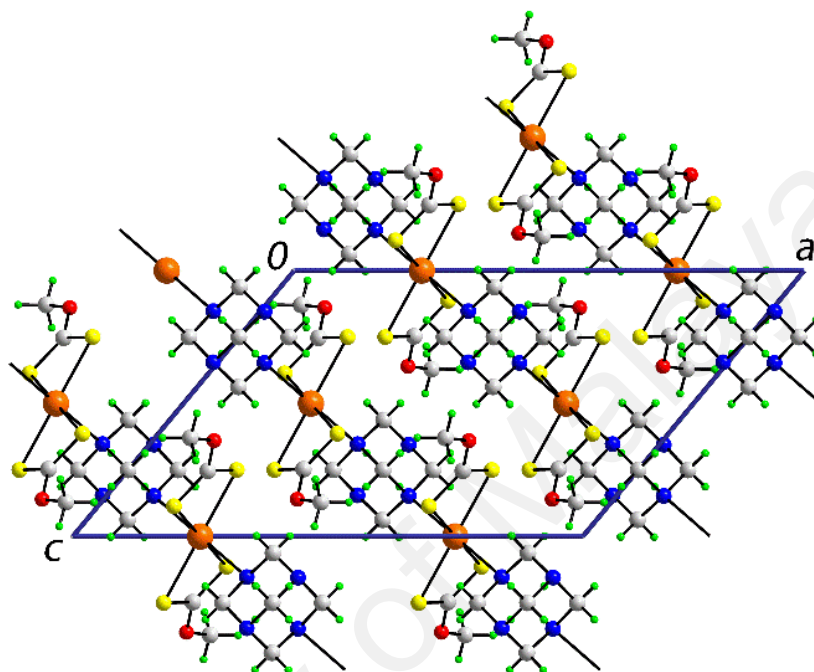


Figure 3.4: View of unit cell of **8**.

A view in projection down the b-axis of the unit cell contents for **8**, showing the supramolecular chains pack without specific interactions between them.

The asymmetric unit in the crystal structure of **9** comprises three distinct cadmium atoms, two of which lie on a centre of inversion with the other in a general position, four distinct ethylxanthate ligands and an entire molecule of hmta, Figure 3.5a, so that there is a 2:1 ratio between $\text{Cd}(\text{S}_2\text{COEt})_2$ and hmta. Each cadmium atom is chelated by two ethylxanthate ligands with the Cd–S bond lengths lying in a relatively narrow range, *i.e.* 2.6056(5) to 2.6683(4) Å. The Cd1 atom is also coordinated by a nitrogen atom from hmta, and from symmetry, each of the Cd2 and Cd3 atoms are coordinated by two nitrogen atoms. The Cd1 atom is penta-coordinated, the NS_4 donor set defining a distorted square pyramidal geometry with the value of $\tau = 0.12$, *cf.* $\tau = 0.00$ and 1.00 for ideal square pyramidal and trigonal bipyramidal geometries, respectively (Addison *et al.*,

1984). Distorted octahedral geometries defined by *trans*-N₂S₄ donor sets, as for **1**, are found for the Cd2 and Cd3 atoms. The Cd2 and Cd3 atoms are bridged by hmta ligands to form a one-dimensional zigzag chain along the *c*-axis, akin to that seen in **8**. The clear difference in **9** arises with the hmta ligand also connected to terminally bound Cd(S₂COEt)₂ entities, indicating that the hmta ligand is μ_3 -tridentate, Figure 3.5b. The terminally bound residues are crucial in assembling chains into a supramolecular layer in the *ac*-plane by C–H \cdots S interactions, which each forming two donor and two acceptor C–H \cdots S interactions, see Figure 3.6a and the figure caption for the geometric details characterising the interactions. The layers stack along the *b*-axis, being separated by hydrophobic interactions, Figure 3.6b.

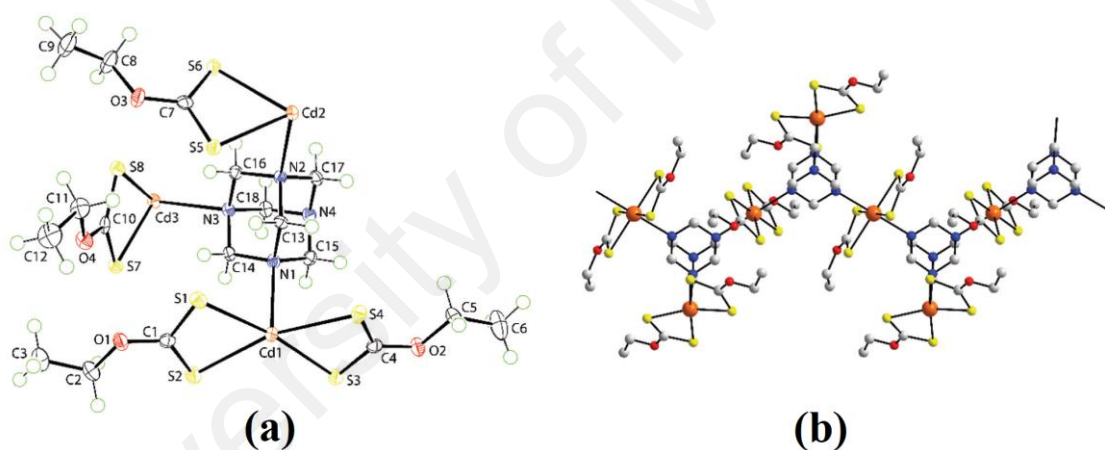


Figure 3.5: Asymmetric, and molecular structures of **9**.

(a) The asymmetric unit in the crystal structure of **9** showing atom-labelling and displacements ellipsoids at the 70% probability level; the Cd2 and Cd3 atoms are located on crystallographic centres of inversion. (b) The 1-D CP in **9**. Selected geometric parameters: Cd1–S1 2.6056(5), Cd1–S2 2.6502(5), Cd1–S3 2.6130(5), Cd1–S4 2.6671(5), Cd1–N1 2.4244(15), Cd2–S5 2.6189(5), Cd2–S6 2.6683(4), Cd2–N2 2.5682(14), Cd3–S7 2.6370(4), Cd3–S8 2.6574(4), Cd3–N3 2.5836(14) Å.

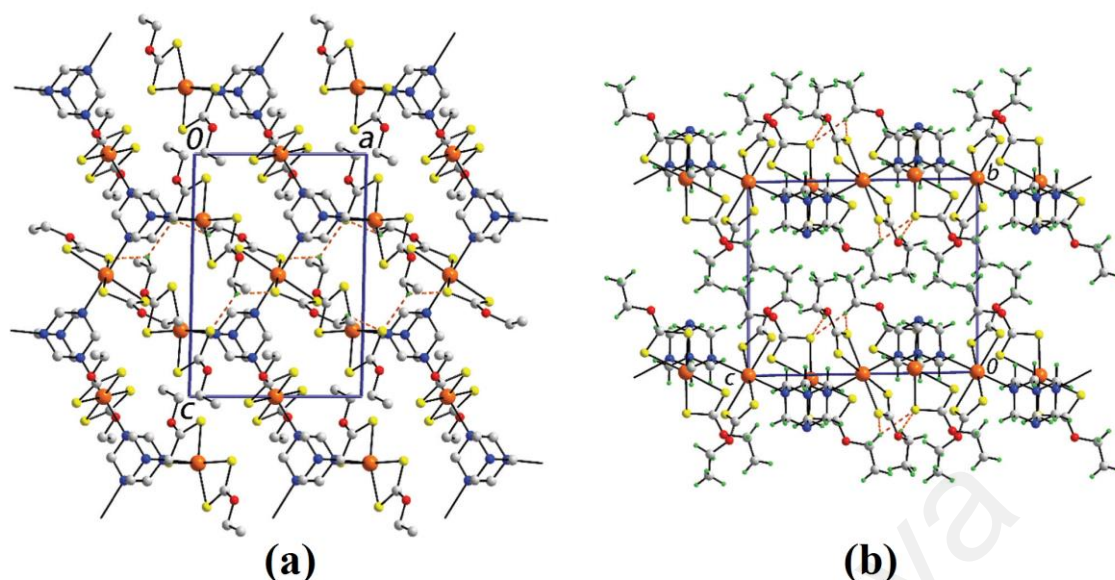


Figure 3.6: Molecular packing in **9**.

(a) The supramolecular layer in the *ac*-plane sustained by C–H···S interactions shown as orange dashed lines, and (b) a view in projection down the *b*-axis of the unit cell contents, showing the supramolecular layers pack along the *c*-axis without specific interactions between them. The geometric parameters for the C–H···S interactions: C5–H5a···S1ⁱ = 2.76 Å, C5···S1ⁱ = 3.4813(19) Å, with angle at H5a = 130° for *i*: -*x*, -*y*, 1-*z*; C5–H5a···S5ⁱ = 2.83 Å, C5···S5ⁱ = 3.544(2) Å, with angle at H5a = 130°; C8–H8b···S1ⁱⁱ = 2.78 Å, C8···S1ⁱⁱ = 3.540(2) Å, with angle at H8b = 134° for *ii*: -1+*x*, *y*, *z*.

The crystal structure of **10** comprises binuclear molecules disposed about a centre of inversion, Figure 3.7. One of the independent isopropylxanthate ligands is chelating, as for **8** and **9**, but the other chelates one cadmium atom while simultaneously bridging another in a $\mu_2\kappa^2$ -tridentate mode. The resulting NS₅ donor set defines an approximate octahedral geometry with distortions again being traced to the restricted bite angle of the xanthate ligands. In the crystal packing, molecules self-assemble into a supramolecular layer in the *ab*-plane being connected by C–H···N and C–H···S interactions, see Figure 3.8a. The layers stack along the *c*-axis, with no specific intermolecular interactions between them, see Figure 3.8b.

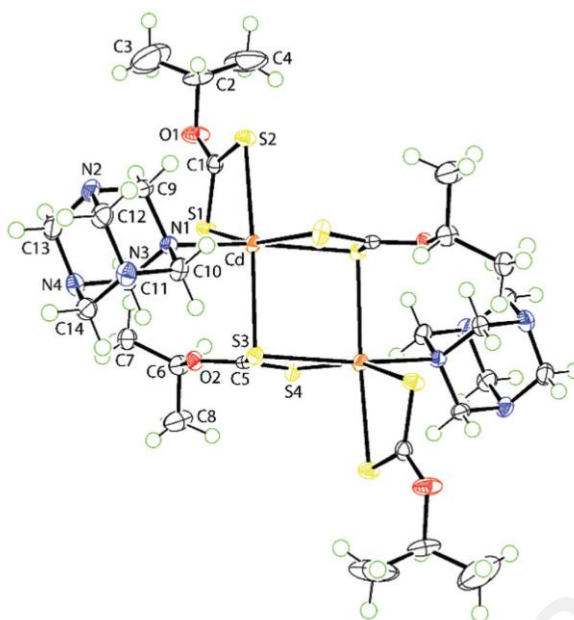


Figure 3.7: Molecular Structure of **10**.

The binuclear molecule in the crystal structure of **10** showing atom-labelling and displacements ellipsoids at the 50% probability level. The molecule is located about a crystallographic centre of inversion; unlabelled atoms are related by the symmetry operation $i: 1-x, 1-y, 1-z$. Selected geometric parameters: Cd–S1 2.6348(6), Cd–S2 2.7107(7), Cd–S3 2.7594(6), Cd–S3ⁱ 2.7101(6), Cd–S4ⁱ 2.7065(6), Cd–N1 2.395(2) Å.

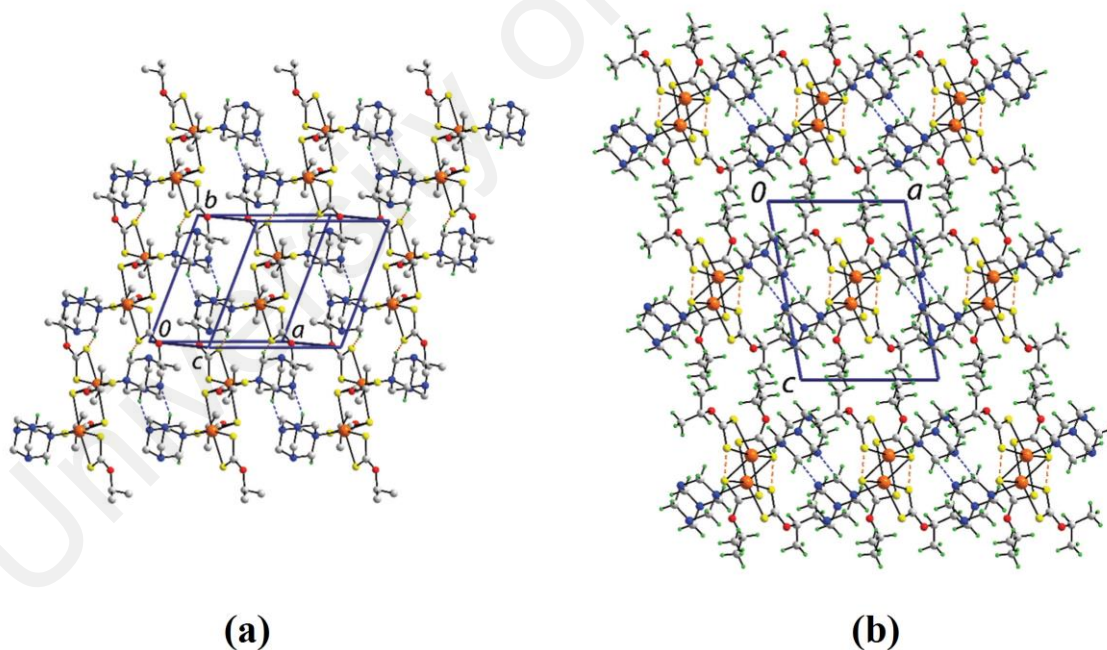


Figure 3.8: Molecular packing in **10**.

(a) The supramolecular layer in the ab -plane sustained by C–H \cdots N and C–H \cdots S interactions shown as blue and orange dashed lines, respectively, and (b) a view in projection down the b -axis of the unit cell contents, showing the supramolecular layers pack along the c -axis without specific interactions between them. Geometric parameters: C10–H10b \cdots N3ⁱⁱ = 2.57 Å, C10 \cdots N3ⁱⁱ = 3.440(3) Å with angle at H10b = 147° for ii: 2- x , 1- y , 1- z ; C9–H9b \cdots S2ⁱ = 2.77 Å, C9 \cdots S2ⁱ = 3.725(2) Å with angle at H9b = 163° for i: 1- x , 2- y , 1- z . In (a), only hydrogen atoms participating in the intermolecular interactions are shown.

The structures of one-dimensional, zigzag CPs **8** and **9** complement the sole previous example of a linear CP constructed from $\text{Cd}(\text{S}_2\text{COiPr})_2$ and a bridging 4,4'-bipyridine ligand, $[\text{Cd}(\text{S}_2\text{COiPr})_2(4,4'\text{-bipy})]_n$ (Abrahams *et al.*, 1990). The zero-dimensional aggregate seen in **10** has only one precedent in the literature, namely in the structure of $[\{\text{Cd}(\text{S}_2\text{COEt})_2\}_2\text{L}_2]$, where L is the S-bound thiourea derivative, bis(4-methoxyphenyl)thiourea (Sun *et al.*, 1994), but resembles the almost universally adopted structural motif adopted by binary cadmium dithiocarbamates (Casas *et al.*, 1989; Cox *et al.*, 1999; Dee *et al.*, 2002; Domenicano *et al.*, 1968; Glinskaya *et al.*, 1999; Ivanov *et al.*, 2006; A. V. Ivanov *et al.*, 2005; Ivanov *et al.*, 2008; F.-F. Jian *et al.*, 1999; F. Jian *et al.*, 1999; Kant *et al.*, 2012; Konarev *et al.*, 2006; Manohar *et al.*, 2005; Saravanan *et al.*, 2004; Thirumaran *et al.*, 2012; Yin *et al.*, 2004; Zhong *et al.*, 2004). As revealed in the previously mentioned review of the inverse coordination propensities of hmta (Kirillov, 2011), μ_2 -, μ_4 - and μ_4 -bridging modes have been observed in CPs but terminally bound examples are comparatively rare. In the context of 1,1'-dithiolate chemistry, there are no literature precedents of cadmium xanthates or dithiocarbamates with hmta but there are three examples of zero-dimensional aggregates for cadmium dithiophosphates and dithiophosphinates (S_2PR_2) with hmta. Thus, a mononuclear bis adduct with hmta coordinating in a monodentate fashion was reported in the structure of $\text{Cd}[\text{S}_2\text{P}(\text{OEt})_2]_2(\text{hmta})_2$ (Shimoi *et al.*, 1982). There are two binuclear hemi adducts with hmta, namely $\{\text{Cd}[\text{S}_2\text{P}(\text{O-sBu})_2]_2\}_2(\text{hmta})$ (Bolundut *et al.*, 2008) and $\{\text{Cd}[\text{S}_2\text{P}(\text{O-iBu})_2]_2\}_2(\text{hmta})$ (Kokina *et al.*, 2010), each having hmta in the μ_2 -bidentate bridging mode.

3.3.3. Rationale for the adoption of different structural motifs in 8–10

Having discussed the structures of **8–10**, the challenge remains to rationalise their formation. First and foremost, DFT calculations show that the electronic profiles of alkylxanthate ligands are independent of R present in **8–10** (Buntine *et al.*, 2003). The difference between CPs **8** and **9** on the one hand, and that of **10** is readily explained in terms of relative size of the iPr substituent. Simply, and consistent with literature precedents (Lai *et al.*, 2002; Lai, Liu, *et al.*, 2004; Lai *et al.*, 2003; Tiekink, 2003, 2006), the bulk of the iPr residue precludes the supramolecular association adopted by the structures with the smaller R groups. The rationalisation of the different compositions of **8** and **9** is more subtle. Figure 3.9 shows end- and side-on views of the CPs. To a first approximation, the CPs are very similar and the Cd...Cd separations vindicate this conclusion, being 6.66 and 6.68 Å for **8** and **9**, respectively. The end-on view of **8** is instructive in that it reveals a very compact arrangement with the methyl groups shielding the non-coordinating nitrogen atoms of hmta from further interaction. By contrast, a more open arrangement is noted in the end-on view of **9**. Presumably, the larger ethyl groups in **9** preclude the adoption of the tight-knit structure in **8**. The common feature immediately apparent from the side-on views in Figure 3.9 is the relative orientation of the –hmta–Cd–hmta–Cd– backbones in both structures. The clear difference relates to the relative orientations of the xanthate ligands. While successive xanthate ligands must be twisted in order to avoid steric clashes between the R substituents, the successive xanthates are not in opposite orientations in **9** and this opens voids in the polymer to allow the additional coordination of the pendent Cd(S₂COEt)₂ entities. The crystal packing efficiencies were calculated with PLATON (Spek, 2009). These are 72.4, 70.9 and 69.2%, respectively, again highlighting the relatively compact structure and efficient packing in **8**.

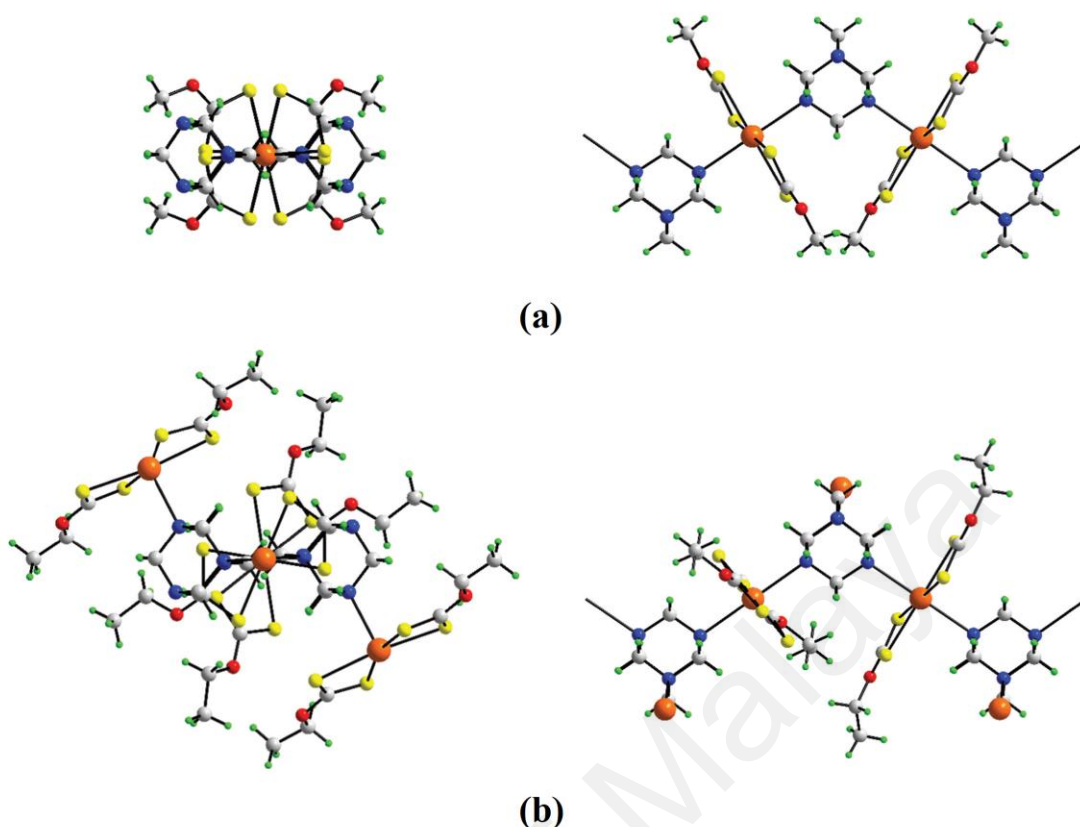


Figure 3.9: End-on and side-on views of the CPs in (a) **8** and (b) **9**.

In the side-on image for **9**, only the cadmium atoms of the pendent $\text{Cd}(\text{S}_2\text{COEt})_2$ entities are shown for reasons of clarity.

3.3.4. UV-visible and photoluminescence studies

In order to probe further whether N4 remained coordinated in solution, the UV-visible characteristics of **8–10** were compared with those of the parent $\text{Cd}(\text{S}_2\text{COR})_2$ compounds, see Table 3.2 for data. The spectra were obtained in ethanol:acetonitrile (1:1) solutions, each at concentrations of 10 and 100 μM , and were very similar to each other. An intense, high-energy band was observed at 296 nm for each of **8–10**. This transition is assigned as an intra-ligand $\pi \rightarrow \pi^*$ charge transfer (Kang *et al.*, 2010). Low intensity bands were observed around 360 nm which are assigned to ligand metal charge transfer (LMCT) bands (Kang *et al.*, 2010). The similarity of the spectra is consistent with lack of significant influence of the alkyl group on electronic transitions (Bevilacqua *et al.*, 1994; Buntine *et al.*, 2003; Kang *et al.*, 2010). The spectra of the $\text{Cd}(\text{S}_2\text{COR})_2$ compounds exhibit very similar absorptions but with distinctive values of ϵ in the case of

the R = Me and Et compounds but, with near equivalence when R = iPr. More distinctive responses were evidenced from a photoluminescence study.

Table 3.2: UV-visible (λ_{max} , nm; ϵ , Lcm⁻¹mol⁻¹) and photoluminescence data (λ , nm; λ_{ex} = 295 and 360 nm) for Cd(S₂COR)₂, R = Me, Et and iPr, and **8–10**.

Compd.	solution		solid-state (77 K)		
	UV-Vis	photoluminescence			
	λ_{max}	λ_{em} (295)	λ_{em} (360)	λ_{em} (295)	λ_{em} (360)
Cd(S ₂ COMe) ₂	296 (11,594)	707	612	589	598
	358 (254)			693	694
Cd(S ₂ COEt) ₂	298 (18,295)	-	642	703	490
	362 (137)				650
Cd(S ₂ COiPr) ₂					698
	299 (20,471)	-	612	493	614
	362 (145)			605	
8				697	
	296 (20,270)	-	554	609	586
	362 (155)			701	
9					
	296 (35,150)	710	554	489	542
	360 (386)			709	
10					
	296 (21,680)	-	-	661	602
	363 (146)			693	

Photoluminescence measurements were carried out at room temperature on 1 mM solutions in acetonitrile:ethanol (1:1) with excitation wavelengths of 295 and 360 nm, Table 3.2. With λ_{ex} = 295 nm, only the R = Me compounds showed emissions at around 710 nm. With λ_{ex} = 360 nm **8** and **9** showed strong emissions at 554 nm; **10** was non-emissive. By contrast, the Cd(S₂COR)₂ compounds showed emissions at wavelengths greater than 610 nm. This distinctive behaviour suggests that the N4 ligands remain coordinated in **8–10**, at least in acetonitrile:ethanol (1:1) solutions.

Photoluminescence measurements were also carried out in the solid-state at the same excitation wavelengths, Table 3.2. Consistent with expectation, blue-shifts and increasing intensities of the bands were observed as the temperatures at which the experiments were measured were decreased. Representative spectra recorded at 77 K for **8–10** are given in Figure 3.10 and show that while distinctive bands for **9** and, especially, zero-dimensional **10** were observed, those for **8** were poorly resolved. With $\lambda_{\text{ex}} = 295$ nm, two bands were observed for each of **8–10** with the high-energy band varying from a low 489 for **9** to a high 661 for **10**. A low-energy band, which was significantly more intense in **9** but had comparable intensities for **8** and **10**, appeared around 700 nm. A single emission appeared when λ_{ex} was 360 nm. The solid-state spectra for **8–10** are quite distinct from those observed for $\text{Cd}(\text{S}_2\text{COR})_2$ indicating that the presence of the hmta ligand influences the electronic transitions involving the xanthate chromophores.

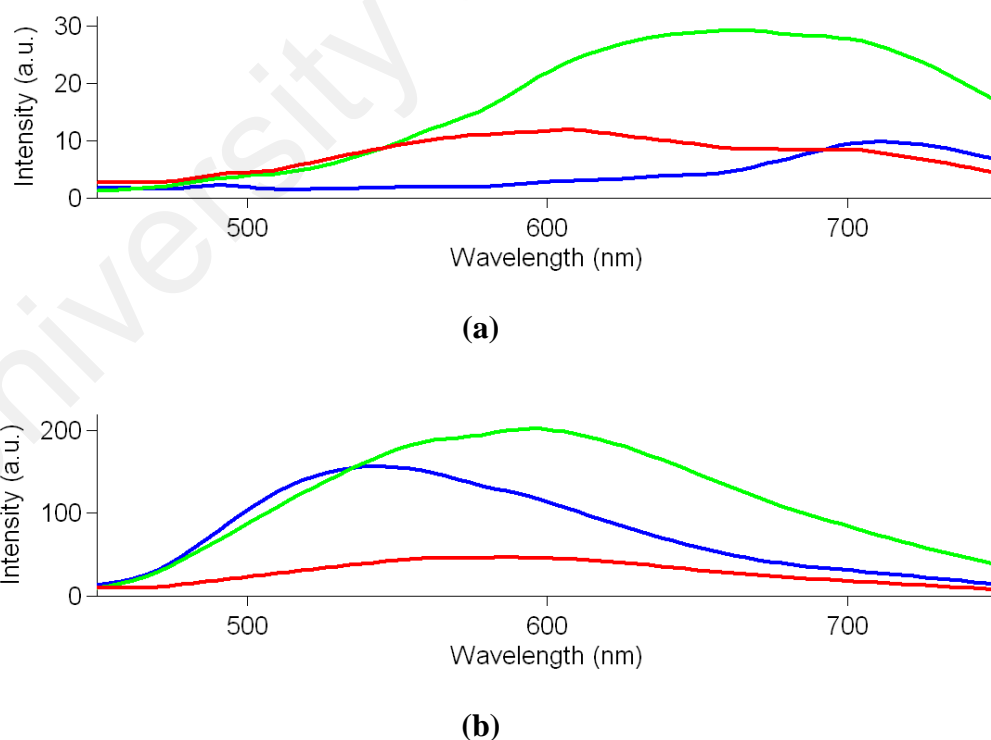


Figure 3.10: Solid-state emission spectra for **8–10**.

(a) $\lambda_{\text{ex}} = 295$ nm and (b) $\lambda_{\text{ex}} = 360$ nm. The red spectrum corresponds to **8** ($\text{R} = \text{Me}$), blue to **9** ($\text{R} = \text{Et}$) and green to **10** ($\text{R} = \text{iPr}$).

3.3.5. Thermogravimetric analysis

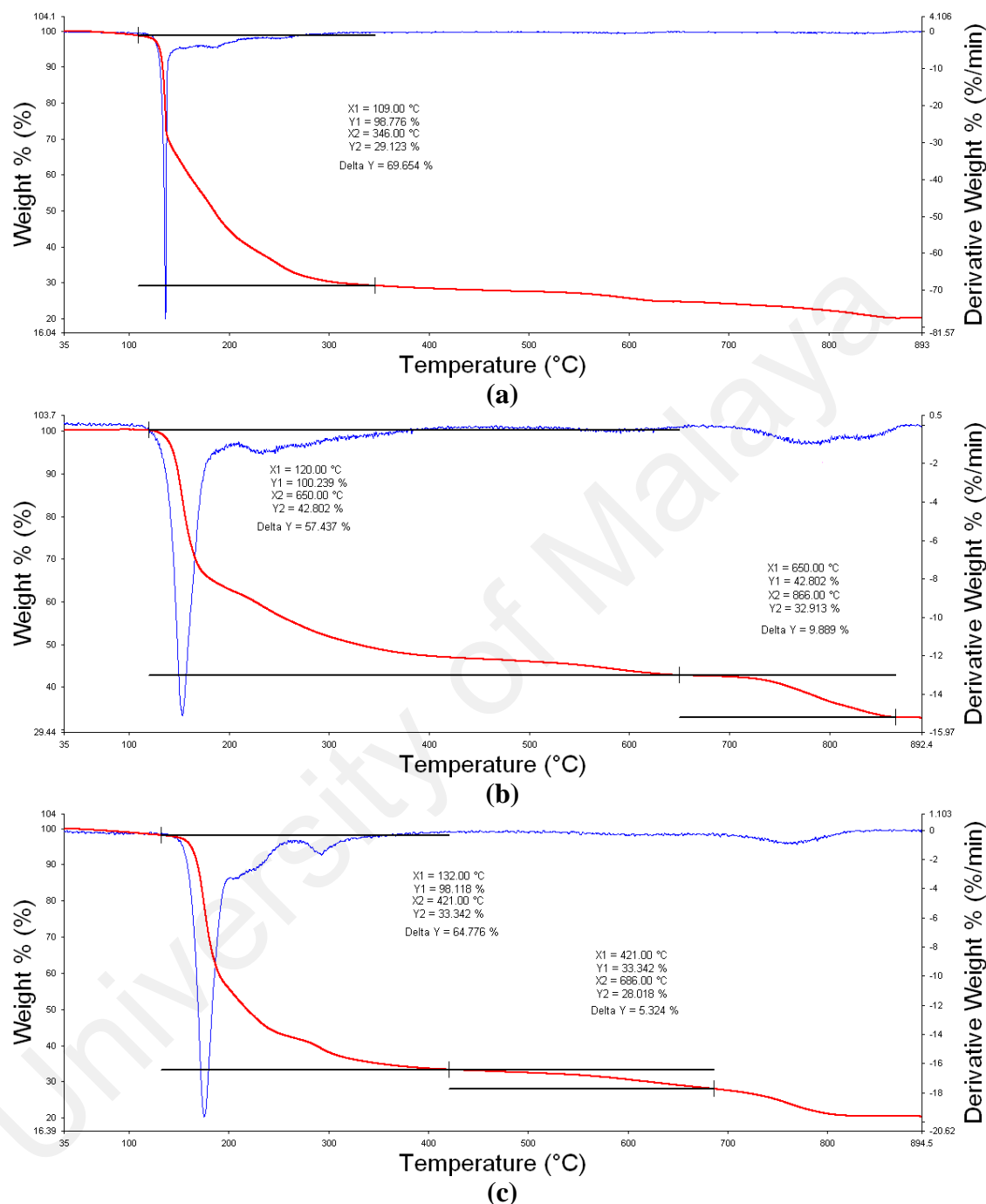


Figure 3.11: TGA (red trace) and DTA (blue trace) for (a) **8**, (b) **9** and (c) **10**.

Traces for the thermogravimetric analysis for **8–10** are given in Figure 3.11. The decomposition mechanisms of **8–10** were relatively straightforward and led to CdS. Decomposition of **8** to CdS was in one step between 109 and 346 °C, with weight loss of 69.7 % cf. calcd. 69.1%. Two discernible steps were noted for **9**. The first step between

120 and 650 °C correlated with the loss of three xanthate anions and hmta with a weight loss of 57.4 % cf. calcd. 59.3 %. The second step between 650 and 866 °C left a 32.9 % residue cf. calcd. 34.0 % corresponding to CdS. The decomposition mechanism of **10** was basically the same as for **9** with three xanthates and two hmta molecules being lost initially between 132 and 421 °C (weight loss 64.8 % cf. calcd. 65.6 %). The following step between 421 and 686 °C left a 28.0 % residue cf. calcd. 27.6 % corresponding to CdS. Cadmium xanthates and nitrogen adducts are well known to be useful as synthetic precursors for CdS nanoparticles (Barreca *et al.*, 2005; Chesman *et al.*, 2014; Onwudiwe *et al.*, 2014), and the results herein suggest that hmta adducts are able to produce CdS relatively cleanly.

3.4. Conclusion

Three new compounds have been isolated from 1:1, 1:2 and 2:1 solutions containing $\text{Cd}(\text{S}_2\text{COR})_2$, R = Me, Et and iPr, and hmta. Compound **8** is a CP with a zig-zag topology. The basic structure of **9** is as for **8** but with pendant $\text{Cd}(\text{S}_2\text{COEt})_2$ entities, indicating the hmta ligand is μ_3 -tridentate. A binuclear molecule is observed in **10** with terminally bound hmta ligands. The zero-dimensional aggregate in **10** is correlated with the steric bulk of the iPr groups. The compact arrangement in **8** cannot accommodate the larger ethyl groups in **9** which enables additional coordination of $\text{Cd}(\text{S}_2\text{COEt})_2$ entities. This study expands the range of cadmium xanthates with potentially bridging ligands and reveals unexpected and interesting structural diversity suggesting further investigations are well warranted.

CHAPTER 4: A COMBINED CRYSTALLOGRAPHIC AND COMPUTATIONAL STUDY OF THE PERSISTENCE OF C–H $\cdots\pi$ (CHELATE RING) INTERACTIONS IN THE CRYSTAL STRUCTURES OF PALLADIUM BIS (O-ALKYLDITHIOCARBONATE)S, Pd(S₂COR)₂

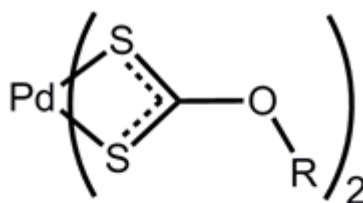
4.1. Introduction and Literature Review

The 1,1'-dithiolates are a class of uninegative ligands comprising, for example, dithiocarbamates, dithiocarbonates (hereafter, xanthates) and dithiophosphates, Figure 1.1a-c (Haiduc, 2003). Transition metal and main group element coordination compounds of these ligands have been thoroughly studied over the years and have been the subject of several bibliographic reviews (Haiduc *et al.*, 1996; Heard, 2005; Hogarth, 2005; Tiekink *et al.*, 2005). Mitigating their wide application in the generation of CPs is the propensity of dithiocarbamate coordination compound to be stabilised by the canonical structure shown in Figure 1.1e, which may contribute up to 40% to the overall resonance structure. The adoption of this canonical structure has two effects. Firstly, dithiocarbamates prove to be very effective chelating agents with the consequence they have a reduced tendency to bridge, compared with xanthates and dithiophosphates (Lai *et al.*, 2003; Tiekink, 2003, 2006). Secondly, the enhanced donation of electrons to the metal centre reduces the Lewis acidity of the latter which in turn diminishes the likelihood of the formation of additional coordinate bonds to, for example, bridging bipyridine-type ligands, ubiquitous in CPs (Adarsh *et al.*, 2012; Du *et al.*, 2013). Conversely, the enhanced metalloaromatic (Masui, 2001) behaviour of chelate rings formed by dithiocarbamate ligands enables the formation of C–H $\cdots\pi$ (chelate ring) interactions in their crystal structures.

For 1,1'-dithiolate compounds, C–H $\cdots\pi$ (MS₂C) interactions, where MS₂C represents the four-membered chelate ring, were possibly first commented upon in the crystal structures of adducts of cadmium(II) bis(xanthates) (Chen *et al.*, 2003) and subsequently identified in a range of transition metal and main group element bis(1,1'-

dithiolate) analogues (Tiekink *et al.*, 2005; Tiekink *et al.*, 2011; Zukerman-Schpector & Tiekink, 2012). These latter bibliographic surveys showed C–H $\cdots\pi$ (MS₂C) interactions occurred most frequently in dithiocarbamates compared with other 1,1'-dithiolates, consistent with significant π -character in the chelate rings formed by these ligands owing to the significant contribution of the canonical structure shown in Figure 1.1e, certainly compared with the putative structure shown in Figure 1.1f for the xanthate anion, and could feature independently of other readily identifiable intermolecular interactions to sustain zero-, one-, two- and three-dimensional architectures, with chains and layers being dominant (Zukerman-Schpector & Tiekink, 2012). A variety of other chelate rings are also known to participate in analogous interactions (Basu Baul *et al.*, 2013; Bogdanović *et al.*, 2002; Câmpian *et al.*, 2013; Gupta *et al.*, 2014; Jiang *et al.*, 2005; Medaković *et al.*, 2012; Medaković *et al.*, 2004; Singh *et al.*, 2013) with the most extensive study being upon chelate rings formed by acetylacetonate and derivatives in square planar transition metal coordination compound (Milčič *et al.*, 2006) Zarić *et al.* (Nangia, 2010) estimate that the energy of association of C–H $\cdots\pi$ (MO₂C₂) is in the range 6–11 kJ mol⁻¹ which is comparable to that for C–H $\cdots\pi$ (arene) of 1–8 kJ mol⁻¹ in organic structures (Nangia, 2010).

In the original survey of the prevalence of C–H $\cdots\pi$ (MS₂C) interactions in metal/main group bis(1,1'-dithiolate)s, for xanthate derivatives it was noted that i) the shortest H \cdots ring centroid(MS₂C) separation was observed in the crystal structure of Pd(S₂CO-iPr)₂ (Singhal *et al.*, 2007) and ii) a relatively large number of nickel(II) xanthate exhibited C–H $\cdots\pi$ (NiS₂C) interactions (Zukerman-Schpector & Tiekink, 2012). In this context, it was thought of interest to evaluate the propensity of C–H $\cdots\pi$ (PdS₂C) interactions in the crystal structures of a series of Pd(S₂COR)₂ compounds, *i.e.* **11–22** (Figure 4.1).



R:

(11)	Me	(17)	n-Pent
(12)	Et	(18)	i-Pent
(13)	n-Pr	(19)	neo-Pent
(14)	i-Pr	(20)	n-Hex
(15)	n-Bu	(21)	i-Hex
(16)	i-Bu	(22)	neo-Hex

Figure 4.1: Chemical structures of the palladium(II) bis(xanthate)s (**11–22**) investigated herein.

Palladium xanthates have been investigated previously owing to interest in developing non-platinum based anti-cancer agents (Friebolin *et al.*, 2005) and to investigate their utility as synthetic precursors for the generation of PdS nanocrystals (Singhal *et al.*, 2007). Several crystal structures are available for $\text{Pd}(\text{S}_2\text{COR})_2$ compounds, namely $\text{R} = \text{Me}$ (Shahzadi *et al.*, 2009; Singhal *et al.*, 2007), Et (Ara *et al.*, 2003), iPr (Singhal *et al.*, 2007), CH_2CF_3 (Romanenko *et al.*, 1979) and 2,4,6-trimethylphenyl (Chen *et al.*, 1978). Herein, the crystal structures of **11–22** are described, their crystal packing patterns analysed. Theoretical methods have been employed to estimate the energy of attraction associated with a $\text{C-H}\cdots\pi(\text{PdS}_2\text{C})$ interaction.

4.2. Methodology

4.2.1. Synthesis

Details of synthesis, yield, physiochemical and spectroscopic (IR, ^1H and $^{13}\{^1\text{H}\}$ NMR and UV-Vis) data are given in Appendix L (L.1- L.12).

4.2.2. X-ray crystallography

Intensity data were measured at 100 K on an Agilent Technologies SuperNova Dual CCD with an Atlas detector fitted with Mo K α ($\lambda = 0.71073$ Å) or Cu K α ($\lambda = 1.54184$ Å) radiation. Data processing and absorption corrections were accomplished with CrysAlis PRO ("CrysAlisPro," 2014). With the use of SHELX programs (Sheldrick, 2015) integrated into WinGX (Farrugia, 2012), the structures were solved by direct methods and refined on F^2 by full-matrix least-squares with anisotropic displacement parameters for all non-hydrogen atoms. The C-bound H atoms were placed on stereochemical grounds and refined in the riding model approximation with $U_{\text{iso}} = 1.2-1.5U_{\text{eq}}(\text{carrier atom})$. A weighting scheme of the form $w = 1/[\sigma^2(F_o^2) + (aP)^2 + bP]$ where $P = (F_o^2 + 2F_c^2)/3$ was introduced in each case. For **11**, the (0 1 1) reflection was omitted from the final refinement owing to poor agreement. Several of the refinements exhibited residual electron density peaks greater than $1 \text{ e } \text{\AA}^{-3}$. For **12**, the maximum and minimum residual electron density peaks of 0.83 and $1.14 \text{ e } \text{\AA}^{-3}$ were located 1.17 and 0.71 Å from the S1 and Pd atoms, respectively. For **14**, 1.68 and $0.85 \text{ e } \text{\AA}^{-3}$, respectively, from S2 and Pd atoms; **16**, 0.82 and $-1.60 \text{ e } \text{\AA}^{-3}$, 0.78 and 0.83 Å from Pd; **17**, 1.30 and $3.02 \text{ e } \text{\AA}^{-3}$, 0.89 and 0.85 Å from Pd; **18**, 1.18 and $1.23 \text{ e } \text{\AA}^{-3}$, 0.96 and 0.87 Å from Pd; **20**, 0.91 and $1.05 \text{ e } \text{\AA}^{-3}$, 1.00 and 0.94 Å from Pd; **22**, 4.37 and $2.03 \text{ e } \text{\AA}^{-3}$, 0.96 and 0.89 Å from Pd. Details of unit cell data, X-ray data collection and structure refinement are given in Appendix M. The programs ORTEP-3 for Windows (Farrugia, 2012), PLATON ("CrysAlisPro," 2014; Farrugia, 2012; Sheldrick, 2015) and DIAMOND (Brandenburg, 2006) were also used in the analysis.

4.3. Results and Discussion

Compounds **11–22** were prepared in crystalline form in good yields. Full details of synthesis, basically the metathetical reaction between $\text{Pd}(\text{NO}_3)_2$ and the potassium salt of the respective xanthate, and characterisation are given in Appendix L. Allowing for

differences in composition, there is significant homogeneity in the spectroscopic characteristics. The key results of the characterisation relate to the narrow range of the chemical shifts due to S₂CO in the ¹³C{¹H} NMR, *i.e.* 232.7- 234.7 ppm, and the similarity of these to the equivalent chemical shifts for the respective uncoordinated xanthate anions (recorded in D₂O) indicating a high degree of delocalisation of π -electron density over the PdS₂C atoms. The UV-Vis spectra were also very similar to each other, consistently exhibiting four absorptions (Garje *et al.*, 2003; Mohamed *et al.*, 2004; Winter, 1980). Two intense high-energy bands in the narrow ranges 236-238 and 282-285 nm are assigned to metal-ligand charge-transfer $n \rightarrow \sigma^*$ and intra-ligand $\pi \rightarrow \pi^*$ transitions, respectively. Weaker ligand-metal charge-transfer (CT, $n \rightarrow \pi^*$) bands are observed in the range 378-381 nm, and even weaker $d-d$ (¹A_{1g} \rightarrow ¹E_g) transitions occur in the range 448-461 nm. In order to confirm these assignments, Gaussian (Frisch *et al.*, 2009) calculations were run to confirm the source of the observed electronic transitions. The UV-Vis spectrum for the molecule in **13** (R = nPr) was calculated using time-dependent DFT. The geometry was relaxed using B3LYP/6-31+g(d,p) (Becke, 1993; Lee *et al.*, 1988) except for Pd, for which aug-cc-pVDZ-PP (Peterson *et al.*, 2005) was used. Sixty singlet-singlet vertical transitions were calculated. A polarizable continuum model (PCM) (Tomasi *et al.*, 2005) was used in order to reproduce the effects of the solvent (acetonitrile). The resulting spectrum is shown in Figure 4.2, which was calculated using the Gausssum program (O'Boyle *et al.*, 2008). The calculated high-energy transitions have wavelengths of 286.4 nm and 224.3 nm, in excellent agreement with the experimental values (284 nm and 237 nm, respectively). The most intense absorption (284 nm) can be clearly identified as being derived from the π -orbitals in the chelate (PdS₂C) ring. The remaining transitions, including the 237 nm one, involve charge transfer excitations between Pd and the xanthate ligands.

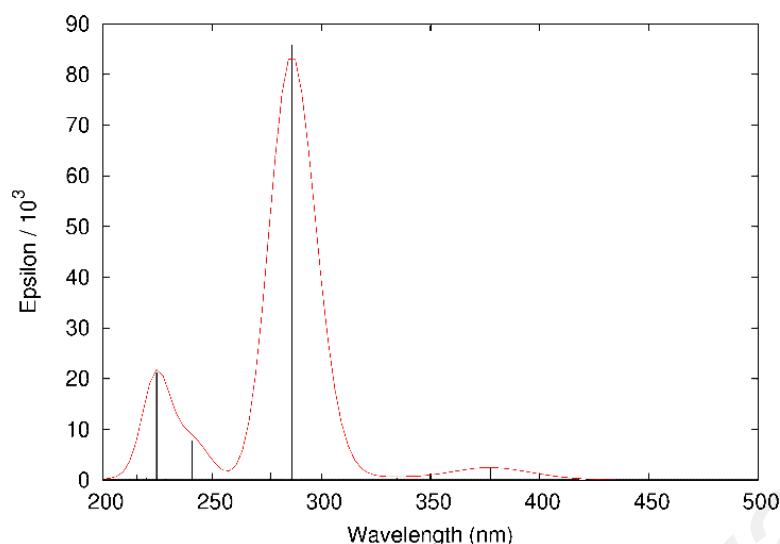


Figure 4.2: Calculated UV/visible spectrum for bis(O-n-propylxanthato)palladium(II), [Pd(S₂COPr)₂] (**13**).

The NMR and UV-Vis data suggest the xanthate ligands have a very similar electronic profile which is independent of the alkyl group and consistent with the results of their geometry-optimised structures (Buntine *et al.*, 2003). In keeping with the above, the molecular structures of **11–22** are also very similar. The structures of **11**, **12** and **14** have been described previously. New data are reported here, recorded at low temperature and under similar experimental conditions, in order to obtain a consistent data set of 12 structures. Compound **11** has been described twice (Shahzadi *et al.*, 2009; Singhal *et al.*, 2007), and the new results are consistent with these. The structure of **12** has been described in both centrosymmetric *Pbca* (Ara *et al.*, 2003) and non-centrosymmetric *Pca*₂₁ (Wang *et al.*, 2005). The centrosymmetric model is employed herein. Finally, the original report (Singhal *et al.*, 2007) of the structure of **14** is matched by the new determination.

4.3.1. Molecular Structures

The molecular structure of **18**, being an exemplar of the remaining Pd(S₂COR)₂ structures, is illustrated in Figure 4.3; illustrations of all molecular structures are given in Appendix L. The asymmetric unit of each of **11** and **13** comprises an entire molecule, whereas the Pd atom in the remaining structures is located on a centre of inversion. In

each of **11–22** the Pd atom is chelated by two xanthate ligands which define a square planar geometry. Selected interatomic parameters are collated in Appendix N from which it can be seen that the range of Pd–S bond lengths is narrow, *i.e.* 2.3210(6)–2.3432(15) Å, indicating that the xanthate ligands are symmetrically chelating, as indicated by the solution spectroscopy. Reflecting this is the experimental equivalence of the associated C–S bond lengths, which lie in the range 1.693(5)–1.706(3) Å. In spite of the similarity in the molecular structures, disparate crystal packing patterns are observed, as discussed below.

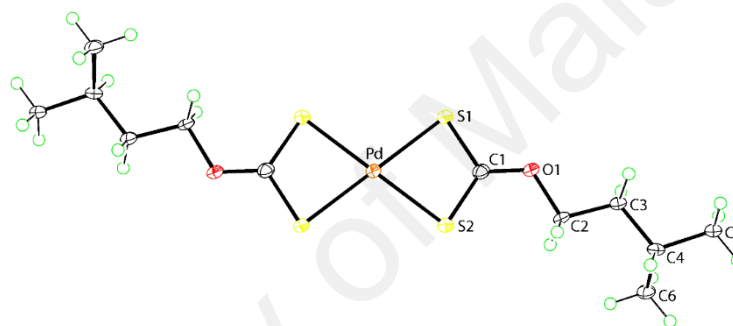


Figure 4.3: Molecular structure of **18**.

An exemplar of the molecular structures described herein, showing the atom labelling and displacement ellipsoids at the 50% probability level. The molecule is located about a centre of inversion with the unlabelled atoms related by the symmetry operation: 1-x, 1-y, 1-z.

4.3.2. Supramolecular Structures

Compounds **11–22** crystallise in five different crystal packing patterns that can be roughly divided into those structures that exhibit intermolecular Pd \cdots S or C–H \cdots S interactions and those that do not. In **11**, R = Me, with no crystallographically imposed symmetry in the molecule, centrosymmetrically related molecules are connected into dimeric aggregates by Pd \cdots S1ⁱ secondary interactions (Alcock, 1972), Figure 4.4a; symmetry operation: 1-x, 2-y, 1-z. The Pd \cdots S1ⁱ separation of 3.3165(13) Å is within the sum of the van der Waals radii of Pd (1.63 Å) and S (1.80 Å), *i.e.* 3.43 Å (Bondi, 1964). Molecules assemble into layers that stack along the b-axis with no directional interactions

between them in accord with the criteria embodied in PLATON (Spek, 2003); see Figure 4.5. However, it is noted that there are weak $S1 \cdots S2^{ii}$ interactions of $3.6206(18) \text{ \AA}$, which are just beyond the sum of the van der Waals radii for sulphur, that assemble dimeric aggregates into rows along the a-axis; ii: $-1+x, y, z$. The second molecule without crystallographically imposed symmetry is **13**. These, too, assemble into centrosymmetric dimeric aggregates via $Pd \cdots S2^i$ secondary interactions of $3.3678(9) \text{ \AA}$; i: $2-x, 1-y, 1-z$. As shown in Figure 4.4b, two other noteworthy features of the crystal packing are highlighted. Firstly, within the dimeric aggregates there are methylene-C-H $\cdots\pi$ (PdS₂C) interactions, Appendix O. As noted in the original bibliographic reviews of these types of interaction (Tiekink et al., 2011; Zukerman-Schpector & Tiekink, 2012), the geometric parameters characterising these appear in the PLATON (Spek, 2003) output as possible examples of C-H $\cdots\pi$ interactions. The connections between dimeric aggregates leading to supramolecular chains aligned along the a-axis are anagostic (Brookhart et al., 2007; Scherer et al., 2015; Taubmann et al., 2009; Zhang et al., 2006) methylene-C-H \cdots Pd interactions, Appendix O, so that the methylene acts a bridge between two adjacent molecules in the chain. This type of interaction is attracting increasing attention in the structural chemistry of metal 1,1'-dithiolates owing largely to the work of Singh et al (Gupta et al., 2014; Kumar, Singh, Gupta, Drew, et al., 2015; Kumar, Singh, Gupta, Singh, et al., 2015; Poirier et al., 2015; Rajput et al., 2013; Singh et al., 2013). The chains pack in the crystal structure separated by hydrophobic interactions, Figure 4.6.

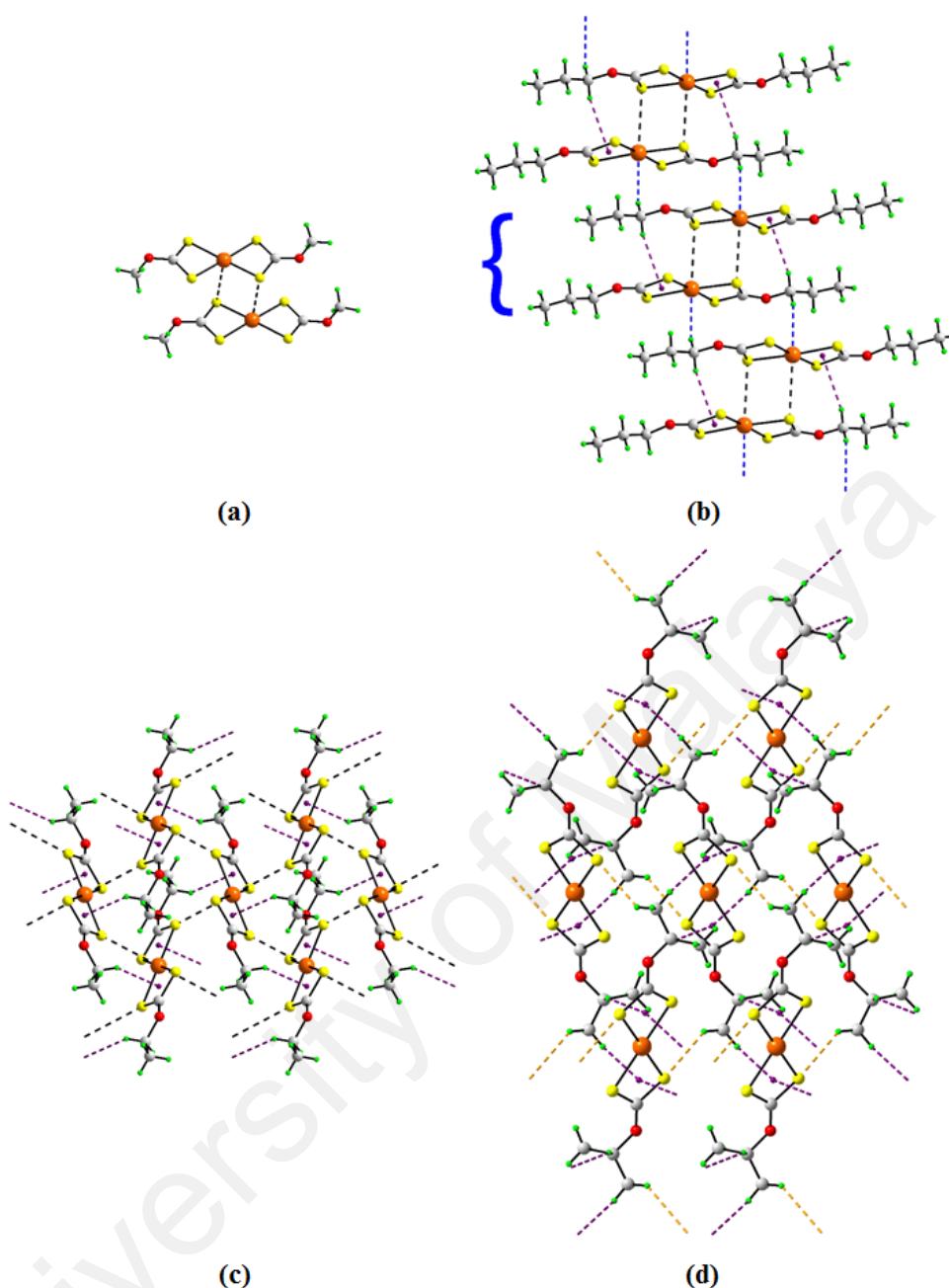


Figure 4.4: Supramolecular aggregation in **11**, **13**, **12**, and **14**.

(a) **11**, Dimeric aggregate sustained by Pd \cdots S secondary interactions shown as black dashed lines; (b) **13**, supramolecular chain whereby dimeric aggregates, sustained by Pd \cdots S interactions and enclosing C–H \cdots π (PdS₂C) interactions (purple dashed lines), are linked by anagostic C–H \cdots Pd interactions (blue dashed lines). The blue brace indicates one dimeric aggregate; (c) centrosymmetric **12**, supramolecular layer sustained by Pd \cdots S interactions and enclosing two C–H \cdots π (PdS₂C) interactions per molecule; (d) **14**, sustained by C–H \cdots S interactions and enclosing four C–H \cdots π (PdS₂C) interactions per molecule.

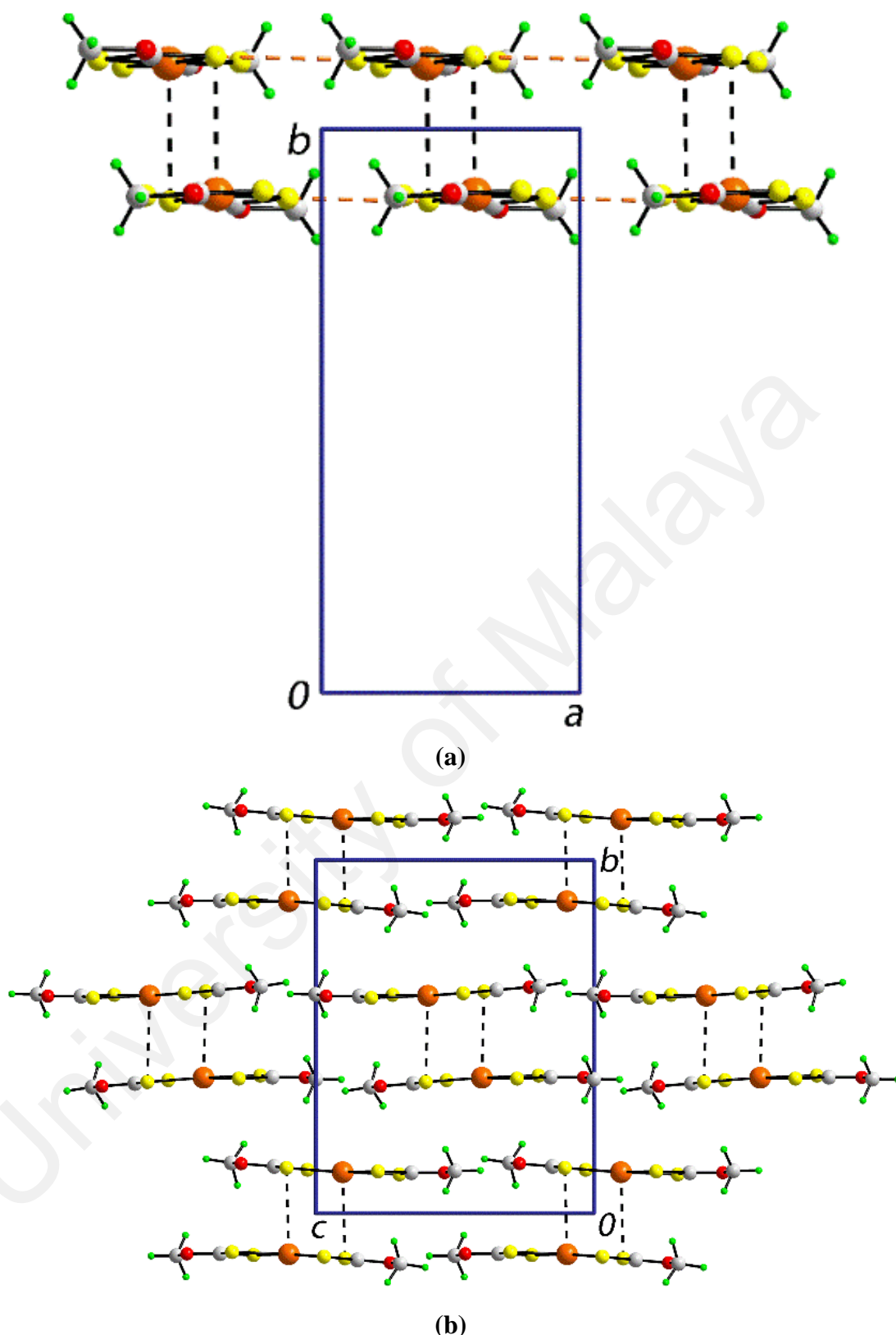


Figure 4.5: Views of the unit cell contents for bis(O-methylxanthato)palladium(II). [Pd(S₂COMe)₂] (**11**).

In projection down the (a) *c*-axis, and (b) *a*-axis. No directional interactions are noted other than the Pd...S1ⁱ interactions [3.3165(13) Å; black dashed lines] leading to dimeric aggregates; symmetry operation *i*: 1-*x*, 2-*y*, 1-*z*. In (a), the orange dotted lines indicate S1...S2ⁱⁱ interactions of 3.6206(18) Å, which are just beyond the sum of the van der Waals radii; *ii*: -1+*x*, *y*, *z*.

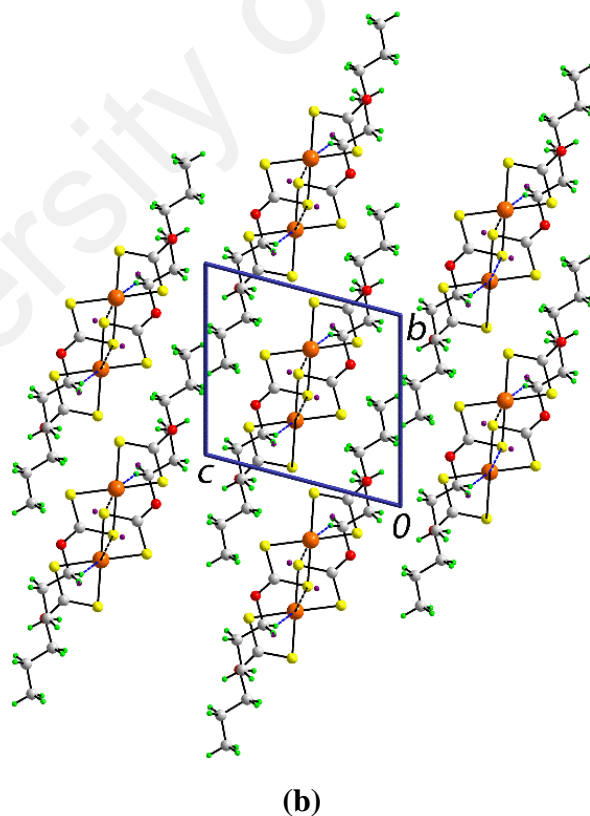
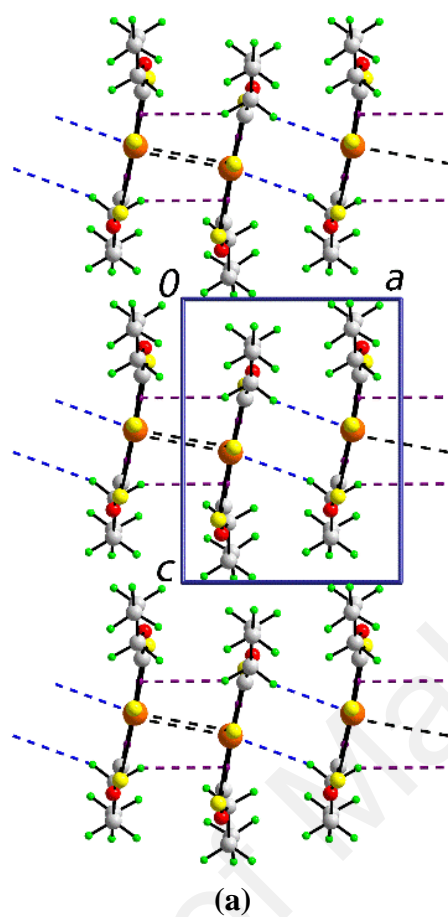


Figure 4.6: Views of the unit cell contents for bis(O-n-propylxanthato)palladium(II), $[\text{Pd}(\text{S}_2\text{COPr})_2]$ (**13**).

In projection down the (a) b-axis, and (b) a-axis. Chains are separated by hydrophobic interactions. The $\text{Pd}\cdots\text{S}$, $\text{C}-\text{H}\cdots\pi(\text{PdS}_2\text{C})$ and $\text{Pd}\cdots\text{H}$ interactions are shown as black, purple and blue dashed lines, respectively.

At this point, it is worthwhile to consider the C–H $\cdots\pi$ (PdS₂C) and Pd \cdots H interactions in the context of their van der Waals radii. For the putative C–H $\cdots\pi$ (PdS₂C) interactions, the van der Waals radius of the chelate ring is taken as 1.90 Å, being the value accepted as the half-thickness of a phenyl ring, based on the upper value estimated for half the separation between the two centroids in parallel phenyl rings (Janiak, 2000). Thus, adding this to 1.20 Å, the Bondi van der Waals radius for hydrogen (Bondi, 1964), the sum of the van der Waals radii becomes 3.10 Å. However, if the widely accepted value of 1.09 Å (Rowland *et al.*, 1996) is used for a hydrogen atom, the sum of the van der Waals radii reduces to 2.99 Å. In searching for C–H $\cdots\pi$ (MS₂C) and allied M(lp) $\cdots\pi$ (phenyl) (Caracelli *et al.*, 2013, 2014; Caracelli *et al.*, 2012; Tiekink *et al.*, 2010; Zukerman-Schpector, Haiduc, *et al.*, 2011, 2012; Zukerman-Schpector, Otero-de-la-Roza, *et al.*, 2011; Zukerman-Schpector *et al.*, 2014) interactions in the crystallographic literature, *i.e.* in the CSD (Groom *et al.*, 2014), 10% of the value of the sum of the van der Waals radii is usually added in order to capture all possible interactions, a practice which seems to be widely accepted as there is no absolute cut-off for a putative interaction (Mukherjee *et al.*, 2014). Therefore, the C–H $\cdots\pi$ (PdS₂C) contacts in **13** (2.91 Å) clearly fall within the sum of the van der Waals radii of the interacting species. Concerning the Pd \cdots H interactions, the sum of the van der Waals radii for palladium (Alcock, 1972) and hydrogen (1.09 Å) (Atwood *et al.*, 2004) is 2.72 Å, a value shorter than 2.83 Å for the C–H \cdots Pd interaction in **13** but well within the sum of the van der Waals radii + 10% criterion.

As mentioned above, the remaining molecular structures are centrosymmetric. In **12**, R = Et, supramolecular layers are formed in the *ab*-plane sustained by Pd \cdots S interactions (3.3612(6) Å; 1/2+x, 3/2-y, 1-z) above and below the square plane, Figure 4.4c. Within this framework are methylene-C–H $\cdots\pi$ (PdS₂C) interactions, Appendix O, with, from symmetry, each chelate ring participating in one such contact. Layers stack along the *c*-axis being separated by hydrophobic interactions, Figure 4.7.

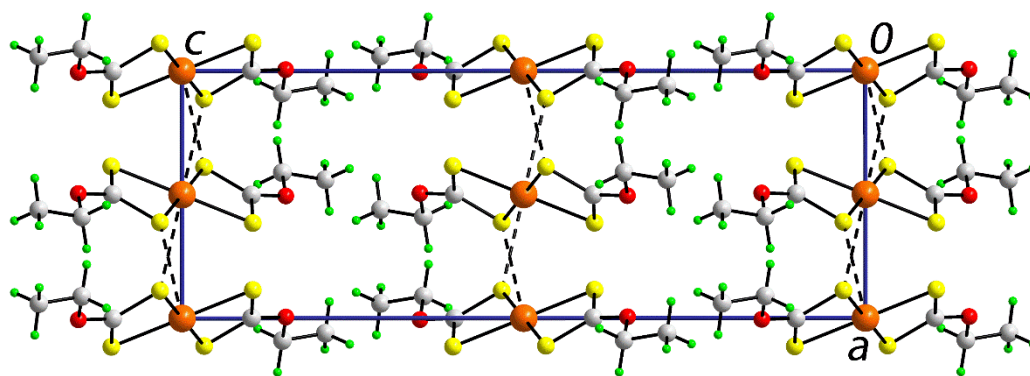


Figure 4.7: View of the unit cell contents for bis(O-ethylxanthato)palladium(II), $[\text{Pd}(\text{S}_2\text{COEt})_2]$ (**12**).

In projection down the (a) b-axis. Layers are separated by hydrophobic interactions.

In keeping with the well-established principal in the structural chemistry of metal 1,1'-dithiolates, namely that increasing the steric bulk of the R group will “turn-off” secondary $\text{M}\cdots\text{S}$ interactions (Liu *et al.*, 2005; Tiekink, 2003, 2006, 2008; Tiekink *et al.*, 2010), branching in **14**, $\text{R} = \text{iPr}$, and increasing size in **15–22**, leads to crystal packing patterns devoid of $\text{Pd}\cdots\text{S}$ interactions. In **14**, $\text{C-H}\cdots\text{S}$ interactions cooperate with methine- and methyl- $\text{C-H}\cdots\pi(\text{PdS}_2\text{C})$ interactions to generate a supramolecular layer parallel to $(-1\ 0\ 1)$, Figure 4.4d. In all there are four $\text{C-H}\cdots\pi(\text{PdS}_2\text{C})$ interactions per molecule. Layers pack with no directional interactions between them, Figure 4.8.

The structures of **15–22** exhibit the same global crystal packing patterns with each featuring $\text{C-H}\cdots\pi(\text{PdS}_2\text{C})$ interactions operating independently of other recognisable supramolecular synthons leading to supramolecular chains. While the crystal packing of **15** also features $\text{C-H}\cdots\text{S}$ interactions, which link chains, those of **16–22** do not. In fact, no other recognisable intermolecular synthons are apparent in **16–22**. Despite these similarities and the fact that all molecules are centrosymmetric, crystallising with half a molecule in the asymmetric unit in the triclinic (*PI*) space group, the mode of association between molecules *via* $\text{C-H}\cdots\pi(\text{PdS}_2\text{C})$ interactions is not consistent across the series with five different supramolecular motifs discerned. These are now discussed below in terms of complexity of modes of association.

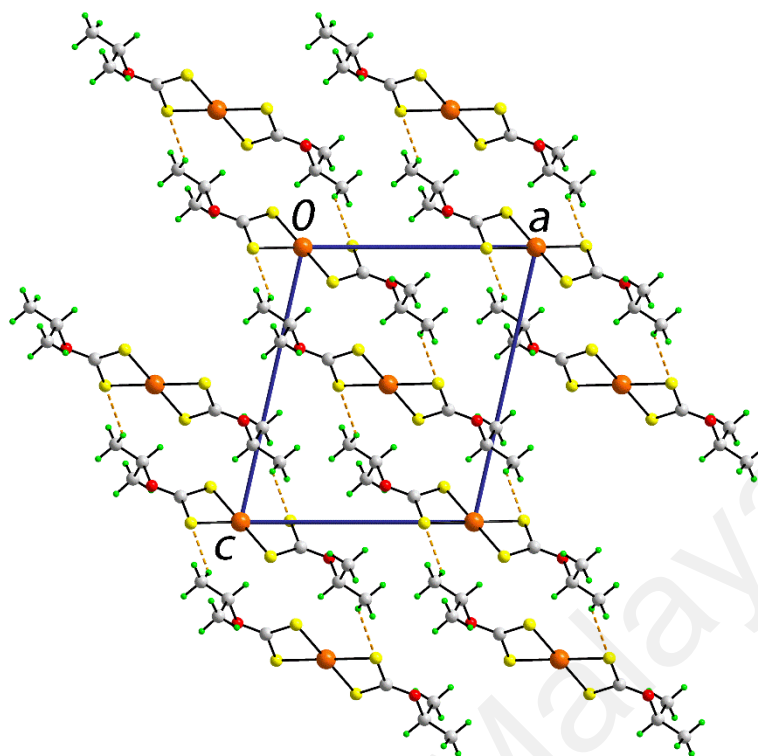


Figure 4.8: View of the unit cell contents for bis(O-isopropylxanthato)palladium(II), $[\text{Pd}(\text{S}_2\text{CO-i-Pr})_2]$ (**14**).

In projection down the *b*-axis. Layers parallel to $(-1\ 0\ 1)$, sustained by weak $\text{C-H}\cdots\text{S}$ hydrogen bonds shown as orange dashed lines, are separated by hydrophobic interactions.

The simplest mode of association between molecules based on $\text{C-H}\cdots\pi(\text{PdS}_2\text{C})$ interactions leading to supramolecular chains is found in the crystal packing of **19** ($\text{R} = \text{neoPent}$) where methylene- $\text{C-H}\cdots\pi(\text{PdS}_2\text{C})$ interactions, one per chelate ring, on opposite sides of the molecule from symmetry, link molecules into chains aligned along the *b*-axis, Fig. 4.10a and Appendix O. As for all other supramolecular chains described below, the chains in **19** pack with no directional interactions between them, Figure 4.10. In **15** ($\text{R} = n\text{-Bu}$), supramolecular rows of molecules aligned along the *b*-axis are sustained by four methylene- $\text{C-H}\cdots\pi(\text{PdS}_2\text{C})$ interactions per molecule, Figure 4.9b. These are connected into layers by $\text{C-H}\cdots\text{S}$ hydrogen bonds that stack along the *c*-axis, being separated by hydrophobic interactions, Figure 4.11. The other two structures with straight alkyl chains, *i.e.* **17** ($\text{R} = n\text{-Pent}$), and **20** ($\text{R} = n\text{-Hex}$), exhibit the same patterns of 1,3-methylene- $\text{C-H}\cdots\pi(\text{PdS}_2\text{C})$ supramolecular association as for **15**, Figure 4.12 and 4.13. A similar

aggregation is found for **21** (R = *i*-Hex) where branching occurs at the penultimate carbon, Figure 4.14. The mode of association for **18** (R = *i*-Pent) is as just described for **15** but, with the hydrogen atoms derived from 1,3-related methylene- and methyl-hydrogens, Figure 4.9c and Figure 4.15. The aggregation in **16** (R = *i*-Bu) leading to chains aligned along the *a*-axis resembles that seen for **19** but there are two contacts per chelate ring instead of one, involving 1,3-related methylene- and methyl-hydrogen atoms, Figure 4.9d and Figure 4.16. Finally, in **22** (R = neoHex), chains are formed along the *b*-axis with six C–H $\cdots\pi$ (PdS₂C) interactions per molecule. Here, 1,2-related methylene hydrogens span two chelate rings, with the oxygen-bound methylene interacting with one chelate ring, and both methylene hydrogen atoms interacting with the other chelate ring on the same side of the PdS₄ square-plane, Figure 4.9e and Figure 4.17.

A common feature of the aggregation patterns involving C–H $\cdots\pi$ (PdS₂C) interactions, when formed, is the participation of an oxygen-bound methylene hydrogen atom in in all examples except in **19**, Figure 4.9a, where steric pressures presumably preclude the close approach of this group. This observation is consistent with the notion that these hydrogens would be the most acidic in these molecules. An evaluation of the data included in Appendix O suggests no correlations between the H \cdots centroid(PdS₂C) distance and the nature of the hydrogen atom participating in a C–H $\cdots\pi$ (PdS₂C) interaction nor between these distances and the angles subtended at the hydrogen atom. This lack of correlation is not unexpected for weak interactions (Dunitz *et al.*, 1997; Tiekink *et al.*, 2011; Zukerman-Schpector & Tiekink, 2012).

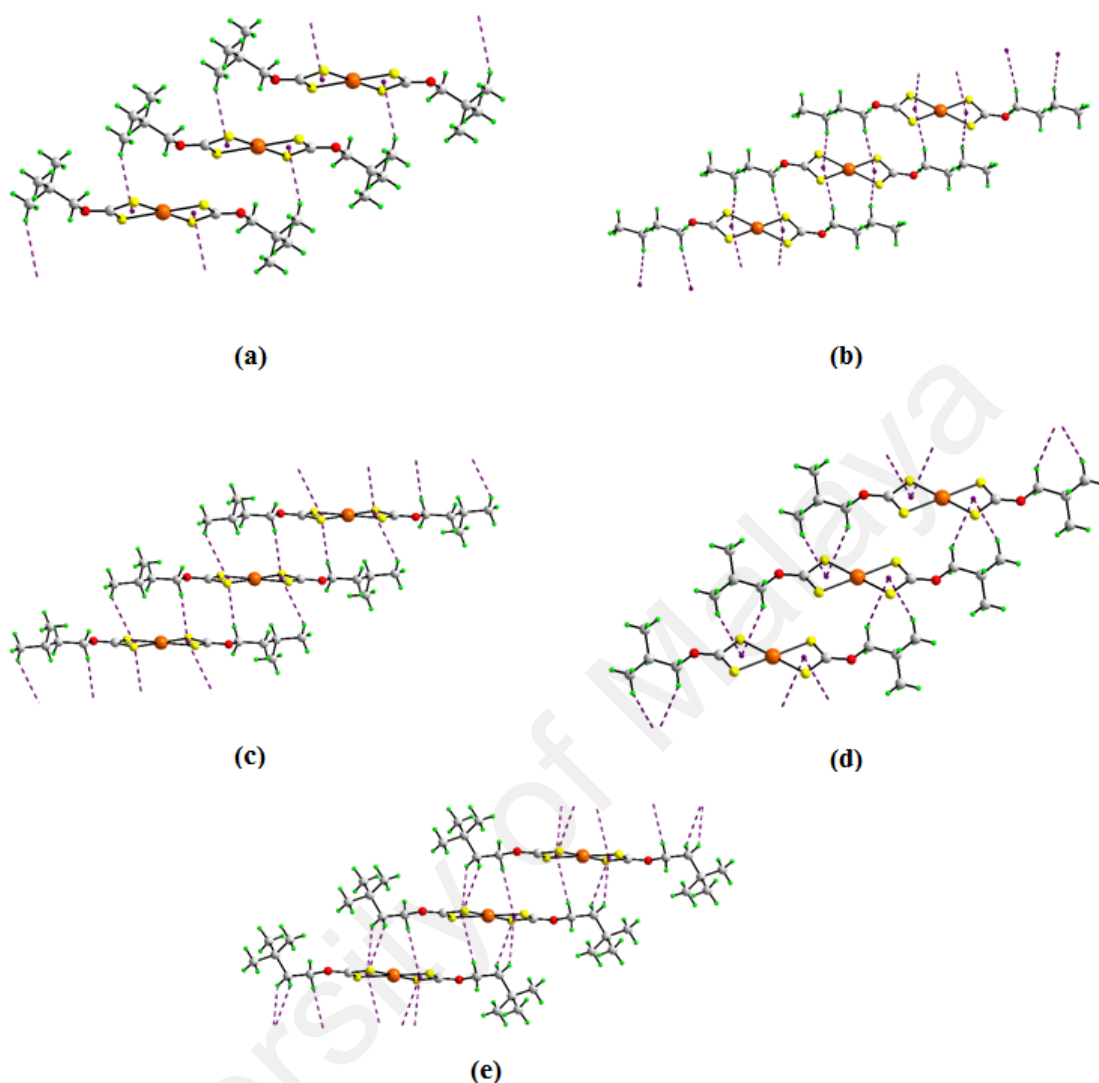


Figure 4.9: Supramolecular aggregation in **19**, **15**, **18**, **16**, and **22**.

(a) **19**, Chains along the *a*-axis sustained by two C–H \cdots π (PdS₂C) interactions per molecule, one per chelate ring and involving methyl-hydrogens; (b) **15**, chains along the *b*-axis sustained by four C–H \cdots π (PdS₂C) interactions per molecule, one on either side of each chelate ring and involving 1,3-related methylene-hydrogens. Similar aggregation is observed in each of **17**, **20** and **21**; (c) **18**, as for **15** but involving 1,4-related methylene- and methyl-hydrogens; (d) **16**, chains along the *a*-axis sustained by four C–H \cdots π (PdS₂C) interactions per molecule, two to one side of each chelate ring and involving 1,3-related methylene- and methyl- hydrogens; and (e) **22**, chains along the *b*-axis sustained by six C–H \cdots π (PdS₂C) interactions per molecule, two to one side and one to the other for each chelate ring and involving 1,2-related methylene-hydrogens.

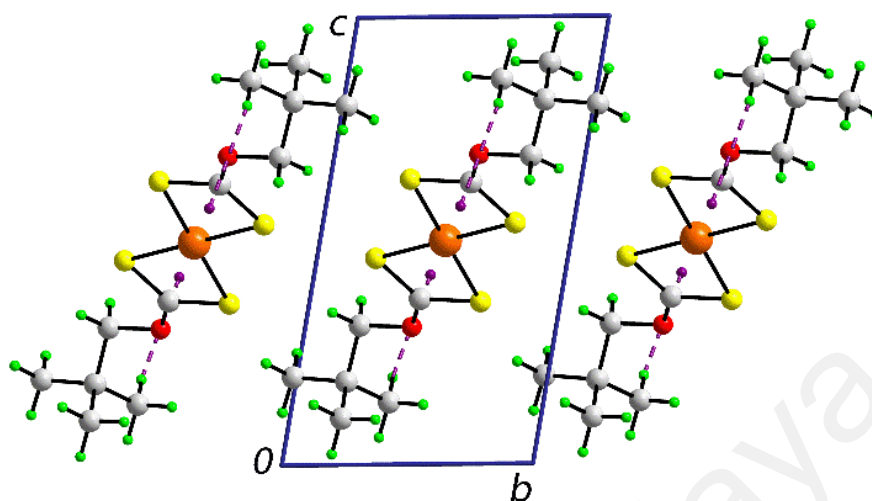


Figure 4.10: View of the unit cell contents for bis(O-neopentylxanthato)palladium(II), $[\text{Pd}(\text{S}_2\text{CO-neo-Pent})_2]$ (**19**).

In projection down the b-axis. Rows of molecules, along the b-axis and connected by $\text{C-H}\cdots\pi(\text{PdS}_2\text{C})$ interactions are separated by hydrophobic interactions.

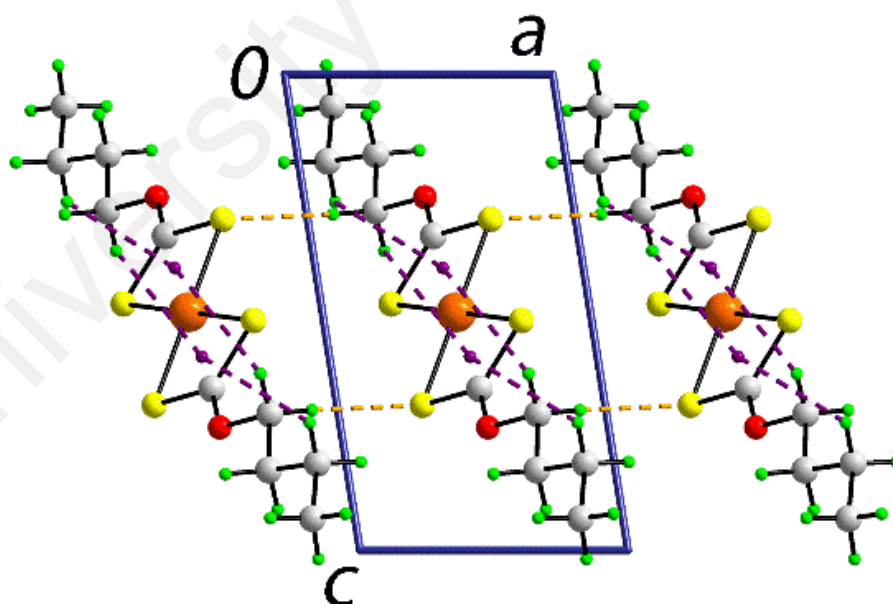
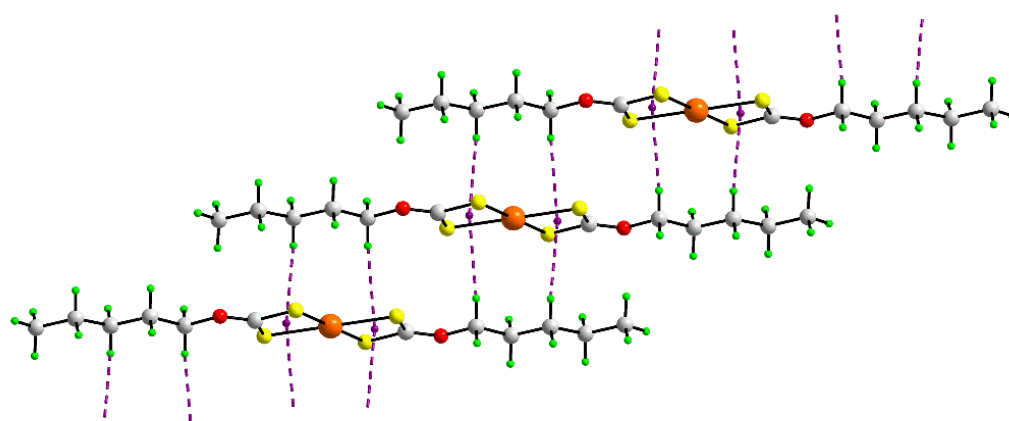
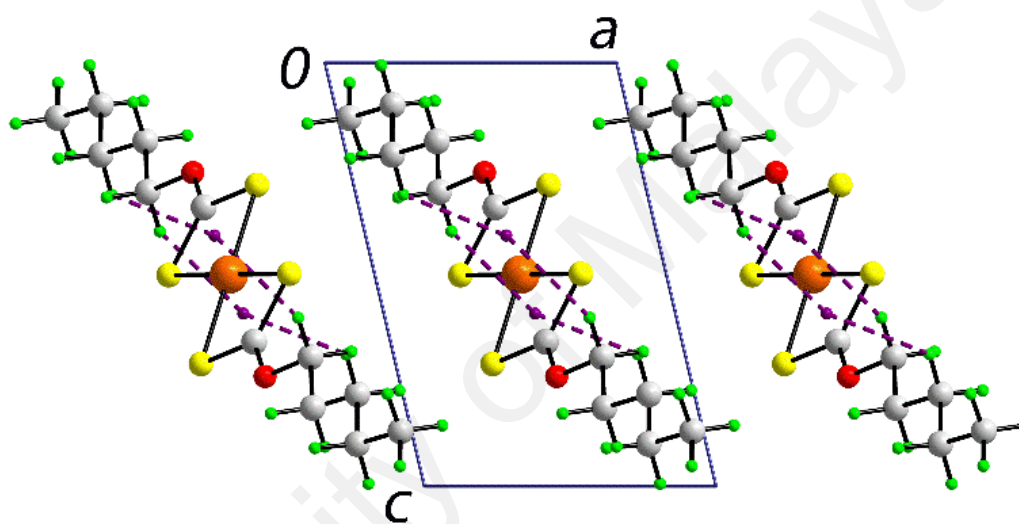


Figure 4.11: View of the unit cell contents for bis(O-n-butylxanthato)palladium(II), $[\text{Pd}(\text{S}_2\text{CO-n-Bu})_2]$ (**15**).

In projection down the b-axis. Rows of molecules, along the b-axis and connected by $\text{C-H}\cdots\pi(\text{PdS}_2\text{C})$ interactions, are linked by weak $\text{C-H}\cdots\text{S}$ hydrogen bonds, shown as orange dashed lines, to form layers that are separated by hydrophobic interactions.



(a)



(b)

Figure 4.12: Views of the crystal packing in bis(O-n-pentylxanthato)palladium(II), $[\text{Pd}(\text{S}_2\text{CO-n-Pent})_2]$ (**17**).

(a) Supramolecular chain aligned along the b-axis, being connected by $\text{C-H}\cdots\pi(\text{PdS}_2\text{C})$ interactions; and (b) the unit cell contents in projection down the b-axis. Chains of molecules do not form specific interactions in the crystal packing.

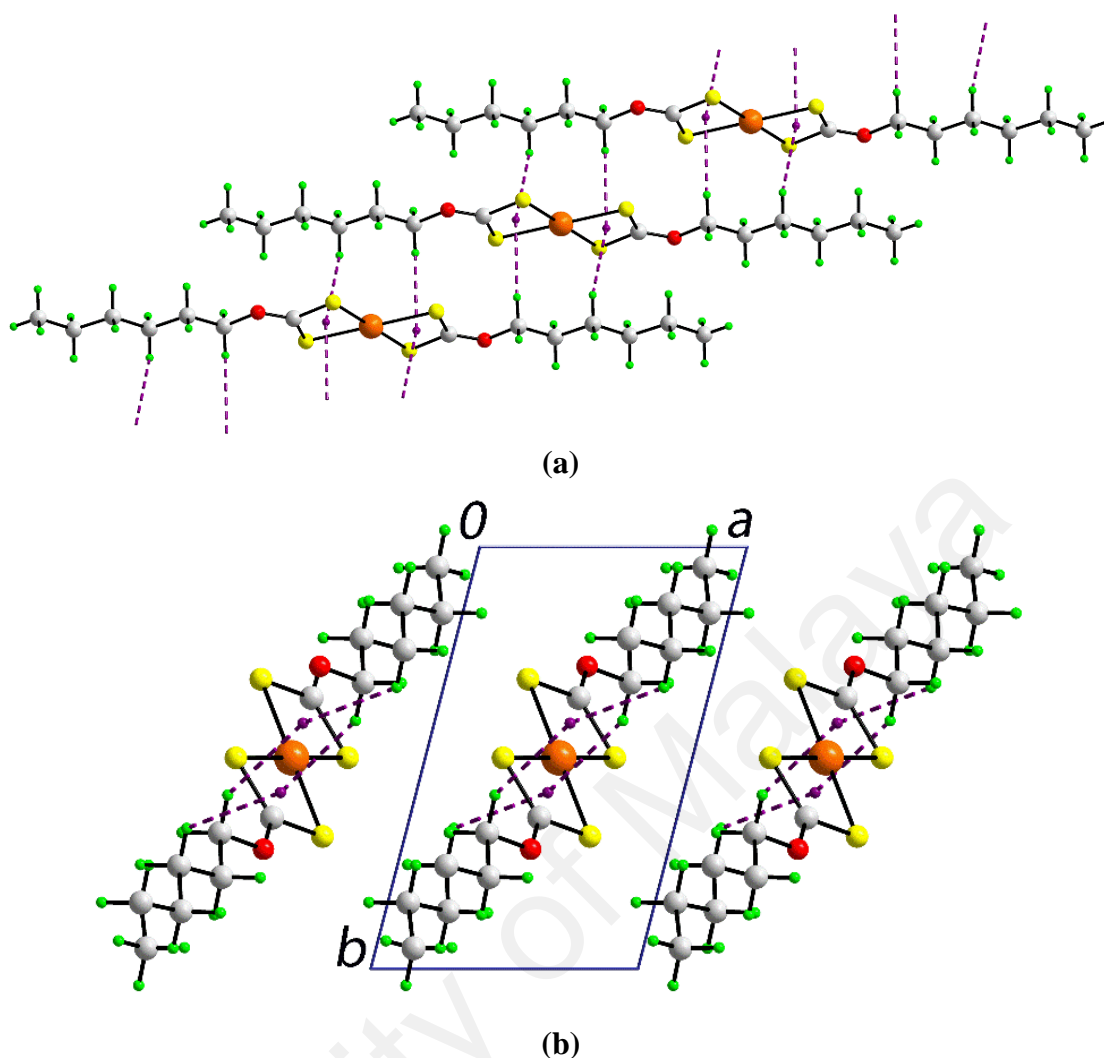


Figure 4.13: Views of the crystal packing in bis(O-n-hexylxanthato)palladium(II), $[\text{Pd}(\text{S}_2\text{CO-n-Hex})_2]$ (**20**).

(a) Supramolecular chain aligned along the b-axis, being connected by $\text{C-H}\cdots\pi(\text{PdS}_2\text{C})$ interactions; and (b) the unit cell contents in projection down the b-axis. Chains of molecules do not form specific interactions in the crystal packing.

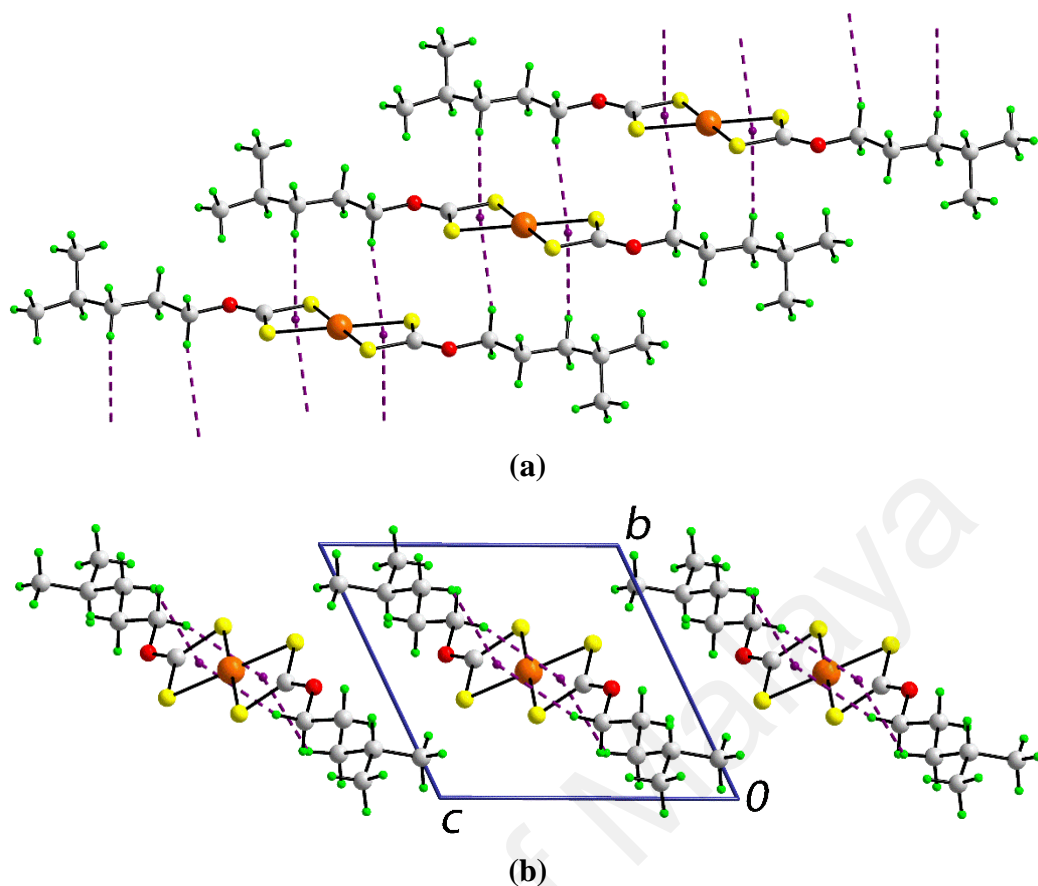


Figure 4.14: Views of the crystal packing in bis(O-isohexylxanthato)palladium(II), $[\text{Pd}(\text{S}_2\text{CO-i-Hex})_2]$ (**21**).

(a) Supramolecular chain aligned along the b-axis, being connected by $\text{C-H}\cdots\pi(\text{PdS}_2\text{C})$ interactions; and (b) the unit cell contents in projection down the b-axis. Chains of molecules do not form specific interactions in the crystal packing.

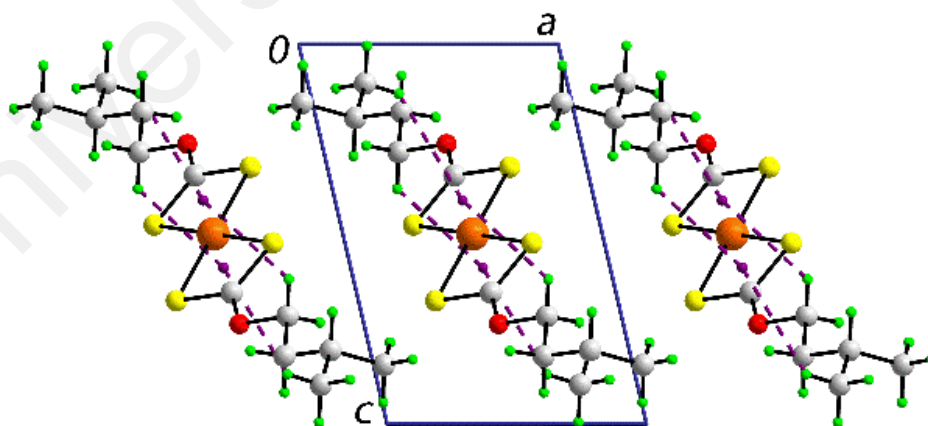


Figure 4.15: View of the crystal packing in bis(O-isopentylxanthato)palladium(II), $[\text{Pd}(\text{S}_2\text{CO-i-Pent})_2]$ (**18**).

The unit cell contents in projection down the b-axis. Chains of molecules do not form specific interactions in the crystal packing.

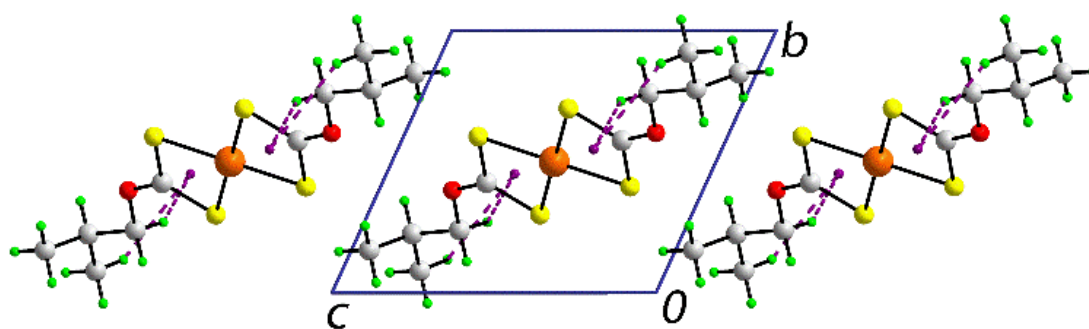


Figure 4.16:View of the crystal packing in bis(O-isobutylxanthato)palladium(II), $[\text{Pd}(\text{S}_2\text{CO-i-Bu})_2]$ (**16**).

The unit cell contents in projection down the a-axis. Chains of molecules do not form specific interactions in the crystal packing.

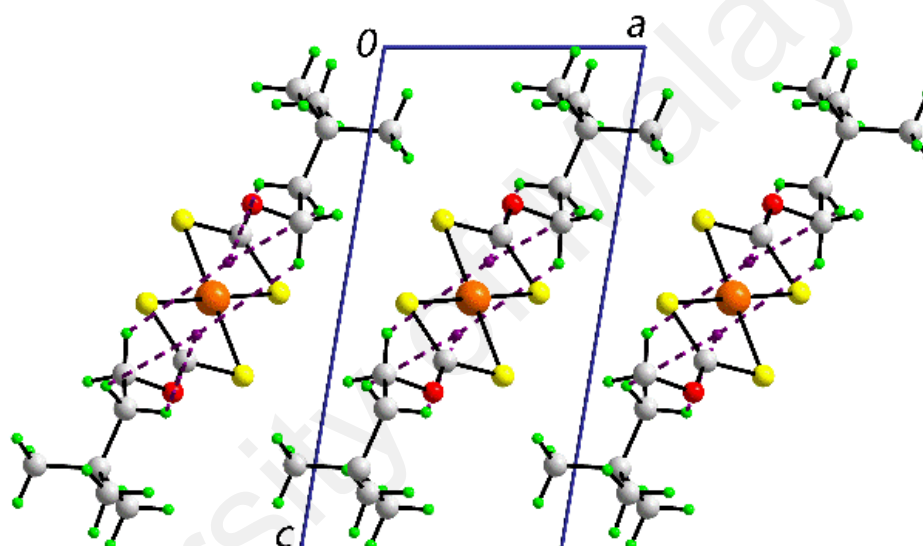


Figure 4.17:View of the crystal packing in bis(O-neohexylxanthato)palladium(II), $[\text{Pd}(\text{S}_2\text{CO-neo-Hex})_2]$ (**22**).

The unit cell contents in projection down the b-axis. Chains of molecules do not form specific interactions in the crystal packing.

4.3.3. Computational Study

As noted above and illustrated in Figure 4.4b, the crystal packing of **13** features secondary Pd \cdots S as well as C–H $\cdots\pi$ and methylene–C–H \cdots Pd interactions. This structure was therefore chosen for a computational study in order to delineate the importance and nature of these interactions. Several calculations were conducted for this study. First, the experimental crystal geometry was relaxed using DFT, corrected using the exchange-hole dipole moment (XDM) model (Becke *et al.*, 2007; Otero-de-la-Roza *et al.*, 2012, 2013). The XDM dispersion energy has been shown to efficiently represent the intermolecular interactions in molecular crystals (Otero-de-la-Roza *et al.*, 2012) and in the gas-phase (Otero-de-la-Roza *et al.*, 2013), particularly in systems involving transition metals (Otero-de-la-Roza *et al.*, 2014). For the crystal structure, the calculations were carried out using Quantum ESPRESSO (Giannozzi *et al.*, 2009), and the XDM correction was coupled with the B86BPBE exchange-correlation functional (Becke, 1986; Perdew *et al.*, 1996). The plane-wave energy cut-off was 60 Ry and the density cut-off was 600 Ry. A 4 x 4 x 4 k-point grid was used. To calculate the lattice energy, the geometry of **13** was relaxed inside a supercell with 50 bohr cell length. The equilibrium crystal structure shows a cell volume of 642.4 Å³ and a lattice energy of 141.83 kJ/mol per molecule. This lattice energy is relatively high, compared to crystals of roughly the same size (Otero-de-la-Roza *et al.*, 2012), especially considering there are no strong hydrogen bonds or other directional interactions, *e.g.* halogen.

At the converged crystal geometry, the B86BPBE electron density was obtained and the non-covalent interaction (NCI) plots (Otero-de-la-Roza *et al.*, 2012, 2013) were calculated for the relevant intermolecular contacts using the critic2 program (Becke, 1986; Giannozzi *et al.*, 2009; Perdew *et al.*, 1996). There are four non-equivalent contacts in the crystal structure of **13**: a) a stacked contact involving two methylene–C–H $\cdots\pi$ (PdS₂C), b) a stacked contact with two Pd \cdots S interactions, and two distinct side-by-

side intermolecular contacts involving mostly the aliphatic substituents (c and d); these are illustrated in Figure 4.18.

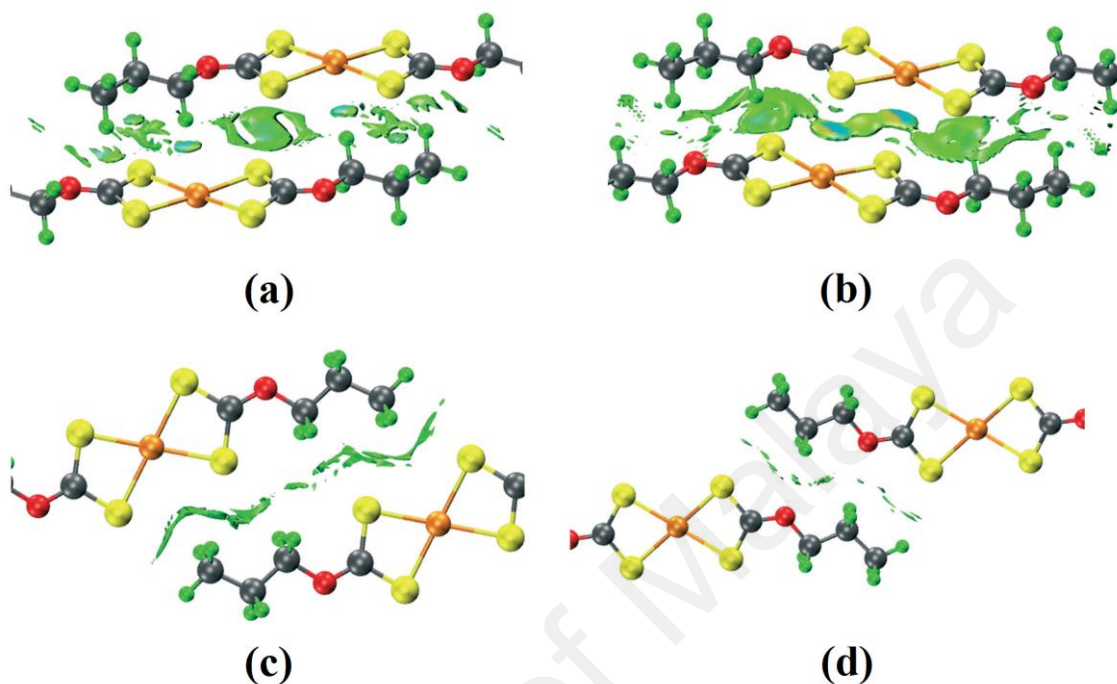


Figure 4.18: NCI plots in the molecular packing of **13**.

- a) A stacked contact involving two methylene $C-H\cdots\pi(PdS_2C)$ interactions, b) a stacked contact with two $Pd\cdots S$ interactions, and (c and d) two distinct side-by-side intermolecular contacts involving the aliphatic substituents.

The NCI plots shows that the dominant contributions to the lattice energy, in order of relative importance, come from the $Pd\cdots S$ interactions, the methylene- $C-H\cdots\pi(PdS_2C)$ contacts followed by the hydrophobic contacts. While the latter contributions are not specific and likely originate from dispersion, as evidenced by the low-density extensive NCI regions, the two types of secondary contacts, *i.e.* ($Pd\cdots S$ and $C-H\cdots\pi(PdS_2C)$), are directional and give localised high-density NCI domains. It is important to notice the high efficiency of the molecular packing in this crystal structure. The green NCI domains in Figure 4.18c and d follow the hydrophobic surface of the molecules in contact, indicating that the bumps and hollows match between molecules.

In order to quantify the relative contributions to the lattice energy from each of the four intermolecular contacts in the crystal, the binding energies in the gas-phase of

the four dimers shown in Figure 4.18 were calculated; the different species were frozen at the crystal geometry. The calculations were run using Gaussian (Frisch *et al.*, 2009), the LC-wPBE-XDM functional (Johnson *et al.*, 2013; Vydrov, Heyd, *et al.*, 2006; Vydrov & Scuseria, 2006), and the pc-2-spd basis set. The latter is particularly well-suited for the calculation of non-covalent interactions (Vydrov, Heyd, *et al.*, 2006). For the Pd atom, the basis-set/pseudopotential combination aug-cc-pVDZ-PP (Peterson *et al.*, 2005) was employed. Referring to Figure 4.18, the calculated binding energies were: (a) 62.92, (b) 67.37, (c) 29.85 and (d) 20.85 kJ/mol. Thus, in agreement with the NCI plots, the directional Pd \cdots S and C–H $\cdots\pi$ (PdS₂C) contacts are the main contributors to the stability of the crystal structure, and the Pd \cdots S interaction is marginally stronger than C–H $\cdots\pi$ (PdS₂C).

However, the contribution from the two hydrophobic contacts (c and d) is by no means negligible, which explains the disparate crystal packing observed for the other crystals (**11**, **12**, **14-22**). For the crystal structures involving larger substituents, it is expected that global crystal packing effects will become more important, eventually overcoming the Pd \cdots S and C–H $\cdots\pi$ (PdS₂C) contributions and therefore, controlling the crystal structure.

4.3.4. Conclusion

Amongst the 12 palladium(II) xanthates isolated, 11 compounds demonstrated C–H $\cdots\pi$ (PdS₂C) interactions. Compound **13** showed the presence of one C–H $\cdots\pi$ (PdS₂C) interactions, while each of **12** and **19** exhibited two of the interactions aforementioned. A total of four C–H $\cdots\pi$ (PdS₂C) interactions were determined from each of the crystal structures of **14–18**, **20** and **21**, and up to a maximum of six C–H $\cdots\pi$ (PdS₂C) interactions contributed to the crystal system stabilization. Over and above, DFT calculations of selected compound, **13**, provide evidence of contribution of C–H $\cdots\pi$ (PdS₂C) in stabilising the crystal system with the binding energy comparable to Pd \cdots S interaction. In addition to the two types of interactions mentioned in the former, C–H \cdots Pd and hydrophobic interactions from side by side of aliphatic hydrocarbon chain imparted vital but at smaller extent of stabilization energy.

CHAPTER 5: CONCLUSION

In summary, CE were studied and applied in current research program through the three respective projects. A total of 22 compounds were successfully synthesised and characterised using various spectroscopic techniques and material analysis.

In the first project, a total of seven polymorphs were isolated from various crystallisation techniques and synthesis methods, as described in Chapter 2. The crystallisation process of all polymorphs, including the two noteworthy structure motifs for cadmium(II) dithiocarbamate compound, one-dimensional coordination polymers (CP), were observed. Remarkably, single crystal to single crystal transformations (SCSC) led to the formation of two pairs of supramolecular isomers (SI), ascribed to the stabilisation energy of crystal systems and atmospheric moisture for SCSC transformation of **1** to **2**, and **6** to **7**, respectively. The above 'non-reversible' SCSCs of these two pair of SIs can be interconverted by developing solvent-induced reversible transformations. Compounds **3** (cocrystal) and **4** (salt cocrystal) each presented a dimeric structure whilst **5** forms a salt from a tris(dithiocarbamato)cadmium(II) cation and a protonated amine anion.

The denticity of hexamethylenetetramine (hmta) was evaluated in the second project and the results were discussed in Chapter 3. The denticity of hmta was manipulated by the types of precursors applied while varying the mole ratio of hmta:precursors (1:1, 1:2, and 2:1) resulted in indifferent outcomes. The molecular structures obtained for **8** and **9** revealed that the various coordination modes of hmta attributed to steric effect induced by xanthate side groups. Unexpected phenomena was observed in xanthate bearing ethyl group, which provided more space for insertion to the third ligating nitrogen atom from hmta. The high packing density of **8** bearing methyl side group prevented the close contact of cadmium(II) xanthate to uncoordinated nitrogen atom of hmta. In the contrary, steric effect of ethyl side group in compound **9** led to an

orientation with the presence of a void, resulted in the third coordination of hmta. The binuclear compound **10** however displayed a distinctive structure with terminally bound hmta ligands. Dissimilar from compounds **8** and **9**, compound **10** formed a zero-dimensional aggregate ascribed to the steric bulk of the iPr groups.

In the third project, 12 palladium(II) xanthate compounds were prepared, with 11 of them demonstrated the presence of anticipated C–H $\cdots\pi$ (PdS₂C) interactions. Amongst these 11 structures, a range of one to maximum of six interactions were observed. Over and above, some of the crystal systems were found constructed from Pd \cdots S, and anagostic C–H \cdots Pd interactions. The above was further supported by DFT calculations of selected compound **13**. The calculations revealed that the C–H $\cdots\pi$ (PdS₂C) interactions play a vital role in stabilising the crystal system with binding energy of 62.92 kJ mol⁻¹, followed after the slightly stronger Pd \cdots S interactions of 67.37 kJ mol⁻¹ in compound **13**.

The study of related 1,1'-dithiolate coordination compounds reported as attached in publication: the applications of compounds prepared as single source precursor for nanoparticle generation and as potential anti-cancer agents are explored. The above findings aid in the exploration of related research areas and they can be extended by, *e.g.* manipulating crystal systems formation by selection of crystallisation techniques, adoption of linkers other than utropine and pyridine types, and assessing the importance of C–H $\cdots\pi$ (MS₂C) in crystal system construction in other coordination compounds.

REFERENCES

- Abrahams, B. F., Hoskins, B. F., Tiekink, E. R. T., & Winter, G. (1988). Investigation Of A New Xanthate Ligand. The Crystal And Molecular Structures Of Nickel And Cadmium (Methoxyethyl)Xanthates. *Australian Journal of Chemistry*, 41(7), 1117-1122.
- Abrahams, B. F., Hoskins, B. F., & Winter, G. (1990). The Structure Of Cadmium Bis(isopropylxanthate)-4,4'-Bipyridine. *Australian Journal of Chemistry*, 43(10), 1759-1765.
- Adarsh, N. N., & Dastidar, P. (2012). Coordination Polymers: What Has Been Achieved In Going From Innocent 4,4'-Bipyridine To Bis-pyridyl Ligands Having A Non-Innocent Backbone? *Chemical Society Reviews*, 41(8), 3039-3060.
- Addison, A. W., Rao, T. N., Reedijk, J., van Rijn, J., & Verschoor, G. C. (1984). Synthesis, Structure, And Spectroscopic Properties Of Copper(II) Compounds Containing Nitrogen-Sulphur Donor Ligands; The Crystal And Molecular Structure Of Aqua[1,7-bis(N-methylbenzimidazol-2'-yl)-2,6-dithiaheptane]copper(II) Perchlorate. *Journal of the Chemical Society, Dalton Transactions*(7), 1349-1356.
- Afzaal, M., Malik, M. A., & O'Brien, P. (2010). Chemical Routes To Chalcogenide Materials As Thin Films Or Particles With Critical Dimensions With The Order Of Nanometres. *Journal of Materials Chemistry*, 20(20), 4031-4040.
- Akhbari, K., & Morsali, A. (2013). Solid- And Solution-State Structural Transformations In Flexible Lead(II) Supramolecular Polymers. *CrystEngComm*, 15(44), 8915-8918.
- Alcock, N. W. (1972). Secondary Bonding To Nonmetallic Elements. In H. J. Emeléus & A. G. Sharpe (Eds.), *Advances in Inorganic Chemistry and Radiochemistry* (Vol. Volume 15, pp. 1-58): Academic Press.
- Aly, A. A., Brown, A. B., Bedair, T. M. I., & Ishak, E. A. (2012). Dithiocarbamate Salts: Biological Activity, Preparation, And Utility In Organic Synthesis. *Journal of Sulfur Chemistry*, 33(5), 605-617.
- An, S.-W., Mei, L., Wang, C.-Z., Xia, C.-Q., Chai, Z.-F., & Shi, W.-Q. (2015). The First Case Of Actinide Triple Helices: pH-Dependent Structural Evolution And Kinetically-Controlled Transformation Of Two Supramolecular Conformational Isomers. *Chemical Communications*, 51(43), 8978-8981.

- Ara, I., El Bahij, F., Lachkar, M., & Ben Larbi, N. (2003). Bis(O-ethyl dithiocarbonato- k^2S,S')palladium(II). *Acta Crystallographica Section C*, 59(5), m199-m200.
- Arman, H. D., Poplaukhin, P., & Tiekink, E. R. T. (2012). Bis[N-(2-hydroxyethyl)-N-methyldithiocarbamate- kS][2,4,6-tris(pyridin-2-yl)-1,3,5-triazine- k^3N^1,N^2,N^6]zinc dioxane sesquisolvate. *Acta Crystallographica Section E*, 68(3), m319-m320.
- Atwood, J. L., & Steed, J. (2004). *Encyclopedia of Supramolecular Chemistry*. New York: Marcel Dekker Inc.
- Avila, V., Benson, R. E., Broker, G. A., Daniels, L. M., & Tiekink, E. R. T. (2006). Catena-Poly[[bis(N,N-diethyldithiocarbamate- k^2S,S')cadmium(II)]-m-trans-1,2-di-4-pyridylethane- $k^2N:N'$]. *Acta Crystallographica Section E*, 62(6), m1425-m1427.
- Barreca, D., Gasparotto, A., Maragno, C., Seraglia, R., Tondello, E., Venzo, A., Krishnan, V., & Bertagnolli, H. (2005). Cadmium O-Alkylxanthates As CVD Precursors Of CdS: A Chemical Characterization. *Applied Organometallic Chemistry*, 19(1), 59-67.
- Basu Baul, T. S., Kundu, S., Ng, S. W., Guchhait, N., & Tiekink, E. R. T. (2013). Synthesis, Characterization, Photoluminescent Properties And Supramolecular Aggregations In Diimine Chelated Cadmium Dihalides. *Journal of Coordination Chemistry*, 67(1), 96-119.
- Batten, S. R., Champness, N. R., Chen, X.-M., Garcia-Martinez, J., Kitagawa, S., Ohrstrom, L., O'Keeffe, M., Suh, M. P., & Reedijk, J. (2012). Coordination Polymers, Metal-Organic Frameworks And The Need For Terminology Guidelines. *CrystEngComm*, 14(9), 3001-3004.
- Becke, A. D. (1986). On The Large-Gradient Behavior Of The Density Functional Exchange Energy. *The Journal of Chemical Physics*, 85(12), 7184-7187.
- Becke, A. D. (1993). Density-Functional Thermochemistry. III. The Role Of Exact Exchange. *The Journal of Chemical Physics*, 98(7), 5648-5652.
- Becke, A. D., & Johnson, E. R. (2007). Exchange-Hole Dipole Moment And The Dispersion Interaction Revisited. *The Journal of Chemical Physics*, 127(15), 154108.

- Bevilacqua, J. M., & Eisenberg, R. (1994). Synthesis And Characterization Of Luminescent Square-Planar Platinum(II) Complexes Containing Dithiolate Or Dithiocarbamate Ligands. *Inorganic Chemistry*, 33(13), 2913-2923.
- Biradha, K., Ramanan, A., & Vittal, J. J. (2009). Coordination Polymers Versus Metal–Organic Frameworks. *Crystal Growth & Design*, 9(7), 2969-2970.
- Bogdanović, G. A., Biré, A. S.-D., & Zarić, S. D. (2002). Evidence Based On Crystal Structures And Calculations Of A C–H $\cdots\pi$ Interaction Between An Organic Moiety And A Chelate Ring In Transition Metal Complexes. *European Journal of Inorganic Chemistry*, 2002(7), 1599-1602.
- Bolundut, L., Haiduc, I., Mahon, M. F., & Molloy, K. C. (2008). A Dinuclear Adduct Of Bis (di-sec-butyl dithiophosphato) Cadmium(II) Built Around The Hexamethylenetetramine Cage As Coordination Center. *Revista De Chimie*, 59(11), 1194-1196.
- Bondi, A. (1964). Van der Waals Volumes And Radii. *The Journal of Physical Chemistry*, 68(3), 441-451.
- Brandenburg, K. (2006). DIAMOND. Bonn, Germany: Crystal Impact GbR.
- Brandenburg, K. (2006). DIAMOND, Visual Crystal Structure Information System, Version 3.1. Postfach 1251, D-53002 Bonn, Germany: CRYSTAL IMPACT.
- Broker, G. A., & Tiekink, E. R. T. (2011). Bis[N-(2-hydroxyethyl)-N-propyldithiocarbamato-k²S,S']bis(4-[(pyridin-4-ylmethylidene)hydrazinylidene]methyl}pyridine-kN¹)cadmium. *Acta Crystallographica Section E*, 67(3), m320-m321.
- Brookhart, M., Green, M. L. H., & Parkin, G. (2007). Agostic Interactions In Transition Metal Compounds. *Proceedings of the National Academy of Sciences*, 104(17), 6908-6914.
- Buntine, M. A., Cox, M. J., Lim, Y. X., Yap, T. C., & Tiekink, E. R. T. (2003). Crystal Structure Of Anhydrous Potassium O-*n*-Propyldithiocarbonate. Theoretical Calculations Of O-Alkyl Dithiocarbonates *Zeitschrift für Kristallographie/International journal for structural, physical, and chemical aspects of crystalline materials* (Vol. 218, pp. 56).

- Câmpian, M., Haiduc, I., & Tiekink, E. R. T. (2013). Steric Control Over C=O...C=O Interactions In $M(S_2COR)_2$ (dafone) Compounds: M = Zn And Cd; R = Me, Et And iPr; dafone = 4,5-diazafluoren-9-one-N,N' *Zeitschrift für Kristallographie - Crystalline Materials* (Vol. 228, pp. 187).
- Caracelli, I., Haiduc, I., Zukerman-Schpector, J., & Tiekink, E. R. T. (2013). Delocalised Antimony(Lone Pair)- And Bismuth-(Lone Pair)... π (Arene) Interactions: Supramolecular Assembly And Other Considerations. *Coordination Chemistry Reviews*, 257(21–22), 2863-2879.
- Caracelli, I., Haiduc, I., Zukerman-Schpector, J., & Tiekink, E. R. T. (2014). $M \cdots \pi$ (Arene) Interactions For M = Gallium, Indium And Thallium: Influence Upon Supramolecular Self-Assembly And Prevalence In Some Proteins. *Coordination Chemistry Reviews*, 281(0), 50-63.
- Caracelli, I., Zukerman-Schpector, J., & Tiekink, E. R. T. (2012). Supramolecular Aggregation Patterns Based On The Bio-Inspired Se(Lone Pair)... π (Aryl) Synthon. *Coordination Chemistry Reviews*, 256(3–4), 412-438.
- Casas, J., Castiñeiras, A., Garcia-Tasende, M. S., Sánchez, A., Sordo, J., & Vázquez-López, E. M. (1995). The X-Ray Crystal Structure Of Bis(dicyclohexyldithiophosphato)cadmium(II). *Polyhedron*, 14(15–16), 2055-2058.
- Casas, J. S., Sánchez, A., Bravo, J., García-Fontán, S., Castellano, E. E., & Jones, M. M. (1989). Cadmium Coordination Chemistry Related To Chelate Therapy. *Inorganica Chimica Acta*, 158(1), 119-126.
- Chai, J., Lai, C. S., Yan, J., & Tiekink, E. R. T. (2003). Crystallographic Report: Polymeric [Bis(N,N-diethyldithiocarbamato) (trans-1,2-bis(4-pyridyl)ethylene)cadmium(II)]. *Applied Organometallic Chemistry*, 17(4), 249-250.
- Chan, M. Y., Lai, C. S., & Tiekink, E. R. T. (2004). Crystallographic Report: Bis(N-cyclohexyl,N-methyldithiocarbamato)zinc(II). *Applied Organometallic Chemistry*, 18(6), 298-298.
- Chen, D.-S., Sun, L.-B., Liang, Z.-Q., Shao, K.-Z., Wang, C.-G., Su, Z.-M., & Xing, H.-Z. (2013). Conformational Supramolecular Isomerism In Two-Dimensional Fluorescent Coordination Polymers Based On Flexible Tetracarboxylate Ligand. *Crystal Growth & Design*, 13(9), 4092-4099.

- Chen, D., Lai, C. S., & Tiekink, E. R. T. (2003). Crystal Structures Of 2,2'-Bipyridine Adducts Of Two Cadmium O-Alkyl Dithiocarbonates: Rationalisation Of Disparate Coordination Geometries Based On Different Crystal Packing Environments *Zeitschrift für Kristallographie/International journal for structural, physical, and chemical aspects of crystalline materials* (Vol. 218, pp. 747).
- Chen, H. W., & Fackler, J. P. (1978). Sulfur Chelates. 30. Crystal And Molecular Structures Of Aryl Xanthates. Bis(O-4-tert-butylphenyl dithiocarbonato)nickel(II), Tris(O-2,4,6-trimethylphenyl dithiocarbonato)cobalt(III), And Bis(O-2,4,6-trimethylphenyl dithiocarbonato)Palladium(II). *Inorganic Chemistry*, 17(1), 22-26.
- Chesman, A. S. R., Duffy, N. W., Martucci, A., De Oliveira Tozi, L., Singh, T. B., & Jasieniak, J. J. (2014). Solution-Processed CdS Thin Films From A Single-Source Precursor. *Journal of Materials Chemistry C*, 2(17), 3247-3253.
- Cookson, J., & Beer, P. D. (2007). Exploiting The Dithiocarbamate Ligand In Metal-Directed Self-Assembly. *Dalton Transactions*(15), 1459-1472.
- Coucouvannis, D. (2007). The Chemistry Of The Dithioacid And 1, 1-Dithiolate Complexes, 1968–1977 *Progress in Inorganic Chemistry* (Vol. 26, pp. 301-469): John Wiley & Sons, Inc.
- Cox, M. J., & Tiekink, E. R. T. (1999). Structural Characteristics Of Cadmium(II) Bis(N,N-dialkyldithiocarbamate) Compounds *Zeitschrift für Kristallographie* (Vol. 214, pp. 670).
- Cox, M. J., & Tiekink, E. R. T. (1999). Structural Diversity In Mercury(II) Bis(O-alkyldithiocarbonate) Compounds *Zeitschrift für Kristallographie* (Vol. 214, pp. 486).
- Cox, M. J., Tiekink, E.R.T. (1999). Structural Features Of Zinc(II) Bis(O-alkyldithiocarbonate) And Zinc(II) Bis(N,N-dialkyldithiocarbamate) Compounds. *Zeitschrift für Kristallographie*, 214, 184. doi: Zeitschrift für Kristallographie
- . CrysAlisPro. (2014). Santa Clara, CA, USA: Agilent Technologies.
- . CrystalClear. User Manual. Rigaku/MSI Inc. (2005). The Woodlands, TX: Rigaku Corporation.

- Decken, A., Gossage, R. A., Chan, M. Y., Lai, C. S., & Tiekink, E. R. T. (2004). Crystallographic Report: Bis(N,N-dibenzylthiocarbamato)zinc(II). *Applied Organometallic Chemistry*, 18(2), 101-102.
- Dee, C. M., & Tiekink, E. R. T. (2002). Refinement Of The Crystal Structure Of Dimeric Bis(N,N-diethyldithiocarbamato) Cadmium(II), $[\text{Cd}(\text{S}_2\text{CNEt}_2)_2]_2$ *Zeitschrift für Kristallographie - New Crystal Structures* (Vol. 217, pp. 85).
- Desiraju, G. R. (1989). *Crystal Engineering: The Design Of Organic Solids*. Amsterdam: Elsevier.
- Desiraju, G. R. (2001). Crystal Engineering: Outlook And Prospects. *Current Science*, 81(8), 1038-1042.
- Dobrzańska, L. (2015). Concomitant, Genuine 1D Supramolecular Isomers Of An Ag(I) Complex With 1,3-Bis(imidazol-1-ylmethyl)-2,4,6-trimethylbenzene and BF_4^- As Counterion. *Inorganic Chemistry Communications*, 55(0), 21-24.
- Domenicano, A., Torelli, L., Vaciago, A., & Zambonelli, L. (1968). Structural Studies Of Metal Dithiocarbamates. Part Iv. The Crystal And Molecular Structure Of Cadmium(II) N,N'-Diethyldithiocarbamate. *Journal of the Chemical Society A: Inorganic, Physical, Theoretical*(0), 1351-1361.
- Drake, J. E., Mislankar, A. G., & Yang, J. (1992). Synthesis, Spectroscopy, And Structural Studies Of Tetrakis(O-alkyl dithiocarbonato)germanium. Crystal Structures Of $\text{Ge}[\text{S}_2\text{COR}]_4$, Where R = Me, Et, And Iso-Pr. *Inorganic Chemistry*, 31(26), 5543-5548.
- Du, M., Li, C.-P., Liu, C.-S., & Fang, S.-M. (2013). Design And Construction Of Coordination Polymers With Mixed-Ligand Synthetic Strategy. *Coordination Chemistry Reviews*, 257(7–8), 1282-1305.
- du Plessis, M., & Barbour, L. J. (2012). Supramolecular Isomerism And Solvatomorphism In A Novel Coordination Compound. *Dalton Transactions*, 41(14), 3895-3898.
- Dubraja, L. A., Matkovic-Calogovic, D., & Planinic, P. (2015). Crystal Disassembly And Reassembly Of Heterometallic Ni^{II} - Ta^{V} Oxalate Compounds. *CrystEngComm*, 17(9), 2021-2029.

- Duhme, A.-K., Pohl, S., & Strasdeit, H. (1990). Formation And Properties Of $[\text{Cd}(\text{S}_2\text{CNEt}_2)\text{I}]_\infty$, An Alternating Copolymer Of Cadmium N,N-Diethyldithiocarbamate And Cadmium Iodide. *Inorganica Chimica Acta*, 175(1), 5-8.
- Dunitz, J. D., & Taylor, R. (1997). Organic Fluorine Hardly Ever Accepts Hydrogen Bonds. *Chemistry – A European Journal*, 3(1), 89-98.
- Ewings, P. F. R., Harrison, P. G., & King, T. J. (1976). Derivatives Of Bivalent Germanium, Tin, And Lead. Part XVI. Crystal And Molecular Structure Of Tin(II) Bis(O-methyl dithiocarbonate). *Journal of the Chemical Society, Dalton Transactions*(14), 1399-1403.
- Farrugia, L. (2012). WinGX And ORTEP For Windows: An Update. *Journal of Applied Crystallography*, 45(4), 849-854.
- Fiorillo, A. A., & Galbraith, J. M. (2004). A Valence Bond Description Of Coordinate Covalent Bonding. *The Journal of Physical Chemistry A*, 108(23), 5126-5130.
- Frahm, D., Hoffmann, F., & Fröba, M. (2014). Two Metal–Organic Frameworks With A Tetratopic Linker: Solvent-Dependent Polymorphism And Postsynthetic Bromination. *Crystal Growth & Design*, 14(4), 1719-1725.
- Friebolin, W., Schilling, G., Zöller, M., & Amtmann, E. (2005). Antitumoral Activity Of Non-Platinum Xanthate Complexes. *Journal of Medicinal Chemistry*, 48(25), 7925-7931.
- Frisch, M. J., Trucks, G. W., Schlegel, H. B., Scuseria, G. E., Robb, M. A., Cheeseman, J. R., Scalmani, G., Barone, V., Mennucci, B., Petersson, G. A., Nakatsuji, H., Caricato, M., Li, X., Hratchian, H. P., Izmaylov, A. F., Bloino, J., Zheng, G., Sonnenberg, J. L., Hada, M., Ehara, M., Toyota, K., Fukuda, R., Hasegawa, J., Ishida, M., Nakajima, T., Honda, Y., Kitao, O., Nakai, H., Vreven, T., Montgomery Jr., J. A., Peralta, J. E., Ogliaro, F., Bearpark, M. J., Heyd, J., Brothers, E. N., Kudin, K. N., Staroverov, V. N., Kobayashi, R., Normand, J., Raghavachari, K., Rendell, A. P., Burant, J. C., Iyengar, S. S., Tomasi, J., Cossi, M., Rega, N., Millam, N. J., Klene, M., Knox, J. E., Cross, J. B., Bakken, V., Adamo, C., Jaramillo, J., Gomperts, R., Stratmann, R. E., Yazyev, O., Austin, A. J., Cammi, R., Pomelli, C., Ochterski, J. W., Martin, R. L., Morokuma, K., Zakrzewski, V. G., Voth, G. A., Salvador, P., Dannenberg, J. J., Dapprich, S., Daniels, A. D., Farkas, Ö., Foresman, J. B., Ortiz, J. V., Cioslowski, J., & Fox, D. J. (2009). Gaussian 09. Wallingford, CT, USA: Gaussian, Inc.

- Gangavaram, S., Raghavender, S., Sanphui, P., Pal, S., Manjunatha, S. G., Nambiar, S., & Nangia, A. (2012). Polymorphs And Cocrystals Of Nalidixic Acid. *Crystal Growth & Design*, 12(10), 4963-4971.
- Garje, S. S., & Jain, V. K. (2003). Chemistry Of Arsenic, Antimony And Bismuth Compounds Derived From Xanthate, Dithiocarbamate And Phosphorus Based Ligands. *Coordination Chemistry Reviews*, 236(1–2), 35-56.
- Garnovskii, A. D., Sennikova, E. V., & Kharisov, B. I. (2009). Coordination Aspects In Modern Inorganic Chemistry. *The Open Inorganic Chemistry Journal*, 3, 1-20.
- Giannozzi, P., Baroni, S., Bonini, N., Calandra, M., Car, R., Cavazzoni, C., Ceresoli, D., Chiarotti, G. L., Cococcioni, M., Dabo, I., Dal Corso, A., Fabris, S., Fratesi, G., de Gironcoli, S., Gebauer, R., Gerstmann, U., Gougoussis, C., Kokalj, A., Lazzeri, M., Martin-Samos, L., Marzari, N., Mauri, F., Mazzarello, R., Paolini, S., Pasquarello, A., Paulatto, L., Sbraccia, C., Scandolo, S., Sclauzero, G., Seitsonen, A. P., Smogunov, A., Umari, P., Wentzcovitch, R. M., Giannozzi, P., Baroni, S., Bonini, N., Calandra, M., Car, R., Cavazzoni, C., Ceresoli, D., Chiarotti, G. L., Cococcioni, M., Dabo, I., Dal Corso, A., Fabris, S., Fratesi, G., de Gironcoli, S., Gebauer, R., Gerstmann, U., Gougoussis, C., Kokalj, A., Lazzeri, M., Martin-Samos, L., Marzari, N., Mauri, F., Mazzarello, R., Paolini, S., Pasquarello, A., Paulatto, L., Sbraccia, C., Scandolo, S., Sclauzero, G., Seitsonen, A. P., Smogunov, A., Umari, P., & Wentzcovitch, R. M. (2009). QUANTUM ESPRESSO: A Modular And Open-Source Software Project For Quantum Simulations Of Materials. *Journal of Physics Condensed Matter*, 21(39), 395502.
- Glinskaya, L. A., Zemskova, S. M., & Klevtsova, R. F. (1999). Molecular And Crystal Structure Of Cadmium(II) Diisobutyldithiocarbamate $\{Cd[(i-C_4H_9)_2NCS_2]_2\}_2$. *Journal of Structural Chemistry*, 40(6), 979-983.
- Glinskaya, L. A., Zemskova, S. M., Klevtsova, R. F., Larionov, S. V., & Gromilov, S. A. (1992). The Preparation, Structures And Thermal Properties Of $[MEN_3][Cd(S_2CNEt_2)_3]_2$ [M = Zinc(II), Cadmium(II)] Complexes. *Polyhedron*, 11(22), 2951-2956.
- Groom, C. R., & Allen, F. H. (2014). The Cambridge Structural Database In Retrospect And Prospect. *Angewandte Chemie International Edition*, 53(3), 662-671.
- Gupta, A. N., Kumar, V., Singh, V., Manar, K. K., Drew, M. G. B., & Singh, N. (2014). Intermolecular Anagostic Interactions In Group 10 Metal Dithiocarbamates. *CrystEngComm*, 16(39), 9299-9307.
- Haiduc, I. (2003). 1.15 - 1,1-Dithiolato Ligands. In J. A. M. J. Meyer (Ed.), *Comprehensive Coordination Chemistry II* (pp. 349-376). Oxford: Pergamon.

- Haiduc, I. (2007). Chapter 10.2 1,1-Dithiolato Ligands And Related Selenium And Tellurium Compounds *Handbook of Chalcogen Chemistry: New Perspectives in Sulfur, Selenium and Tellurium* (pp. 593-643): The Royal Society of Chemistry.
- Haiduc, I. (2007). Secondary Bonding *Encyclopedia of Supramolecular Chemistry* (Vol. null, pp. 1215-1224): Taylor & Francis.
- Haiduc, I., & Sowerby, D. B. (1996). Stereochemical Aspects Of Phosphor-1,1-dithiolato Metal Complexes: Coordination Patterns, Molecular Structures And Supramolecular Associations In Dithiophosphinates And Related Compounds. *Polyhedron*, 15(15), 2469-2521.
- Han, L.-L., Hu, T.-P., Mei, K., Guo, Z.-M., Yin, C., Wang, Y.-X., Zheng, J., Wang, X.-P., & Sun, D. (2015). Solvent-Controlled Three Families Of Zn(II) Coordination Compounds: Synthesis, Crystal Structure, Solvent-Induced Structural Transformation, Supramolecular Isomerism And Photoluminescence. *Dalton Transactions*, 44(13), 6052-6061.
- Heard, P. J. (2005). Main Group Dithiocarbamate Complexes *Progress in Inorganic Chemistry* (Vol. 53, pp. 1-69): John Wiley & Sons, Inc.
- Higashi, T. (1995). ABSCOR. Tokyo, Japan: Rigaku Corporation.
- Hogarth, G. (2005). Transition Metal Dithiocarbamates: 1978–2003 *Progress in Inorganic Chemistry* (Vol. 53, pp. 71-561): John Wiley & Sons, Inc.
- Hogarth, G. (2012). Metal-dithiocarbamate complexes: chemistry and biological activity. *Mini Review in Medicinal Chemistry*, 12(12), 1202 – 1215.
- Hou, S.-S., Huang, X., Guo, J.-G., Zheng, S.-R., Lei, J., Tan, J.-B., Fan, J., & Zhang, W.-G. (2015). Assembly Of Cd(II) Coordination Polymers: Structural Variation, Supramolecular Isomers, And Temperature/Anion-Induced Solvent-Mediated Structural Transformations. *CrystEngComm*, 17(4), 947-959.
- Hwang, I. H., Kim, H.-Y., Lee, M. M., Na, Y. J., Kim, J. H., Kim, H.-C., Kim, C., Huh, S., Kim, Y., & Kim, S.-J. (2013). Zn-MOFs Containing Flexible α,ω -Alkane (Or Alkene)-Dicarboxylates And 1,2-Bis(4-pyridyl)ethane Ligands: CO₂ Sorption And Photoluminescence. *Crystal Growth & Design*, 13(11), 4815-4823.
- Iimura, Y. (1973). *Sci. Pap. Inst. P. C. R. (Jpn.)*, 67, 43-46.

- Imura, Y., Ito, T., & Hagihara, H. (1972). The Crystal Structure Of Cadmium Ethylxanthate. *Acta Crystallographica Section B*, 28(7), 2271-2279.
- Ikeda, T., & Hagihara, H. (1966). The Crystal Structure Of Zinc Ethylxanthate. *Acta Crystallographica*, 21(6), 919-927.
- Ito, T., & Otake, M. (1996). Linear-Chain Structure Of Bis(O,O'-dimethyldithiophosphato)cadmium(II). *Acta Crystallographica Section C*, 52(12), 3024-3025.
- Ivanov, A. V., Gerasimenko, A. V., Antzutkin, O. N., & Forsling, W. (2005). The Unique Alternation Of Conformationally Different ('Chair'-'Saddle') Eight-Membered Metallocycles [Cd₂S₄P₂] In The Chains Of Cadmium Dialkyldithiophosphates: ¹³C, ³¹P, ¹¹³Cd CP/MAS NMR And Single-Crystal X-Ray Diffraction Studies. *Inorganica Chimica Acta*, 358(9), 2585-2594.
- Ivanov, A. V., Gerasimenko, A. V., Konzelko, A. A., Ivanov, M. A., Antzutkin, O. N., & Forsling, W. (2006). Conformational Isomerism Of The Binuclear N,N-Pentamethylenedithiocarbamate Cadmium(II) Complex, [Cd₂{S₂CN(CH₂)₅}₄] On Multinuclear (¹⁵N, ¹¹³Cd) CP/MAS NMR And Single-Crystal X-Ray Diffraction Data. *Inorganica Chimica Acta*, 359(12), 3855-3864.
- Ivanov, A. V., Konzelko, A. A., Gerasimenko, A. V., Ivanov, M. A., Antzutkin, O. N., & Forsling, W. (2005). Structural Organization Of Cadmium(II) And Copper(II) Dithiocarbamate Complexes With Dialkyl-Substituted And Cyclic Ligands: Synthesis, Single-Crystal X-Ray Diffraction, EPR, And CP/MAS ¹³C, ¹⁵N, And ¹¹³Cd NMR. *Russian Journal of Inorganic Chemistry*, 50(11), 1710-1726.
- Ivanov, A. V., Loseva, O. V., & Gerasimenko, A. V. (2008). Chemisorption Of Copper(II) At Zinc And Cadmium Dialkyldithiocarbamates: EPR And X-Ray Diffraction Studies. *Russian Journal of Coordination Chemistry*, 34(6), 413-421.
- Ivanov, A. V., Loseva, O. V., Ivanov, M. A., Konfederatov, V. A., Gerasimenko, A. V., Antzutkin, O. N., & Forsling, W. (2007). Crystalline Cadmium Dialkyl Phosphorodithioate Complexes: Synthesis And Structural Organization As Probed By Multinuclear ¹³C, ³¹P, And ¹¹³Cd CP/MAS NMR And Single-Crystal X-Ray Diffraction. *Russian Journal of Inorganic Chemistry*, 52(10), 1595-1602.
- Janiak, C. (2000). A Critical Account On p-p Stacking In Metal Complexes With Aromatic Nitrogen-Containing Ligands. *Journal of the Chemical Society, Dalton Transactions*(21), 3885-3896.

- Javed, F., Ali, S., Shah, W., Tahir, M. N., & Ullah, H. (2013). (O-Methyl dithiocarbonato-kS)triphenyltin(IV). *Acta Crystallographica Section E*, 69(6), m316.
- Jeon, Y., Cheon, S., Cho, S., Lee, K. Y., Kim, T. H., & Kim, J. (2014). Controlled Reversible Crystal Transformation Of Cu(I) Supramolecular Isomers. *Crystal Growth & Design*, 14(5), 2105-2109.
- Jian, F.-F., Wang, Z.-X., Fun, H.-K., Bai, Z.-P., & You, X.-Z. (1999). A Binuclear Cadmium(II) Complex: Bis[bis(N,N-Diisopropylthiocarbamato)Cadmium(II)]. *Acta Crystallographica Section C*, 55(2), 174-176.
- Jian, F., Wang, Z., Bai, Z., You, X., Fun, H.-K., & Chinnakali, K. (1999). Structure Of Bis(dipropylthiocarbamate) Cadmium(II), $[\text{Cd}_2(\text{n-Pr}_2\text{dtc})_4]$ (dtc = Dithiocarbamate). *Journal of Chemical Crystallography*, 29(2), 227-231.
- Jiang, X., Zhang, W., Zhong, Z., Wei, F., & Wang, S. (2002). Synthesis and Crystal Structures of Cadmium (II) n-butylxathate Complexes. *Chinese Journal of Inorganic Chemistry*, 18(6), 615 - 618.
- Jiang, Y.-F., Xi, C.-J., Liu, Y.-Z., Niclós-Gutiérrez, J., & Choquesillo-Lazarte, D. (2005). Intramolecular "CH $\cdots\pi$ (Metal Chelate Ring) Interactions" As Structural Evidence For Metalloaromaticity In Bis(pyridine-2,6-diimine)Ru^{II} Complexes. *European Journal of Inorganic Chemistry*, 2005(8), 1585-1588.
- Johnson, E. R., Otero-de-la-Roza, A., Dale, S. G., & DiLabio, G. A. (2013). Efficient Basis Sets For Non-Covalent Interactions In XDM-Corrected Density-Functional Theory. *The Journal of Chemical Physics*, 139(21), 214109.
- Kaneko, W., Ohba, M., & Kitagawa, S. (2007). A Flexible Coordination Polymer Crystal Providing Reversible Structural And Magnetic Conversions. *Journal of the American Chemical Society*, 129(44), 13706-13712.
- Kang, J.-G., Shin, J.-S., Cho, D.-H., Jeong, Y.-K., Park, C., Soh, S. F., Lai, C. S., & Tiekink, E. R. T. (2010). Steric Control Over Supramolecular Polymer Formation In Trans-1,2-Bis(4-pyridyl)ethylene Adducts Of Zinc Xanthates: Implications For Luminescence. *Crystal Growth & Design*, 10(3), 1247-1256.
- Kant, R., Gupta, V. K., Kapoor, K., Valarmathi, P., & Thirumaran, S. (2012). Bis(m-N-benzyl-N-furfuryldithiocarbamato)-1:2k³S,S':S';2:1k³S,S':S'-Bis[(N-benzyl-N-furfuryldithiocarbamato-k²S,S')cadmium]. *Acta Crystallographica Section E*, 68(1), m12-m13.

- Kimble, W. L., Rousseau, R. W., & Sambanis, A. (1995). Lysozyme Crystallization By Vapor Diffusion: Characterization And Modeling In The Absence And Presence Of Exogenous Minerals. *Journal of Crystal Growth*, 147(1–2), 165-171.
- Kirillov, A. M. (2011). Hexamethylenetetramine: An Old New Building Block For Design Of Coordination Polymers. *Coordination Chemistry Reviews*, 255(15–16), 1603-1622.
- Kokina, T. E., Klevtsova, R. F., Glinskaya, L. A., & Larionov, S. V. (2010). Synthesis And Crystal Structures Of Binuclear Complexes Of Cobalt(II) And Cadmium(II) Diisobutyldithiophosphinates With Hexamethylenetetramine. *Russian Journal of Inorganic Chemistry*, 55(1), 56-60.
- Konarev, D. V., Khasanov, S. S., Kovalevsky, A. Y., Lopatin, D. V., Rodaev, V. V., Saito, G., Náfrádi, B., Forró, L., & Lyubovskaya, R. N. (2008). Supramolecular Approach To The Synthesis Of [60]Fullerene–Metal Dithiocarbamate Complexes, $\{(M^{II}(R_2dtc)_2)_x \cdot L\} \cdot C_{60}$ ($M = Zn, Cd, Hg, Fe, \text{ And } Mn; x = 1 \text{ And } 2$). The Study Of Magnetic Properties And Photoconductivity. *Crystal Growth & Design*, 8(4), 1161-1172.
- Konarev, D. V., Kovalevsky, A. Y., Khasanov, S. S., Saito, G., Lopatin, D. V., Umrikhin, A. V., Otsuka, A., & Lyubovskaya, R. N. (2006). Synthesis, Crystal Structures, Magnetic Properties And Photoconductivity Of C_{60} And C_{70} Complexes With Metal Dialkyldithiocarbamates $M(R_2dtc)_x$, Where $M = Cu^{II}, Cu^I, Ag^I, Zn^{II}, Cd^{II}, Hg^{II}, Mn^{II}, Ni^{II}, \text{ And } Pt^{II}$; $R = Me, Et, \text{ And } nPr$. *European Journal of Inorganic Chemistry*, 2006(9), 1881-1895.
- Kumar, V., Singh, V., Gupta, A. N., Drew, M. G. B., & Singh, N. (2015). Intermolecular $Tl \cdots H-C$ Anagostic Interactions In Luminescent Pyridyl Functionalized Thallium(I) Dithiocarbamates. *Dalton Transactions*, 44(4), 1716-1723.
- Kumar, V., Singh, V., Gupta, A. N., Manar, K. K., Drew, M. G. B., & Singh, N. (2014). Influence Of Ligand Environments On The Structures And Luminescence Properties Of Homoleptic Cadmium(II) Pyridyl Functionalized Dithiocarbamates. *CrystEngComm*, 16(29), 6765-6774.
- Kumar, V., Singh, V., Gupta, A. N., Singh, S. K., Drew, M. G. B., & Singh, N. (2015). Cooperative Influence Of Ligand Frameworks In Sustaining Supramolecular Architectures Of Ni(II)/Pd(II) Heteroleptic Dithio-Dipyrrin Complexes Via Non-Covalent Interactions. *Polyhedron*, 89(0), 304-312.

- Lago, A. B., Carballo, R., Rodriguez-Hermida, S., & Vazquez-Lopez, E. M. (2013). Control Over The Preparation Of Two pH-Dependent Cu(II) Supramolecular Isomers Based On 1,3,5-Benzenetricarboxylic Acid And The Bis(4-pyridylthio)methane Ligand. *CrystEngComm*, 15(8), 1563-1570.
- Lai, C. S., Lim, Y. X., Yap, T. C., & Tiekink, E. R. T. (2002). Molecular Paving With Zinc Thiolates. *CrystEngComm*, 4(99), 596-600.
- Lai, C. S., Liu, S., & Tiekink, E. R. T. (2004). Steric Control Over Polymer Formation And Topology In Adducts Of Zinc Dithiophosphates Formed With Bridging Bipyridine Ligands. *CrystEngComm*, 6(38), 221-226.
- Lai, C. S., & Tiekink, E. R. T. (2003). Supramolecular Association In Organomercury(II) 1,1-Dithiolates. Complementarity between HgS And Hydrogen Bonding Interactions In Organomercury(II) 2-Amino-cyclopent-1-ene-1-carbodithioates. *CrystEngComm*, 5(44), 253-261.
- Lai, C. S., & Tiekink, E. R. T. (2004). Engineering Polymers With Variable Topology - Bipyridine Adducts Of Cadmium Dithiophosphates. *CrystEngComm*, 6(97), 593-605.
- Lai, C. S., & Tiekink, E. R. T. (2006). Delineating The Principles Controlling Polymer Formation And Topology In Zinc(II)- And Cadmium(II)-Dithiophosphate Adducts Of Diimine-Type Ligands. *Journal of Molecular Structure*, 796(1-3), 114-118.
- Lai, C. S., & Tiekink, E. R. T. (2006). Polymeric Topologies In Cadmium(Ii) Dithiophosphate Adducts Of The Isomeric N-Pyridinealdazines, n = 2, 3 and 4 *Zeitschrift fur Kristallographie* (Vol. 221, pp. 288).
- Larionov, S. V., Glinskaya, L. A., Leonova, T. G., & Klevtsova, R. F. (2005). Synthesis And Crystal And Molecular Structure Of Mixed-Ligand Complexes Cd(2,2'-Bipy)(i-PrOCS₂)₂ And (2,2'-Bipy)(i-BuOCS₂)₂. *Journal of Structural Chemistry*, 46(6), 1023-1030.
- Lawton, S. L., & Kokotailo, G. T. (1969). Crystal And Molecular Structures Of Zinc And Cadmium O,O-Diisopropyl Phosphorodithioates. *Inorganic Chemistry*, 8(11), 2410-2421.
- Lee, C. T., Yang, W. T., & Parr, R. G. (1988). Development Of The Colle-Salvetti Correlation-Energy Formula Into A Functional Of The Electron-Density. *Physical Review B*, 37(2), 785-789.

- Lee, E., Kim, J.-Y., Lee, S. S., & Park, K.-M. (2013). Molar-Ratio-Dependent Supramolecular Isomerism: AgI Coordination Polymers With Bis(cyanobenzyl)sulfides. *Chemistry – A European Journal*, 19(41), 13638-13645.
- Leong, W. L., & Vittal, J. J. (2011). One-Dimensional Coordination Polymers: Complexity and Diversity in Structures, Properties, and Applications. *Chemical Reviews*, 111(2), 688-764.
- Li, C.-P., & Du, M. (2011). Role Of Solvents In Coordination Supramolecular Systems. *Chemical Communications*, 47(21), 5958-5972.
- Li, G., Wang, C., & Zhang, X. (2013). Two Supramolecular Isomers With Different Structural Features: Reversible Transformation And Fluorescence Properties. *Journal of Coordination Chemistry*, 66(7), 1107-1117.
- Li, S.-H., Han, M.-L., Liu, G.-Z., Ma, L.-F., & Wang, L.-Y. (2015). Guest-Induced Single-Crystal-To-Single-Crystal Transformations Of A New 4-Connected 3D Cadmium(II) Metal-Organic Framework. *RSC Advances*, 5(23), 17588-17591.
- Li, T., Li, Z.-H., & Du, S.-W. (2004). Catena-Poly[[bis(O,O'-diethyl dithiophosphato- k^2S,S')cadmium(II)]-m-4,4'-bipyridine-N:N']. *Acta Crystallographica Section E*, 60(12), m1912-m1914.
- Li, T., LI, Z.-H., & Du, S.-W. (2005). Catena-Poly[[bis(O,O'-dimethyl dithiophosphato- k^2S,S')cadmium(II)]-m-4,4'-bipyridine-N:N']. *Acta Crystallographica Section E*, 61(1), m95-m97.
- Li, T., Li, Z.-H., Hu, S.-M., & Du, S.-W. (2006). Syntheses, Crystal Structures And Luminescence Properties Of Cadmium(II) O,O'-Dialkyldithiophosphates With Nitrogen Donors. *Journal of Coordination Chemistry*, 59(8), 945-952.
- Liu, B., Pang, L.-Y., Hou, L., Wang, Y.-Y., Zhang, Y., & Shi, Q.-Z. (2012). Two Solvent-Dependent Zinc(II) Supramolecular Isomers: Structure Analysis, Reversible And Nonreversible Crystal-To-Crystal Transformation, Highly Selective CO₂ Gas Adsorption, And Photoluminescence Behaviors. *CrystEngComm*, 14(19), 6246-6251.
- Liu, Y., & Tiekink, E. R. T. (2005). Supramolecular Associations In Binary Antimony(III) Dithiocarbamates: Influence Of Ligand Steric Bulk, Influence On Coordination Geometry, And Competition With Hydrogen-Bonding. *CrystEngComm*, 7(2), 20-27.

- López-Mejías, V., Kampf, J. W., & Matzger, A. J. (2012). Nonamorphism In Flufenamic Acid And A New Record For A Polymorphic Compound With Solved Structures. *Journal of the American Chemical Society*, 134(24), 9872-9875.
- Luo, L., Chen, K., Liu, Q., Lu, Y., Okamura, T.-A., Lv, G.-C., Zhao, Y., & Sun, W.-Y. (2013). Zinc(II) And Cadmium(II) Complexes With 1,3,5-Benzenetricarboxylate And Imidazole-Containing Ligands: Structural Variation Via Reaction Temperature And Solvent. *Crystal Growth & Design*, 13(6), 2312-2321.
- Malik, M. A., O'Brien, P., & Motevalli, M. (1996). Bis(m-diethyldithiocarbamato)-1kS,1:2k²S';2kS,1:2k²S'-bis(ethylzinc). *Acta Crystallographica Section C*, 52(8), 1931-1933.
- Manna, B., Singh, S., Karmakar, A., Desai, A. V., & Ghosh, S. K. (2015). Selective Anion Exchange And Tunable Luminescent Behaviors Of Metal–Organic Framework Based Supramolecular Isomers. *Inorganic Chemistry*, 54(1), 110-116.
- Manohar, A., Ramalingam, I., Bocelli, G., & Cantoni, A. (2005). Synthesis And Spectral Studies On 2 : 1 Adducts Involving Cadmium Dithiocarbamates And 4,4-Bipyridine. Single Crystal X-Ray Structural Studies On Bis(piperidinecarbodithioato-S,S')cadmium(II) Benzene Solvate. *Polish Journal of Chemistry*, 79(4), 671-678.
- Masui, H. (2001). Metalloaromaticity. *Coordination Chemistry Reviews*, 219–221(0), 957-992.
- McCleverty, J. A., Gill, S., Kowalski, R. S. Z., Bailey, N. A., Adams, H., Lumbard, K. W., & Murphy, M. A. (1982). Aspects Of The Inorganic Chemistry Of Rubber Vulcanisation. Part 3. Anionic Cadmium Complexes Derived From Dialkyldithiocarbamates, 2-Mercaptobenzothiazole And Its Derivatives, And Dialkyl Dithiophosphates, And The Crystal And Molecular Structures Of [NⁿBuⁿ][Cd(S₂CNEt₂)₃], [NEt₄][Cd(C₇H₄NS₂)₃], And [NMe₄][Cd{S₂P(OPrⁱ)₂}₃]. *Journal of the Chemical Society, Dalton Transactions*(3), 493-503.
- Medaković, V. B., Bogdanović, G. A., Milčić, M. K., Janjić, G. V., & Zarić, S. D. (2012). CH/π Interactions In Metal–Porphyrin Complexes With Pyrrole And Chelate Rings As Hydrogen Acceptors. *Journal of Inorganic Biochemistry*, 117(0), 157-163.
- Medaković, V. B., Milčić, M. K., Bogdanović, G. A., & Zarić, S. D. (2004). C–H⋯π Interactions In The Metal–Porphyrin Complexes With Chelate Ring As The H Acceptor. *Journal of Inorganic Biochemistry*, 98(11), 1867-1873.

- Meng, X., Song, X.-Z., Song, S.-Y., Su, S.-Q., Zhu, M., Hao, Z.-M., Zhao, S.-N., & Zhang, H.-J. (2013). Supramolecular Isomerism, Single-Crystal To Single-Crystal Transformation Induced By Release Of In Situ Generated I₂ Between Two Supramolecular Frameworks. *Dalton Transactions*, 42(16), 5619-5622.
- Mensforth, E. J., Hill, M. R., & Batten, S. R. (2013). Coordination Polymers Of Sulphur-Donor Ligands. *Inorganica Chimica Acta*, 403, 9-24.
- Milčič, M. K., Medaković, V. B., Sredojević, D. N., Juranić, N. O., & Zarić, S. D. (2006). Electron Delocalization Mediates The Metal-Dependent Capacity For CH/ π Interactions Of Acetylacetonato Chelates. *Inorganic Chemistry*, 45(12), 4755-4763.
- Mishra, M. K., Sanphui, P., Ramamurty, U., & Desiraju, G. R. (2014). Solubility-Hardness Correlation In Molecular Crystals: Curcumin And Sulfathiazole Polymorphs. *Crystal Growth & Design*, 14(6), 3054-3061.
- Mlowe, S., Lewis, D. J., Malik, M. A., Raftery, J., Mubofu, E. B., O'Brien, P., & Revaprasadu, N. (2014). Bis(piperidinedithiocarbamato)pyridinecadmium(II) As A Single-Source Precursor For The Synthesis Of CdS Nanoparticles And Aerosol-Assisted Chemical Vapour Deposition (AACVD) Of CdS Thin Films. *New Journal of Chemistry*, 38(12), 6073-6080.
- Mohamed-Ibrahim, M. I., Chee, S. S., Buntine, M. A., Cox, M. J., & Tiekink, E. R. T. (2000). Structural Variation In Diorganotin Dimethylxanthates, R₂Sn(S₂COMe)₂: A Combined Crystallographic And Theoretical Investigation. *Organometallics*, 19(25), 5410-5415.
- Mohamed, A. A., Kani, I., Ramirez, A. O., & Fackler, J. P. (2004). Synthesis, Characterization, And Luminescent Properties Of Dinuclear Gold(I) Xanthate Complexes: X-Ray Structure Of [Au₂(ⁿBu-xanthate)₂]. *Inorganic Chemistry*, 43(13), 3833-3839.
- Mothes, R., Jakob, A., Waechtler, T., Schulz, S. E., Gessner, T., & Lang, H. (2015). [Ag{S₂CNR(C₂H₄OH)}] As Single-Source Precursor For Ag₂S – Synthesis, Decomposition Mechanism, And Deposition Studies. *European Journal of Inorganic Chemistry*, 2015(10), 1726-1733.
- Moulton, B., & Zaworotko, M. J. (2001). From Molecules to Crystal Engineering: Supramolecular Isomerism and Polymorphism in Network Solids. *Chemical Reviews*, 101(6), 1629-1658.

- Mukherjee, A., & Desiraju, G. R. (2014). Halogen Bonds In Some Dihalogenated Phenols: Applications To Crystal Engineering. *IUCrJ*, 1(1), 49-60.
- Nabipour, H., Ghammamy, S., Ashuri, S., & Aghbolagh, Z. S. (2010). Synthesis Of A New Dithiocarbamate Compound And Study Of Its Biological Properties. *Organic Chemistry Journal*, 2, 75-80.
- Nagarkar, S. S., Chaudhari, A. K., & Ghosh, S. K. (2012). Role Of Temperature On Framework Dimensionality: Supramolecular Isomers Of $Zn_3(RCOO)_8$ Based Metal Organic Frameworks. *Crystal Growth & Design*, 12(2), 572-576.
- Nangia, A. (2010). Supramolecular Chemistry And Crystal Engineering. *Journal of Chemical Sciences*, 122(3), 295-310.
- Nangia, A., & Desiraju, G. R. (1999). Pseudopolymorphism: Occurrences Of Hydrogen Bonding Organic Solvents In Molecular Crystals. *Chemical Communications*(7), 605-606.
- Nomura, R., Kori, M., & Matsuda, H. (1985). Preparation And Reactions Of Novel m-Oxo-Bisantimony Aminoalkoxide. *Chemistry Letters*, 14(5), 579-580.
- Nugent, P., Belmabkhout, Y., Burd, S. D., Cairns, A. J., Luebke, R., Forrest, K., Pham, T., Ma, S., Space, B., Wojtas, L., Eddaoudi, M., & Zaworotko, M. J. (2013). Porous Materials With Optimal Adsorption Thermodynamics And Kinetics For CO_2 Separation. *Nature*, 495(7439), 80-84.
- O'Boyle, N. M., Tenderholt, A. L., & Langner, K. M. (2008). cclib: A Library For Package-Independent Computational Chemistry Algorithms. *Journal of Computational Chemistry*, 29(5), 839-845.
- Okubo, T., Anma, H., Tanaka, N., Himoto, K., Seki, S., Saeki, A., Maekawa, M., & Kuroda-Sowa, T. (2013). Crystal Structure And Carrier Transport Properties Of A New Semiconducting 2D Coordination Polymer With A 3,5-Dimethylpiperidine Dithiocarbamate Ligand. *Chemical Communications*, 49(39), 4316-4318.
- Okubo, T., Kuwamoto, H., Kim, K. H., Hayami, S., Yamano, A., Shiro, M., Maekawa, M., & Kuroda-Sowa, T. (2011). Intervalence Charge-Transfer System By 1D Assembly Of New Mixed-Valence Octanuclear $Cu^I/Cu^{II}/Cu^{III}$ Cluster Units. *Inorganic Chemistry*, 50(7), 2708-2710.

- Okubo, T., Tanaka, N., Kim, K. H., Anma, H., Seki, S., Saeki, A., Maekawa, M., & Kuroda-Sowa, T. (2011). Crystal Structure And Carrier Transport Properties Of A New 3D Mixed-Valence Cu(I)-Cu(II) Coordination Polymer Including Pyrrolidine Dithiocarbamate Ligand. *Dalton Transactions*, 40(10), 2218-2224.
- Onwudiwe, D. C., Krüger, T. P. J., & Strydom, C. A. (2014). Laser Assisted Solid State Reaction For The Synthesis Of ZnS And CdS Nanoparticles From Metal Xanthate. *Materials Letters*, 116(0), 154-159.
- Otero-de-la-Roza, A., & Johnson, E. R. (2012). A Benchmark For Non-Covalent Interactions In Solids. *The Journal of Chemical Physics*, 137(5), 054103.
- Otero-de-la-Roza, A., & Johnson, E. R. (2012). Van der Waals Interactions In Solids Using The Exchange-Hole Dipole Moment Model. *The Journal of Chemical Physics*, 136(17), 174109.
- Otero-de-la-Roza, A., & Johnson, E. R. (2013). Non-Covalent Interactions And Thermochemistry Using XDM-Corrected Hybrid And Range-Separated Hybrid Density Functionals. *The Journal of Chemical Physics*, 138(20), 204109.
- Otero-de-la-Roza, A., Mallory, J. D., & Johnson, E. R. (2014). Metallophilic Interactions From Dispersion-Corrected Density-Functional Theory. *The Journal of Chemical Physics*, 140(18), 18A504.
- Park, I.-H., Chanthapally, A., Zhang, Z., Lee, S. S., Zaworotko, M. J., & Vittal, J. J. (2014). Metal–Organic Organopolymeric Hybrid Framework By Reversible [2+2] Cycloaddition Reaction. *Angewandte Chemie International Edition*, 53(2), 414-419.
- Park, I.-H., Lee, S. S., & Vittal, J. J. (2013). Guest-Triggered Supramolecular Isomerism In A Pillared-Layer Structure With Unusual Isomers Of Paddle-Wheel Secondary Building Units By Reversible Single-Crystal-To-Single-Crystal Transformation. *Chemistry – A European Journal*, 19(8), 2695-2702.
- Peedikakkal, A. M. P., & Vittal, J. J. (2011). Structural Transformations Of Pb(II)-trans-1,2-bis(4'-pyridyl)ethene Coordination Polymers In Solution. *Crystal Growth & Design*, 11(10), 4697-4703.
- Perdew, J. P., Burke, K., & Ernzerhof, M. (1996). Generalized Gradient Approximation Made Simple. *Physical Review Letters*, 77(18), 3865-3868.

- Peterson, K. A., & Puzzarini, C. (2005). Systematically Convergent Basis Sets For Transition Metals. II. Pseudopotential-Based Correlation Consistent Basis Sets For The Group 11 (Cu, Ag, Au) And 12 (Zn, Cd, Hg) Elements. *Theoretical Chemistry Accounts*, 114(4-5), 283-296.
- Poirier, S., Roberts, R. J., Le, D., Leznoff, D. B., & Reber, C. (2015). Interpreting Effects Of Structure Variations Induced By Temperature And Pressure On Luminescence Spectra Of Platinum(II) Bis(dithiocarbamate) Compounds. *Inorganic Chemistry*, 54(8), 3728-3735.
- Poplaukhin, P., Arman Hadi, D., & Tiekink, E. R. T. (2012). Supramolecular Isomerism In Coordination Polymers Sustained By Hydrogen Bonding: Bis[Zn(S₂CN(Me)CH₂CH₂OH)₂](N,N'-bis(pyridin-3-ylmethyl)thioxalamide) *Zeitschrift für Kristallographie Crystalline Materials* (Vol. 227, pp. 363).
- Poplaukhin, P., & Tiekink, E. R. T. (2010). Interwoven Coordination Polymers Sustained By Tautomeric Forms Of The Bridging Ligand. *CrystEngComm*, 12(4), 1302-1306.
- Prasanna, S., Bijini, B. R., Rajendra Babu, K., Eapen, S. M., Deepa, M., & Nair, C. M. K. (2011). Growth And Characterisation Of A Novel Polymer Of Manganese(II) Nicotinate Single Crystal. *Journal of Crystal Growth*, 333(1), 36-39.
- Rajput, G., Singh, V., Gupta, A. N., Yadav, M. K., Kumar, V., Singh, S. K., Prasad, A., Drew, M. G. B., & Singh, N. (2013). Unusual C-H...Ni Anagostic Interactions In New Homoleptic Ni(II) Dithio Complexes. *CrystEngComm*, 15(23), 4676-4683.
- Rietveld, H. M., & Maslen, E. N. (1965). The Crystal Structure Of Cadmium N-Butyl Xanthate. *Acta Crystallographica*, 18(3), 429-436.
- Rojas-Leon, I., Guerrero-Alvarez, J. A., Hernandez-Paredes, J., & Hopfl, H. (2012). Solvent-Solvent And Solvent-Solute Interactions In A 3D Chloroform Clathrate With Diorganotin Macrocycles In The Nano-Sized Pores. *Chemical Communications*, 48(3), 401-403.
- Romanenko, G. V., Podberezskaya, N. V., Baidina, I. A., Bakakin, V. V., & Borisov, S. V. (1979). The crystal structure of bis(trifluoroethylxanthato)palladium(II) Pd(S₂COCH₂CF₃)₂ and various crystal-chemical characteristics of alkylxanthates. *Journal of Structural Chemistry*, 20(3), 439-445.

- Rowland, R. S., & Taylor, R. (1996). Intermolecular Nonbonded Contact Distances In Organic Crystal Structures: Comparison With Distances Expected From Van der Waals Radii. *The Journal of Physical Chemistry*, 100(18), 7384-7391.
- Saravanan, M., Ramalingam, K., Bocelli, G., & Olla, R. (2004). Crystallographic Report: A New Polymorph For Bis[bis(N,N-dibenzylthiocarbamato)cadmium(II)]. *Applied Organometallic Chemistry*, 18(2), 103-103.
- Scherer, W., Dunbar, A. C., Barquera-Lozada, J. E., Schmitz, D., Eickerling, G., Kratzert, D., Stalke, D., Lanza, A., Macchi, P., Casati, N. P. M., Ebad-Allah, J., & Kuntscher, C. A. (2015). Anagostic Interactions Under Pressure: Attractive Or Repulsive? *Angewandte Chemie*, 127(8), 2535-2539.
- Shahzadi, S., Ali, S., Jabeen, R., & Khosa, M. K. (2009). Pd(Me-Xanthate)₂ : Synthesis, Characterization, And X-Ray Structure. *Turkish Journal of Chemistry*, 33(2), 307-312.
- Sheldrick, G. (2008). A Short History Of Shelx. *Acta Crystallographica Section A*, 64(1), 112-122.
- Sheldrick, G. (2015). Crystal Structure Refinement With SHELXL. *Acta Crystallographica Section C*, 71(1), 3-8.
- Sheldrick, G. M. (1996). SADABS. Germany: University of Göttingen.
- Shimoi, M., Ouchi, A., Aikawa, M., Sato, S., & Saito, Y. (1982). Syntheses And Structure Of Bis(O,O'-diethyl dithiophosphato)bis(hexamethylenetetramine)cadmium(II) And Related Adducts. *Bulletin of the Chemical Society of Japan*, 55(7), 2089-2093.
- Singh, S. K., Drew, M. G. B., & Singh, N. (2013). Self Assembly Of Homoleptic Ni(II) Dithiocarbamates And Dithiocarbimates Via Ni...H-C Anagostic And C-H...p(Chelate) Interactions. *CrystEngComm*, 15(47), 10255-10265.
- Singhal, A., Dutta, D. P., Tyagi, A. K., Mobin, S. M., Mathur, P., & Lieberwirth, I. (2007). Palladium(II)/allylpalladium(II) Complexes With Xanthate Ligands: Single-Source Precursors For The Generation Of Palladium Sulfide Nanocrystals. *Journal of Organometallic Chemistry*, 692(23), 5285-5294.

- Smith, A. J., Kavuru, P., Arora, K. K., Kesani, S., Tan, J., Zaworotko, M. J., & Shytle, R. D. (2013). Crystal Engineering Of Green Tea Epigallocatechin-3-gallate (EGCg) Cocrystals And Pharmacokinetic Modulation In Rats. *Molecular Pharmaceutics*, 10(8), 2948-2961.
- Smith, A. J., Kim, S.-H., Duggirala, N. K., Jin, J., Wojtas, L., Ehrhart, J., Giunta, B., Tan, J., Zaworotko, M. J., & Shytle, R. D. (2013). Improving Lithium Therapeutics By Crystal Engineering Of Novel Ionic Cocrystals. *Molecular Pharmaceutics*, 10(12), 4728-4738.
- Spek, A. (2003). Single-Crystal Structure Validation With The Program PLATON. *Journal of Applied Crystallography*, 36(1), 7-13.
- Spek, A. (2009). Structure Validation In Chemical Crystallography. *Acta Crystallographica Section D*, 65(2), 148-155.
- Srinivasan, N., Jamuna Rani, P., & Thirumaran, S. (2009). Synthesis And Spectral Studies On Mixed Ligand Complexes Of Cd(II) Dithiocarbamates With Nitrogen Donors: Single Crystal X-Ray Structure Of Bis(4-methylpiperidinecarbodithioato-S,S')(1,10-phenanthroline)cadmium(II). *Journal of Coordination Chemistry*, 62(8), 1271-1277.
- Stang, P. J., & Olenyuk, B. (1997). Self-Assembly, Symmetry, And Molecular Architecture: Coordination As The Motif In The Rational Design Of Supramolecular Metallacyclic Polygons And Polyhedra. *Accounts of Chemical Research*, 30(12), 502-518.
- Sun, D., Ke, Y., Mattox, T. M., Ooro, B. A., & Zhou, H.-C. (2005). Temperature-Dependent Supramolecular Stereoisomerism In Porous Copper Coordination Networks Based On A Designed Carboxylate Ligand. *Chemical Communications*(43), 5447-5449.
- Sun, Z.-F., Duan, C.-Y., You, X.-Z., & Huang, X.-Y. (1994). A Mixed-Ligand Cadmium(II) Complex Of Xanthic Acid And N,N'-Bis(4-methoxyphenyl)thiourea. *Acta Crystallographica Section C*, 50(7), 1012-1014.
- Tan, Y. S., Abdul Halim, S. N., & Tiekink, E. R. T. (2014). Crystal Structure Of 3-(Propan-2-yl)-1,3-oxazolidine-2-thione, C₆H₁₁NOS *Zeitschrift für Kristallographie - New Crystal Structures* (Vol. 229, pp. 55).

- Tan, Y. S., Sudlow, A. L., Molloy, K. C., Morishima, Y., Fujisawa, K., Jackson, W. J., Henderson, W., Abdul Halim, S. N., Ng, S. W., & Tiekink, E. R. T. (2013). Supramolecular Isomerism In A Cadmium Bis(N-Hydroxyethyl, N-Isopropylthiocarbamate) Compound: Physiochemical Characterization Of Ball ($n = 2$) And Chain ($n = \infty$) Forms Of $\{Cd[S_2CN(iPr)CH_2CH_2OH]_2 \cdot \text{solvent}\}_n$. *Crystal Growth & Design*, 13(7), 3046-3056.
- Tanaka, D., Nakagawa, K., Higuchi, M., Horike, S., Kubota, Y., Kobayashi, T. C., Takata, M., & Kitagawa, S. (2008). Kinetic Gate-Opening Process In A Flexible Porous Coordination Polymer. *Angewandte Chemie International Edition*, 47(21), 3914-3918.
- Taubmann, C., Öfele, K., Herdtweck, E., & Herrmann, W. A. (2009). Complexation Of (5H)-Dibenzo[a,d]cyclohepten-5-ylidene To Palladium(II) Via The Diazo Route And Evidence Of C-H \cdots Pd Interactions. *Organometallics*, 28(15), 4254-4257.
- Thirumaran, S., Srinivasan, N., Sharma, V., Gupta, V. K., & Rajnikant. (2012). Crystal Structure Of Bis(m-4-methylpiperidine-1-carbodithioato-1:2k³S,S':S';2:1k³S,S':S')bis[(4-methylpiperidine-1-carbodithioato-k²S,S')cadmium(II)]. *X-ray Structure Analysis Online*, 28, 21-22.
- Tiekink, E. R. T. (1987). Bis(O-methyldithiocarbonato)mercury(II). *Acta Crystallographica Section C*, 43(3), 448-450.
- Tiekink, E. R. T. (1988). Polymeric Bis(O-methyldithiocarbonato)lead(II). *Acta Crystallographica Section C*, 44(2), 250-253.
- Tiekink, E. R. T. (2000). On The Structure Of Cadmium Isopropylxanthate. Corrigendum. *Acta Crystallographica Section C*, 56(9), 1176.
- Tiekink, E. R. T. (2001). Crystal Structure Of 2,2'-Bipyridyl Adduct Of Bis(dibutyldithiocarbamate)zinc(II), $[Zn(S_2CNBu_2)_2(\text{bipy})]$ *Zeitschrift für Kristallographie - New Crystal Structures*, 216(4), 575.
- Tiekink, E. R. T. (2003). Molecular Architecture And Supramolecular Association In The Zinc-Triad 1,1-Dithiolates. Steric Control As A Design Element In Crystal Engineering? *CrystEngComm*, 5(21), 101-113.
- Tiekink, E. R. T. (2006). Aggregation Patterns In The Crystal Structures Of Organometallic Group XV 1,1-Dithiolates: The Influence Of The Lewis Acidity Of The Central Atom, Metal- And Ligand-Bound Steric Bulk, And Coordination Potential Of The 1,1-Dithiolate Ligands Upon Supramolecular Architecture. *CrystEngComm*, 8(2), 104-118.

- Tiekink, E. R. T. (2008). Tin Dithiocarbamates: Applications And Structures. *Applied Organometallic Chemistry*, 22(9), 533-550.
- Tiekink, E. R. T., & Haiduc, I. (2005). Stereochemical Aspects Of Metal Xanthate Complexes: Molecular Structures And Supramolecular Self-Assembly *Progress in Inorganic Chemistry* (Vol. 54, pp. 127-319): John Wiley & Sons, Inc.
- Tiekink, E. R. T., & Haiduc, I. (2005). Stereochemical Aspects Of Metal Xanthate Complexes: Molecular Structures And Supramolecular Self-Assembly *Progress in Inorganic Chemistry* (pp. 127-319): John Wiley & Sons, Inc.
- Tiekink, E. R. T., & Zukerman-Schpector, J. (2010). Pb $\cdots\pi$ Aryl Interactions As Supramolecular Synthons. *Australian Journal of Chemistry*, 63(4), 535-543.
- Tiekink, E. R. T., & Zukerman-Schpector, J. (2010). Stereochemical Activity Of Lone Pairs Of Electrons And Supramolecular Aggregation Patterns Based On Secondary Interactions Involving Tellurium In Its 1,1-Dithiolate Structures. *Coordination Chemistry Reviews*, 254(1–2), 46-76.
- Tiekink, E. R. T., & Zukerman-Schpector, J. (2011). Emerging Supramolecular Synthons: C-H \cdots p(chelate) Interactions In Metal Bis(1,1-dithiolates). *Chemical Communications*, 47(23), 6623-6625.
- Tomasi, J., Mennucci, B., & Cammi, R. (2005). Quantum Mechanical Continuum Solvation Models. *Chemical Reviews*, 105(8), 2999-3094.
- Tomlin, D. W., Cooper, T. M., Zelmon, D. E., Gebeyehu, Z., & Hughes, J. M. (1999). Cadmium Isopropylxanthate. *Acta Crystallographica Section C*, 55(5), 717-719.
- Upreti, M., Smit, J. P., Hagen, E. J., Smolenskaya, V. N., & Prakash, I. (2011). Single Crystal Growth And Structure Determination Of The Natural “High Potency” Sweetener Rebaudioside A. *Crystal Growth & Design*, 12(2), 990-993.
- van Poppel, L. H., Groy, T. L., & Caudle, M. T. (2004). Carbon–Sulfur Bond Cleavage In Bis(N-alkyldithiocarbamato)cadmium(II) Complexes: Heterolytic Desulfurization Coupled To Topochemical Proton Transfer. *Inorganic Chemistry*, 43(10), 3180-3188.

- van Poppel, L. H., Groy, T. L., & Tyler Caudle, M. (2004). Carbon–Sulfur Bond Cleavage In Bis(N-alkyldithiocarbamato)cadmium(II) Complexes: Heterolytic Desulfurization Coupled To Topochemical Proton Transfer. *Inorganic Chemistry*, 43(10), 3180-3188.
- van Zyl, W. E., & Woollins, J. D. (2013). The Coordination Chemistry Of Dithiophosphonates: An Emerging And Versatile Ligand Class. *Coordination Chemistry Reviews*, 257(3–4), 718-731.
- Vittal, J. J. (2007). Supramolecular Structural Transformations Involving Coordination Polymers In The Solid State. *Coordination Chemistry Reviews*, 251(13–14), 1781-1795.
- Vydrov, O. A., Heyd, J., Krukau, A. V., & Scuseria, G. E. (2006). Importance Of Short-Range Versus Long-Range Hartree-Fock Exchange For The Performance Of Hybrid Density Functionals. *The Journal of Chemical Physics*, 125(7), 074106.
- Vydrov, O. A., & Scuseria, G. E. (2006). Assessment Of A Long-Range Corrected Hybrid Functional. *The Journal of Chemical Physics*, 125(23), 234109.
- Wang, S., Peng, Y., Wei, X., Zhang, Q., Wang, D., Dou, J., Li, D., & Bai, J. (2011). Temperature-Dependent Supramolecular Isomerism In Three Zinc Coordination Polymers With Pamoic Acid And 1,4-Bis(imidazol-1-ylmethyl)-benzene. *CrystEngComm*, 13(17), 5313-5316.
- Wang, Y., Yan, L., Fu, J., & Chai, M. (2005). *Huaxue Tong bao*, 68, w036.
- Winter, G. (1980). Inorganic Xanthates. *Rev. Inorg. Chem.*, 2, 253-342.
- . X'Pert HighScore Plus. (2009). Almelo, The Netherlands: PANalytical B.V.
- Xia, Q., Ren, Y., Cheng, M.-L., Liu, X., Chen, S., Zhai, C., & Liu, Q. (2015). Ligand Concentration-Dependent Supramolecular Complexes With Uncoordinated Carbonyl Groups Based On A New Pyrazole Carboxylic Acid Ligand. *Journal of Coordination Chemistry*, 68(10), 1688-1704.
- Yaghi, O. M., O'Keeffe, M., Ockwig, N. W., Chae, H. K., Eddaoudi, M., & Kim, J. (2003). Reticular Synthesis And The Design Of New Materials. *Nature*, 423(6941), 705-714.

- Yang Farina, A. A., Othman, A. H., Baba, I., Sivakumar, K., Fun, H.-K., & Ng, S. W. (2000). Bis[N,N-bis(2-hydroxyethyl)dithiocarbamato]dimethyltin(IV). *Acta Crystallographica Section C*, 56(3), e84-e85.
- Yin, X., Zhang, W., Zhang, Q., Fan, J., Lai, C. S., & Tiekink, E. R. T. (2004). Crystallographic Report: Bis[bis(N,N-dibenzylidithiocarbamato)cadmium(II)]. *Applied Organometallic Chemistry*, 18(3), 139-140.
- Yin, Y.-G., Fording, W., Antzutkin, O., Lindbergh, M., Ivanov, A., & Boström, D. (2003). Polymeric Structure And Solid NMR Spectra Of Cadmium (II) Dialkyldithiophosphates (Alkyl = Propyl, Butyl, Isopropyl And Isobutyl). *Chinese Journal of Chemistry*, 21(3), 291-295.
- Young Jr, V. G., & Tiekink, E. R. T. (2002). Bis(O-methyldithiocarbonato)cadmium(II). *Acta Crystallographica Section E*, 58(10), m537-m539.
- Zemskova, S. M., Glinskaya, L. A., Klevtsova, R. F., Fedotov, M. A., & Larionov, S. V. (1999). Structure And Properties Of Mono- And Heterometallic Cadmium, Zinc, And Nickel Complexes Containing Diethyldithiocarbamate Ions And Ethylenediamine Molecules. *Journal of Structural Chemistry*, 40(2), 284-292.
- Zhang, J.-P., Huang, X.-C., & Chen, X.-M. (2009). Supramolecular Isomerism In Coordination Polymers. *Chemical Society Reviews*, 38(8), 2385-2396.
- Zhang, J.-P., Lin, Y.-Y., Zhang, W.-X., & Chen, X.-M. (2005). Temperature- Or Guest-Induced Drastic Single-Crystal-To-Single-Crystal Transformations Of A Nanoporous Coordination Polymer. *Journal of the American Chemical Society*, 127(41), 14162-14163.
- Zhang, Y., Bhadbhade, M., Price, J. R., Karatchevtseva, I., Collison, D., & Lumpkin, G. R. (2014). Kinetics Vs. Thermodynamics: A Unique Crystal Transformation From A Uranyl Peroxo-Nanocluster To A Nanoclustered Uranyl Polyborate. *RSC Advances*, 4(65), 34244-34247.
- Zhang, Y., Lewis, J. C., Bergman, R. G., Ellman, J. A., & Oldfield, E. (2006). Nmr Shifts, Orbitals, And M···H-X Bonding In d⁸ Square Planar Metal Complexes. *Organometallics*, 25(14), 3515-3519.
- Zhong, Y., Zhang, W., Fan, J., Tan, M., Lai, C. S., & Tiekink, E. R. T. (2004). Bis[m-N,N-bis(2-hydroxyethyl)dithiocarbamato]-1:2k³S,S':S';2:1k³S,S':S'-bis{[N,N-bis(2-hydroxyethyl)dithiocarbamato-k²S,S']cadmium(II)}. *Acta Crystallographica Section E*, 60(11), m1633-m1635.

- Zohir, N., Mustapha, B., & Abdul Elbak, i. D. (2009). Synthesis And Structural Characterization Of Xanthate (KEX) In Sight Of Their Utilization In The Processes Of Sulphides Flotation *Journal of Minerals & Materials Characterization & Engineering*, 8(6), 469-477.
- Zou, G.-D., He, Z.-Z., Tian, C.-B., Zhou, L.-J., Feng, M.-L., Zhang, X.-D., & Huang, X.-Y. (2014). Microwave And Conventional Hydro(Solvo)Thermal Syntheses Of Three Co(II) Coordination Polymers: Supramolecular Isomerism And Structural Transformations Accompanied By Tunable Magnetic Properties. *Crystal Growth & Design*, 14(9), 4430-4438.
- Zukerman-Schpector, J., Haiduc, I., & Tiekink, E. R. T. (2011). The Metal-Carbonyl...p(Aryl) Interaction As A Supramolecular Synthone For The Stabilisation Of Transition Metal Carbonyl Crystal Structures. *Chemical Communications*, 47(47), 12682-12684.
- Zukerman-Schpector, J., Haiduc, I., & Tiekink, E. R. T. (2012). Chapter Two - Supramolecular Self-Assembly Of Transition Metal Carbonyl Molecules Through M-CO(Lone Pair)... π (Arene) Interactions. In F. H. Anthony & J. F. Mark (Eds.), *Advances in Organometallic Chemistry* (Vol. Volume 60, pp. 49-92): Academic Press.
- Zukerman-Schpector, J., Otero-de-la-Roza, A., Luana, V., & Tiekink, E. R. T. (2011). Supramolecular Architectures Based On As(Lone Pair)...p(Aryl) Interactions. *Chemical Communications*, 47(27), 7608-7610.
- Zukerman-Schpector, J., & Tiekink, E. R. T. (2012). Intermolecular C-H... π (Chelate) Interactions – Prevalence In The Crystal Structures Of Metal 1,1-Dithiolates *The Importance of Pi-Interactions in Crystal Engineering* (pp. 275-299): John Wiley & Sons, Ltd.
- Zukerman-Schpector, J., & Tiekink, E. R. T. (2014). On The Role Of DMSO-O(Lone Pair)...p(Arene), DMSO-S(Lone Pair)...p(Arene) And S=O...p(Arene) Interactions In The Crystal Structures Of Dimethyl Sulphoxide (DMSO) Solvates. *CrystEngComm*, 16(28), 6398-6407.

LIST OF SELECTED PUBLICATION AND CONFERENCE ATTENDED

PUBLICATION

- PUBLICATION 1** 119
Supramolecular Isomerism in a Cadmium Bis(*N*-Hydroxyethyl, *N*-isopropylthiocarbamate) Compound: Physiochemical Characterization of Ball ($n = 2$) and Chain ($n = \infty$) Forms of $\{\text{Cd}[\text{S}_2\text{CN}(\text{iPr})\text{CH}_2\text{CH}_2\text{OH}]_2 \cdot \text{solvent}\}_n$.
- PUBLICATION 2** 120
Exploring the crystallization landscape of cadmium bis(*N*-hydroxyethyl, *N*-isopropylthiocarbamate), $\text{Cd}[\text{S}_2\text{CN}(\text{iPr})\text{CH}_2\text{CH}_2\text{OH}]_2$.
- PUBLICATION 3** 121
Serendipitous compositional and structural diversity in urotropine adducts of binary cadmium xanthates.
- PUBLICATION 4** 122
Persistence of $\text{C}-\text{H} \cdots \pi$ (chelate ring) interactions in the crystal structures of $\text{Pd}(\text{S}_2\text{COR})_2$. The utility of $\text{Pd}(\text{S}_2\text{COR})_2$ as precursors for palladium sulphide materials.

CONFERENCE

- CONFERENCE 1** 123
Poster: The Influence of Water on The Transformation Between Supramolecular Isomers of Bis(*N*-Hydroxyethyl-*N*-isopropyl-dithiocarbamate)Cadmium(II)
- CONFERENCE 2** 124
Oral: Supramolecular Isomer Transformation of Bis(*N*-hydroxyethyl-*N*-isopropyl-dithiocarbamate)Cadmium(II).
- CONFERENCE 3** 125
Poster: The Influence of Water on The Transformation Between Supramolecular Isomers of Bis(*N*-Hydroxyethyl-*N*-isopropyl-dithiocarbamate)Cadmium(II)
- CONFERENCE 4** 126
Oral & Poster: Single crystal-single crystal transformation of supramolecular isomers of Bis(*N*-hydroxyethyl-*N*-isopropyl dithiocarbamate)cadmium(II).
- CONFERENCE 5** 127
Oral: Pseudo-Reversible Single Crystal to Single Crystal Transformation for Non-Reversible Supramolecular Isomerism Transformation of Cadmium(II) Dithiocarbamate Complex.
- CONFERENCE 6** 128
Poster: Single Crystal to Single Crystal Transformations of Bis(*N*-hydroxyethyl-*N*-isopropyl-dithiocarbamate)Cadmium(II) Supramolecular Isomers.

Supramolecular Isomerism in a Cadmium Bis(*N*-Hydroxyethyl, *N*-isopropylthiocarbamate) Compound: Physiochemical Characterization of Ball ($n = 2$) and Chain ($n = \infty$) Forms of $\{\text{Cd}[\text{S}_2\text{CN}(\text{iPr})\text{CH}_2\text{CH}_2\text{OH}]_2 \cdot \text{solvent}\}_n$

Yee Seng Tan,[†] Anna L. Sudlow,[‡] Kieran C. Molloy,[‡] Yui Morishima,[§] Kiyoshi Fujisawa,[§] Wendy J. Jackson,^{||} William Henderson,^{||} Siti Nadiah Binti Abdul Halim,[†] Seik Weng Ng,^{†,⊥} and Edward R.T. Tiekink^{*,†}

[†]Department of Chemistry, University of Malaya, 50603 Kuala Lumpur, Malaysia

[‡]Department of Chemistry, University of Bath, Bath BA2 7AY, United Kingdom

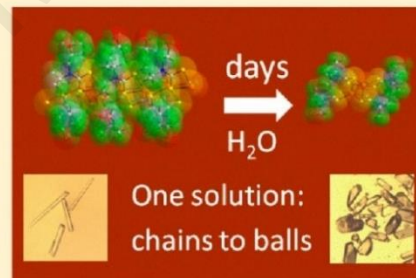
[§]College of Science, Department of Chemistry, Ibaraki University, 2-1-1 Bunkyo, Mito, Ibaraki 310-8512, Japan

^{||}Department of Chemistry, University of Waikato, Private Bag 3105, Hamilton 3240, New Zealand

[⊥]Chemistry Department, Faculty of Science, King Abdulaziz University, PO Box 80203, Jeddah, Saudi Arabia

Supporting Information

ABSTRACT: Needles of $\{\{\text{Cd}[\text{S}_2\text{CN}(\text{iPr})\text{CH}_2\text{CH}_2\text{OH}]_2\}_3 \cdot \text{MeCN}\}_\infty$ (**2**) were harvested from a dry acetonitrile solution of $\text{Cd}[\text{S}_2\text{CN}(\text{iPr})\text{CH}_2\text{CH}_2\text{OH}]_2$ after one or two days and proved to be a coordination polymer in which all dithiocarbamate ligands are μ_2, κ^2 -tridentate, bridging two cadmium atoms and simultaneously chelating one of these. If the same solution was allowed to stand for at least several days, **2** is replaced by blocks comprising a supramolecular isomer of **2**, dimeric **1**, with formula $\{\text{Cd}[\text{S}_2\text{CN}(\text{iPr})\text{CH}_2\text{CH}_2\text{OH}]_2\}_2 \cdot 2\text{H}_2\text{O} \cdot 2\text{MeCN}$, and two ligands coordinating μ_2, κ^2 as in **2** and the other two purely κ^2 -chelating. The time dependency correlates with the pivotal role of water in driving the conversion of “chain” **2** to “ball” **1**; crystals of **2** could not be isolated from “wet” acetonitrile. When each of **1** and **2** are dissolved in solution, they exhibit comparable spectroscopic attributes (^1H , ^{13}C , and ^{113}Cd NMR and UV/vis), indicating the solution structures are the same. Both **1** and **2** are luminescent in the solid state with **1** being significantly brighter than **2**. Greenockite CdS nanoparticles are generated by the thermal decomposition of both **1** and **2**.



1. INTRODUCTION

In the construction of coordination polymers incorporating three-dimensional (3D) metal–organic frameworks (MOFs),^{1,2} the crystal engineer is faced with opportunities whereby systematic variation of a metal center's oxidation state, coordination number, geometry, etc. can be tailored, along with a choice of ancillary ligand(s), to generate a rich diversity of structural motifs with potential applications ranging from gas storage to catalysis.^{3–5} One challenge facing practitioners in this area relates to the phenomenon of supramolecular isomerism (SI).⁶ Here, quite different supramolecular architectures can be constructed from the same molecular constituents. An early and dramatic example of this is found in the structure of copper(I) ethylimidazolate, where from a polar solvent (water) a triple-stranded helix is formed by contrast to the zigzag polymer formed from the less polar solvent system (e.g. water/cyclohexane).⁷ These are examples of solvent-induced supramolecular isomerism, and given the empirical formulas are the same, they can be classified as “genuine” supramolecular

isomers,⁸ as opposed to different supramolecular aggregates cocrystallized with solvent.⁶ Herein, an example of the latter scenario is presented where supramolecular isomers (as different solvates) of a cadmium bis(*N*-hydroxyethyl, *N*-isopropylthiocarbamate) compound, $\{\text{Cd}[\text{S}_2\text{CN}(\text{iPr})\text{CH}_2\text{CH}_2\text{OH}]_2 \cdot \text{solvent}\}_n$, are described, i.e., ball ($n = 2$) and chain ($n = \infty$) forms. Here, the basic building block is considered to be $\text{Cd}[\text{S}_2\text{CN}(\text{iPr})\text{CH}_2\text{CH}_2\text{OH}]_2$, which dimerizes to a ball (**2**) or polymerizes to a chain (**1**). The terminology “pseudo polymorphism” was rejected on the basis that the species feature different coordination geometries.

In crystal engineering endeavors of 1,1-dithiolate ligands, of which dithiocarbamate is a prominent example, metal 1,1-dithiolates are known to serve as reliable precursors of nanosized metal sulfide crystals, especially of the main group

Received: March 26, 2013

Revised: May 21, 2013

Published: May 27, 2013



ACS Publications

© 2013 American Chemical Society

3046

dx.doi.org/10.1021/cg400453x | Cryst. Growth Des. 2013, 13, 3046–3056

Yee Seng Tan, Siti Nadiyah Abdul Halim and Edward R.T. Tiekink*

Exploring the crystallization landscape of cadmium bis(*N*-hydroxyethyl, *N*-isopropylthiocarbamate), $\text{Cd}[\text{S}_2\text{CN}(\text{iPr})\text{CH}_2\text{CH}_2\text{OH}]_2$

DOI 10.1515/zkr-2015-1889

Received August 16, 2015; accepted September 30, 2015; published online October 31, 2015

Abstract: Crystallization of $\text{Cd}[\text{S}_2\text{CN}(\text{iPr})\text{CH}_2\text{CH}_2\text{OH}]_2$ from ethanol yields the coordination polymer $[\{\text{Cd}[\text{S}_2\text{CN}(\text{iPr})\text{CH}_2\text{CH}_2\text{OH}]_2\cdot\text{EtOH}\}]_n$ (1) within 3 h. When the solution is allowed to stand for another hour, the needles begin to dissolve and prisms emerge of the supramolecular isomer (SI), binuclear $[\text{Cd}[\text{S}_2\text{CN}(\text{iPr})\text{CH}_2\text{CH}_2\text{OH}]_2]_2\cdot 2\text{EtOH}$ (2). These have been fully characterized spectroscopically and by X-ray crystallography. Polymeric 1 has 2-fold symmetry and features dithiocarbamate ligands coordinating two octahedral Cd atoms in a μ_2 -tridentate mode. Binuclear 2 is centrosymmetric with two ligands being μ_2 -tridentate as for 1 but the other two being κ^2 -chelating leading to square pyramidal geometries. The conversion of the kinetic crystallization product, 1, to thermodynamic 2 is irreversible but transformations mediated by recrystallization (ethanol and acetonitrile) to related literature SI species, namely coordination polymer $[\{\text{Cd}[\text{S}_2\text{CN}(\text{iPr})\text{CH}_2\text{CH}_2\text{OH}]_2\cdot\text{MeCN}\}]_n$ and binuclear $[\text{Cd}[\text{S}_2\text{CN}(\text{iPr})\text{CH}_2\text{CH}_2\text{OH}]_2]_2\cdot 2\text{H}_2\text{O}\cdot 2\text{MeCN}$, are demonstrated, some of which are reversible. Three other crystallization outcomes are described whereby crystal structures were obtained for the 1:2 co-crystal $[\text{Cd}[\text{S}_2\text{CN}(\text{iPr})\text{CH}_2\text{CH}_2\text{OH}]_2]_2\cdot 2\{3\text{-(propan-2-yl)-1,3-oxazolidine-2-thione}\}$ (3), the salt co-crystal $[\text{iPrNH}_2(\text{CH}_2\text{CH}_2\text{OH})]_2[\text{SO}_4]_2\cdot [\text{Cd}[\text{S}_2\text{CN}(\text{iPr})\text{CH}_2\text{CH}_2\text{OH}]_2]$ (4) and the salt $[\text{iPrNH}_2(\text{CH}_2\text{CH}_2\text{OH})][\text{Cd}[\text{S}_2\text{CN}(\text{iPr})\text{CH}_2\text{CH}_2\text{OH}]_2]$ (5). These arise as a result of decomposition/oxidation of the dithiocarbamate ligands. In each of 3 and 4 the binuclear $[\text{Cd}[\text{S}_2\text{CN}(\text{iPr})\text{CH}_2\text{CH}_2\text{OH}]_2]$ SI, as in 2, is observed strongly suggesting a thermodynamic preference for this form.

Keywords: cadmium; crystal structure analysis; dithiocarbamate; supramolecular isomerism; X-ray diffraction.

Introduction

Contemporary applications, e.g. medicinal [1] and as single source precursors for nanoparticle generation of metal chalcogenides [2], complement well-established uses, e.g. as lubricants, in the vulcanization of rubber, as flotation agents, etc. [3–5] of metal 1,1'-dithiolates comprising ligands such as dithiocarbamate ($^-\text{S}_2\text{CNR}_2$), xanthate ($^-\text{S}_2\text{COR}$), and dithiophosphate ($^-\text{S}_2\text{P}(\text{OR})_2$). Therefore, it is not surprising that a vast amount of structural data for this class of compound exists as summarized in a number of bibliographic reviews [6–10]. These prove that an enormous range of structures have been characterized, ranging from zero- to three-dimensional architectures, and their adoption often rationalized in terms of the role of steric bulk of the remote substituents in mitigating secondary M–S interactions [11, 12], offering a new paradigm in the design of supramolecular assembly [13–16]. In the context of the present study, the structural diversity of these systems is very well illustrated in the binary cadmium xanthates, $\text{Cd}(\text{S}_2\text{COR})_2$, where zero- (mononuclear) [17], one- [18] and two-dimensional [19–24] aggregation patterns are observed, depending on the bridging propensity of the xanthate ligands. For the cadmium dithiophosphates both zero- (binuclear) [25–27] and one-dimensional [28–30] aggregation is found. By contrast to this diversity, the structural chemistry of cadmium dithiocarbamates is remarkably less varied. In the almost 50 years since the original report of the crystal structure of binuclear $[\text{Cd}(\text{S}_2\text{CNEt}_2)_2]_2$ [31], a large number of related dialkyl species have been described as having the same binuclear structural motif, i.e. with two each of κ^2 -chelating and μ_2 -tridentate dithiocarbamate ligands leading to penta-coordinate geometries, regardless of whether the R groups were the same [31–44], dissimilar [39, 45], incorporated within a cyclic system [46–49], or whether the compound was co-crystallized with another species [35, 39, 47], or that the R group carried additional potential oxygen donor atoms [44, 49]. However, this situation changed in 2013 with the report of a coordination polymer, $[\{\text{Cd}[\text{S}_2\text{CN}(\text{iPr})\text{CH}_2\text{CH}_2\text{OH}]_2\cdot\text{MeCN}\}]_n$ [50]. Further diversity was described in 2014 with the report of

*Corresponding author: Edward R.T. Tiekink, Department of Chemistry, University of Malaya, 50603 Kuala Lumpur, Malaysia; and Centre for Chemical Crystallography, Faculty of Science and Technology, Sunway University, 47500 Bandar Sunway, Selangor Darul Ehsan, Malaysia, E-mail: edward@sunway.edu.my
Yee Seng Tan and Siti Nadiyah Abdul Halim: Department of Chemistry, University of Malaya, 50603 Kuala Lumpur, Malaysia

Yee Seng Tan, Aliaa Diyana Azizuddin, Marius V. Cămpian, Ionel Haiduc and Edward R.T. Tiekink*

Serendipitous compositional and structural diversity in urotropine adducts of binary cadmium xanthates

DOI 10.1515/zkri-2015-1899

Received August 17, 2015; accepted October 29, 2015

Abstract: Three new compounds, $\text{Cd}(\text{S}_2\text{COMe})_2(\text{hmta})$ (1), $\text{Cd}(\text{S}_2\text{COEt})_2(\text{hmta})_2$ (2) and $\text{Cd}(\text{S}_2\text{COiPr})_2(\text{hmta})$ (3), have been isolated from a systematic study of adduct formation between $\text{Cd}(\text{S}_2\text{COR})_2$, $\text{R} = \text{Me}$, Et and iPr , precursors and potentially polydentate hmta; hmta is urotropine (hexamethylenetetramine). The compounds have been characterised by a variety of spectroscopic techniques including a photoluminescence study in both solution and the solid-state, as well as by thermal methods. Crystallography shows 1 to have μ_2 -bridging hmta leading to a one-dimensional coordination polymer. This framework is essentially repeated in 2 but with a μ_2 -bridging hmta so that $\text{Cd}(\text{S}_2\text{COEt})_2$ entities decorate the chain. By contrast, a binuclear zero-dimensional aggregate with terminally bound hmta is found in 3. The influence of steric bulk of the alkyl substituents in $\text{Cd}(\text{S}_2\text{COR})_2$ is pivotal in determining the ultimate structural outcome.

Keywords: cadmium; crystal structure analysis; urotropine; xanthate; X-ray diffraction.

Introduction

Dithiocarbonates (xanthates), dithiocarbamates and dithiophosphates are important members of the 1,1-dithiolate class of compounds, Figure 1a–c [1–7]. Being easy to prepare and having a great propensity for complexing

heavy elements ranging from the transition metals, lanthanides, and relevant to the present study, main group elements, it is not surprising that there is an enormous wealth of structural data for metal 1,1-dithiolates [1–7]. Amongst these, the structural chemistry exhibited by the binary cadmium xanthates, $\text{Cd}(\text{S}_2\text{COR})_2$, is remarkable for its diversity and complexity [1].

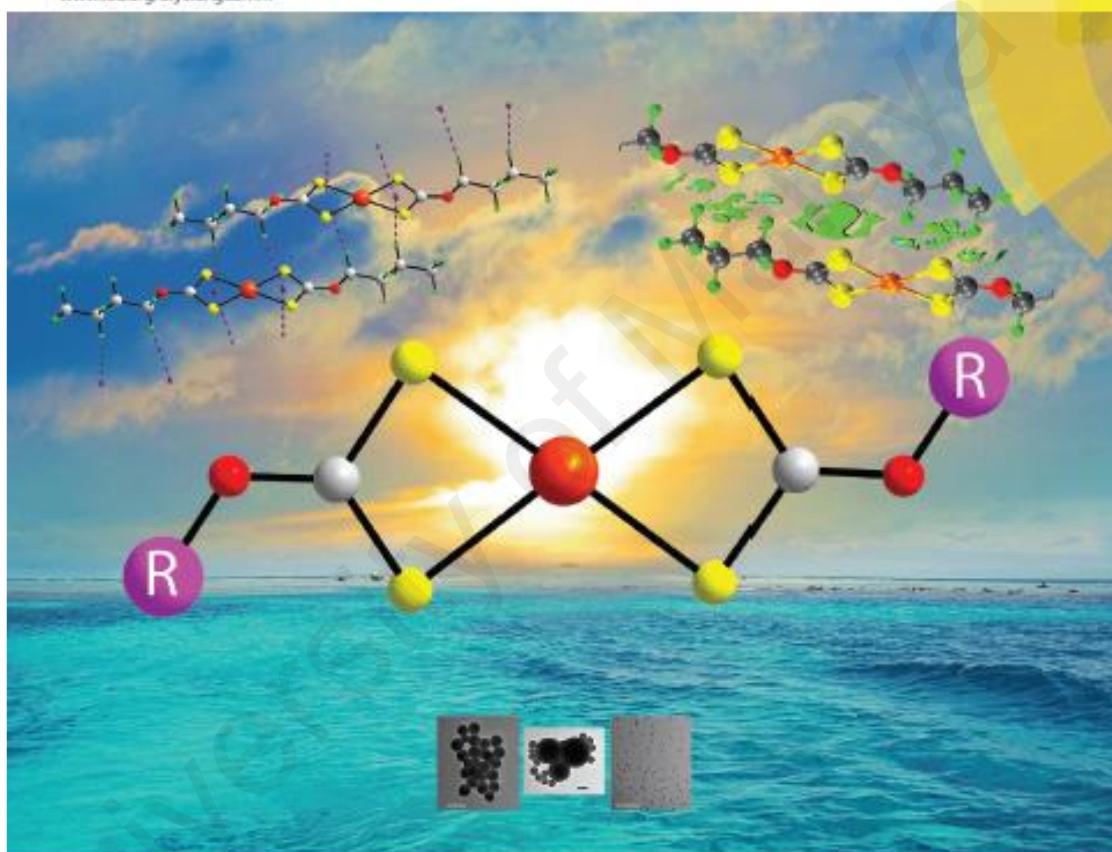
As seen from Figure 2, three very distinct structural motifs are observed for these compounds, ranging from zero-dimensional in the case of the mononuclear compound found for $\text{R} = \text{CH}_2\text{CH}_2\text{OMe}$ [8], one-dimensional in the form of a supramolecular chain when $\text{R} = \text{Me}$ [9], and two-dimensional, as extended sheets, when $\text{R} = \text{Et}$, iPr and $n\text{-Bu}$ [10–15].

Contrasting the behaviour of the cadmium xanthates is the structural chemistry of the binary cadmium dithiocarbamates, $\text{Cd}(\text{S}_2\text{CNR})_2$, which normally features a binuclear, zero-dimensional aggregate as a result of two chelating ligands and two ligands which simultaneously chelate one cadmium centre while bridging another, i.e. μ_2 -tridentate [16–34]. This dramatic difference in structural outcomes is rationalised in terms of the significant contribution of the canonical structure shown in Figure 1e, up to 40%, which makes dithiocarbamate ligands effective chelating agents certainly compared with the xanthate ligand where the equivalent canonical structure, Figure 1d, contributes no more than 20% to the overall electronic structure of the anion [1]. The above notwithstanding, the relatively “staid” coordination chemistry for $\text{Cd}(\text{S}_2\text{CNR})_2$ has been challenged recently by the characterisation of supramolecular isomers [35, 36] of the one-dimensional coordination polymers, $[\{\text{Cd}(\text{S}_2\text{CN}(\text{iPr})\text{CH}_2\text{CH}_2\text{OH})_2\}_n\text{MeCN}]$ [37] and $[\{\text{Cd}(\text{S}_2\text{CN}(\text{iPr})\text{CH}_2\text{CH}_2\text{OH})_2\}_n\text{ZnEtOH}]$ [38] for which all dithiocarbamate ligands are μ_2 -tridentate. Further, a zero-dimensional trinuclear aggregate has been isolated recently, $\{\text{Cd}(\text{S}_2\text{CN}(\text{methylbenzyl})\text{(methylfurfuryl)})_2\}_n$, where the ratio of μ_2 -tridentate to chelating ligands is 2:1 leading to a central octahedrally coordinated cadmium flanked by two square pyramidal cadmium atoms [39]. The structural chemistry of the

*Corresponding author: Edward R.T. Tiekink, Department of Chemistry, University of Malaya, 50603 Kuala Lumpur, Malaysia; and Faculty of Science and Technology, Centre for Crystalline Material, Sunway University, 47500 Bandar Sunway, Selangor Darul Ehsan, Malaysia, E-mail: edwardt@sunway.edu.my
Yee Seng Tan and Aliaa Diyana Azizuddin: Department of Chemistry, University of Malaya, 50603 Kuala Lumpur, Malaysia
Marius V. Cămpian and Ionel Haiduc: Department of Chemistry, Babes-Bolyai University, RO-400028, Cluj-Napoca, Romania

CrystEngComm

www.rsc.org/crystengcomm



PAPER

Kieran C. Molloy, A. Otero-de-la-Roza, Edward R. T. Tiekink et al.
Persistence of C–H... π (chelate ring) interactions in the crystal structures of $\text{Pd}(\text{S}_2\text{COR})_2$. The utility of $\text{Pd}(\text{S}_2\text{COR})_2$ as precursors for palladium sulphide materials

175

YEARS

CrystEngComm

PAPER



Cite this: *CrystEngComm*, 2016, 18, 1122

Persistence of C–H... π (chelate ring) interactions in the crystal structures of $\text{Pd}(\text{S}_2\text{COR})_2$. The utility of $\text{Pd}(\text{S}_2\text{COR})_2$ as precursors for palladium sulphide materials†

Yee Seng Tan,^a Siti Nadiyah Abdul Halim,^a Kieran C. Molloy,^{a,b} Anna L. Sudlow,^b A. Otero-de-la-Roza^{a,c} and Edward R. T. Tiekink^{a,*}



15TH ASIAN
CHEMICAL CONGRESS

Chemistry at the Centre of Molecular Science & Nanotechnology


CERTIFICATE OF ATTENDANCE

This is to certify that

Yee Seng Tan

attended

15th Asian Chemical Congress, 19 – 23 August 2013



Professor T.S. Hor, Andy
Chair, 15th Asian Chemical Congress 2013
President, Singapore National Institute of Chemistry

CONFERENCE 2

CERTIFICATE

This document certifies the presence of

TAN YEE SENG (University of Malaya)

at the *4th Asian Conference of Coordination Chemistry* which
was held at the Jeju International Convention Center, Jeju,
South Korea from November 4 to 7, 2013.

Organizing Committee Co-Chair

Prof. Myunghyun Paik Suh

Prof. Kimoon Kim

ACCC4 The 4th Asian Conference
on Coordination Chemistry

CONFERENCE 3



CONFERENCE 4

Certificate of Participation

This is to certify that

TAN YEE SENG

(Oral & Poster Presenter)

has successfully attended the

University of Malaya Chemical Crystallography Symposium 2014

Organized by



on

28th May 2014



"Celebrating the International Year of Crystallography, IYCr2014"

Professor Dr. Sharifuddin Md Zain
Head
Department of Chemistry
University of Malaya

Certificate of Participation

This certificate is awarded to

TAN YEE SENG

(Oral)

For attending

**University of Malaya
Pharmaceutical Co-Crystal Symposium 2014**

"Celebrating the International Year of Crystallography, IYCr2014"

Organized by

Malaysian Crystallographic Association
(Persatuan Kristalografi Malaysia)

and



on

19th July 2014

Professor Dr. Sharifuddin Md Zain
Head
Department of Chemistry
University of Malaya

2014 international year of crystallography



JSPS Certifies that

Yee Seng Tan

ID: MY1403

Is hereby named a

JSPS HOPE Fellow

*in recognition of successful participation in
the 7th HOPE Meeting*

March 1 –5, 2015

Tokyo, Japan

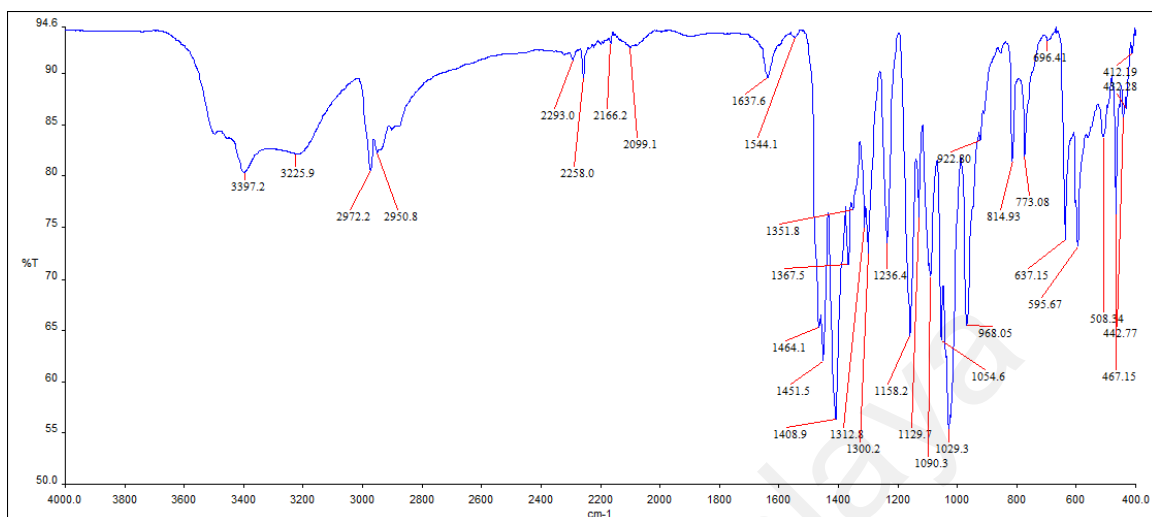


HOPE MEETINGS
with Nobel Laureates

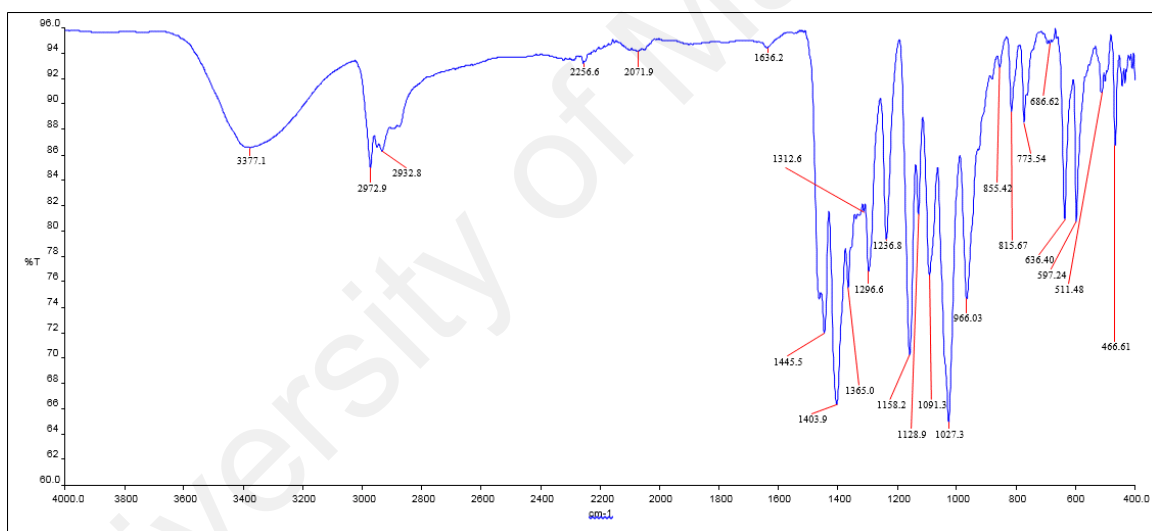
HOPE Meeting Organizing Committee

Prof. Makoto Kobayashi, Chair

APPENDIX A



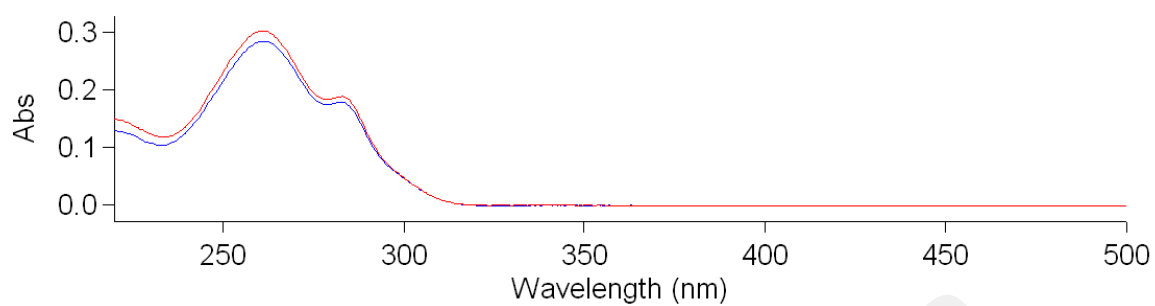
(a)



(b)

IR spectra for **1** (a), and **2** (b).

APPENDIX B



UV-Vis spectra measured in an 1:1 acetonitrile:ethanol solution at a concentration = 10 μM (based on Cd) for **1** (blue trace) and **2** (red).

APPENDIX C

C.1: Selected geometric parameters (Å) for **1** and **2**^a.

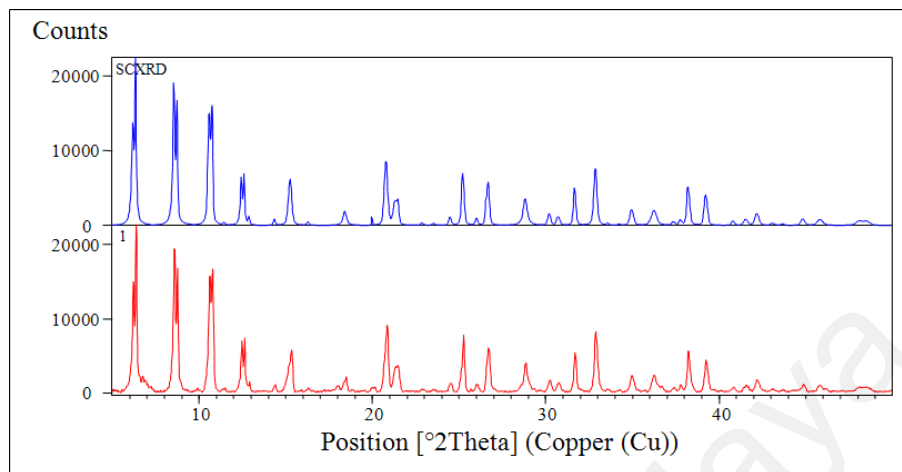
Compound	Parameter
1	
Cd1–S1, S2, S4	2.6331(8), 2.7412(9), 2.6890(9)
Cd2–S3, S4, S2 ⁱ	2.6556(9), 2.7122(9), 2.6811(9)
2	
Cd–S1, S2	2.5462(8), 2.6152(9)
Cd–S3, S4, S4 ⁱⁱ	2.5289(8), 2.8067(8), 2.6090(9)

^a Symmetry operations, *i*: $x, -1+y, z$; *ii*: $1-x, 1-y, -z$.

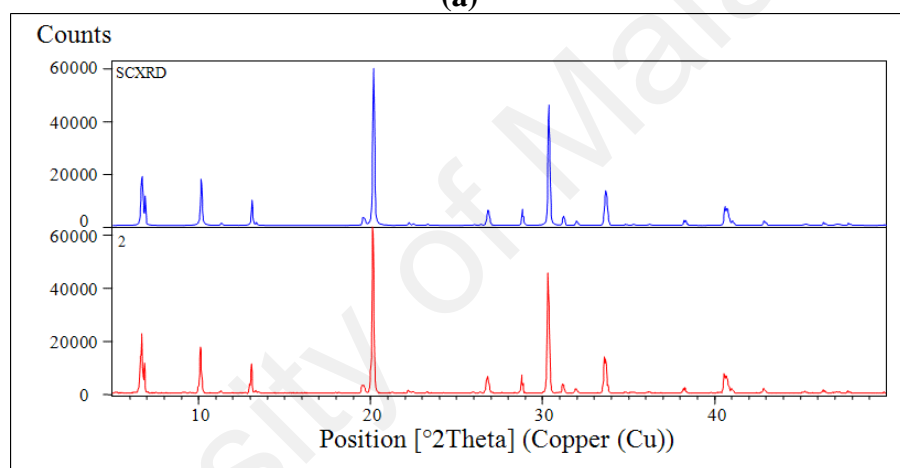
C.2: Geometric characteristics (Å, °) of the intermolecular interactions (A–H...B) operating in the crystal structures of **1** and **2**.

A	H	B	H...B	A...B	A–H...B	symmetry operation
1						
O1	H1o	O2	1.93	2.716(4)	157	$1-x, 1-y, 1-z$
O1	H1o'	O1	2.00	2.717(4)	142	$1-x, 1-y, 1-z$
O2	H2o'	O1	1.89	2.716(4)	170	$1-x, 1-y, 1-z$
O2	H2o	O3	1.89	2.718(5)	172	x, y, z
O3	H3o	O3	1.91	2.744(5)	174	$-x, 1-y, 1-z$
O3'	H3o'	O2	1.90	2.718(5)	163	x, y, z
2						
O1	H1o	O3	1.94(2)	2.739(6)	168(3)	$1-x, 1-y, 1-z$
O2	H2o	O1	1.939(14)	2.769(6)	174(2)	$x, 1+y, -1+z$
O2	H2o	O1'	1.975(17)	2.785(6)	164(3)	$x, 1+y, -1+z$
O3	H3o	O2	1.96(5)	2.787(4)	167(5)	$-1+x, y, 1+z$
O3'	H3o'	O2	1.88(4)	2.713(3)	170(5)	$1-x, 1-y, -z$

APPENDIX D



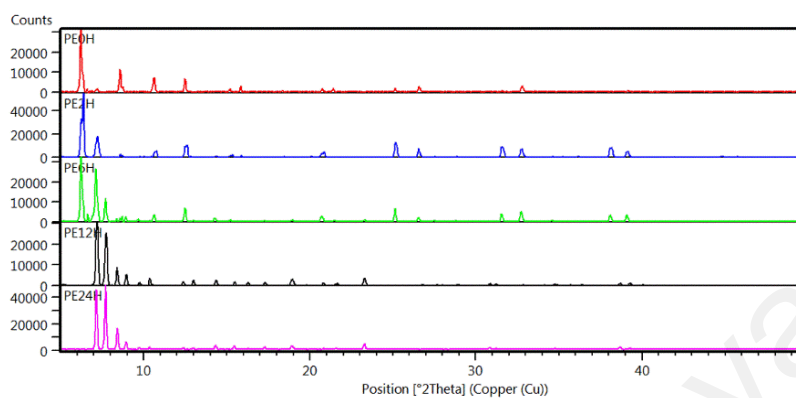
(a)



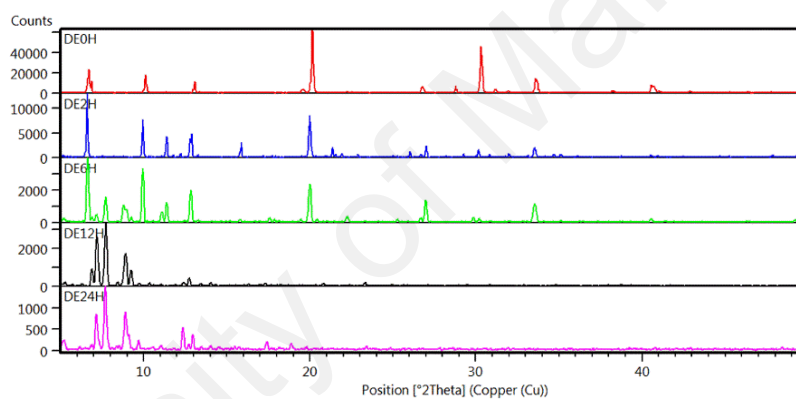
(b)

Experimental (red trace) and calculated (blue) PXRD patterns for **1** (a), and **2** (b).

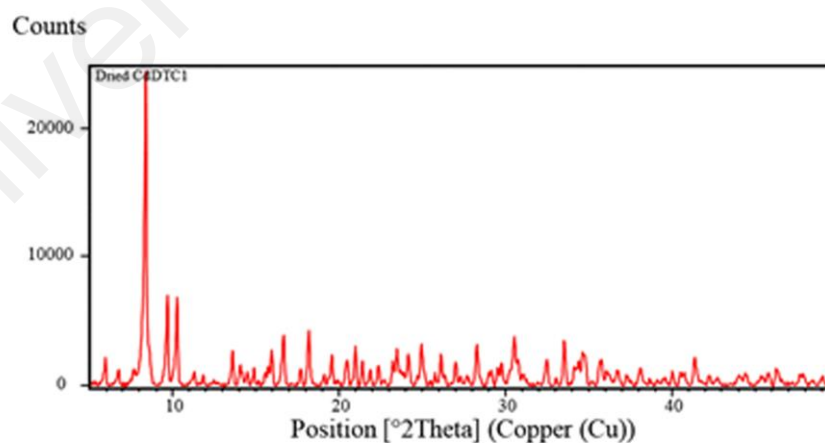
APPENDIX E



(a)



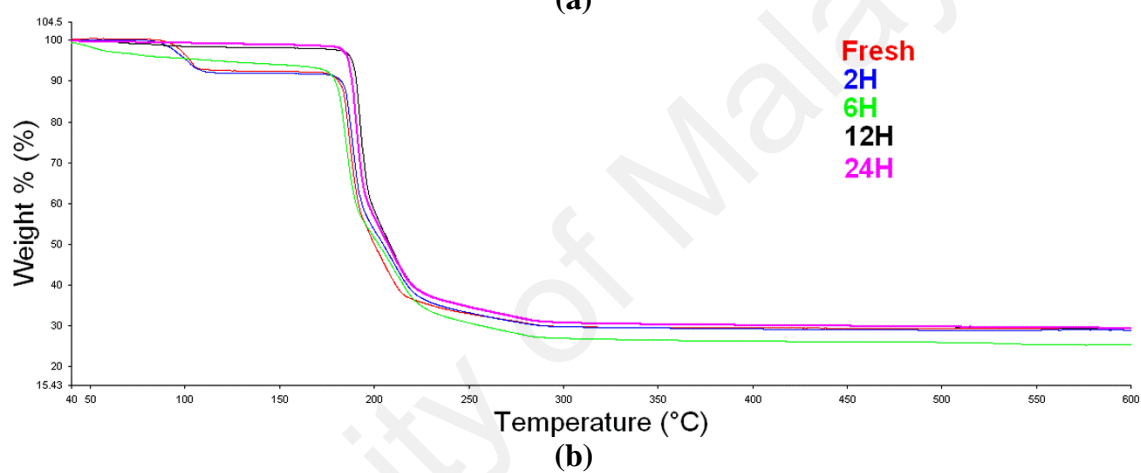
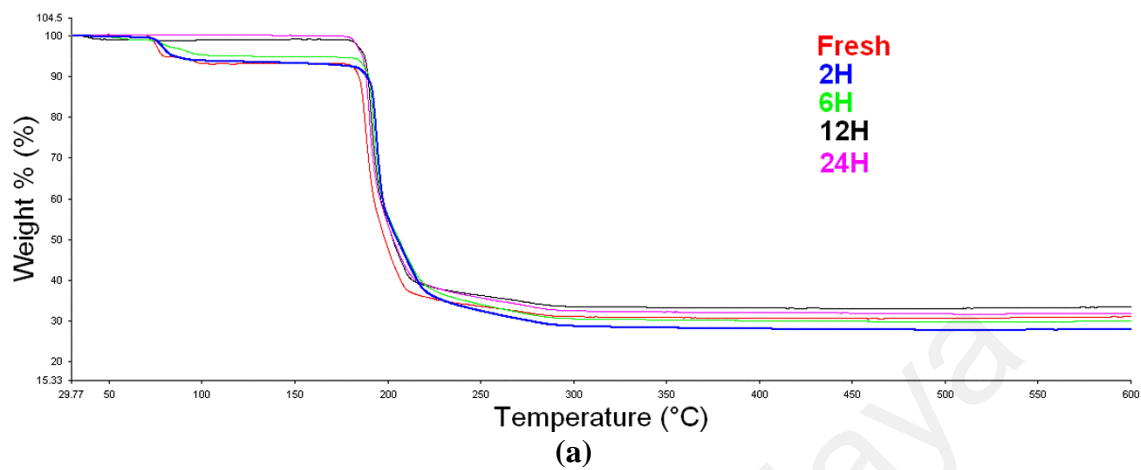
(b)



(c)

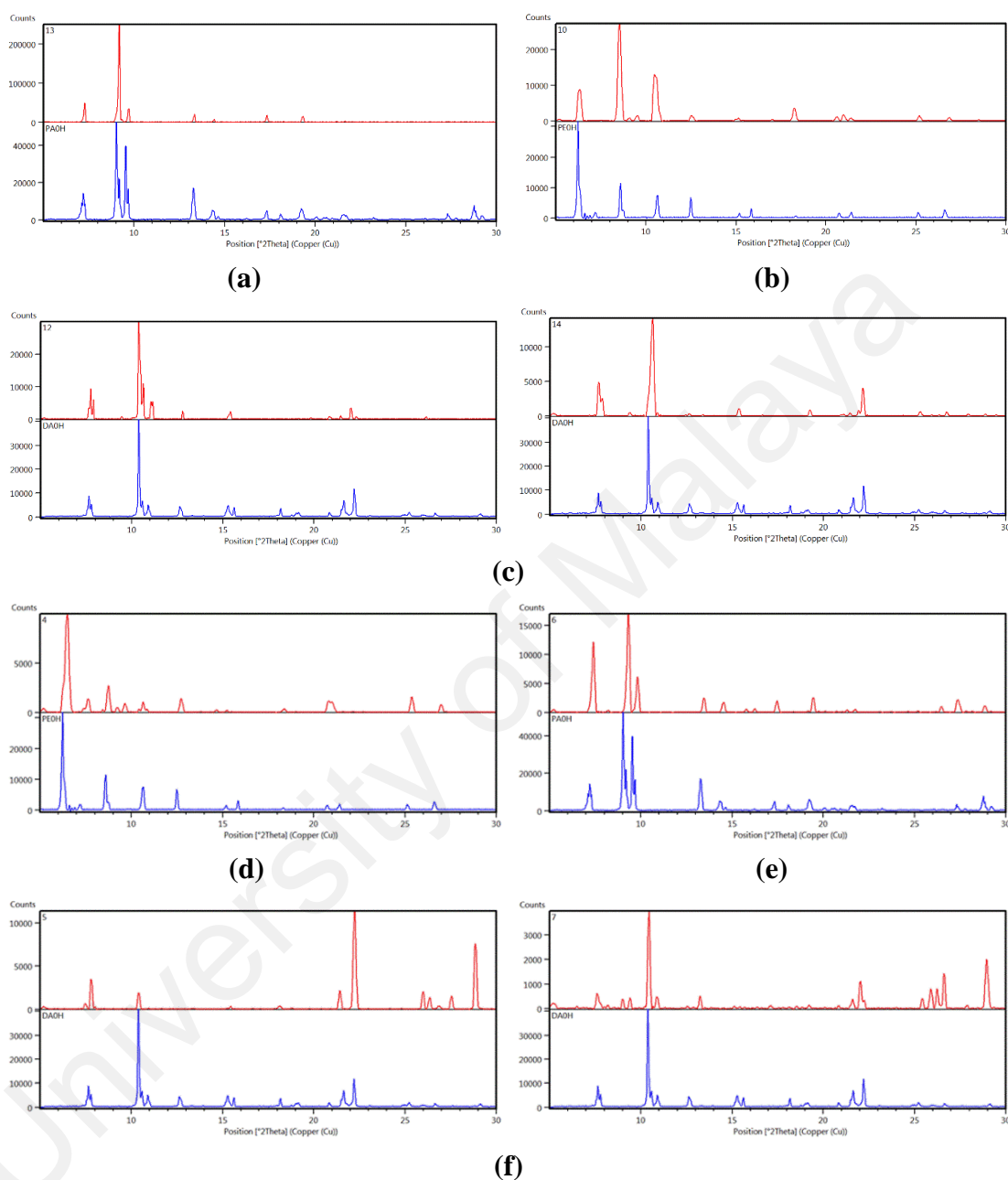
Time-dependent PXRD patterns for **1** (a) and **2** (b) measured at 0 h (red traces), 2 h (blue), 6 h (green), 12 h (black) and 24 (purple). These indicate changes in crystal structure occurred before 2 h in each case. PXRD pattern for $\text{Cd}[\text{S}_2\text{CN}(\text{iPr})\text{CH}_2\text{CH}_2\text{OH}]_2$, the starting material used for recrystallization (c).

APPENDIX F



Time-dependent TGA measurements for **1** (a) and **2** (b), showing the samples had lost most of the ethanol of crystallization after 6 h.

APPENDIX G



PXRD showing the formation of **6** from recrystallization of **1** from dry MeCN in a desiccator (a). **1** from **6**: Dry EtOH, desiccator (b). **7** from **1**: Ambient, left – dry MeCN and right – laboratory grade MeCN, (c). **1** from **7**: Ambient, laboratory grade EtOH; the small extra peaks are due to original **7** (d). **6** from **2**: dry MeCN, desiccator (e). **7** from **2**: Ambient, left – dry MeCN and right – laboratory grade MeCN; the small extra peaks in the right-hand image are due to an unidentified species (f). The top (red) trace is of the product of the recrystallization and the bottom (blue) trace is of an authenticated sample.

APPENDIX H

H.1: Selected geometric parameters (Å) for **3–5**^a.

Compound	Parameter
3	
Cd–S1, S2, S2 ⁱ	2.4236(7), 3.0448(9), 2.5545(11)
Cd–S3, S4	2.5109(8), 2.7159(10)
4	
Cd–S1, S2	2.5590(5), 2.5952(5)
Cd–S3, S4, S4 ⁱⁱ	2.5619(5), 2.7915(5), 2.5879(5)
5	
Cd–S1, S2	2.6534(6), 2.7040(6)
Cd–S3, S4	2.6787(6), 2.7039(6)
Cd–S5, S6	2.7079(5), 2.7279(5)

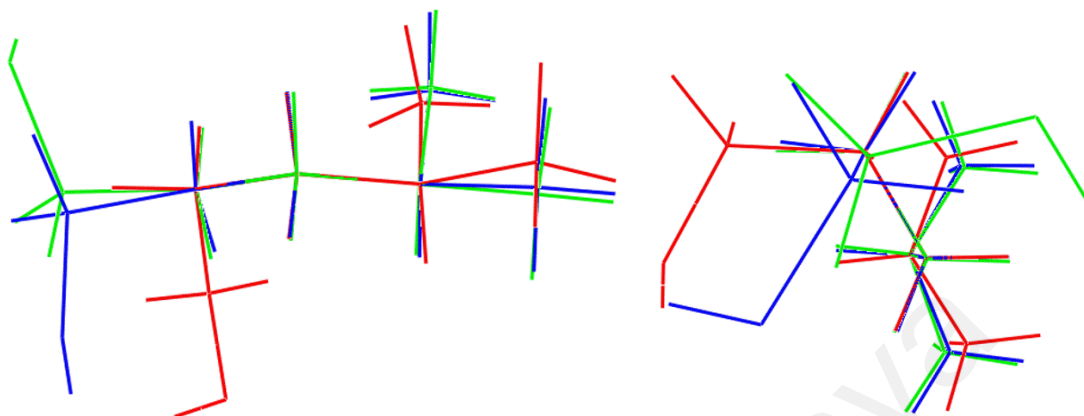
^a Symmetry operations, *i*: -*x*, 1-*y*, 1-*z*; and *ii*: 1-*x*, 2-*y*, 1-*z*

APPENDIX H- Continued

H.2: Geometric characteristics (Å, °) of the intermolecular interactions (A–H...B) operating in the crystal structures of **3–5**.

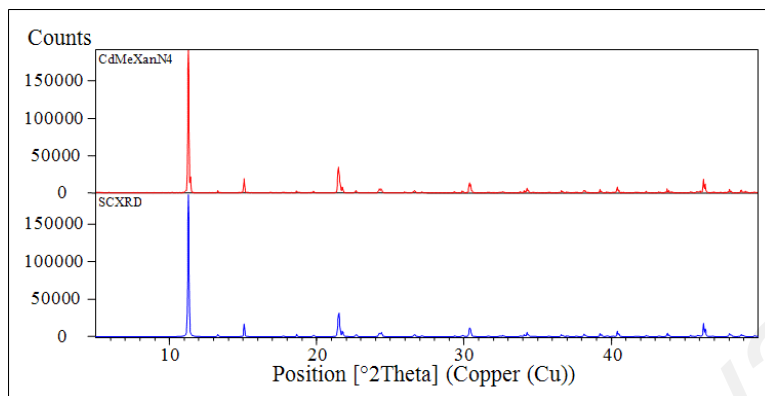
A	H	B	H...B	A...B	A–H...B	symmetry operation
3						
O1	H1o	S5	2.56(2)	3.349(2)	158(2)	-1+x, y, -1+z
O2	H2o	O1	1.96(2)	2.781(3)	172(4)	1-x, 1-y, 1-z
C6	H6c	O2	2.19	3.104(3)	155	-1+x, y, -1+z
C9	H9a	S1	2.64	3.536(2)	151	1-x, 1-y, 1-z
C14	H14a	S2	2.77	3.744(3)	169	1-x, 1-y, 1-z
C18	H18b	S4	2.78	3.629(3)	146	1-x, 1-y, 1-z
4						
O1	H1o	O4	2.02(2)	2.850(2)	174(2)	$\frac{1}{2}$ -x, $1\frac{1}{2}$ -y, 1-z
O2	H2o	O5	2.03(2)	2.815(2)	157.7(16)	x, y, z
O3	H3o	O6	1.904(14)	2.7258(18)	167(2)	x, y, z
O4	H4o	O7	1.968(14)	2.7757(19)	164(2)	x, y, z
N3	H1n	O8	1.851(18)	2.727(2)	162.9(17)	x, 1-y, $\frac{1}{2}$ +z
N3	H2n	O7	1.982(18)	2.8199(19)	153.6(17)	x, y, z
N4	H3n	O5	1.905(15)	2.804(2)	172.3(19)	x, y, z
N4	H4n	O8	1.865(16)	2.761(2)	168.6(19)	x, 1-y, $\frac{1}{2}$ +z
5						
O1	H1o	S3	2.545(13)	3.3189(17)	156(2)	$-\frac{1}{2}$ +x, $1\frac{1}{2}$ -y, $-\frac{1}{2}$ +z
O2	H2o	S6	2.538(17)	3.3283(16)	160(2)	1+x, y, z
O3	H3o	S5	2.350(13)	3.1475(15)	162(2)	x, y, z
O4	H4o	O2	1.971(19)	2.758(2)	159(2)	x, y, z
N4	H1n	O4	2.38(2)	2.835(3)	111.5(14)	x, y, z
N4	H1n	O4	2.329(18)	2.964(2)	127.4(17)	2-x, 1-y, 1-z
N4	H2n	O1	1.916(13)	2.781(2)	158(2)	1-x, 1-y, 1-z
C9	H9a	O3	2.51	3.423(3)	153	$\frac{1}{2}$ +x, $1\frac{1}{2}$ -y, $-\frac{1}{2}$ +z

APPENDIX I

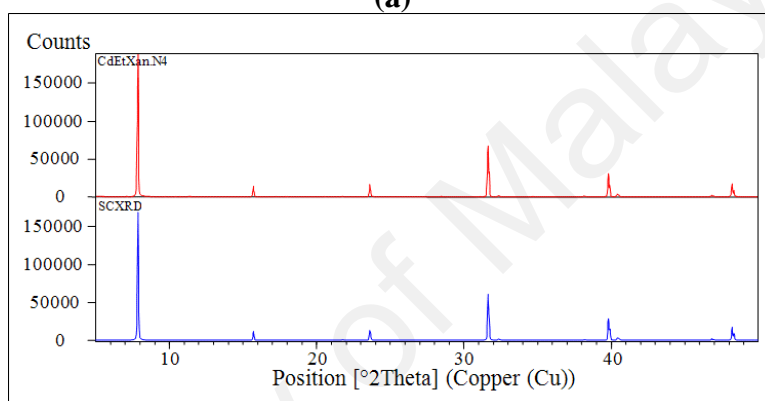


Overlay diagram of the cations in **4**, N3-molecule (red image) and inverted-N4-cation (green), and inverted **5** (blue). The cations have been overlapped so that the central C–N–C residues are coincident. In order to ensure the isopropyl groups have the same orientation to highlight the important differences between the conformations, inverted versions of the N4-cation in **4** and the cation in **5** are illustrated. The key torsion angle data quantify the differences in the cations, *i.e.* N–C–C–O is 48.5(2), -73.6(2) and 59.3(2)° for the N3-cation and N4-cation in **4**, and **5**-cation, respectively. The wide variety in conformations is highlighted in the right-hand image which is a projection down the CH₂CH₂ bonds of the hydroxyethyl groups.

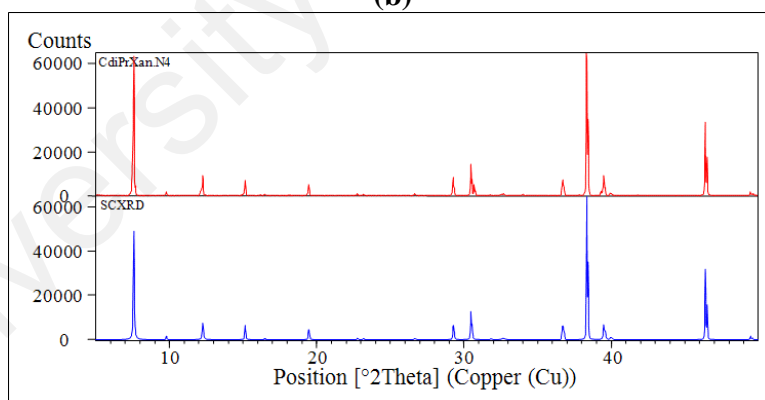
APPENDIX J



(a)



(b)

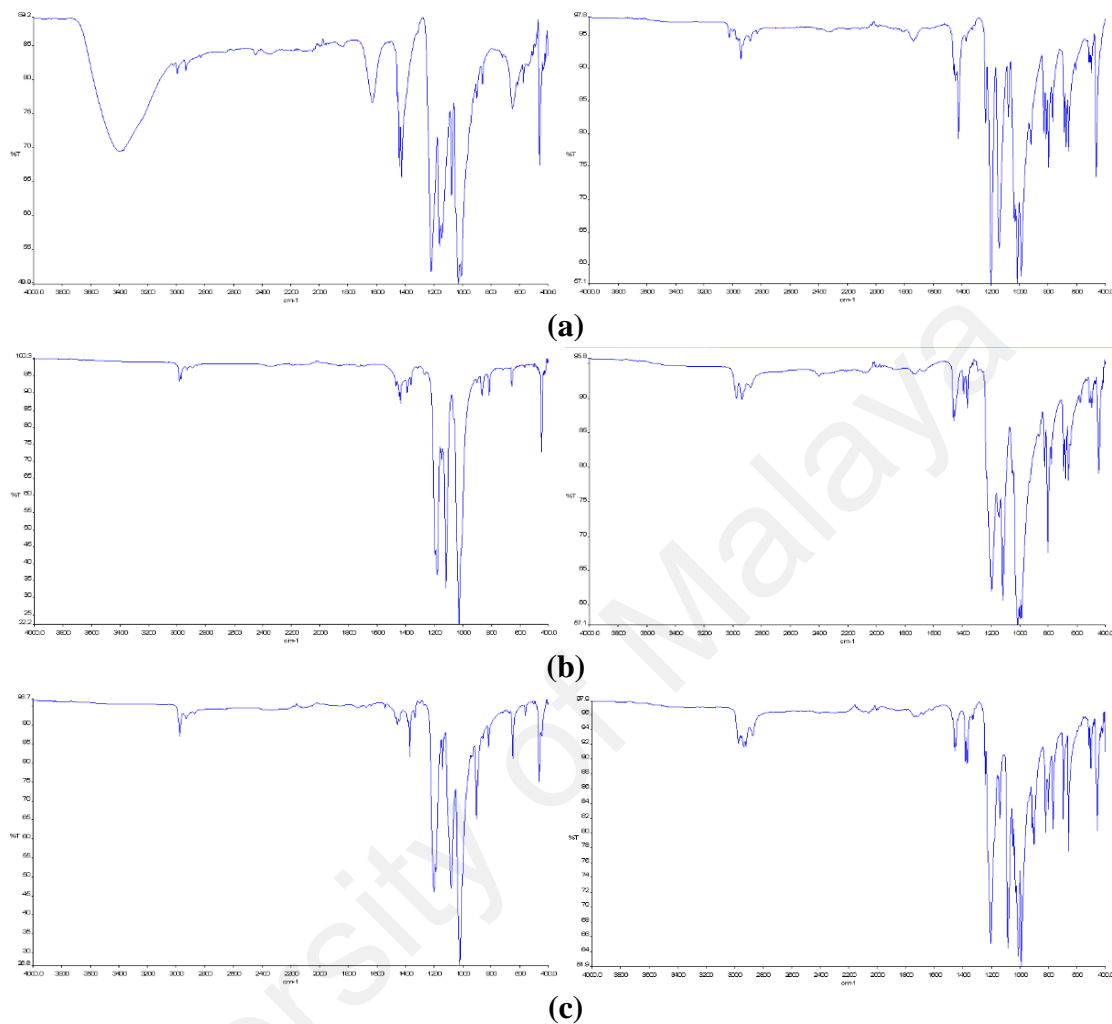


(c)

Experimental (red trace) and simulated based on the single crystal structure (blue trace)

PXRD patterns for (a) **8**, (b) **9** and (c) **10**. These show that the single crystal data reported herein for each of **8–10** match the structure of the bulk material in each case.

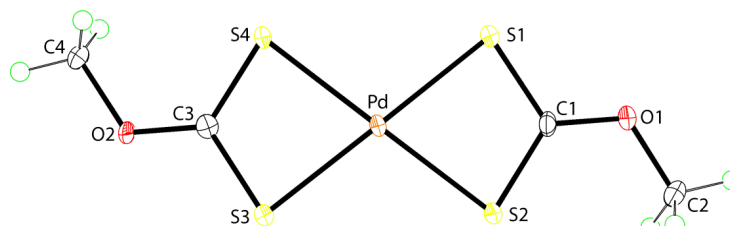
APPENDIX K



IR data for (a) $\text{Cd}(\text{S}_2\text{COMe})_2$ (left-hand image) and **8** (right-hand image), (b) $\text{Cd}(\text{S}_2\text{COEt})_2$ and **9**, and (c) $\text{Cd}(\text{S}_2\text{COiPr})_2$ and **10**.

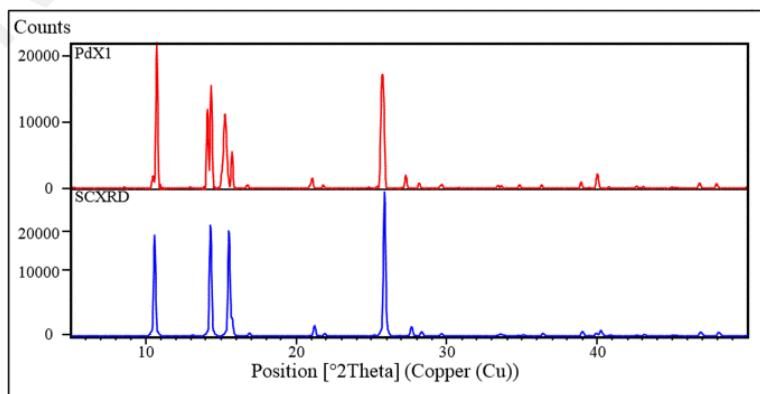
APPENDIX L

L.1 Molecular structure of bis(*O*-methylxanthato)palladium(II), [Pd(S₂COMe)₂] (**11**), showing atom labelling and displacement ellipsoids at the 50% probability level.



Synthesis and characterisation:

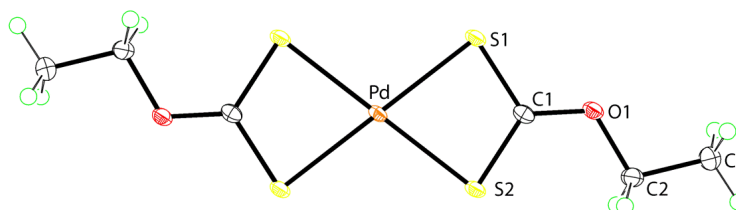
Potassium methylxanthate (0.0125 mol, 1.8283 g) and palladium(II) nitrate (0.0063 mol, 1.4402 g) were each dissolved in water (50 ml). The Pd(NO₃)₂ solution was added into the ligand solution drop-wise with stirring; a brown precipitate formed immediately. The precipitate was extracted with chloroform (100 ml). The chloroform layer was filtered off and the aqueous layer was further extracted with chloroform (5 x 100 ml) until no colour was evident in the chloroform extract. The orange blocks formed after a few days of slow evaporation of the combined chloroform extracts. Recrystallisation was performed by dissolving the obtained crystals from a dichloromethane and hexane mixture (200 ml; 1:1 v/v). Orange blocks formed after 2 days. Yield: 1.76 g, 88 %. M. pt: 388.8–390.7 K. *Anal.* Calc'd for C₄H₆O₂PdS₄: C, 14.98; H, 1.89. Found: C, 14.69; H, 1.92 %. FTIR (cm⁻¹): 1232 (*s*) ν(C-O), 1028 (*s*) ν(C-S). ¹H NMR {CDCl₃}: δ 4.18 (*s*, 3H, CH₃) ppm. ¹³C{¹H} NMR {CDCl₃}: δ 234.7 (CS); 57.8 (CH₃) ppm. UV-Vis (ACN; nm, cm⁻¹ mol⁻¹ L): 236 (ε = 15690; n → σ*, CT); 282 (ε = 35190; π → π*); 379 (ε = 3250; n → π*, CT); 457 (ε = 110; *d-d*, ¹A_{1g} → ¹E_g).



Experimental (red trace) and simulated based on the single crystal structure (blue trace) PXRD pattern.

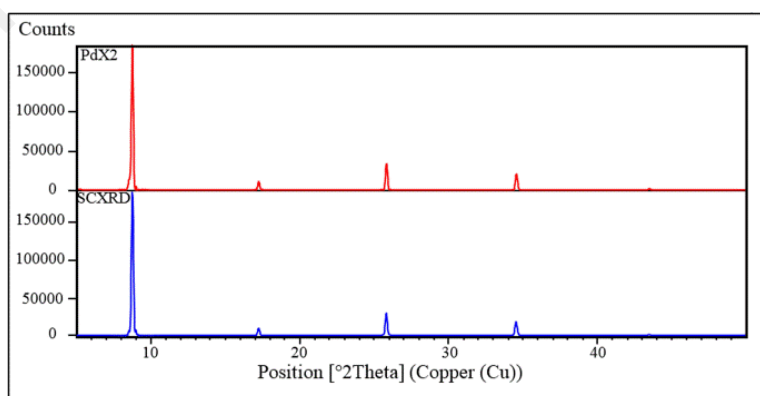
APPENDIX L- Continued

L.2 Molecular structure of bis(*O*-ethylxanthato)palladium(II), [Pd(S₂COEt)₂] (**12**), showing atom labelling and displacement ellipsoids at the 50% probability level.



Synthesis and characterisation:

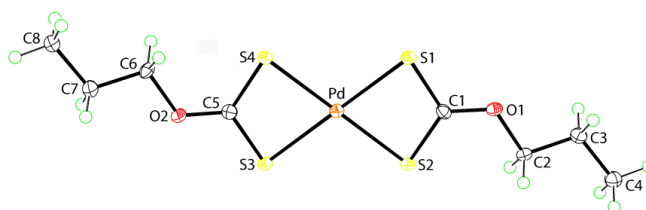
Potassium ethylxanthate (0.0115 mol, 1.8382 g) and palladium(II) nitrate (0.0058 mol, 1.3213 g) were each dissolved in water (50 ml). The Pd(NO₃)₂ solution was added into the ligand solution drop-wise with stirring; a brown precipitate formed immediately. The precipitate was extracted with chloroform (100 ml). The chloroform layer was filtered off and the aqueous layer was further extracted with chloroform (5 x 100 ml) until no colour was evident in the chloroform extract. The orange plates formed after a few days of slow evaporation of the combined chloroform extracts. Recrystallisation was performed by dissolving the obtained crystals from a dichloromethane and hexane mixture (200 ml; 1:1 v/v). Orange plates formed after 2 days. Yield: 1.85 g, 93 %. M. pt: 413.3–414.4 K. *Anal.* Calc'd for C₆H₁₀O₂PdS₄: C, 20.66; H, 2.89. Found: C, 21.02; H, 2.50 %. FTIR (cm⁻¹): 1244 (*s*) ν(C-O), 1015 (*s*) ν(C-S). ¹H NMR {CDCl₃}: δ 4.70 (*q*, 2H, CH₂, *J* = 7.1 Hz), 1.52 (*t*, 3H, CH₃, *J* = 7.1 Hz) ppm. ¹³C{¹H} NMR {CDCl₃}: δ 233.7 (CS), 68.3 (CH₂), 13.8 (CH₃) ppm. UV-Vis (ACN; nm, cm⁻¹ mol⁻¹ L): 237 (ε = 20840; n → σ*, CT); 284 (ε = 50080; π → π*); 379 (ε = 4400; n → π*, CT); 457 (ε = 150; *d-d*, ¹A_{1g} → ¹E_g).



Experimental (red trace) and simulated based on the single crystal structure (blue trace) PXRD patterns.

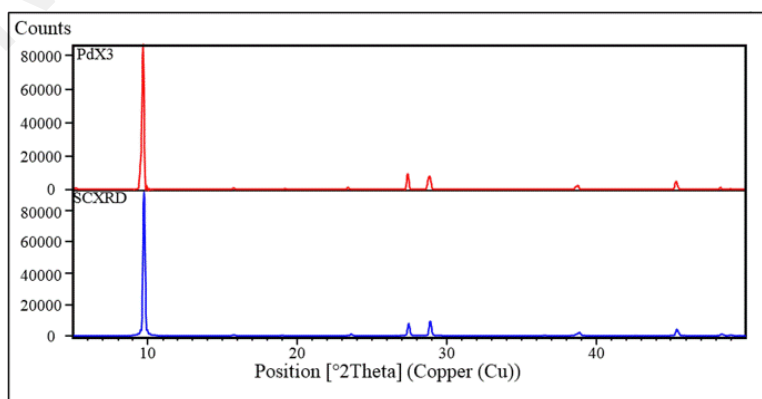
APPENDIX L- Continued

L.3 Molecular structure of bis(*O*-*n*-propylxanthato)palladium(II), [Pd(S₂CO-*n*-Pr)₂] (**13**), showing atom labelling and displacement ellipsoids at the 50% probability level.



Synthesis and characterisation:

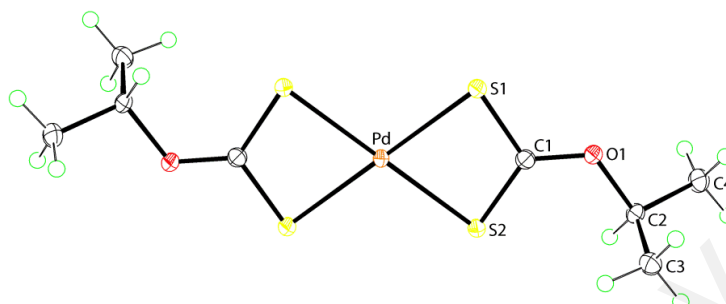
Potassium *n*-propylxanthate (0.0106 mol, 1.8477 g) and palladium(II) nitrate (0.0053 mol, 1.2213 g) were each dissolved in water (50 ml). The Pd(NO₃)₂ solution was added into the ligand solution drop-wise with stirring; a brown precipitate formed immediately. The precipitate was extracted with chloroform (100 ml). The chloroform layer was filtered off and the aqueous layer was further extracted with chloroform (4 x 100 ml) until no colour was evident in the chloroform extract. The orange plates formed after a few days of slow evaporation of the combined chloroform extracts. Recrystallisation was performed by dissolving the obtained crystals from a dichloromethane and hexane mixture (200 ml; 1:1 v/v). Orange plates formed after 2 days. Yield: 1.67 g, 84 %. M. pt: 402.7–403.4 K. *Anal.* Calc'd for C₈H₁₄O₂PdS₄: C, 25.50; H, 3.74. Found: C, 25.62; H, 3.42 %. FTIR (cm⁻¹): 1236 (*s*) ν(C-O), 1023 (*s*) ν(C-S). ¹H NMR {CDCl₃}: δ 4.59 (*t*, 2H, OCH₂, *J* = 6.6 Hz), 1.91 (*tq*, 2H, CH₂CH₃, *J*_t = 7.0, *J*_q = 7.1 Hz), 1.05 (*t*, 3H, CH₃, *J* = 7.4 Hz) ppm. ¹³C{¹H} NMR {CDCl₃}: δ 233.8 (CS), 73.6 (OCH₂), 21.7 (CH₂CH₃), 10.3 (CH₃) ppm. UV-Vis (ACN; nm, cm⁻¹ mol⁻¹ L): 237 (ε = 18500; n → σ*, CT); 284 (ε = 45650; π → π*); 380 (ε = 3920; n → π*, CT); 461 (ε = 140; *d-d*, ¹A_{1g} → ¹E_g).



Experimental (red trace) and simulated based on the single crystal structure (blue trace) PXRD patterns.

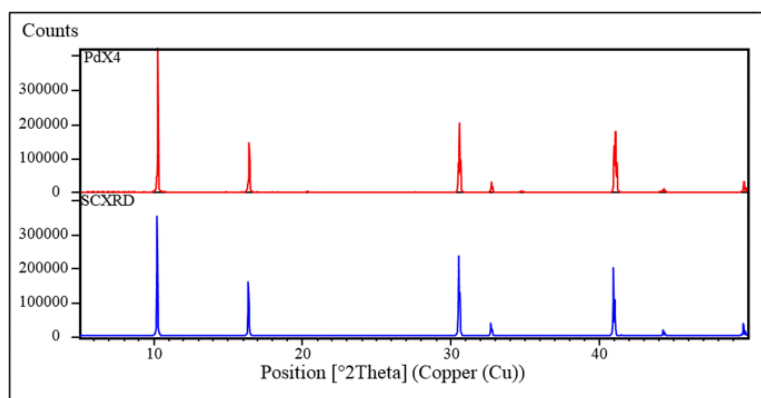
APPENDIX L- Continued

L.4 Molecular structure of bis(*O*-isopropylxanthato)palladium(II), [Pd(S₂CO-i-Pr)₂] (**14**), showing atom labelling and displacement ellipsoids at the 50% probability level.



Synthesis and characterisation:

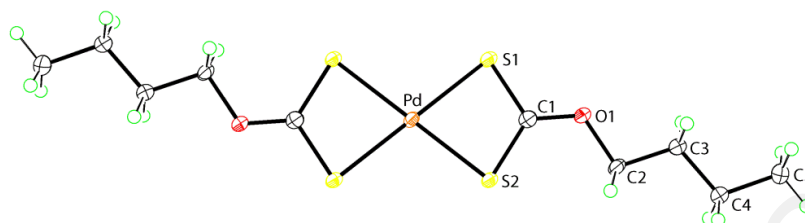
Potassium isopropylxanthate (0.0106 mol, 1.8477 g) and palladium(II) nitrate (0.0053 mol, 1.2213 g) were each dissolved in water (50 ml). The Pd(NO₃)₂ solution was added into the ligand solution drop-wise with stirring; a brown precipitate formed immediately. The precipitate was extracted with chloroform (100 ml). The chloroform layer was filtered off and the aqueous layer was extracted with further chloroform (3 x 100 ml) until no colour was evident in the chloroform extract. The orange blocks formed after a few days of slow evaporation of the combined chloroform extracts. Recrystallisation was performed by dissolving the obtained crystals from a dichloromethane and hexane mixture (200 ml; 1:1 v/v). Orange blocks formed after 2 days. Yield: 1.58 g, 79 %. M. pt: 416.8–417.4 K. *Anal.* Calc'd for C₈H₁₄O₂PdS₄: C, 25.50; H, 3.74. Found: C, 25.59; H, 3.50 %. FTIR (cm⁻¹): 1271 (s) ν(C-O), 1006 (s) ν(C-S). ¹H NMR {CDCl₃}: δ 5.61 (*sept*, 1H, CH, *J* = 6.2 Hz), 1.49 (*d*, 6H, CH₃, *J* = 6.2 Hz) ppm. ¹³C{¹H} NMR {CDCl₃}: δ 232.7 (CS), 77.8 (CH), 21.7 (CH₃) ppm. UV-Vis (ACN; nm, cm⁻¹ mol⁻¹ L): 238 (ε = 20240; n → σ*, CT); 285 (ε = 52030; π → π*); 379 (ε = 4420; n → π*, CT); 461 (ε = 160; *d-d*, ¹A_{1g} → ¹E_g).



Experimental (red trace) and simulated based on the single crystal structure (blue trace) PXRD patterns.

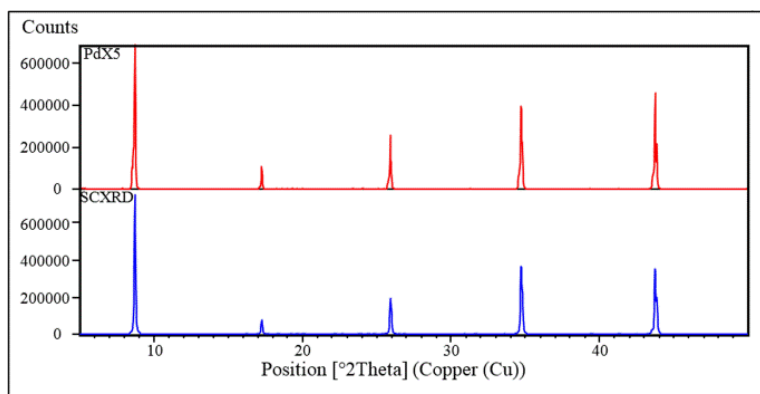
APPENDIX L- Continued

L.5 Molecular structure of bis(*O*-n-butylxanthato)palladium(II), [Pd(S₂CO-n-Bu)₂] (**15**), showing atom labelling and displacement ellipsoids at the 50% probability level.



Synthesis and characterisation:

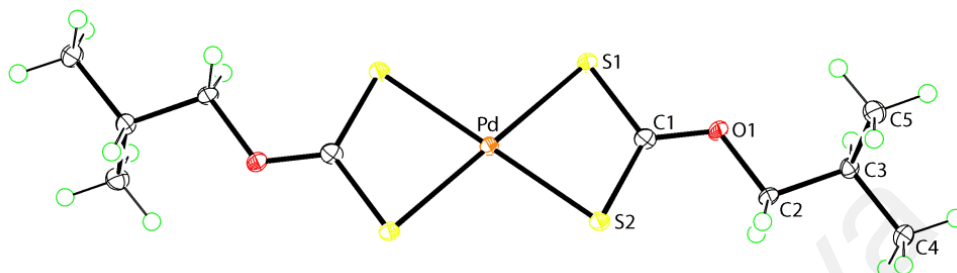
Potassium n-butylxanthate (0.0099 mol, 1.8606 g) and palladium(II) nitrate (0.0049 mol, 1.1382 g) were each dissolved in water (50 ml). The Pd(NO₃)₂ solution was added into the ligand solution drop-wise with stirring; a brown precipitate formed immediately. The precipitate was extracted with chloroform (100 ml). The chloroform layer was filtered off and the aqueous layer was further extracted with chloroform (3 x 100 ml) until no colour was evident in the chloroform extract. The orange plates formed after a few days of slow evaporation of the combined chloroform extracts. Recrystallisation was performed by dissolving the obtained crystals from a dichloromethane and hexane mixture (200 ml; 1:1 v/v). Orange needles formed after 2 days. Yield: 1.82 g, 91 %. M. pt: 392.4–392.9 K. *Anal.* Calc'd for C₁₀H₁₈O₂PdS₄: C, 29.66; H, 4.48. Found: C, 29.75; H, 4.62 %. FTIR (cm⁻¹): 1266 (s) ν (C-O), 1010 (s) ν (C-S). ¹H NMR {CDCl₃}: δ 4.63 (t, 2H, OCH₂, *J* = 6.5 Hz), 1.86 (tt, 2H, OCH₂CH₂, *J* = 6.1 Hz, *J* = 7.6 Hz), 1.49 (tq, 2H, CH₂CH₃, *J*_t = 7.5 Hz, *J*_q = 7.5 Hz), 0.98 (t, 3H, CH₃, *J* = 7.4 Hz) ppm. ¹³C{¹H} NMR {CDCl₃}: δ 233.8 (CS), 72.0 (OCH₂), 30.2 (OCH₂CH₂), 19.0 (CH₂CH₃), 13.6 (CH₃) ppm. UV-Vis (ACN; nm, cm⁻¹ mol⁻¹ L): 237 (ϵ = 18260; $n \rightarrow \sigma^*$, CT); 284 (ϵ = 45650; $\pi \rightarrow \pi^*$); 380 (ϵ = 3840; $n \rightarrow \pi^*$, CT); 457 (ϵ = 120; *d-d*, ¹A_{1g} \rightarrow ¹E_g).



Experimental (red trace) and simulated based on the single crystal structure (blue trace) PXRD patterns.

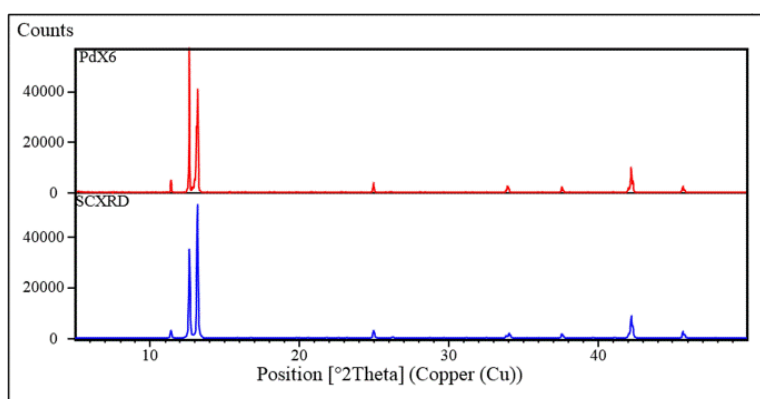
APPENDIX L- Continued

L.6 Molecular structure of bis(*O*-isobutylxanthato)palladium(II), [Pd(S₂CO-i-Bu)₂] (**16**), showing atom labelling and displacement ellipsoids at the 50% probability level.



Synthesis and characterisation:

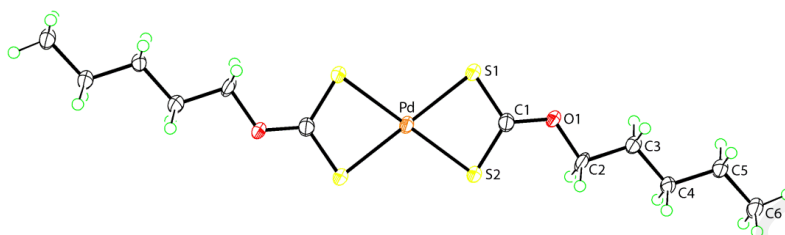
Potassium isobutylxanthate (0.0099 mol, 1.8606 g) and palladium(II) nitrate (0.0049 mol, 1.1382 g) were each dissolved in water (50 ml). The Pd(NO₃)₂ solution was added into the ligand solution drop-wise with stirring; a brown precipitate formed immediately. The precipitate was extracted with chloroform (100 ml). The chloroform layer was filtered off and the aqueous layer was further extracted with chloroform (3 x 100 ml) until no colour was evident in the chloroform extract. The orange plates formed after a few days of slow evaporation of the combined chloroform extracts. Recrystallisation was performed by dissolving the obtained crystals from a chloroform and acetonitrile mixture (200 ml; 3:1 v/v). Orange blocks formed after 2 days. Yield: 1.90 g, 95 %. M. pt: 439.0–439.6 K. *Anal.* Calc'd for C₁₀H₁₈O₂PdS₄: C, 29.66; H, 4.48. Found: C, 29.67; H, 4.39 %. FTIR (cm⁻¹): 1233 (*s*) ν(C-O), 1030 (*s*) ν(C-S). ¹H NMR {CDCl₃}: δ 4.40 (*d*, 2H, OCH₂, *J* = 6.6 Hz), 2.20 (*tsept*, 1H, CH, *J* = 6.7 Hz, *J* = 6.7 Hz), 1.04 (*d*, 6H, CH₃, *J* = 6.7 Hz) ppm. ¹³C{¹H} NMR {CDCl₃}: δ 233.8 (CS), 77.8 (OCH₂), 27.7 (CH), 19.0 (CH₃) ppm. UV-Vis (ACN; nm, cm⁻¹ mol⁻¹ L): 237 (ε = 18790; n → σ*, CT); 285 (ε = 48130; π → π*); 381 (ε = 3990; n → π* CT); 461 (ε = 110; *d-d*, ¹A_{1g} → ¹E_g).



Experimental (red trace) and simulated based on the single crystal structure (blue trace) PXRD patterns.

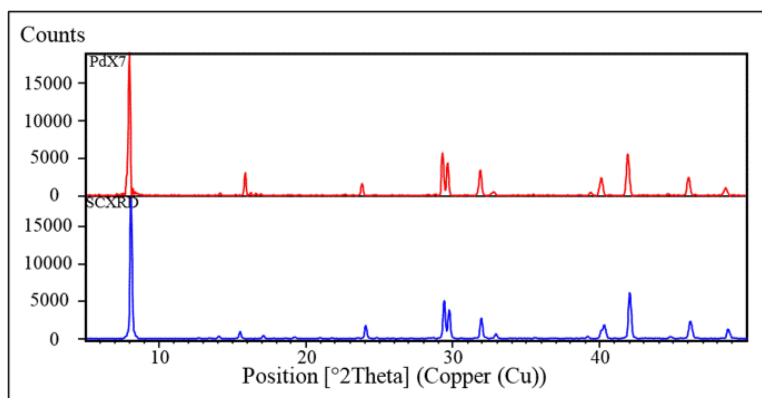
APPENDIX L- Continued

L.7 Molecular structure of bis(*O*-*n*-pentylxanthato)palladium(II), [Pd(S₂CO-*n*-Pent)₂] (**17**), showing atom labelling and displacement ellipsoids at the 50% probability level.



Synthesis and characterisation:

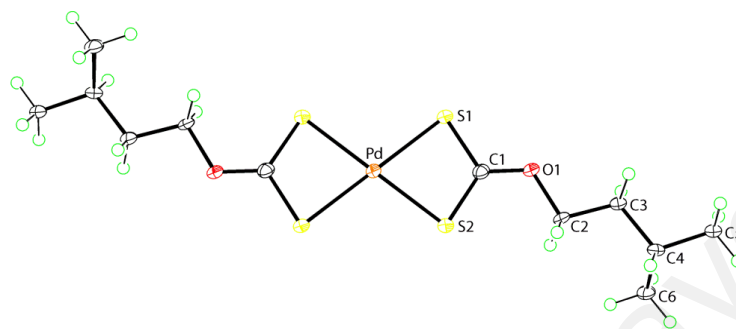
Potassium *n*-pentylxanthate (0.0092 mol, 1.8696 g) and palladium(II) nitrate (0.0046 mol, 1.0644 g) were each dissolved in water (50 ml). The Pd(NO₃)₂ solution was added into the ligand solution drop-wise with stirring; a brown precipitate formed immediately. The precipitate was extracted with chloroform (100 ml). The chloroform layer was filtered off and the aqueous layer was further extracted with chloroform (3 x 100 ml) until no colour was evident in the chloroform extract. The orange needles formed after a few days of slow evaporation of the combined chloroform extracts. Recrystallisation was performed by dissolving the obtained crystals from a chloroform and acetonitrile mixture (200 ml; 3:1 v/v). Orange needles formed after 2 days. Yield: 1.73 g, 87 %. M. pt: 364.8–365.6 K. *Anal.* Calc'd for C₁₂H₂₂O₂PdS₄: C, 33.29; H, 5.12. Found: C, 33.30; H, 5.43 %. FTIR (cm⁻¹): 1249 (*s*) ν(C-O), 1045 (*s*) ν(C-S). ¹H NMR {CDCl₃}: δ 4.62 (*t*, 2H, OCH₂, *J* = 6.6 Hz), 1.88 (*tt*, 2H, OCH₂CH₂, *J* = 6.4 Hz, *J* = 7.3 Hz), 1.50–1.32 (*m*, 4H, CH₂CH₂CH₃), 0.93 (*t*, 3H, CH₃, *J* = 7.1 Hz) ppm. ¹³C{¹H} NMR {CDCl₃}: δ 233.8 (CS), 72.3 (OCH₂), 27.9, 27.8 (OCH₂CH₂CH₂), 22.2 (CH₂CH₃), 13.9 (CH₃) ppm. UV-Vis (ACN; nm, cm⁻¹ mol⁻¹ L): 237 (ε = 18930; n → σ*, CT); 284 (ε = 45030; π → π*); 378 (ε = 3950; n → π*, CT); 448 (ε = 300; *d-d*, ¹A_{1g} → ¹E_g).



Experimental (red trace) and simulated based on the single crystal structure (blue trace) PXRD patterns.

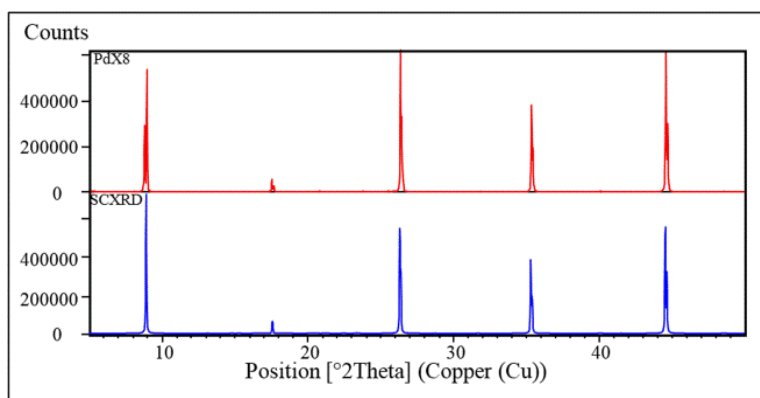
APPENDIX L- Continued

L.8 Molecular structure of bis(*O*-isopentylxanthato)palladium(II), [Pd(S₂CO-i-Pent)₂] (**18**), showing atom labelling and displacement ellipsoids at the 50% probability level.



Synthesis and characterisation:

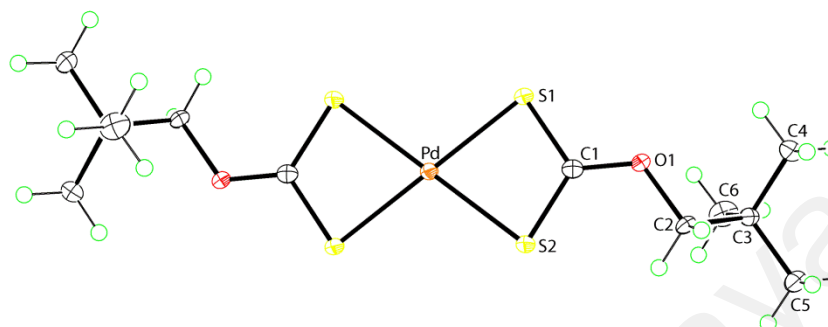
Potassium isopentylxanthate (0.0092 mol, 1.8696 g) and palladium(II) nitrate (0.0046 mol, 1.0644 g) were each dissolved in water (50 ml). The Pd(NO₃)₂ solution was added into the ligand solution drop-wise with stirring; a brown precipitate formed immediately. The precipitate was extracted with chloroform (100 ml). The chloroform layer was filtered off and the aqueous layer was further extracted with chloroform (2 x 100 ml) until no colour was evident in the chloroform extract. The orange plates formed after a few days of slow evaporation of the combined chloroform extracts. Recrystallisation was performed by dissolving the obtained crystals from a chloroform and acetonitrile mixture (200 ml; 3:1 v/v). Orange plates formed after 2 days. Yield: 1.73 g, 87 %. M. pt: 392.5–393.3 K. *Anal.* Calc'd for C₁₂H₂₂O₂PdS₄: C, 33.29; H, 5.12. Found: C, 33.42; H, 5.30 %. FTIR (cm⁻¹): 1267 (*s*) ν(C-O), 1018 (*s*) ν(C-S). ¹H NMR {CDCl₃}: δ 4.66 (*t*, 2H, OCH₂, *J* = 6.5 Hz), 1.90–1.70 (*m*, 3H, CH₂CH), 0.97 (*d*, 6H, CH₃, *J* = 6.4 Hz) ppm. ¹³C{¹H} NMR {CDCl₃}: δ 233.7 (CS), 70.8 (OCH₂), 36.7 (CH), 24.9 (CH₂CH), 23.3 (CH₃) ppm. UV-Vis (ACN; nm, cm⁻¹ mol⁻¹ L): 237 (ε = 21160; n → σ*, CT); 285 (ε = 52980; π → π*); 380 (ε = 4450; n → π*, CT); 461 (ε = 180; *d-d*, ¹A_{1g} → ¹E_g).



Experimental (red trace) and simulated based on the single crystal structure (blue trace) PXRD patterns.

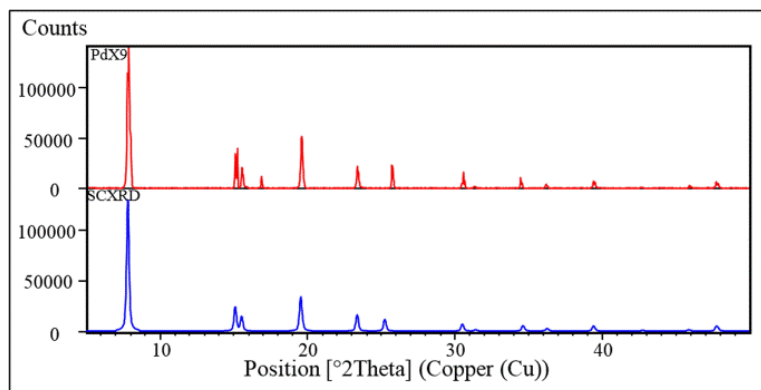
APPENDIX L- Continued

L.9 Molecular structure of bis(*O*-neopentylxanthato)palladium(II), [Pd(S₂CO-neo-Pent)₂] (**19**), showing atom labelling and displacement ellipsoids at the 50% probability level.



Synthesis and characterisation:

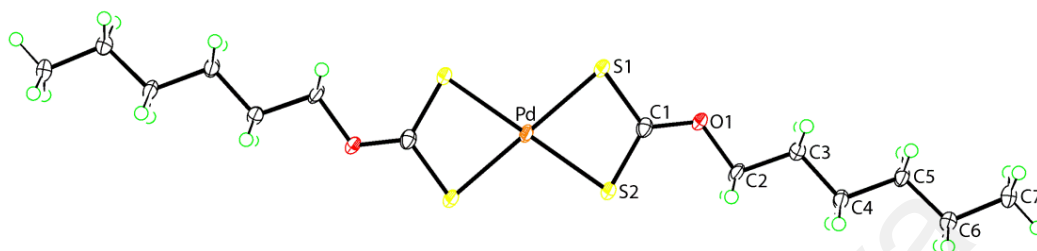
Potassium neopentylxanthate (0.0092 mol, 1.8696 g) and palladium(II) nitrate (0.0046 mol, 1.0644 g) were each dissolved in water (50 ml). The Pd(NO₃)₂ solution was added into the ligand solution drop-wise with stirring; a brown precipitate formed immediately. The precipitate was extracted with chloroform (100 ml). The chloroform layer was filtered off and the aqueous layer was further extracted with chloroform (2 x 100 ml) until no colour was evident in the chloroform extract. The orange plates formed after a few days of slow evaporation of the combined chloroform extracts. Recrystallisation was performed by dissolving the obtained crystals from a chloroform and acetonitrile mixture (200 ml; 3:1 v/v). Orange plates formed after 2 days. Yield: 1.49 g, 75 %. M. pt: 498.5–504.4 K. *Anal.* Calc'd for C₁₂H₂₂O₂PdS₄: C, 33.29; H, 5.12. Found C, 33.26; H, 5.20 %. FTIR (cm⁻¹): 1247 (*s*) ν(C-O), 1020 (*s*) ν(C-S). ¹H NMR {CDCl₃}: δ 4.29 (*s*, 2H, OCH₂), 1.05 (*s*, 9H, CH₃) ppm. ¹³C{¹H} NMR {CDCl₃}: δ 233.9 (CS), 80.9 (OCH₂), 31.8 (CH₂C), 26.3 (CH₃) ppm. UV-Vis (ACN; nm, cm⁻¹ mol⁻¹ L): 237 (ε = 22080; n → σ*, CT); 285 (ε = 55430; π → π*); 379 (ε = 4680; n → π*, CT); 451 (ε = 290; *d-d*, ¹A_{1g} → ¹E_g).



Experimental (red trace) and simulated based on the single crystal structure (blue trace) PXRD patterns.

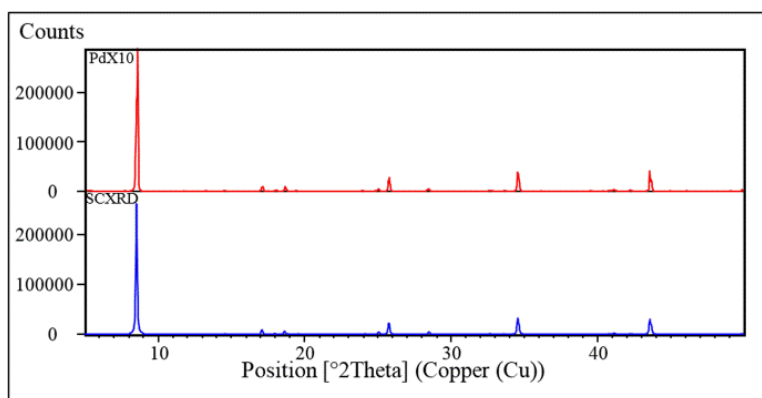
APPENDIX L- Continued

L.10 Molecular structure of bis(*O*-n-hexylxanthato)palladium(II), [Pd(S₂CO-n-Hex)₂] (**20**), showing atom labelling and displacement ellipsoids at the 50% probability level.



Synthesis and characterisation:

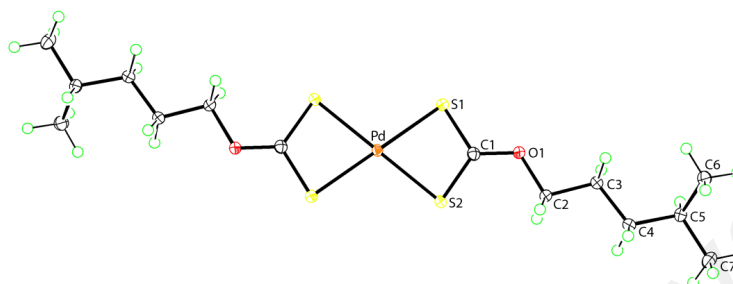
Potassium n-hexylxanthate (0.0087 mol, 1.8776 g) and palladium(II) nitrate (0.0043 mol, 0.9997 g) were each dissolved in water (50 ml). The Pd(NO₃)₂ solution was added into the ligand solution drop-wise with stirring; a brown precipitate formed immediately. The precipitate was extracted with chloroform (100 ml). The chloroform layer was filtered off and the aqueous layer was further extracted with chloroform (3 times, 100 ml) until no colour was evident in the chloroform extract. The chloroform was removed by rotary-evaporation, yielding a yellow-orange powder. Recrystallisation was performed by dissolving the obtained powder from hexane (600 ml). Orange plates formed after 8 days. Yield: 1.77 g, 89 %. M. pt: 355.5–356.0 K. *Anal.* Calc'd for C₁₄H₂₆O₂PdS₄: C, 36.47; H, 5.68. Found: C, 36.54; H, 5.89 %. FTIR (cm⁻¹): 1251 (s) ν(C-O), 1017 (s) ν(C-S). ¹H NMR {CDCl₃}: δ 4.55 (*t*, 2H, OCH₂, *J* = 6.6 Hz), 1.80 (*tt*, 2H, OCH₂CH₂, *J* = 7.1 Hz, *J* = 7.3 Hz), 1.46-1.14 (*m*, 6H, CH₂CH₂CH₂CH₃), 0.84 (*t*, 3H, CH₃, *J* = 6.3 Hz) ppm. ¹³C{¹H} NMR {CDCl₃}: δ 233.8 (CS), 72.3 (OCH₂), 31.3 (OCH₂CH₂), 28.2 (OCH₂CH₂CH₂), 25.5 (CH₂CH₂CH₃), 22.6 (CH₂CH₃), 14.0 (CH₃) ppm. UV-Vis (ACN; nm, cm⁻¹ mol⁻¹ L): 237 (ε = 21440; n → σ*, CT); 284 (ε = 55570; π → π*); 379 (ε = 4550; n → π*, CT); 457 (ε = 110; *d-d*, ¹A_{1g} → ¹E_g).



Experimental (red trace) and simulated based on the single crystal structure (blue trace) PXRD patterns.

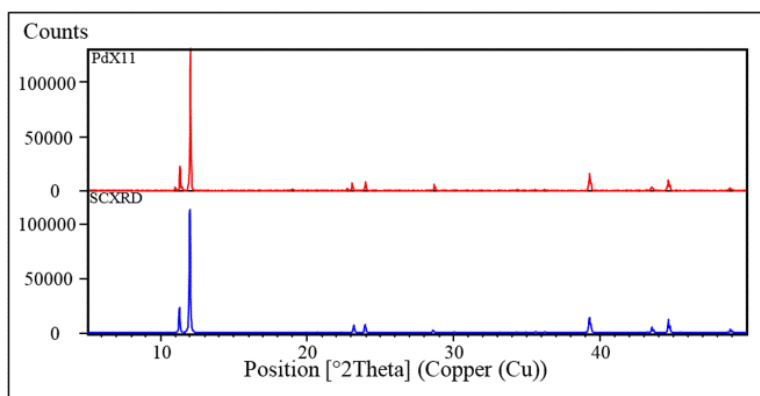
APPENDIX L- Continued

L.11 Molecular structure of bis(*O*-isohexylxanthato)palladium(II), [Pd(S₂CO-i-Hex)₂] (**21**), showing atom labelling and displacement ellipsoids at the 50% probability level.



Synthesis and characterisation:

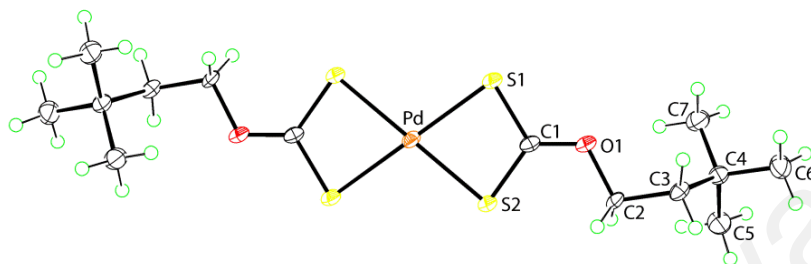
Potassium isohexylxanthate (0.0087 mol, 1.8776 g) and palladium(II) nitrate (0.0043 mol, 0.9997 g) were each dissolved in water (50 ml). The Pd(NO₃)₂ solution was added into the ligand solution drop-wise with stirring; a brown precipitate formed immediately. The precipitate was extracted with chloroform (100 ml). The chloroform layer was filtered off and the aqueous layer was further extracted with chloroform (2 x 100 ml) until no colour was evident in the chloroform extract. The chloroform was removed by rotary-evaporation, yielding a yellow-orange powder. Recrystallisation was performed by dissolving the obtained powder from a chloroform and acetonitrile mixture (200 ml; 3:1 v/v). Orange blocks formed after 2 days. Yield: 1.90 g, 95 %. M. pt: 361.3–361.8 K. *Anal.* Calc'd for C₁₄H₂₆O₂PdS₄: C, 36.47; H, 5.68. Found C, 36.52; H, 5.82 %. FTIR (cm⁻¹): 1253 (*s*) ν (C-O), 1019 (*s*) ν (C-S). ¹H NMR {CDCl₃}: δ 4.61 (*t*, 2H, OCH₂, *J* = 6.7 Hz), 1.87 (*tt*, 2H, OCH₂CH₂, *J* = 6.5 Hz, *J* = 7.9 Hz), 1.50-1.70 (*m*, 3H, CH₂CH), 1.32 (*t*, 6H, CH₃, *J* = 6.6 Hz) ppm. ¹³C{¹H} NMR {CDCl₃}: δ 233.7 (CS), 72.6 (OCH₂), 34.6 (CH), 27.7 (CH₂CH), 26.1 (OCH₂CH₂), 22.4 (CH₃) ppm. UV-Vis (ACN; nm, cm⁻¹ mol⁻¹ L): 237 (ϵ = 17820; $n \rightarrow \sigma^*$, CT); 284 (ϵ = 46280; $\pi \rightarrow \pi^*$); 379 (ϵ = 3780; $n \rightarrow \pi^*$, CT); 459 (ϵ = 90; *d-d*, ¹A_{1g} → ¹E_g).



Experimental (red trace) and simulated based on the single crystal structure (blue trace) PXRD patterns.

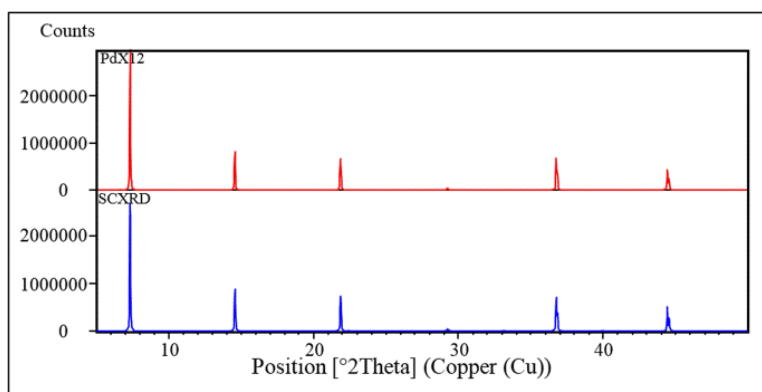
APPENDIX L- Continued

L.12 Molecular structure of bis(*O*-neohexylxanthato)palladium(II), [Pd(S₂CO-neo-Hex)₂] (**22**), showing atom labelling and displacement ellipsoids at the 50% probability level.



Synthesis and characterisation:

Potassium neohexylxanthate (0.0087 mol, 1.8776 g) and palladium(II) nitrate (0.0043 mol, 0.9997 g) were each dissolved in water (50 ml). The Pd(NO₃)₂ solution was added into the ligand solution drop-wise with stirring; a brown precipitate formed immediately. The precipitate was extracted with chloroform (100 ml). The chloroform layer was filtered off and the aqueous layer was further extracted with chloroform (2 x 100 ml) until no colour was evident in the chloroform extract. The chloroform was removed by rotary-evaporation, yielding a yellow-orange powder. Recrystallisation was performed by dissolving the obtained powder from a chloroform and hexane mixture (200 ml; 1:1 v/v). Orange plates formed after 5 days. Yield: 1.49 g, 75 %. M. pt: 436.2–437.2 K. *Anal.* Calc'd for C₁₄H₂₆O₂PdS₄: C, 36.47; H, 5.68. Found C, 36.60; H, 5.88 %. FTIR (cm⁻¹): 1240 (*s*) ν(C-O), 1017 (*s*) ν(C-S). ¹H NMR {CDCl₃}: δ 4.62 (*t*, 2H, OCH₂, *J* = 6.7 Hz), 1.74 (*t*, 2H, OCH₂CH₂, *J* = 6.7 Hz), 0.92 (*s*, 9H, CH₃) ppm. ¹³C{¹H} NMR {CDCl₃}: δ 233.6 (CS), 70.1 (OCH₂), 41.2 (CCH₃), 29.9 (OCH₂CH₂), 29.5 (CH₃) ppm. UV-Vis (I; nm, cm⁻¹ mol⁻¹ L): 237 (ε = 21270; n → σ*, CT); 285 (ε = 53560; π → π*); 379 (ε = 4410; n → π*, CT); 455 (ε = 170; *d-d*, ¹A_{1g} → ¹E_g).



Experimental (red trace) and simulated based on the single crystal structure (blue trace) PXRD patterns.

APPENDIX M

M.1 Crystallographic data and refinement details for 11–14

Compound	11	12	13	14
Formula	C ₄ H ₆ O ₂ PdS ₄	C ₆ H ₁₀ O ₂ PdS ₄	C ₈ H ₁₄ O ₂ PdS ₄	C ₈ H ₁₄ O ₂ PdS ₄
Formula weight	320.73	348.78	376.83	376.83
Crystal colour	Orange	Orange	Orange	Orange
Crystal size/mm ³	0.05x0.05x0.05	0.05x0.10x0.20	0.07x0.09x0.21	0.19x0.27x0.34
Crystal system	monoclinic	orthorhombic	triclinic	monoclinic
Space group	<i>P</i> 2 ₁ / <i>c</i>	<i>Pbca</i>	<i>P</i> $\bar{1}$	<i>P</i> 2 ₁ / <i>n</i>
<i>a</i> /Å	6.2713(5)	7.5034(4)	7.4778(4)	9.9077(6)
<i>b</i> /Å	13.5593(11)	7.2125(4)	9.5272(6)	5.8720(3)
<i>c</i> /Å	10.7931(8)	20.7854(12)	9.8084(5)	11.9621(6)
α /°	90	90	74.832(5)	90
β /°	97.635(9)	90	86.458(4)	102.752(5)
γ /°	90	90	76.292(5)	90
<i>V</i> /Å ³	909.65(12)	1124.87(11)	655.22(7)	678.77(6)
<i>Z</i>	4	4	2	2
<i>D</i> _c /g cm ⁻³	2.342	2.059	1.910	1.844
<i>F</i> (000)	624	688	376	376
μ (MoK α)/mm ⁻¹	2.903	—	2.031	1.961
μ (CuK α)/mm ⁻¹	—	19.997	—	—
Measured data	4854	9418	5652	5337
θ range/°	3.0 – 27.5	4.3 – 75.0	3.2 – 27.5	3.0 – 27.5
Unique data	2080	1154	3011	1555
Observed data (<i>I</i> ≥ 2.0 σ (<i>I</i>))	1455	1044	2414	1452
No. parameters	102	62	136	72
<i>R</i> , obs. Data; all data	0.042; 0.071	0.025; 0.028	0.033; 0.047	0.028; 0.031
<i>a</i> ; <i>b</i> in weighting scheme	0.021; 0	0.046; 0	0.029; 0	0.048; 0.292
<i>R</i> _w , obs. Data; all data	0.071; 0.083	0.069; 0.072	0.069; 0.077	0.072; 0.074
GoF	1.02	1.13	1.07	1.05
Range of residual electron density peaks/E α ⁻³	-0.88 – 0.67	-1.14 – 0.83	-0.97 – 0.93	-0.85 – 1.68

APPENDIX M- Continued

M.2 Crystallographic data and refinement details for 15–18

Compound	15	16	17	18
Formula	C ₁₀ H ₁₈ O ₂ PdS ₄	C ₁₀ H ₁₈ O ₂ PdS ₄	C ₁₂ H ₂₂ O ₂ PdS ₄	C ₁₂ H ₂₂ O ₂ PdS ₄
Formula weight	404.88	404.88	432.93	432.93
Crystal colour	Yellow	Orange	Orange	Orange
Crystal size/mm ³	0.05x0.05x0.20	0.06x0.11x0.16	0.05x0.10x0.20	0.10x0.20x0.40
Crystal system	triclinic	triclinic	triclinic	triclinic
Space group	<i>P</i> $\bar{1}$	<i>P</i> $\bar{1}$	<i>P</i> $\bar{1}$	<i>P</i> $\bar{1}$
<i>a</i> /Å	5.7038(4)	6.0243(4)	6.8820(11)	6.5622(4)
<i>b</i> /Å	6.7822(4)	8.0461(6)	7.3531(12)	6.8643(5)
<i>c</i> /Å	10.5967(8)	8.9366(7)	10.0455(10)	9.8385(7)
α /°	72.420(6)	111.050(7)	70.305(12)	84.811(6)
β /°	78.467(6)	99.851(6)	70.788(12)	76.424(6)
γ /°	79.852(5)	103.836(6)	67.164(15)	83.388(6)
<i>V</i> /Å ³	379.94(5)	376.42(5)	429.42(12)	427.00(5)
<i>Z</i>	1	1	1	1
<i>D</i> _c /g cm ⁻³	1.770	1.786	1.674	1.684
<i>F</i> (000)	204	204	220	220
μ (Mo <i>K</i> α)/mm ⁻¹	1.758	—	—	1.570
μ (Cu <i>K</i> α)/mm ⁻¹	—	15.036	13.223	—
Measured data	5606	2501	3253	6326
θ range/°	3.2 – 27.5	5.5 – 75.0	6.7 – 75.0	3.0 – 27.5
Unique data	1752	1552	1748	1955
Observed data (<i>I</i> ≥ 2.0σ(<i>I</i>))	1646	1551	1619	1812
No. parameters	80	81	89	90
<i>R</i> , obs. data; all data	0.024; 0.026	0.028; 0.028	0.054; 0.058	0.029; 0.033
<i>a</i> ; <i>b</i> in weighting scheme	0.036; 0.263	0.060; 0.187	0.119; 0.851	0.046; 0.080
<i>R</i> _w , obs. data; all data	0.061; 0.064	0.077; 0.077	0.158; 0.166	0.078; 0.083
GoF	1.10	1.05	1.09	1.13
Range of residual electron density peaks/eÅ ⁻³	-0.82 – 0.98	-1.60 – 0.82	-3.03 – 1.30	-1.23 – 1.18

APPENDIX M- Continued

M.3 Crystallographic data and refinement details for 19–22

Compound	19	20	21	22
Formula	C ₁₂ H ₂₂ O ₂ PdS ₄	C ₁₄ H ₂₆ O ₂ PdS ₄	C ₁₄ H ₂₆ O ₂ PdS ₄	C ₁₄ H ₂₆ O ₂ PdS ₄
Formula weight	432.93	460.99	460.99	460.99
Crystal colour	Orange	Yellow	Yellow	Yellow
Crystal size/mm ³	0.20x0.30x0.40	0.03x0.20x0.30	0.05x0.20x0.20	0.05x0.10x0.20
Crystal system	triclinic	triclinic	triclinic	triclinic
Space group	<i>P</i> $\bar{1}$	<i>P</i> $\bar{1}$	<i>P</i> $\bar{1}$	<i>P</i> $\bar{1}$
<i>a</i> /Å	6.2746(3)	6.8083(5)	7.0663(5)	6.1398(6)
<i>b</i> /Å	6.3302(4)	7.5446(4)	8.4457(3)	6.7176(5)
<i>c</i> /Å	11.4138(6)	10.4837(8)	9.2536(4)	11.9393(10)
α /°	79.690(5)	101.008(6)	63.740(4)	90.020(7)
β /°	88.152(4)	98.983(6)	73.752(3)	99.397(7)
γ /°	86.065(5)	112.048(6)	83.782(3)	95.377(7)
<i>V</i> /Å ³	444.89(4)	474.33(6)	475.40(5)	483.63(7)
<i>Z</i>	1	1	1	1
<i>D</i> _c /g cm ⁻³	1.616	1.614	1.610	1.583
<i>F</i> (000)	220	236	236	236
μ (MoK α)/mm ⁻¹	1.507	1.419	1.416	—
μ (CuK α)/mm ⁻¹	—	—	—	11.778
Measured data	3533	3938	7620	7538
θ range/°	3.3 – 27.5	3.0 – 27.6	3.0 – 27.5	3.8 – 75.0
Unique data	2037	2192	2173	1979
Observed data (<i>I</i> ≥ 2.0 σ (<i>I</i>))	1872	2006	2069	1861
No. parameters	91	98	99	100
<i>R</i> , obs. data; all data	0.023; 0.028	0.029; 0.033	0.017; 0.018	0.056; 0.059
<i>a</i> ; <i>b</i> in weighting scheme	0.018; 0	0.023; 0.082	0.021; 0.219	0.130; 0.375
<i>R</i> _w , obs. data; all data	0.047; 0.049	0.064; 0.068	0.042; 0.043	0.158; 0.164
GoF	1.07	1.08	1.04	1.08
Range of residual electron density peaks/eÅ ⁻³	-0.39 – 0.70	-1.05 – 0.91	-0.43 – 0.43	-2.03 – 4.37

APPENDIX N

N.1 Selected bond lengths and angles (Å, °) for **11–22**

Parameter	11	12 ^{a,i}	13	14 ^{a,i}	15 ^{a,i}	16 ^{a,ii}	17 ^{a,i}	18 ^{a,i}	19 ^{a,i}	20 ^{a,iii}	21 ^{a,iv}	22 ^{a,i}
Pd–S1	2.3233(15)	2.3387(5)	2.3253(9)	2.3229(6)	2.3233(6)	2.3243(7)	2.3322(13)	2.3318(7)	2.3210(6)	2.3249(7)	2.3256(4)	2.3368(12)
Pd–S2	2.3376(15)	2.3341(6)	2.3414(9)	2.3366(6)	2.3398(5)	2.3333(7)	2.3397(13)	2.3332(6)	2.3283(5)	2.3354(6)	2.3370(4)	2.3202(12)
Pd–S3	2.3320(15)	2.3387(5)	2.3386(9)	2.3229(6)	2.3233(6)	2.3243(7)	2.3322(13)	2.3318(7)	2.3210(6)	2.3249(7)	2.3256(4)	2.3368(12)
Pd–S4	2.3432(15)	2.3341(6)	2.3371(9)	2.3366(6)	2.3398(5)	2.3333(7)	2.3397(13)	2.3332(6)	2.3283(5)	2.3354(6)	2.3370(4)	2.3202(12)
C1–S1	1.702(6)	1.705(3)	1.700(3)	1.706(3)	1.698(2)	1.700(3)	1.693(6)	1.706(3)	1.696(2)	1.700(2)	1.6968(15)	1.704(5)
C1–S2	1.698(6)	1.695(2)	1.697(3)	1.697(3)	1.702(2)	1.701(3)	1.694(6)	1.698(3)	1.696(2)	1.697(3)	1.7028(15)	1.705(5)
C–S3	1.698(5)	1.705(3)	1.700(3)	1.706(3)	1.698(2)	1.700(3)	1.693(6)	1.706(3)	1.696(2)	1.700(2)	1.6968(15)	1.704(5)
C–S4	1.693(5)	1.695(2)	1.702(3)	1.697(3)	1.702(2)	1.701(3)	1.694(6)	1.698(3)	1.696(2)	1.697(3)	1.7028(15)	1.705(5)
C1–O1	1.304(6)	1.311(3)	1.304(4)	1.300(3)	1.301(3)	1.306(4)	1.309(7)	1.302(3)	1.304(2)	1.298(3)	1.3025(17)	1.296(6)
C–O2	1.307(6)	1.311(3)	1.304(4)	1.300(3)	1.301(3)	1.306(4)	1.309(7)	1.302(3)	1.304(2)	1.298(3)	1.3025(17)	1.296(6)
S1–Pd–S2	75.66(5)	75.50(2)	75.51(3)	75.39(2)	75.57(2)	75.83(3)	75.50(5)	75.62(2)	75.624(19)	75.60(2)	75.647(13)	75.60(4)
S1–Pd–S3	177.93(5)	180	177.62(3)	180	180	180	180	180	180	180	180	180
S1–Pd–S4	103.99(5)	104.50(2)	103.84(3)	104.61(2)	104.43(2)	104.17(2)	104.50(5)	104.38(2)	104.376(19)	104.40(2)	104.353(13)	104.40(4)
S2–Pd–S3	104.80(5)	104.50(2)	104.97(3)	104.61(2)	104.43(2)	104.17(2)	104.50(5)	104.38(2)	104.376(19)	104.40(2)	104.353(13)	104.40(4)
S2–Pd–S4	176.91(4)	180	176.34(3)	180	180	180	180	180	180	180	180	180
S3–Pd–S4	75.44(5)	75.50(2)	75.53(3)	75.39(2)	75.57(2)	75.83(3)	75.50(5)	75.62(2)	75.624(19)	75.60(2)	75.647(13)	75.60(4)
Pd–S1–C1	85.13(19)	84.79(8)	85.20(11)	85.60(9)	85.35(8)	84.94(10)	84.7(2)	84.89(9)	85.10(7)	85.06(9)	85.16(5)	85.08(17)
Pd–S2–C1	84.76(19)	85.14(10)	84.76(12)	85.34(9)	84.73(8)	84.63(10)	84.5(2)	85.02(9)	84.87(7)	84.79(8)	84.67(5)	85.59(17)
Pd–S3–C	84.89(19)	84.79(8)	84.91(12)	85.60(9)	85.35(8)	84.94(10)	84.7(2)	84.89(9)	85.10(7)	85.06(9)	85.16(5)	85.08(17)
Pd–S4–C	84.65(19)	85.14(10)	84.91(12)	85.34(9)	84.73(8)	84.63(10)	84.5(2)	85.02(9)	84.87(7)	84.79(8)	84.67(5)	85.59(17)
S1–C1–O1	119.2(4)	119.66(17)	119.2(2)	118.86(19)	119.29(17)	119.2(2)	119.5(4)	119.5(2)	118.77(16)	119.58(18)	119.55(11)	120.8(4)
S2–C1–O1	126.3(4)	125.8(2)	126.3(3)	127.46(19)	126.35(17)	126.2(2)	125.2(4)	126.2(2)	126.86(16)	125.91(18)	125.95(11)	125.4(4)
S3–C–O2	118.5(4)	119.66(17)	119.8(2)	118.86(19)	119.29(17)	119.2(2)	119.5(4)	119.5(2)	118.77(16)	119.58(18)	119.55(11)	120.8(4)
S4–C–O2	126.5(4)	125.8(2)	125.6(3)	127.46(19)	126.35(17)	126.2(2)	125.2(4)	126.2(2)	126.86(16)	125.91(18)	125.95(11)	125.4(4)

^a The Pd atom is located at a centre of inversion, with symmetry operations: *i* 1-x, 1-y, 1-z; *ii* -x, 1-y, 1-z; *iii* 1-x, -y, 1-z; *iv* 2-x, 1-y, 1-z.

APPENDIX O

O.1 Summary of intermolecular interactions (A–H...B; Å, °) operating in the crystal structures of 12–22

A	H	B	A–H	H...B	A...B	A–H...B	Symmetry operation
12							
C2	H2a	Cg(PdS1S2C1)	0.99	2.86	3.672(3)	140	1/2-x, 1/2+y, z
13							
C2	H2a	Cg(PdS1S2C1)	0.99	2.91	3.753(4)	143	2-x, 1-y, 1-z
C2	H2b	Pd	0.99	2.83	3.759(4)	156	1-x, 1-y, 1-z
14							
C4	H4a	S1	0.98	2.83	3.617(2)	138	1/2+x, 1/2-y, -1/2+z
C2	H2	Cg(PdS1S2C1)	1.00	2.91	3.796(2)	151	1/2-x, 1/2+y, 1/2-z
C4	H4b	Cg(PdS1S2C1)	0.98	2.96	3.845(2)	151	-1/2+x, 1/2-y, -1/2+z
15							
C2	H2a	S1	0.99	2.87	3.850(2)	170	-1+x, y, z
C2	H2b	Cg(PdS1S2C1)	0.99	2.97	3.873(2)	153	1-x, -y, 1-z
C4	H4b	Cg(PdS1S2C1)	0.99	2.96	3.747(2)	138	x, -1+y, z
16							
C2	H2a	Cg(PdS1S2C1)	0.99	3.11	3.952(3)	144	1+x, y, z
C4	H4a	Cg(PdS1S2C1)	0.99	3.07	3.928(4)	147	1+x, y, z
17							
C2	H2b	Cg(PdS1S2C1)	0.99	2.86	3.779(6)	155	1-x, -y, 1-z
C4	H4b	Cg(PdS1S2C1)	0.99	3.01	3.763(5)	133	x, -1+y, z
18							
C2	H2a	Cg(PdS1S2C1)	0.99	3.11	3.858(3)	134	1-x, 2-y, 1-z
C5	H5a	Cg(PdS1S2C1)	0.98	3.14	3.895(3)	136	x, 1+y, z
19							
C4	H4b	Cg(PdS1S2C1)	0.98	3.09	3.995(2)	155	-1+x, y, z
20							
C2	H2b	Cg(PdS1S2C1)	0.99	2.86	3.739(2)	148	1-x, 1-y, 1-z
C4	H4b	Cg(PdS1S2C1)	0.99	3.08	3.873(2)	153	1-x, -y, 1-z
21							
C2	H2a	Cg(PdS1S2C1)	0.99	2.98	3.9274(17)	160	1-x, 1-y, 1-z
C4	H4a	Cg(PdS1S2C1)	0.99	3.10	3.836(2)	132	-1+x, y, z
22							
C2	H2a	Cg(PdS1S2C1)	0.99	3.12	3.826(5)	130	1-x, 1-y, 1-z
C3	H3a	Cg(PdS1S2C1)	0.99	3.06	3.561(5)	113	x, -1+y, z
C3	H3b	Cg(PdS1S2C1)	0.99	3.11	3.561(5)	109	x, -1+y, z